

MAGNETOM Flash

The Magazine of MR

Issue no.2/2007
CMR Edition
Not for distribution in the USA

SIEMENS
medical

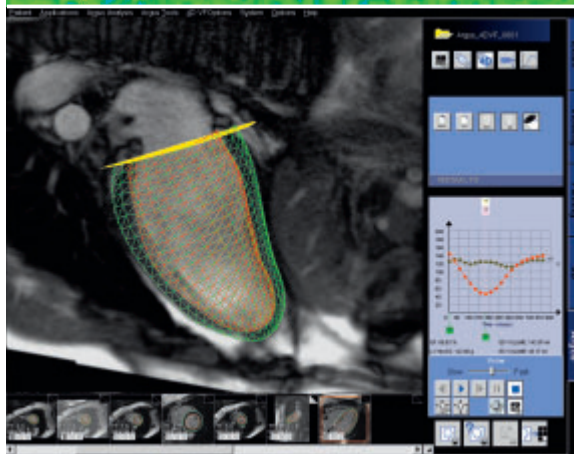
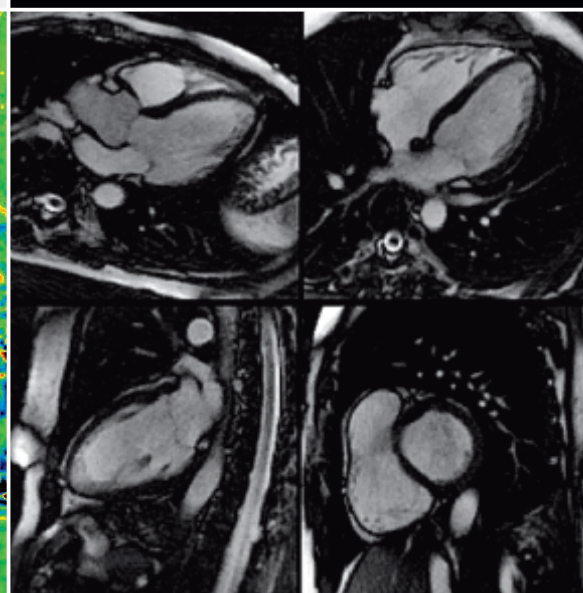
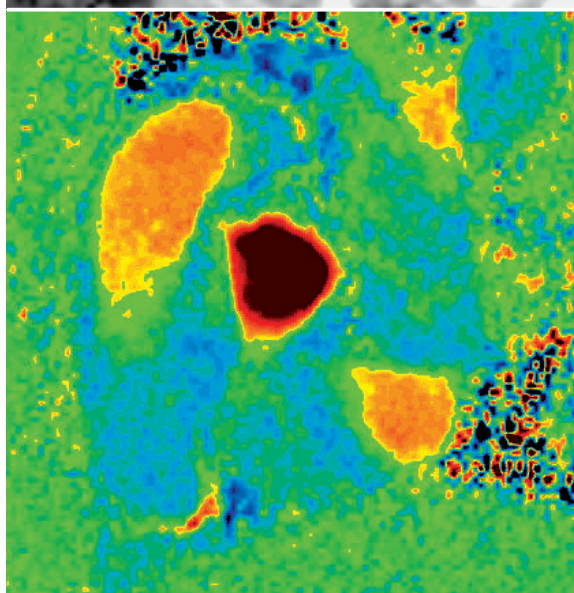
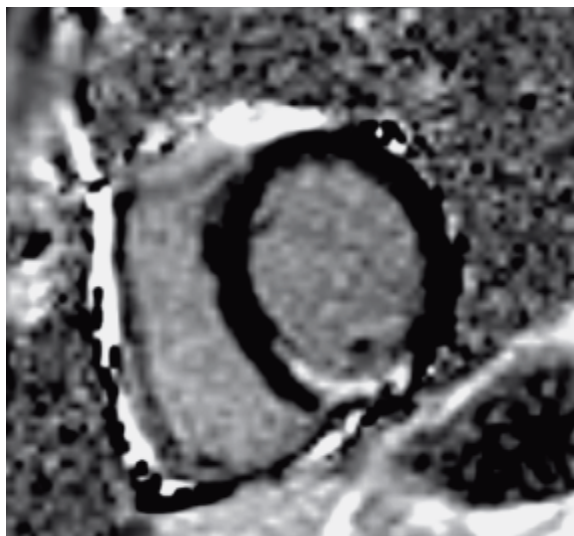
Cardiovascular Magnetic Resonance

Delayed Enhancement
Imaging in Coronary
Artery Disease
Page 14

Differentiation of
Cardiomyopathies
Page 22

Myocardial Stress
Perfusion Imaging
Page 34

Contains a CD with
SCMR Recommended
Protocols
Page 107



36

Okan Ekinci, M.D.
Segment Manager,
Cardiovascular MRI



Dear MAGNETOM user,

From vision to clinical practice, Cardiovascular MRI (CMR) emerges as a fully-established technique for routine cardiac imaging. In handling anatomy, function, morphology, tissue characterization, myocardial perfusion, angiography or molecular MRI, there is simply no other single modality in cardiology or radiology to offer as much insight into the heart as CMR.

Today, CMR allows us to detect multiple cardiac diseases such as myocardial infarct or cardiomyopathies more easily and to understand them much better. Indeed, recent studies show that CMR even helps to identify patients at risk of, for example, sudden cardiac death in DCM or HOCM.

This extension of capabilities, however, requires a deep knowledge about the role and use of CMR in clinical routine. From courses and symposia to user meetings, Siemens has consistently supported a broad range of educational activities to enable more institutions to perform CMR. And we are proud that this new issue of MAGNETOM Flash is totally dedicated to the field of CMR from a clinical perspective by authors who are opinion leaders in their respective fields.

The magazine also comes with two valuable bonuses:

Firstly, a CD presenting a comprehensive guide to performing a CMR exam (90+ pages) in accordance with SCMR recommendations, as well as ready-to-use (downloadable) CMR protocols for the most frequent indications. We are very appreciative of the cooperation of the SCMR in this regard.

Secondly, a poster depicting the common imaging planes, types of sequences frequently used in CMR and typical patterns of delayed enhancement imaging, not to mention many other features to offer you an extremely useful and accessible overview of CMR.

We hope you will enjoy and find value in this edition of MAGNETOM Flash.

Your feedback is very welcome.

Please mail any questions or comments to okan.ekinci@siemens.com

A blue ink handwritten signature of Okan Ekinci.

Okan Ekinci, MD
Guest Editor
Segment Manager, Cardiovascular MRI
Head, Application Marketing Center
Siemens Medical Solutions
MR Marketing

Contact

okan.ekinci@siemens.com

The Editorial Team

We appreciate your comments.

Please contact us at magnetomworld.med@siemens.com



A. Nejat Bengi, M.D.
Editor in Chief



Antje Hellwich
Associate Editor



Dagmar Thomsik-Schröpfer,
Ph.D., MR Marketing-Products,
Erlangen, Germany



Cécile Mohr, Ph.D.
Head of Market Segment
Management, Erlangen



Heike Weh,
Clinical Data Manager,
Erlangen, Germany



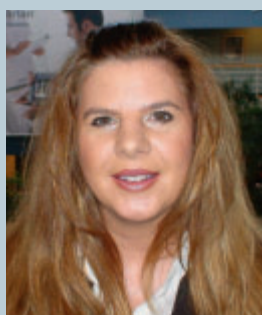
Bernhard Baden,
Clinical Data Manager,
Erlangen, Germany



Peter Kreisler, Ph.D.
Collaborations & Applications,
Erlangen, Germany



Milind Dhamankar, M.D.
Director, MR Product
Marketing, Malvern, USA



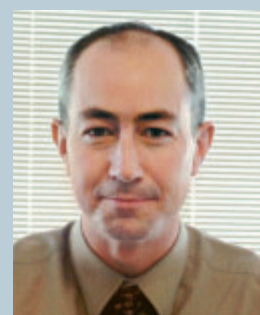
Kathleen Giannini,
US Installed Base Manager,
Malvern, PA, USA



Gary R. McNeal, MS (BME)
Advanced Application Specialist,
Cardiovascular MR Imaging
Hoffman Estates, USA

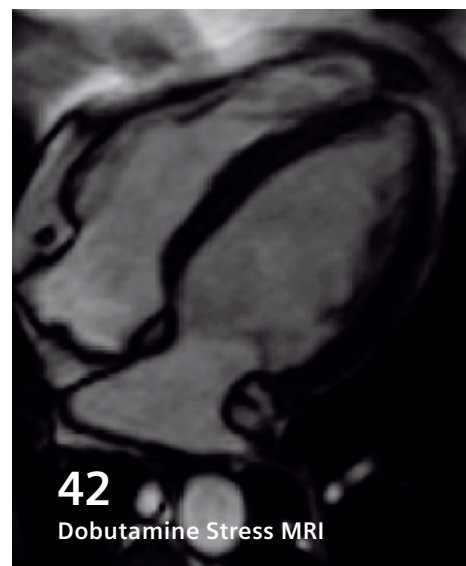
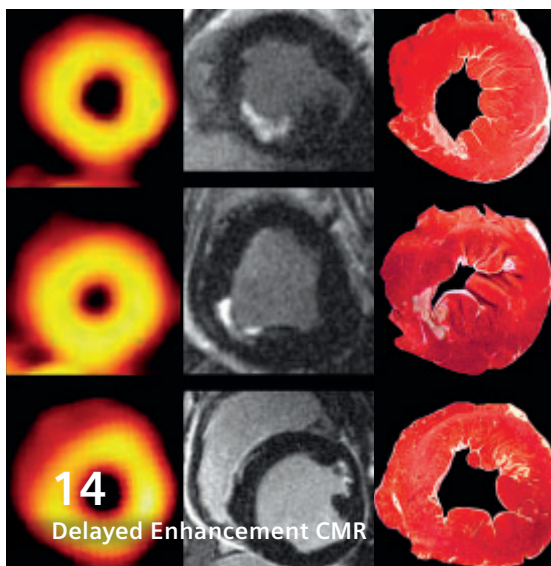


Dr. Sunil Kumar S.L.
Senior Manager Applications,
Canada

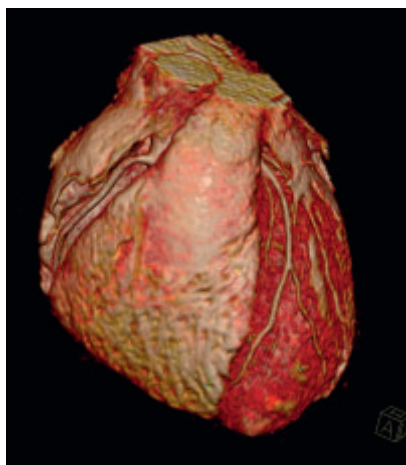


Tony Enright, Ph.D.
Asia Pacific Collaborations,
Australia

Content



Cardiovascular MRI



Due to the increased interest in Cardiovascular MRI we dedicated this issue of MAGNETOM Flash to CMR. Experienced users, opinion leaders in their respective field, provide the key knowledge necessary to understand the role of CMR exams in today's clinical routine.

Clinical Cardiovascular MRI

- 6** CMR Assessment of Global Ventricular Function (Ekinci)
- 14** CMR Delayed Enhancement Imaging in Coronary Artery Disease (Klem)
- 22** Differentiation of Cardiomyopathies by Use of CMR (O'Hanlon, Pennell, Schulz-Menger et al.)
- 34** Stress-MRI: Adenosine Stress Perfusion MRI for Myocardial Ischemia Detection (Arai)
- 42** Stress-MRI: High-Dose Dobutamine Stress MRI for Myocardial Ischemia Detection (Jochims)
- 50** CMR for the Assessment of Valvular Disease (Cowan, Young et al.)
- 56** Evaluation of Cardiac Masses by CMR (Bruder et al.)
- 61** Clinical Application of 3D/4D MR Angiography in Cardiovascular Diseases (Barkhausen et al.)

61 MRA in Cardiovascular Diseases

80 How I do it: Stress Perfusion MRI

126 R&D in Plaque Imaging

68 MR Imaging of Congenital Heart Disease
(Muthurangu, Hansen, Taylor)

74 MR Imaging in the Electrophysiology
Laboratory (Oakes, Marrouche et al.)

Cardiovascular MRI → How I do it

80 Workflow Optimization for CMR Adenosine
Stress Perfusion in Clinical Routine (Recke et al.)

86 CMR Imaging of Myocardial Amyloidosis Using
Late Contrast Enhanced (LCE) Imaging:
Challenges and Potential Solutions (Voros et al.)

89 Flow measurements: Basics and the Applica-
tion to the Main Pulmonary Artery (Abolmaali)

Education / Life

94 Guidelines for Credentialling in CMR
(endorsed by the SCMR)

98 Training Sites / Courses for CMR

102 CMR Site Accreditation Process

107 SCMR Accredited Protocols & Comprehensive
CMR Exam Guide (on CD)

108 Abbreviations

Technology & Trends

110 Dark Blood Delayed Enhancement Imaging:
New Developments in the Imaging of
Myocardial Viability (Rehwald)

118 The Promise of Molecular MRI in
Cardiovascular Imaging (Sosnovik)

126 Nano_AG: Development of New Contrast
Agents for the Detection of Vulnerable
Plaques (Schnorr et al.)

129 Radiofrequency Coil Innovation in
Cardiovascular MRI (Schmitt, Sosnovik et al.)

The information presented in MAGNETOM Flash is for illustration only and is not intended to be relied upon by the reader for instruction as to the practice of medicine. Any health care practitioner reading this information is reminded that they must use their own learning, training and expertise in dealing with their individual patients. This material does not substitute for that duty and is not intended by Siemens Medical Solutions to be used for any purpose in that regard. The drugs and doses mentioned in MAGNETOM Flash are consistent with the approval labeling for uses and/or indications of the drug. The treating physician bears the sole responsibility for the diagnosis and treatment of patients, including drugs and doses prescribed in connection with such use. The Operating Instructions must always be strictly followed when operating the MR System. The source for the technical data is the corresponding data sheets.

Not for distribution in the US.

CMR Assessment of Global Ventricular Function and Mass: Greater Efficiency and Diagnostic Accuracy with Argus 4D VF and Inline VF

Okan Ekin, M.D.

Siemens Medical Solutions, Erlangen, Germany

CMR is considered the gold standard for accurate assessment of left and right ventricular function.

Both cardiac volumes and ejection fraction have important prognostic and therapeutic implications in cardiology, hence the accuracy of the data can significantly affect the appropriateness of certain diagnostic or therapeutic approaches in an individual patient, e.g. when considering the implantation of an Implantable Cardioverter Defibrillator (ICD) in a heart failure patient with an ejection fraction (EF) below 35%.

As a widely available and validated method, transthoracic echocardiography is used most frequently for left ventricular function assessment. But in today's medicine, multiple diagnostic tools are available for ventricular function (VF) assessment including nuclear techniques, CT and CMR. How-

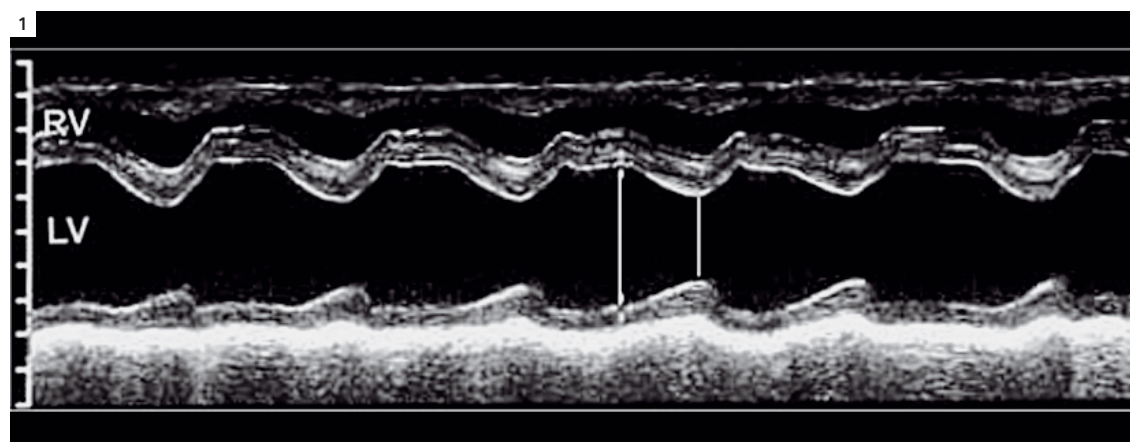
ever, ejection fraction and volume measurements by these techniques are not completely interchangeable due to the different type of data entered into analysis. Normal values for CMR assessed ventricular function and mass are shown in tables 1A–C. In echocardiography there are various approaches for LV EF assessment:

M-mode echo with Teichholz correction (Fig. 1):

$$\text{End-diastolic volume} = [7/(2,4+EDD)] \times EDD^3$$

$$\text{End-systolic volume} = [7/(2,4+ESD)] \times ESD^3$$

(EDD = end-diastolic diameter,
ESD = end-systolic diameter)



1 M-mode echocardiogram of the left ventricle. The long line shows the end-diastolic position; the short line shows the end-systolic position. The length of the lines reflects the LV diameter at end-diastole (EDD) and end-systole (ESD), respectively and can be used for LV function assessment.

Table 1A: CMR Assessed Left Ventricular (LV) Function Indexed by Body Surface Area (BSA)

Parameter	Mean \pm SD		p
	Men	Women	
LVEDVI (mL/m ²)	73.9 \pm 14.7	64.5 \pm 10.8	< 0.0001
LVESVI (mL/m ²)	24.5 \pm 8.8	18.2 \pm 5.1	< 0.0001
LVSVI (mL/m ²)	49.4 \pm 9.9	46.3 \pm 8.4	0.1457
LVEFI (%/m ²)	35.5 \pm 5.9	42.9 \pm 5.6	< 0.0001
LVMI (g/m ²)	85.1 \pm 15.2	66.9 \pm 10.9	< 0.0001
CI (mL/min/m ²)	2.9 \pm 0.6	2.9 \pm 0.6	< 0.1675

Table 1B: CMR Assessed Left Ventricular (LV) Volumes and Mass

Parameter	Mean \pm SD		p
	Men	Women	
LVEDV (mL)	142.2 \pm 34.0	109.2 \pm 22.5	< 0.0001
LVESV (mL)	47.4 \pm 19.4	30.9 \pm 9.5	< 0.0001
LVSV (mL)	94.8 \pm 21.3	78.2 \pm 17.0	< 0.0001
LVEF (%)	67.2 \pm 7.2	71.8 \pm 5.6	< 0.0001
LV mass (g)	163.8 \pm 35.8	113.6 \pm 24.2	< 0.0001
CO (mL/min)	5.6 \pm 1.2	4.9 \pm 1.1	< 0.0001

Table 1C: CMR Assessed Left Ventricular (LV) Function by Ethnicity

Parameter	White (mean \pm SD)	p			AA (mean \pm SD)	p		Hispanics (mean \pm SD)	p	Asian (mean \pm SD)
		AA	Hispanics	Asian		Hispanics	Asian		Asian	
LVEDV (mL)	148.0 \pm 30.5	NS	NS	< 0.05	153.6 \pm 30.9	NS	< 0.05	147.3 \pm 26.7	< 0.05	116.5 \pm 18.4
LVESV (mL)	50.1 \pm 14.7	NS	NS	< 0.05	54.9 \pm 16.5	NS	< 0.05	50.3 \pm 13.6	< 0.05	36.5 \pm 7.0
LVSV (mL)	97.9 \pm 21.4	NS	NS	< 0.05	98.7 \pm 20.9	NS	< 0.05	97.1 \pm 18.2	< 0.05	80.0 \pm 14.9
LVEF (%)	66.3 \pm 6.4	NS	NS	NS	64.5 \pm 6.9	NS	< 0.05	66.2 \pm 6.2	NS	68.5 \pm 4.4
LV mass (g)	170.0 \pm 32.1	NS	NS	< 0.05	181.6 \pm 35.8	< 0.05	< 0.05	163.8 \pm 25.7	< 0.05	129.1 \pm 20.0
CO (L/min)	5.7 \pm 1.4	NS	NS	< 0.05	5.81 \pm 30.9	NS	< 0.05	5.7 \pm 1.1	< 0.05	4.8 \pm 1.0
LVEDVI (mL/m ²)	74.5 \pm 14.0	NS	NS	< 0.05	74.8 \pm 12.1	NS	< 0.05	77.4 \pm 13.0	< 0.05	68.3 \pm 7.4
LVESVI (mL/m ²)	25.2 \pm 7.1	NS	NS	< 0.05	26.7 \pm 7.4	NS	< 0.05	26.4 \pm 7.1	< 0.05	21.4 \pm 3.4
LVSVI (mL/m ²)	49.3 \pm 10.1	NS	NS	NS	48.1 \pm 8.5	NS	NS	51.0 \pm 8.8	NS	46.9 \pm 6.7
LVMI (g/m ²)	85.6 \pm 14.7	NS	NS	< 0.05	38.8 \pm 16.8	NS	< 0.05	85.9 \pm 11.3	< 0.05	75.7 \pm 8.2
CI (L/min/m ²)	2.9 \pm 0.6	NS	NS	NS	2.8 \pm 0.6	NS	NS	3.0 \pm 0.6	NS	2.8 \pm 0.5

Table 1A–C: Normal values for MRI-assessed left ventricular function indexed by BSA (A), for left ventricular volumes and mass by gender (B), and left ventricular function by ethnicity (C). Note – White = white Americans, AA = Africans, Asia = Asian-Americans, NS = not statistically significant, ESVI = end-systolic volume index, EDV = end-diastolic volume, ESV = end-systolic volume, SV = stroke volume, EF = ejection fraction, CO = cardiac output, EDVI = end-diastolic volume index, ESVI = end-systolic volume index, SVI = stroke volume index, MI = mass index, CI = cardiac index. P values based on on Dunnett's two-tailed t test, with the Asian-American group used as the control group [Source: Cardiovascular Function in Multi-Ethnic Study of Atherosclerosis (MESA): Normal Values by Age, Sex, and Ethnicity. Natori S, Lai S, Finn P et al. AJR 2006;186:S357–S365.]

Single-plane area-length method (Fig. 2):

$$V = \pi/6 \times LD^2$$

(L = length of the ventricle,
D = diameter of the ventricle)

Biplane modified Simpson rule (BSR, Fig. 3A, B):

$$V = (\pi/4) \times (LVL/n) \sum_{i=1}^n DiX \times DiY$$

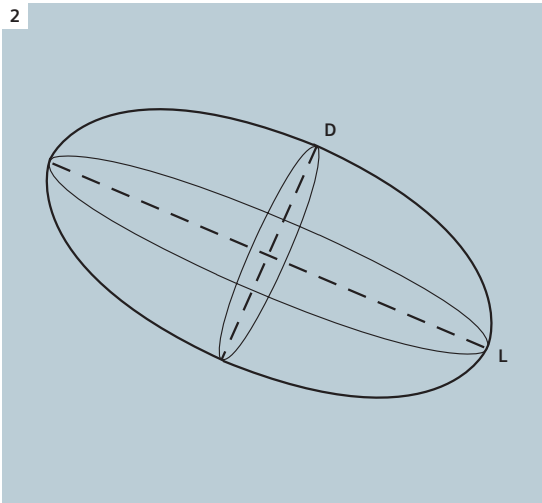
(V = volume,
LVL = length of LV,
n = number of slices,
DiX = diameter in plane X and slice i,
DiY = diameter in plane Y and slice i)

LV mass can be calculated in echocardiography by the corrected ASE simplified cubed equation:

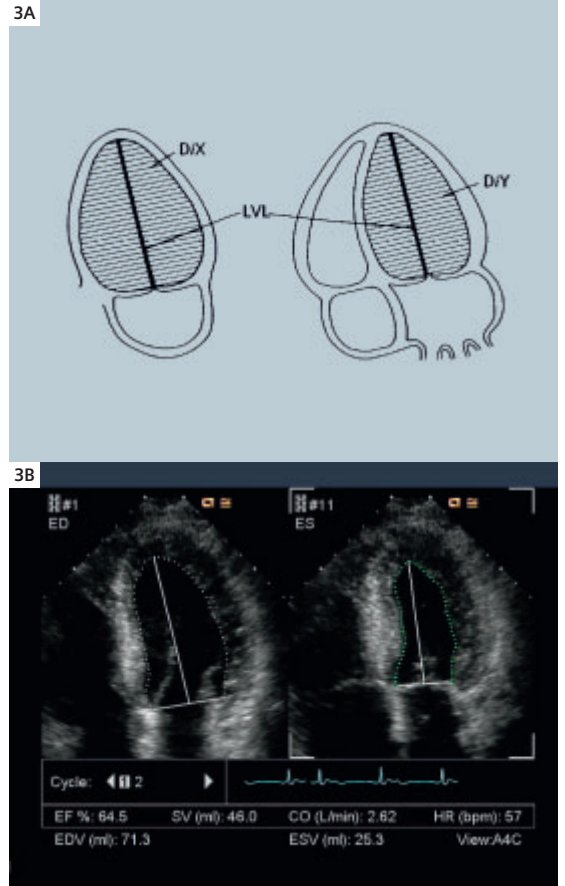
$$LVM \text{ (grams)} = 0.8 [1.05 [(LVID + IVST + PWT)^3 - (LVID)^3]]$$

(LVID = left ventricular internal dimension,
IVST = interventricular septum thickness,
and PWT = posterior wall thickness, 1.05 g/ml is the specific mass of myocardial tissue)

Due to the geometric assumptions in all of these techniques with regard to the left ventricular shape, the accuracy of LV EF assessment using 2D



2 The ellipsoid model is used to make geometric assumptions for the left ventricular function calculation according to the single-plane area-length method (D = diameter of LV, L = length of LV).



3 Illustration of the application of the biplane modified Simpson rule for LV function analysis to 2- and 4-chamber view images in echocardiography (A). Endocardial contours are needed to be drawn in end-diastole and end-systole to calculate volume data for both phases (B). (V = volume, LVL = length of LV, n = number of slices, DiX = diameter in plane X and slice i, DiY = diameter in plane Y and slice i).

echo is low, especially in patients with regional left ventricular wall motion abnormalities (Kuroda T et al., Echocardiography, 1994). Although 3D echocardiography shows much higher correlation to CMR it has not yet replaced 2D VF assessment in cardiology (Table 2, Krenning BJ et al. Cardiovasc. Ultrasound, 2003 and Qi X et al., Echocardiography, 2007). Cardiovascular magnetic resonance is the preferred technique for volume and ejection fraction estimation in heart failure patients, because of its 3D approach for non-symmetric ventricles and superior image quality (Bellenger NG et al., Eur Heart J, 2000) which leads also to less user dependency and higher reproducibility. Due to the difficulties in appropriate

Table 2: Volume and function measurement by 3D Echo reconstruction in comparison with CMR

Author/ref.	Object	N	r.	SE	Mean Diff. \pm SD
Gopal et al.	LV-EDV	15	0.92	7ml	
	LV-ESV	–	0.81	4ml	
Iwase et al.	LV-EDV	30	0.93	–	-17 \pm 23ml
	LV-ESV	–	0.96	–	-4 \pm 18ml
	LV-EF	–	0.85	–	-2 \pm 6%
Buck et al.	LV-EDV	23	0.97	14.7ml	-10.7 \pm 14.5ml
	LV-ESV	–	0.97	12.4ml	-3.4 \pm 12.9ml
	LV-EF	–	0.74	5.6%	-2.5 \pm 6.7%
Altmann et al.	LV-EDV	12	0.98	8.7ml	-14.2 \pm 8.3ml
	LV-ESV	–	0.98	5.6ml	-3.4 \pm 5.5ml
	LV-EF	–	0.85	5.3%	-4.4 \pm 5.3%
Nosir et al.	LV-EDV	46	0.98	–	-1.4 \pm 13.5ml
	LV-ESV	–	0.98	–	-1.5 \pm 10.5ml
	LV-EF	–	0.98	–	0.2 \pm 2.5%
Kim et al.	LV-EDV	18	–	–	6.4 \pm 20ml
	LV-ESV	–	–	–	0.0 \pm 13.3ml
	LV-EF	–	–	–	1.4 \pm 3.5%
Kim et al.	LV-EDV	10	–	–	-3.1 \pm 4.9ml
	LV-ESV	–	–	–	-1.4 \pm 2.2ml
	LV-EF	–	–	–	0.5 \pm 1.8%
Poutanen et al.	LV-EDV	0.80	–	–	4.0 \pm 19.6ml
	LV-ESV	0.88	–	–	0.4 \pm 13.0ml
	LV-EF	0.20	–	–	1.7 \pm 15.1%
Mannaerts et al.	LV-EDV	17	0.74	–	-13.5 \pm 13.5%
	LV-ESV	–	0.88	–	-17.7 \pm 23.9%
	LV-EF	–	0.89	–	-1.8 \pm 5.8%
Krenning et al.	LV-EDV	15	0.98	13.4ml	-22.7 \pm 13.6ml
	LV-ESV	–	0.99	8.7ml	-12.6 \pm 9.9ml
	LV-EF	–	0.97		

Table 2: Volume and function measurement by 3D Echo (reconstruction) in comparison with CMR.

(N = number of subjects; LV = left ventricle; r = correlation coefficient; SE = standard error or regression; Diff. = difference; SD = standard deviation; EDV = end-diastolic volume; ESV = end-systolic volume; EF = ejection fraction). [Mod. from: Krenning BJ, Voormolen MM, Roelandt JRTC. Assessment of left ventricular function by three-dimensional echocardiography. *Cardiovasc Ultrasound*. 2003;1:12].

Argus Function® allows for a comprehensive evaluation of right and left ventricular function.

visualization of the right ventricle in transthoracic echocardiography this holds true even more for the assessment of right ventricular function. MRI is considered also as the ideal method for the determination of LV mass for the same reasons, although transthoracic echo with second harmonic imaging and contrast echocardiographic techniques or 3D echo showed comparable accuracy (Bezante GP et al., Heart, 2005 & Mooney MG et al. Int J Card Imaging, 2000). However, most of the echocardiographic formulas overestimate LV mass, when compared to CMR (Scharhag et al. Z Kardiol, 2003).

CMR for quantification of ventricular function and mass

There are several ways for the acquisition of MR images for LV/RV function and mass assessment. TrueFISP (SSFP) sequences provide high spatial resolution and a high contrast between the dark myocardium and the bright blood-pool and therefore are preferred for this purpose: a stack of short-axis cine images (with a slice thickness of 8–12 mm) by which both ventricles can be covered without a gap in 1–2 breathholds. Preferably, retrospectively ECG-gated sequences should be used to cover the whole R-R interval. Nevertheless, prospectively gated sequences can also be used, without losing accuracy. In a 2-breathhold acquisition, usually 4–6 slices with a gap of 100% from slice to slice are acquired during the first breathhold. Ideally, the acquisition can be planned on 4-chamber and 2-chamber plane. The most basal slice should cover the mitral valve plane in diastole and the stack should be parallel to the mitral valve plane in both orientations. For the second acquisition, the complete stack is shifted with the “gap filling +/-” functionality towards the apex. Using this 2-breathhold approach, a high spatial and temporal resolution can be ensured. The use of integrated Parallel Imaging Techniques – iPAT (e.g. GRAPPA) – can help to accelerate the acquisition or to increase the resolution even further, so that a single breathhold approach can be applied routinely.

Tools for ventricular function and mass assessment

In cardiovascular MRI, Argus Function® has been used as a comprehensive tool for ventricular function and mass assessment by Siemens users for

many years with continuous improvements in the functionalities over time.

The workflow is simple: When loading the acquired images into Argus Function, the images get sorted vertically according to the slice position, from base to apex, and horizontally according to the point in the cardiac cycle from the beginning of the systole to the end-diastole (Fig. 4). After zooming in on the region-of-interest (LV/RV), the endocardial and epicardial contours of LV and RV can be drawn manually or rather semi- or fully automatically on the first image. The contours can be propagated horizontally and vertically to the rest of the images for a fast analysis. Contour changes, e.g. for in- or excluding papillary muscles, can be applied manually with various tools.

The resulting section provides the typical volumetric and functional data for LV and RV including parameters such as EDV, ESV, SV, CO and filling rates. The calculation is done using the modified Simpson’s rule. When both endo- and epicardial contours are drawn, ventricular mass and regional wall thickening can be calculated. Argus Function provides tabular and graphical, color-coded display of the results in parameter maps (e.g., in parameterized bull’s-eye plots with a sector based model) or graphs (e.g., volume-time curve). The customizable layout of the Movie Viewer allows for single movie display or a simultaneous display of up to 8 movies, which is helpful especially in the setting of dobutamine stress MRI. AVI files can be generated and exported easily. Contrast and brightness windowing of the images can be done at any time during the analysis.

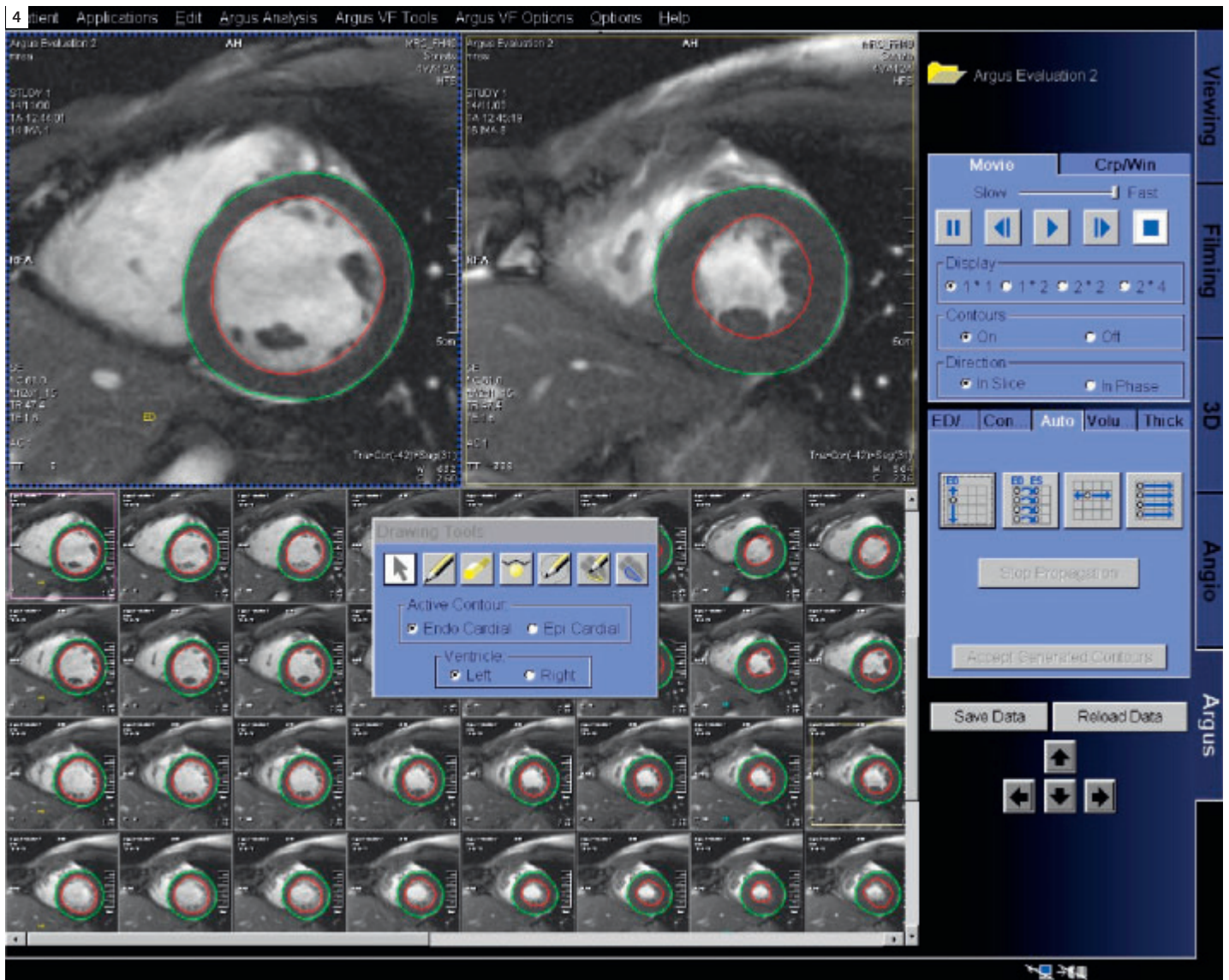
All results including the graphs and summary tables can be integrated in a DICOM structured report and stored to database. Data can be exported as ASCII files when needed.

New tools for LV function and mass assessment using CMR

Argus 4D VF®

In left ventricular analysis, the correct selection of the basal slice is of importance for highly accurate measurement of volume data. Siemens’ new tool for LV function analysis, Argus 4D VF, enables the user to identify the mitral valve insertion points in end-diastole and end-systole on long-axis planes and automatically adapts the basal border of the LV cavity in every single phase of the cardiac cycle. With Argus 4D VF there is neither missing ventric-

With the new Argus 4D VF, LV EF analysis can be performed in less than a minute.



4 User interface of Argus Function®. Contours are drawn initially on one or more slices and then propagated to other slices and phases automatically. Argus Function allows for volume, function and mass analysis for both LV and RV.

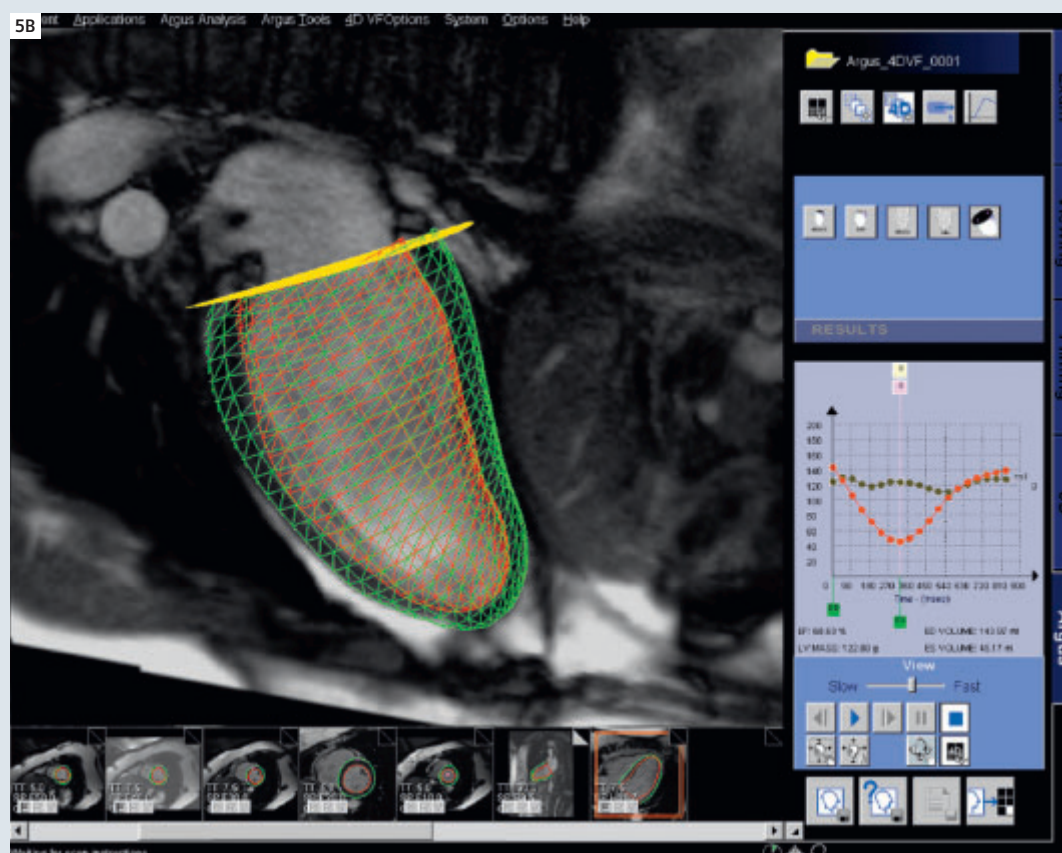
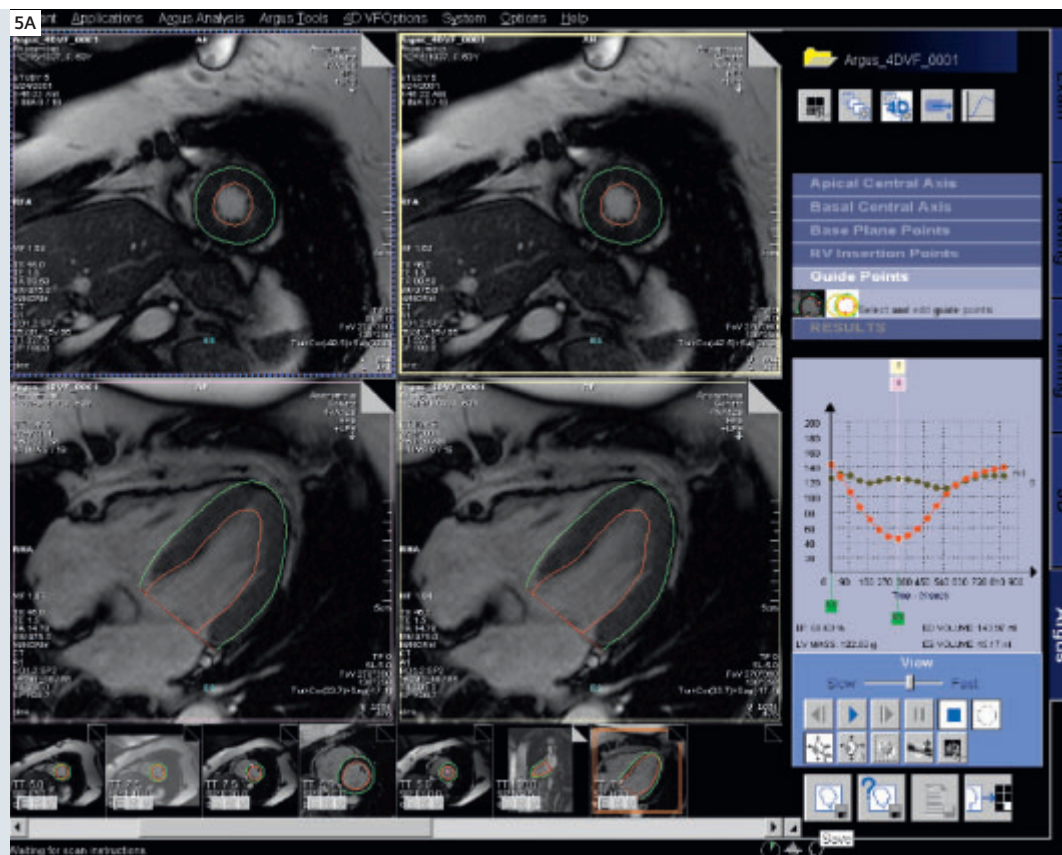
ular volume nor additional atrial volume deteriorating the accuracy of the LV volumetric analysis anymore.

Beyond providing higher accuracy, the tool's main advantage is its speed: Using Argus 4D VF, a typical LV function and mass analysis can be done in less than a minute. The reason for this is a new approach: Instead of contour tracing, a heart model-based algorithm enables the user to limit the input to a few mouse clicks with a guided workflow to identify the following anatomical landmarks:

- Center of the LV apex on a apical short-axis cine
- Center of the LV base on a basal short-axis cine
- Mitral valve insertion points on a 2- and/or 4-chamber plane in diastole and systole

The model-based algorithm provides within a few seconds the appropriate endo- and epicardial contours on all slices and phases as well as a summary table including various data for volume, function and mass. A volume-time curve and the key parameters are also integrated into the main window which allows to see parameter changes immediately

5 The user interface of the new Argus 4DVF[®]. After loading short- and long-axis images, a guided workflow ensures a fast calculation of the contours by use of a heart-model based algorithm and the automatic assessment of LV function (A). Advanced volume rendering options are available for a time-resolved (4D) visualization (B).

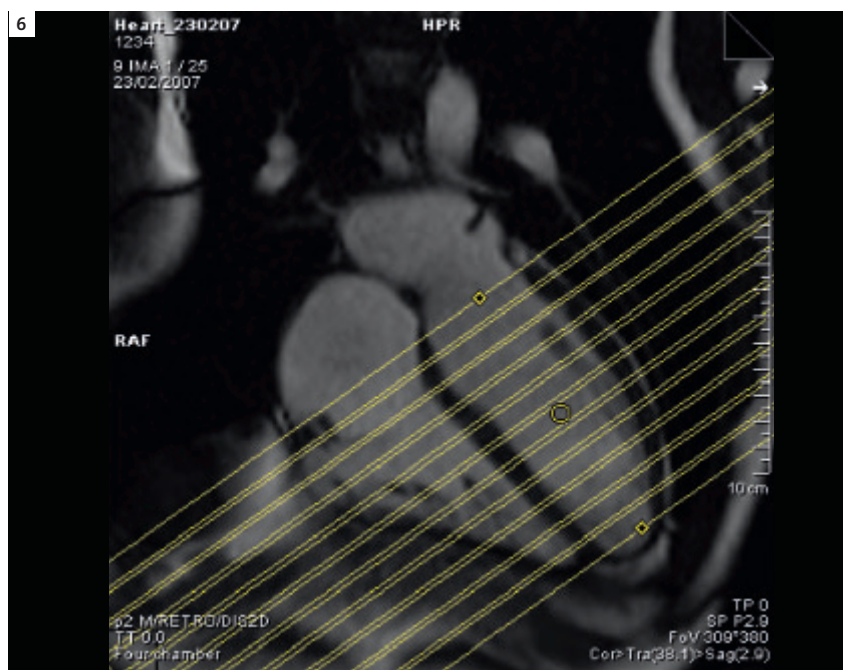


when changes are done on contours (e.g. for papillary muscle inclusion/exclusion, Fig. 5A). A comprehensive visualisation task-card provides various 4D volume visualization options (solid/mesh, endocardium only/epicardium only etc.) with or without spatial integration of the respective 2D cine MR images (Fig. 5B).

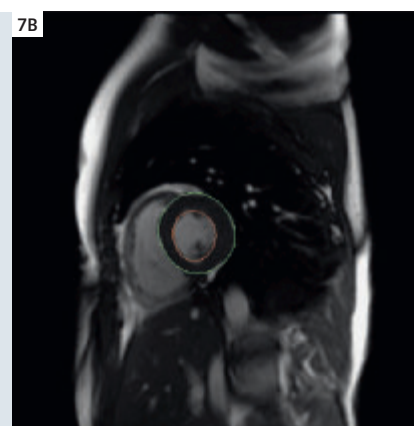
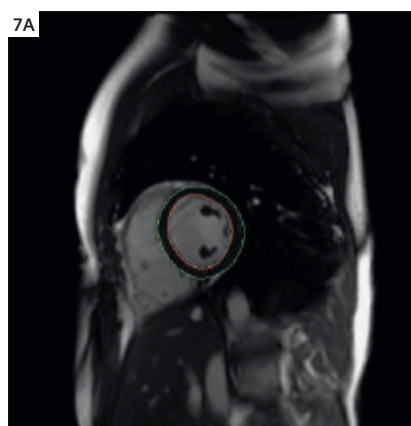
Inline VF®

Especially in a high-throughput setting, instead of the necessity of using post-processing tools, one might expect to have the most relevant data available right after a scan – without any user interaction. With another tool, Inline VF, Siemens introduced the first fully automatic LV function assessment tool implemented on the MR acquisition workplace. Inline VF is integrated directly into the acquisition sequence (Fig. 6), enabling the calculation of functional data already during image acquisition. The heart is localized on the short-axis CMR images automatically with the support of a motion compensation algorithm; endo- and epicardial contours are detected and shown on the inline display with no user interaction (Fig. 7A, B). Subsequently the parameters of LV function are generated and shown on the display without additional mouse clicks (Fig. 7C). The images can be loaded and modified in Argus Function, when needed. Inline VF is embedded in *syngo* BEAT, thus can be used with each triggered 2D cine sequence (GRE or TrueFISP contrast, segmented or real-time acquisition, cartesian or radial sampling scheme).

CMR is the gold standard for functional cardiac diagnostics; the new tools further lead to an efficient workflow and will help to increase the utilization of CMR in clinical routine.



6 Planning of short-axis slices on a 4-chamber view using Inline VF®. The most basal slice is positioned on the mitral valve plane in end-diastole. An automatic algorithm moves the most basal slice for calculation purposes in end-systole to the next slide when necessary, to avoid left atrial volume affecting the volumetric analysis.



7 Inline VF® automatically locates the heart and detects endo- and epicardial contours in all cardiac slices and phases (A, B). Parameters of left ventricular function (e.g., EDV, ESV, EF, SV etc.) are shown on the inline display right after scan (C).

Contact

Okan Ekinci, M.D.
Global Segment Manager
Cardiovascular MRI
Siemens Medical Solutions
Karl-Schall-Str. 6
91052 Erlangen
Germany
Phone: +49 9131/84-4391
okan.ekinci@siemens.com

CMR Delayed Enhancement Imaging in Coronary Artery Disease

Igor Klem, M.D.

Duke Cardiovascular Magnetic Resonance Center, Duke University Medical Center, Durham, USA

Delayed Enhancement MRI – from bench to bedside

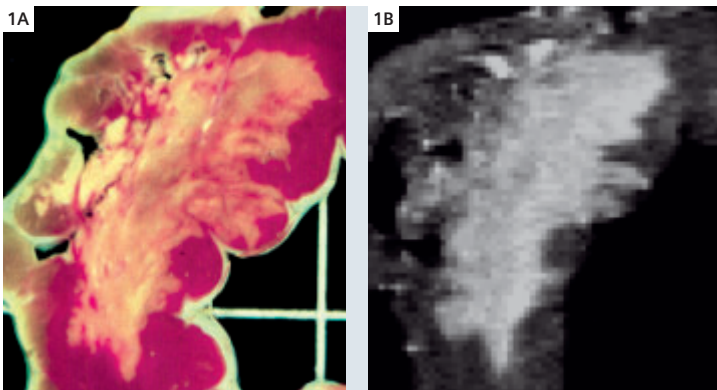
Imaging myocardial injury using T1-weighted pulse sequences after the administration of intravenous gadolinium contrast media has been performed since the mid 1980's. A major advance of this technique was achieved with the development of a pulse sequence (segmented inversion-recovery turbo-FLASH) which allowed an increase in signal difference between "normal" and "hyper-enhanced" tissue 10-fold compared to older pulse sequences. This technique, named **delayed contrast-enhanced MRI** (DE-MRI) was introduced in the late 1990's and may be considered already the gold-standard for the detection of irreversibly damaged myocardium. This development of DE-MRI and its subsequently emerging clinical applications parallels the steadily increasing importance of cardiovascular magnetic resonance in routine clinical patient care.

What is hyperenhanced or "bright" myocardium?

The underlying concept is that infarcted tissue accumulates gadolinium and can be visualized as hyperenhanced or "bright" regions on T1-weighted

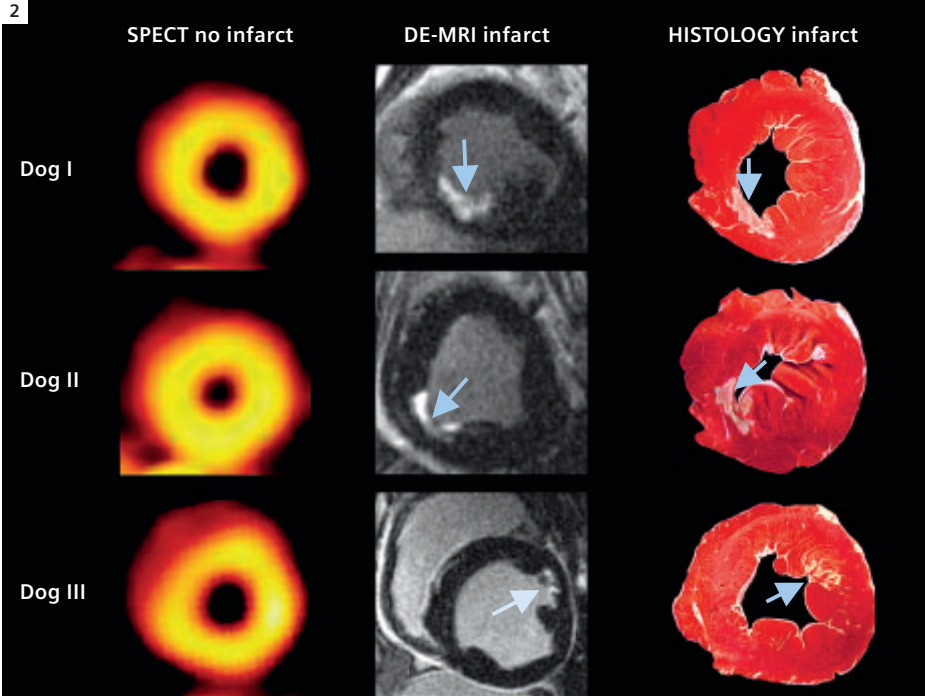
images acquired at least 10 minutes after gadolinium injection. How can we understand that a "non-specific" contrast agent can distinguish between viable and nonviable myocardium, especially across the wide range of tissue environments that occur during infarct healing? One should conceptually not think of DE-MRI as a tissue- or necrosis-specific staining technique or a ligand binding to specific receptors. Gadolinium is an inert extracellular contrast agent and the amount of contrast agent in a given tissue distribution volume determines the image signal intensity – the more contrast per distribution volume the higher the signal. An important physiological fact to remember is that the tissue volume in normal myocardium is predominately intracellular (~ 75% of the water space). Because extracellular contrast media is excluded from this space by the intact sarcolemmal membrane, the volume of distribution of a contrast medium in normal myocardium is quite small (~ 25% of water space), and one can consider viable myocytes as actively excluding contrast media. The unifying mechanism for the hyperenhancement effect of nonviable myocardium may then be the absence of viable myocytes rather than any inherent properties that are specific for acutely

Infarcted myocardium accumulates gadolinium and can be visualized as hyperenhanced or "bright" regions on T1-weighted images.



1 Comparison of high-resolution ex-vivo DE-MRI images (right) with acute myocyte necrosis defined by histopathology (left). Note that the size and shape of the infarcted region (yellowish-white region) defined histologically by staining is nearly exactly matched by the size and shape of the hyper-enhanced (bright) region on DE-MRI.

(Adapted from Kim RJ, Fieno DS, Parrish TB, et al. Relationship of MRI delayed contrast enhancement to irreversible injury, infarct age, and contractile function. *Circulation* 1999; 100: 1996; with permission).



2 Short axis views from three animals with subendocardial infarcts. DE-MRI detected even small infarcts (arrowheads) which were missed by SPECT. (Adapted from Wagner A, Mahrholdt H, Holly TA, et al. Contrast-enhanced MRI and routine single photon emission computed tomography (SPECT) perfusion imaging for detection of sub-endocardial myocardial infarcts: an imaging study. *Lancet* 2003; 361: 376; with permission.)

necrotic tissue, collagenous scar, or other forms of nonviable tissue.

In animal models of ischemic injury directly comparing DE-MRI to histopathology a nearly exact agreement between the size and shape of infarcted myocardium by DE-MRI to that by histopathology was demonstrated (Figure 1). It has been shown that DE-MRI can delineate between reversible and irreversible myocardial injury independent of wall motion, infarct age, or reperfusion status. Human studies demonstrate that DE-MRI is effective in identifying the presence, location, and extent of MI in both the acute and chronic settings. Additionally, DE-MRI provides scar size measurements that are closely correlated with positron emission tomography (PET) in patients with ischemic cardiomyopathy, and provides results superior to single-photon emission computed tomography (SPECT) in patients with subendocardial infarctions.

Advantages of DE-MRI over other viability techniques

A DE-MRI scan for assessment of viability is quite simple (see section on protocol), can be performed in a single exam of less than 30 minutes duration and does not require pharmacological or physical stress. Additionally, DE-MRI is rarely performed in isolation, rather it is one component in a more comprehensive study that is tailored to the specific

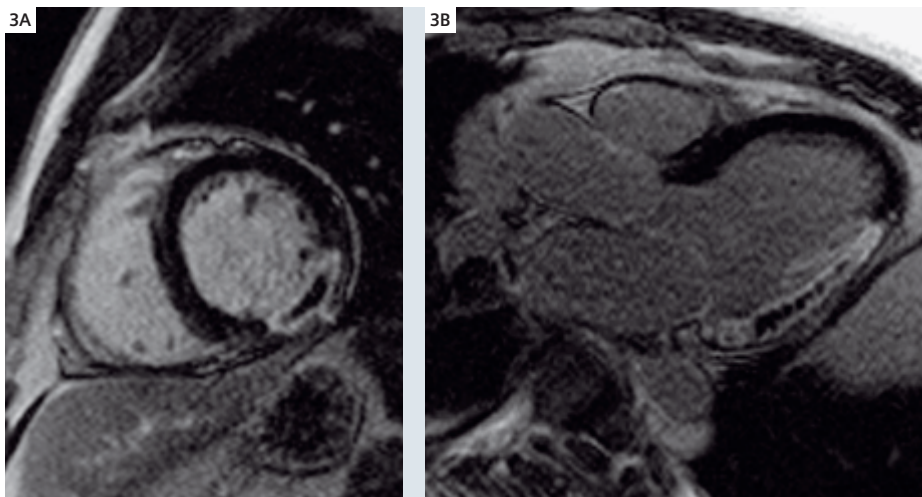
patient. It may be combined with a stress component for ischemia assessment, cine images for functional assessment, flow velocity mapping for evaluation of valvular disease, or a vascular study to assess aortic pathology to mention just a few of the possible combinations.

A major advantage of DE-MRI is the high spatial resolution. With a standard implementation, a group of 10 hyperenhanced pixels (voxel, 1.9 x 1.4 x 6 mm) in a typical image would represent an infarction of 0.16 grams, or a region one thousandth of the LV myocardial mass. This level of resolution, more than 40-fold greater than SPECT, allows visualization of even microinfarcts that cannot be detected by other imaging techniques (Figure 2).

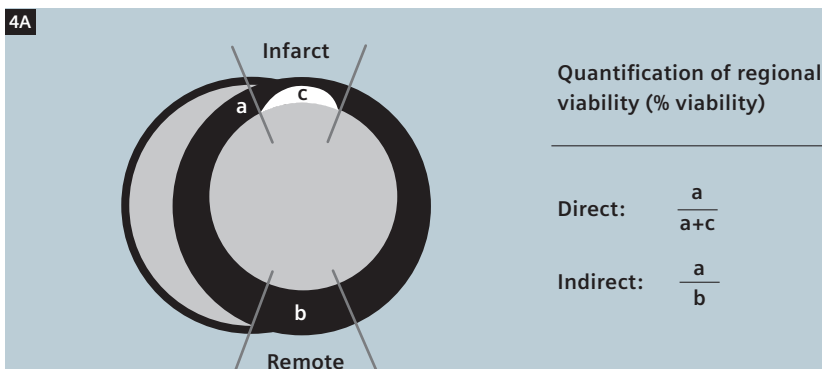
Further, DE-MRI is different from radionuclide imaging in that it provides direct visualization of both non-viable and viable myocardium. For instance, rather than simply identifying a region of acute infarction as non-viable due to reduced tracer activity, DE-MRI can distinguish between acute infarcts with necrotic myocytes and acute infarcts with necrotic myocytes and damaged microvasculature. The latter, termed the "no-reflow phenomenon", indicates compromised tissue perfusion despite restoration of epicardial artery patency. DE-MRI performed 5–10 minutes after contrast provides high image quality and delineates regions with more

DE-MRI can delineate between reversible and irreversible myocardial injury independent of wall motion, infarct age, or reperfusion status.

The voxel resolution of CMR is 40-fold greater than SPECT, allowing visualization of microinfarcts that cannot be detected by other imaging techniques.

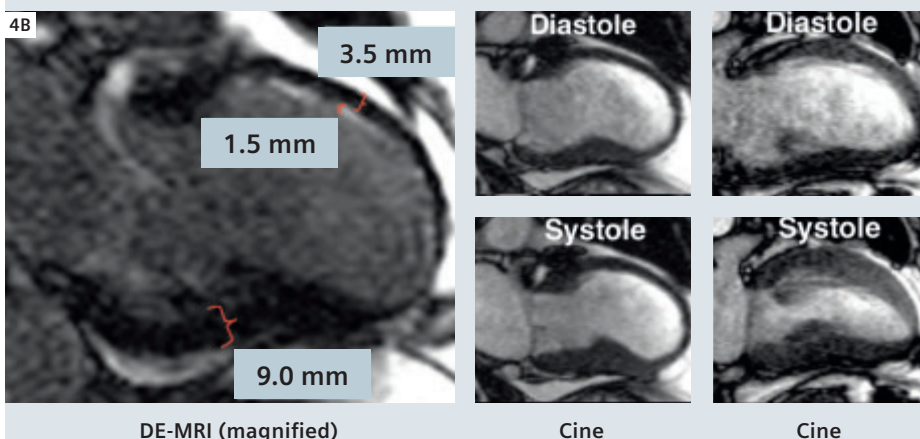


3 Short axis and long axis images from a patient with acute myocardial infarction. Note that the transmural infarct is composed of a bright area with a central black core corresponding to an area of no-reflow.



4 (4A) Illustration of the differences between a direct and indirect method of quantifying regional viability. Viable myocardium is displayed in black and infarcted myocardium displayed in white.

(4B) Long axis MR images of a patient before and two months after revascularization. Although the akinetic anterior wall is “thinned” (diastolic wall thickness = 5 mm; remote zone = 9 mm), DE-MRI demonstrates that there is only a subendocardial infarction (1.5 mm thick). A direct assessment of viability would show that the anterior wall is predominantly viable (3.5 mm / 5 mm = 70% viable), whereas the indirect method would show that the anterior wall is predominantly nonviable (3.5 mm / 9 mm = 39% viable).



Cine MR images obtained following coronary revascularization demonstrate full recovery of wall motion and diastolic wall thickness. Full motion movies can be viewed at <http://dcmrc.duhs.duke.edu/NF10>. (Modified from Heart 2004; 90: 137–140 with permission.)

profound microvascular damage (Figure 3). The ability to simultaneously visualize non-viable and viable myocardium provides additional advantages. For example, DE-MRI can accurately assess ventricular remodeling following acute MI at an early time point before measurements of ventricular volumes, internal dimensions, and ventricular

mass have changed. This is possible since DE-MRI can assess serially, concurrent directionally opposite changes such as resorption of infarcted tissue and hypertrophy of viable myocardium. When only viable myocardium can be visualized, the “percentage of viability” in a given segment is assessed indirectly and generally refers to the

amount of viability in the segment normalized to the segment with the maximum amount of viability. Conversely, when both viable and infarcted myocardium can be visualized, the “percentage of viability” can be assessed directly and expressed as the amount of viability in the segment normalized to the amount of viability plus infarction in the same segment (Figure 4A). These differences in the way in which viability is measured can alter clinical interpretation. Figure 4B demonstrates MR images in a patient with chronic coronary disease and an akinetic anterior wall. Although the anterior wall is thinned, only a small subendocardial portion of the anterior wall is infarcted. In this case, the indirect method would show that the anterior wall is only 39% viable (compared to the remote region), whereas the direct method would show that the anterior wall is 70% viable. The indirect method would predict no recovery of wall motion after revascularization whereas the direct method would predict recovery. The post-revascularization images (bottom-right panel) demonstrate in this patient the direct method was correct.

Clinical applications of DE-MRI

Prediction of functional recovery in ischemic disease

As the patient example in Figure 4 shows, one clinical application of DE-MRI is to identify patients with potentially reversible ventricular dysfunction from those with irreversible dysfunction. With the ability of DE-MRI to directly visualize the transmural extent of infarction (and viability) functional improvement after revascularization can be predicted in both acute and ischemic disease.

In the context of acute myocardial infarction, prompt revascularization therapy has been shown to result in salvage of ischemic but viable myocardium, improvement in ejection fraction (EF), and long-term improvement in survival. In the immediate post-infarction setting, even after successful reperfusion, myocardial dysfunction may persist, and it is difficult to distinguish whether it is due to myocardial necrosis or to myocardial stunning. Differentiation between these two conditions is important because patients with a large area with dysfunction but only little necrosis (i.e. predominantly stunned) would be expected to have marked functional and clinical improvement. In contrast, patients with a dysfunctional region that is predominantly necrotic would not be expected to

have much functional improvement. Studies in patients with acute myocardial infarction and successful revascularization showed that transmural extent of infarction was highly predictive of improvement in wall motion and global function (see recommended reading for details). The transmural extent of infarction determined by DE-MRI has also been shown to predict response to myocardial revascularization in patients with chronic ischemic heart disease. Similar to findings in the acute setting, likelihood of functional improvement was inversely related in a progressive stepwise fashion to transmural extent of infarction. Several studies have demonstrated that there is a progressive relationship between the likelihood of contractile response to revascularization and the transmural extent of infarction as evidenced by DE-MRI.

DE-MRI for heart-failure assessment

We have discussed thus far the ability of DE-MRI to predict the likelihood and magnitude of functional improvement after revascularization in both acute and chronic ischemic disease. There is however a significant proportion of patients, in whom myocardial dysfunction and heart failure (ischemic cardiomyopathy) persists even after revascularization, or in whom revascularization is not possible due to a variety of reasons (e.g. associated comorbidities, poor distal targets, or diffuse atherosclerotic disease). In addition, a significant proportion of patients have dysfunction in the absence of CAD (nonischemic cardiomyopathy). The utility of DE-MRI for diagnostic assessment of heart failure patients is manyfold. We will discuss here some established and emerging applications:

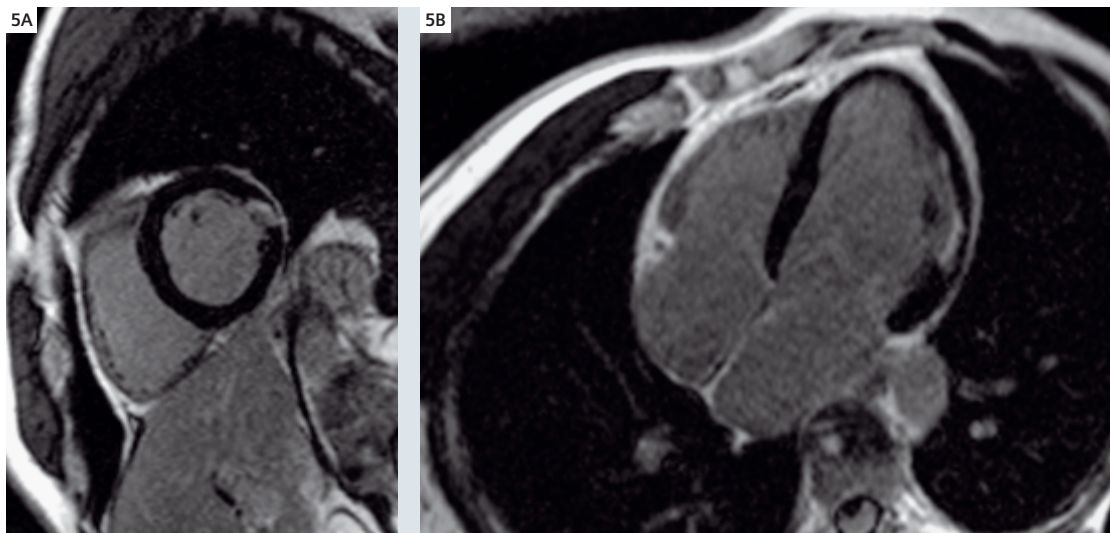
1. The ability of DE-MRI to provide in-vivo images corresponding to ex-vivo pathological sections allows the determination of underlying pathology of cardiomyopathies. This application is based on the concept that both presence and pattern of scar can be used to discriminate between myopathic processes. The typical pattern of hyperenhancement that occurs in patients with myocardial infarction and thus with ischemic cardiomyopathy can be explained by the pathophysiology of myocardial ischemia. Following approximately fifteen minutes of coronary occlusion, a wavefront of myocardial necrosis begins in the subendocardium and progresses transmurally with increasing duration of occlusion. Therefore, hyperenhancement can

DE-MRI allows visualization of the transmural extent of myocardial infarction.

The transmural extent of infarction determined by DE-MRI predicts the response to myocardial revascularization in patients with chronic ischemic heart disease.

The distribution pattern of DE allows the determination of underlying pathology of cardiomyopathies.

2D/3D & PSIR TurboFLASH/TrueFISP IR sequences are provided for delayed enhancement imaging in the Advanced Cardiac Package.



5 Typical DE-MRI images (5A: short-axis and 5B: 4-chamber view) of a patient with coronary artery disease and previous myocardial infarct in the lateral wall. The hyperenhancement of CAD pattern typically involves the subendocardium extending towards the subepicardium. The transmural extent of infarction is well visualized.

Different delayed enhancement patterns can be seen in non-ischemic cardiomyopathies such as HCM, cardiac amyloidosis, cardiac sarcoid or myocarditis.

For CMR stress studies, cine and perfusion studies at rest and stress are combined with DE to identify scar tissue.

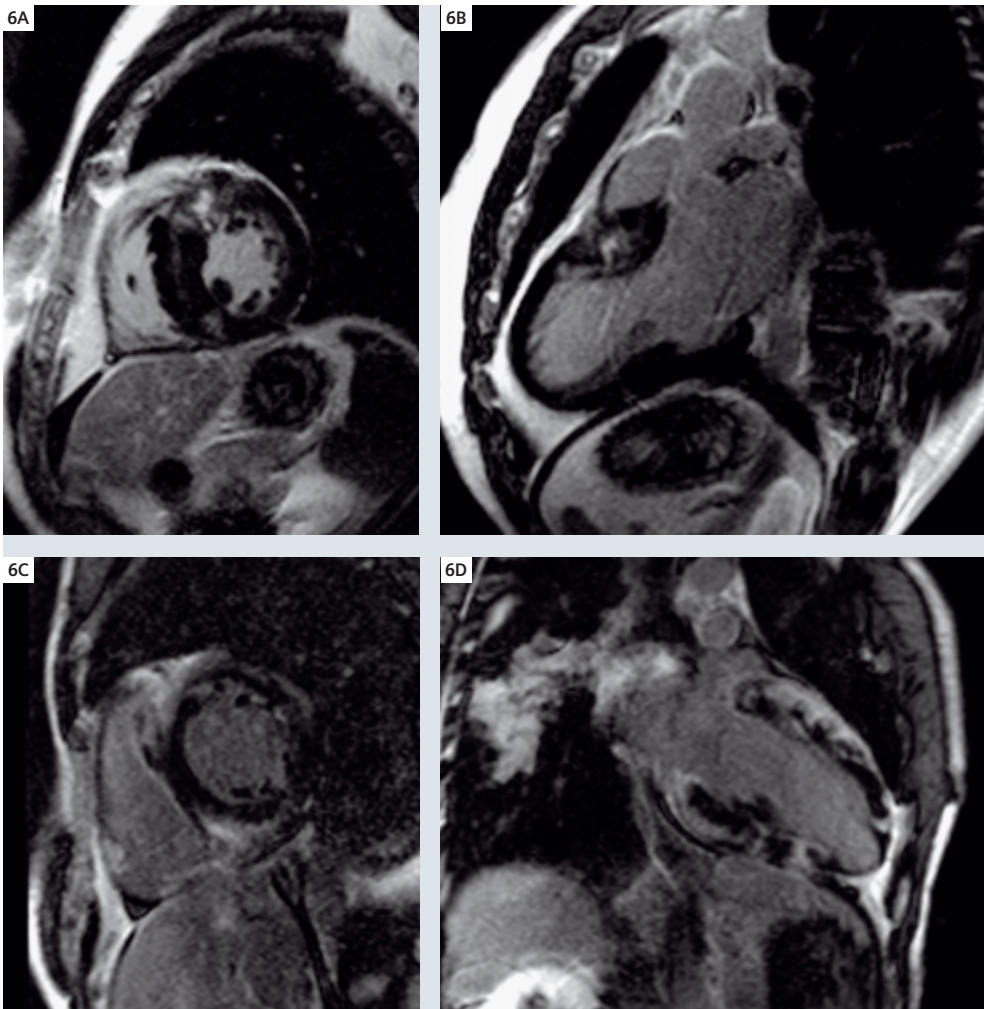
be classified as “ischemic” type or “non-ischemic” type, the former involving the subendocardium (i.e. subendocardial or transmural) and be located in a region that is consistent with the perfusion territory of an epicardial coronary artery (Figure 5). Hyperenhancement pattern has been shown to provide diagnostic utility for distinguishing between ischemic and non-ischemic cardiomyopathies. While classification of cardiomyopathies as ischemic or non-ischemic is an important means of dichotomizing patients with systolic dysfunction, prior studies have found that disease-specific differences in etiology of myocardial dysfunction alter prognosis and therapy. Among patients with non-ischemic cardiomyopathies, therapeutic options include corticosteroids for treatment of cardiac sarcoid or myocarditis, alkylators in the setting of cardiac amyloid, α -galactosidase enzyme replacement therapy in the setting of Anderson-Fabry’s disease, and septal ablation or myomectomy in the setting of hypertrophic cardiomyopathy. DE-MRI evidenced hyperenhancement can occur in all of these conditions, having been reported in inflammatory conditions such as myocarditis, infiltrative cardiomyopathies such as sarcoid, systemic processes such as amyloid or Chagas disease, and genetic abnormalities such as hypertrophic cardiomyopathy or Anderson-Fabry’s disease. Each of these conditions results in myocardial dysfunction as a result of diverse pathological processes and is associated with differences in hyperenhancement patterns (Figure 6).

2. In patients with congestive heart failure, several studies have shown that medical therapy using

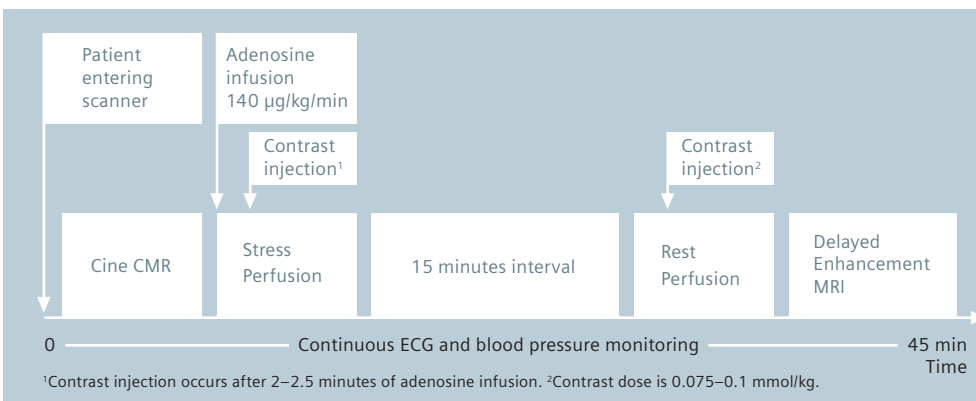
beta-blockers can result in improvement in LV function, heart failure symptoms, and long-term survival. A significant heterogeneity exists, however, in the response to beta-blockers among individual patients. It has been shown that patients with the most advanced disease have less capacity to respond to beta-blockers, because less viable myocardium exists. Similar to the situation in patients undergoing coronary revascularization, an inverse relationship was found between the transmural extent of infarction and the likelihood of improvement in regional contractility and LVEF after beta-blocker therapy. Furthermore, this parameter from DE-MRI was directly related to the magnitude of reverse remodeling (i.e. a decrease in LV enddiastolic volume index and LV end-systolic volume index).

DE-MRI as part of a multi-component stress test

MRI stress testing is being increasingly performed in clinical practice for evaluation of patients with ischemic heart disease. There are two techniques available, dobutamine cine CMR, analogous to dobutamine stress echocardiography, and vasodilator (adenosine) stress perfusion. The latter appears to be more practical and faster in the clinical scenario. In addition to providing information on stress perfusion, which could be obtained in approx. 5 minutes scan time, CMR can provide a very comprehensive evaluation if stress perfusion is combined with other CMR components. In our experience, the optimum combination is stress/rest perfusion CMR with delayed enhancement CMR (Figure 7). While the former detects perfusion



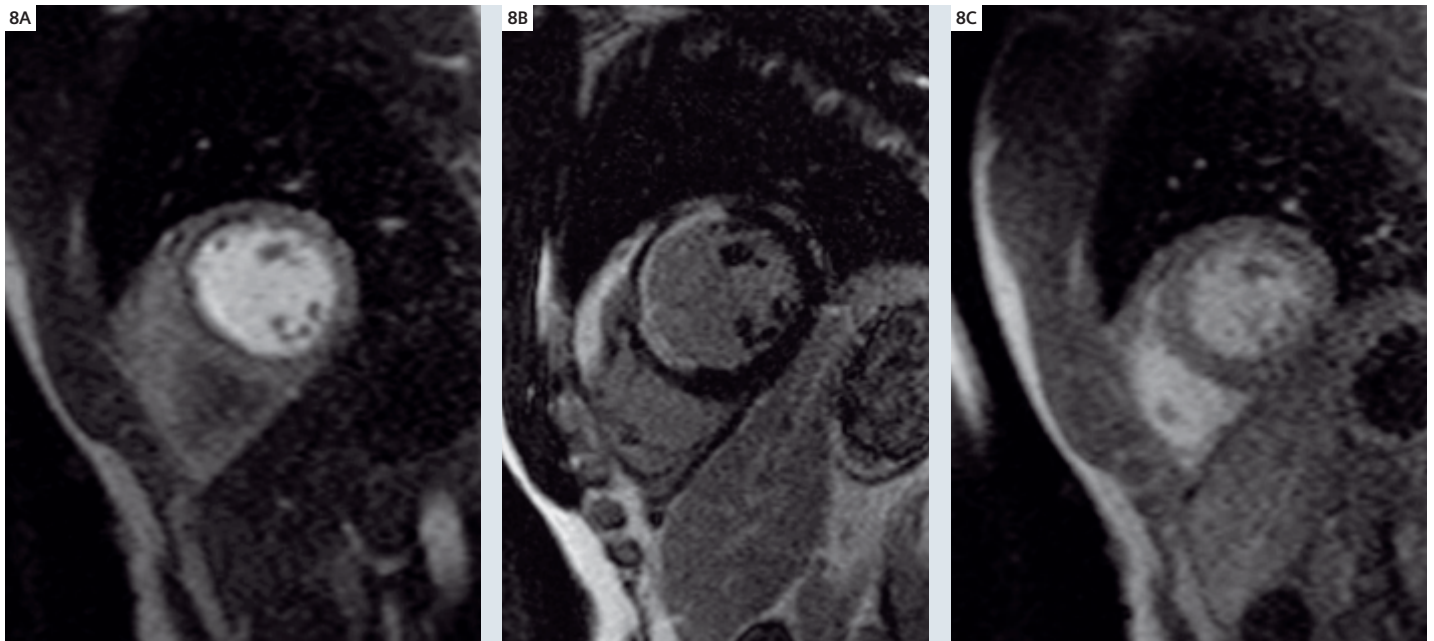
6 Examples of patient images with non-CAD type of hyperenhancement. Patient 1 is a 32-year-old male with hypertrophic cardiomyopathy. DE-MRI revealed extensive scarring at the right ventricular insertion sites into the septum (**A, B**). Patient 2 is a 28-year-old male with pulmonary sarcoidosis, an MRI scan performed for further evaluation of ventricular tachycardia revealed extensive cardiac involvement (**C, D**).



7 Flow-diagram of a multi-component CMR stress perfusion study. Note that DE-MRI is performed after two injections of gadolinium contrast ($2 \times 0.07\text{--}0.1$ mmol/kg) for stress and rest perfusion, which provides sufficient contrast for delayed enhancement imaging without additional contrast injections.

defects, DE-CMR provides further information regarding the cause of those defects. For example, perfusion defects that are matching in spatial extent to bright areas (scar) on DE-CMR are caused by infarcted myocardium (Figure 8). In contrast, a perfusion defect detected in dark (viable) myocardium by DE-CMR is consistent with inducible

ischemia. Occasionally, artifactual defects are observed on perfusion CMR which may impose difficulties in image interpretation. We found DE-CMR to be also useful to differentiate artifactual perfusion defects from true perfusion defects due to coronary artery disease. Artifactual defects occur in identical location, intensity and extent on serial



8 Patient example of a stress CMR study demonstrating complementary information of stress/rest perfusion and DE-MRI. Note that the subendocardial perfusion defect seen during stress (**A**) matches in spatial extent the scarred area on DE-MRI (**B**) indicating that there is infarct but no ischemic viable myocardium. Rest perfusion images (**C**) can be useful for differentiation of true perfusion defects from artifacts.

DE-MRI provides an important non-invasive tool for studying associations between scar characteristics and arrhythmic risk.

DE-MRI can be performed as a stand-alone procedure and takes less than 30 minutes.

image acquisitions if imaging parameters are kept unchanged. Therefore we acquire for every patient both stress and rest perfusion images and compare these to DE-CMR findings. The only physiological scenarios where myocardial perfusion is thus severely reduced to cause rest defects are a) resting ischemia and b) infarcts. In the former scenario, the patient would likely be symptomatic at rest, thus not a good candidate for stress testing. In the latter scenario, which is more common in clinical practice, we have an independent technique for infarct detection to confirm our perfusion findings: DE-CMR. Consequently, if matched defects are not confirmed to be infarcts on DE-CMR they can be identified as artifactual. We found that considering these physiologic principles when interpreting the multi-component CMR stress test can increase the accuracy significantly (see recommended reading for details).

DE-CMR for assessment of patients with arrhythmias

Myocardial scar forms a substrate for ventricular tachyarrhythmias, with a relationship between scar morphology and arrhythmic risk demonstrated in both experimental and epidemiologic studies. Data from animal studies indicates that both scar

size and scar morphology influence arrhythmic risk. DE-MRI evidenced hyperenhancement provides highly accurate assessment of both scar size and morphology, with improved scar detection in comparison to other modalities such as myocardial scintigraphy (SPECT). Thus, DE-MRI provides an important non-invasive tool for studying associations between scar characteristics and arrhythmic risk. Interesting insights into the relationship between hyperenhancement and arrhythmogenic potential has been provided in several investigations and has started to transition into clinical trials to investigate the potential of this technique for prediction of clinical SCD risk.

DE-MRI imaging protocol – as simple as it is

A DE-MRI scan can be performed in a single brief examination which requires only a peripheral intravenous catheter which is placed before the patient enters the MRI scanner, and does not require pharmacologic or physiologic stress. After obtaining scout images to delineate the short and long axis views of the heart, cine images are acquired to provide a matched assessment of left ventricular (LV) morphology and contractile function with the viability characterization from DE-MRI. Short-axis views (e.g. 6 mm slice thickness with 4 mm gap to

match contrast-enhancement images) are taken every 10 mm from mitral valve insertion to LV apex along with two to three long-axis views in order to encompass the entire LV. The patient is then given a bolus of 0.10–0.20 mmol/kg intravenous gadolinium by hand or power injection. After a 10–15 minute delay to allow the contrast media to distribute, high spatial resolution delayed enhancement images of the heart are obtained at the same slice locations as the cine images, using a 2D segmented inversion recovery fast gradient-echo (seg IR-GRE, e.g. 2D IR TurboFLASH) pulse sequence. For patients who are acutely ill and unable to perform breath-holds an alternative is offered by using a subsecond “snapshot” imaging technique. This single-shot, inversion-recovery, steady state free-precession sequence can be used in analogy to the segmented gradient echo sequence. Parallel Acquisition Techniques (iPAT) are used to speed up imaging. This technique has been shown to be highly accurate with only mildly reduced sensitivity and possible underestimation of the transmural extent of infarction. Another option is a 3D sequence during free breathing using the navigator technique to account for breathing motion.

The pulse sequence parameters are set up similar to any other cardiac MRI sequence, the only specific parameter to DE-MRI is the inversion time (TI). This is the time required from the inversion prepulse (which provides T1-weighting) to the center of the read-out portion of the sequence and should be set to “null” signal from normal myocardium. What that means is that the signal from myocardium is minimized i.e. black, thereby the infarct which has different T1-characteristics than normal myocardium has the largest difference in signal and appears bright on the image. The correct TI has to be determined for each scan and depends on factors such as the contrast dose and timing of imaging after administration of contrast. Obtaining the correct TI can be accomplished with little training. For those starting with DE-MRI the cardiac pulse-sequence package includes tools to allow the beginner to identify the right TI time: the TI-Scout displays the identical scan location with an array of different TI-times, which allows the scanner operator to determine the correct TI (where myocardium appears black) for subsequent acquisitions using the IR-GRE sequence. Alternatively a phase-sensitive IR-GRE (e.g. PSIR) sequence can be used

which can be used over a broad range of TI-time, thus making it unnecessary to optimize the TI. In general, most delayed enhancement images are acquired during an 8–10 s breath-hold, single shot phase-sensitive IR-GRE (PSIR) images in even less than 4 seconds. The imaging time for the entire examination is under 30 minutes. Figures 3, 5 and 6 demonstrate DE-MRI images from typical patient scans.

Summary

Delayed enhancement MRI provides clinically important information in a wide range of cardiac pathologies, in those frequently encountered in cardiology practice such as coronary artery disease and heart failure as well as less common problems such as in patients with cardiomyopathies or ventricular arrhythmias. It provides in-vivo information to the clinician that used to be only available to the pathologist on macroscopic exploration. In our institution DE-MRI is part of every cardiac exam. DE-MRI is a very robust technique and can be performed easily on a standard MRI scanner equipped with a cardiac package.

Single-shot PSIR sequences can be used for accurate DE-MRI especially in patients with breath-holding difficulties or arrhythmia.

DE-MRI provides in-vivo information to the clinician that used to be only available to the pathologist on macroscopic exploration.

Contact

Igor Klem, M.D.
Duke Cardiovascular Magnetic Resonance Center
Duke University Medical Center 3934
Durham, NC 27710
USA
igorklem@duke.edu

Recommended Reading

- 1 Kim RJ, Shah DJ, Judd RM. How we perform delayed enhancement imaging. *JCMR* 2003;5:505–514.
- 2 Kim RJ, Fieno DS, Parrish TB, et al. Relationship of MRI delayed contrast enhancement to irreversible injury, infarct age, and contractile function. *Circulation* 1999;100:1992–2002.
- 3 Kim RJ, Wu E, Rafael A, et al. The use of contrast-enhanced magnetic resonance imaging to identify reversible myocardial dysfunction. *N Engl J Med* 2000;343:1445–53.
- 4 Wagner A, Mahrholdt H, Holly TA, et al. Contrast-enhanced MRI and routine single photon emission computed tomography (SPECT) perfusion imaging for detection of subendocardial myocardial infarcts: an imaging study. *Lancet* 2003;361:374–79.
- 5 Choi KM, Kim RJ, Gubernikoff G, et al. Transmural extent of acute myocardial infarction predicts long-term improvement in contractile function. *Circulation* 2001;104:1101–7.
- 6 Klem I, Heitner JF, Shah DJ, et al. Improved detection of coronary artery disease by stress perfusion cardiovascular magnetic resonance with the use of delayed enhancement infarction imaging. *J Am Coll Cardiol* 2006;47:1630–8.

Differentiation of Cardiomyopathies by use of CMR

Rory O'Hanlon, M.D.; Dudley J. Pennell, M.D., FCRP, FESC
CMR Unit, Royal Brompton Hospital, London, UK

Jeanette Schulz-Menger, M.D., FESC; Ralf Waßmuth, M.D.
Charité Campus Buch, Franz-Volhard-Klinik, Berlin, Germany

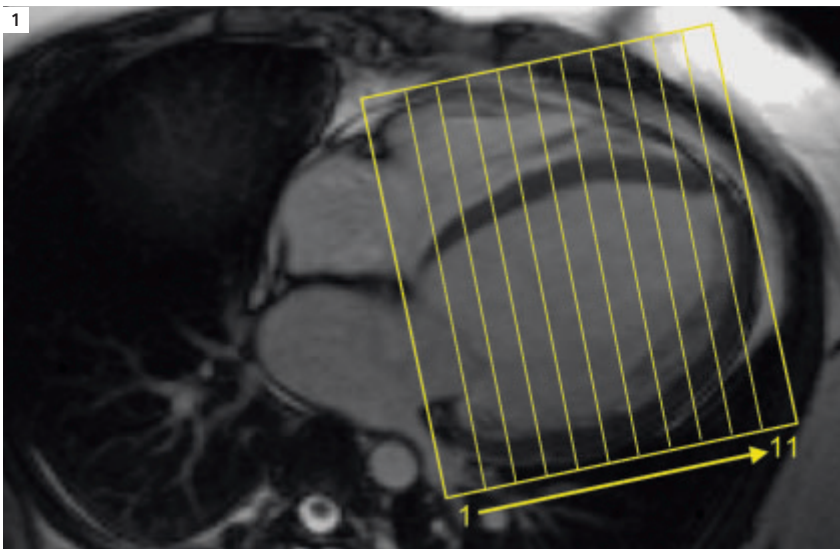
CMR can yield information on cardiac anatomy, function, tissue characterization, perfusion, and valvular flow in one single study.

Introduction

Primary cardiomyopathies (CMP) are diagnosed by exclusion of other cardiac diseases. Secondary or specific cardiomyopathies are defined as distinct myocardial diseases with specific origin as ischemic, hypertensive, inflammatory. The identification of the etiology for a non-ischemic cardiomyopathy is often difficult and suboptimal with conventional imaging and invasive testing. A "standard" investigative route is focused around a detailed history, ECG, transthoracic echocardiography, holter monitoring, exercise treadmill testing, and invasive angiography. These tests often produce a clear diagnosis, such as coronary artery disease, valvular heart disease, dilated cardiomy-

opathy, or hypertrophic cardiomyopathy. Nevertheless, establishing a diagnosis of cardiomyopathy can still be difficult and may be not possible to do with certainty. In recent years, advances in cardiovascular magnetic resonance (CMR) have brought this technology into routine clinical use. In a single 45–60 minute study, CMR can yield information on cardiac anatomy, function, tissue characterization, perfusion, and valvular flow. This technology not only helps to determine the etiology and presence for a cardiomyopathic process, but also provides a robust imaging tool to follow patients over time and provide prognostic information.

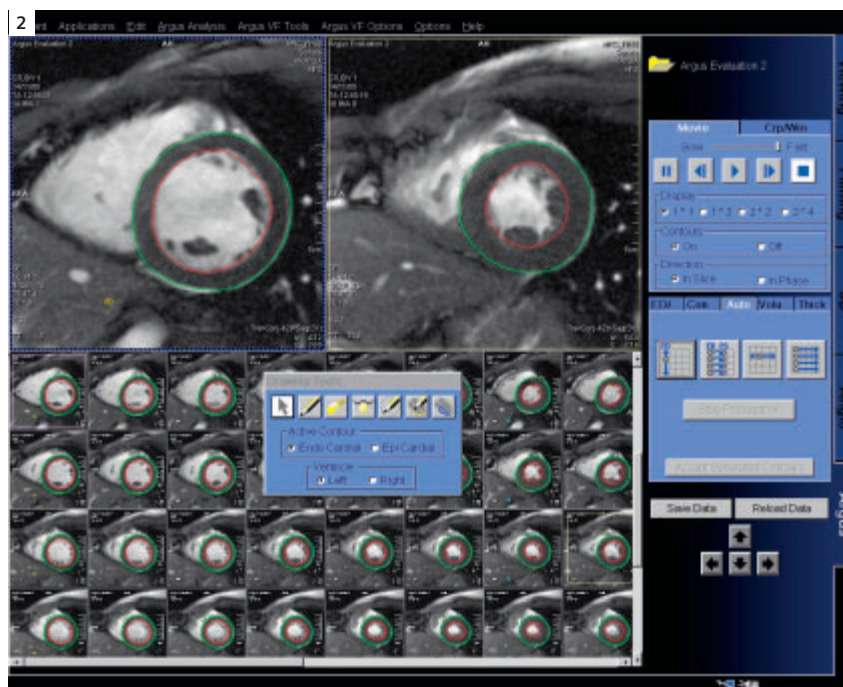
A number of CMR techniques are useful in the assessment of cardiomyopathy. Initially a detailed assessment of cardiac anatomy is performed using at least transaxial (and also usually coronal and sagittal) HASTE (Half-Fourier Acquisition Single-Shot Turbo Spin-Echo) imaging, which can be completed in approximately 3 minutes. This serves to identify at an early stage important shunts, anomalous pulmonary venous drainage, or congenital anomalies which may explain increased chamber dimensions suggestive of a cardiomyopathy. Alternatively, a multislice single-shot TrueFISP morphology sequence can be performed. TrueFISP cine imaging of long and short axis function is performed to assess overall myocardial function, followed by a stack of 8–12 short axis TrueFISP cines of the LV and RV from base to apex, which is regarded as the "gold standard" test for quantitative assessment of biventricular volumes and function (Fig. 1). Assessment of volumes and mass can be performed by manual planimetry of the epi- and endocardial border in diastole and the endocardial border in systole (Fig. 2). Alternatively, the analysis can be performed using semi-



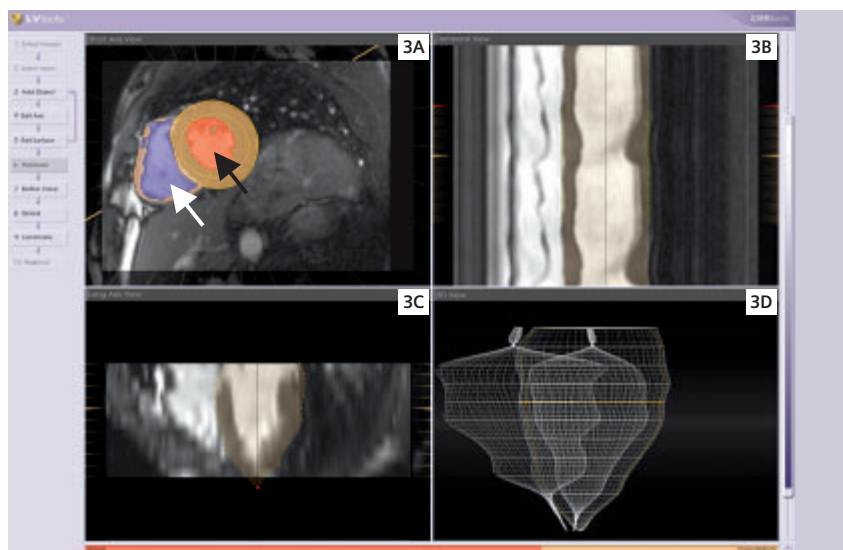
1 Method of acquisition of short axis stack of cine-images from base to apex. The first slice (1) is typically taken parallel to the annulus of the mitral and tricuspid valve. Serial slices 10 mm apart are acquired from base to apex (slice 11) usually with a slice thickness of 7 mm and 3 mm gaps, at our institution. Breath-hold is typically no longer than 8–10 seconds.

automated software (Fig. 3). A completely automatic VF analysis tool has recently been introduced by Siemens Medical Solutions (Inline VF). For patients with subtle reductions in function by echocardiography, CMR can establish ventricular dysfunction with greater confidence because of the availability of normal values which are corrected for age, sex and body surface area. CMR also provides a more suitable method for follow up of serial measurements given the superior interstudy reproducibility over other imaging modalities which are more routinely used, especially 2D echocardiography.

A number of other more specialized imaging sequences are also performed in a patient with suspected cardiomyopathy. T1 and T2-weighted turbo-spin echo (TSE) sequences are useful to assess the pericardium where the clinical question resolves around constrictive vs. restrictive cardiomyopathy. Short T1 Inversion Recovery (STIR) imaging with a triple inversion protocol, nulls signal from fat, is T2-weighted and is used to identify areas of increased myocardial water content, indicative of myocardial oedema and inflammation which are seen in conditions such as acute myocarditis and acute myocardial infarction. Myocardial T2*-weighted imaging is used to quantify myocardial iron. Imaging performed immediately (1–3 minutes) following intravenous gadolinium is a sensitive tool to detect intracardiac thrombi by providing the best delineation between the enhanced blood-pool and myocardium on one side and the dark thrombus on the other side. Further, late gadolinium enhancement (LGE) imaging using sequences such as inversion recovery TurboFLASH (IR GRE) or phase-sensitive inversion recovery (PSIR) sequences is then performed approximately 5–20 minutes after gadolinium administration (the delay between contrast administration and image acquisition depends on the concentration of gadolinium given, typically 0.1–0.2 mmol/kg body weight). The presence of LGE is indicative of abnormal myocardial interstitium such as myocardial fibrosis and infarction. In non-ischemic cardiomyopathy, there are several typical patterns of LGE which are very helpful in determining etiology and providing prognostic information. Please refer to the article of I. Klem (pg. 14) for details about typical LGE pattern caused by ischemic heart disease.



2 Contouring of epicardial and endocardial borders in diastole and systole to measure LV mass, volumes, and function. The volumes are calculated by summing the volume of the blood in each slice. The mass is determined from the volumes of myocardium in diastole multiplied by the myocardial density (1.05 g/cm³).



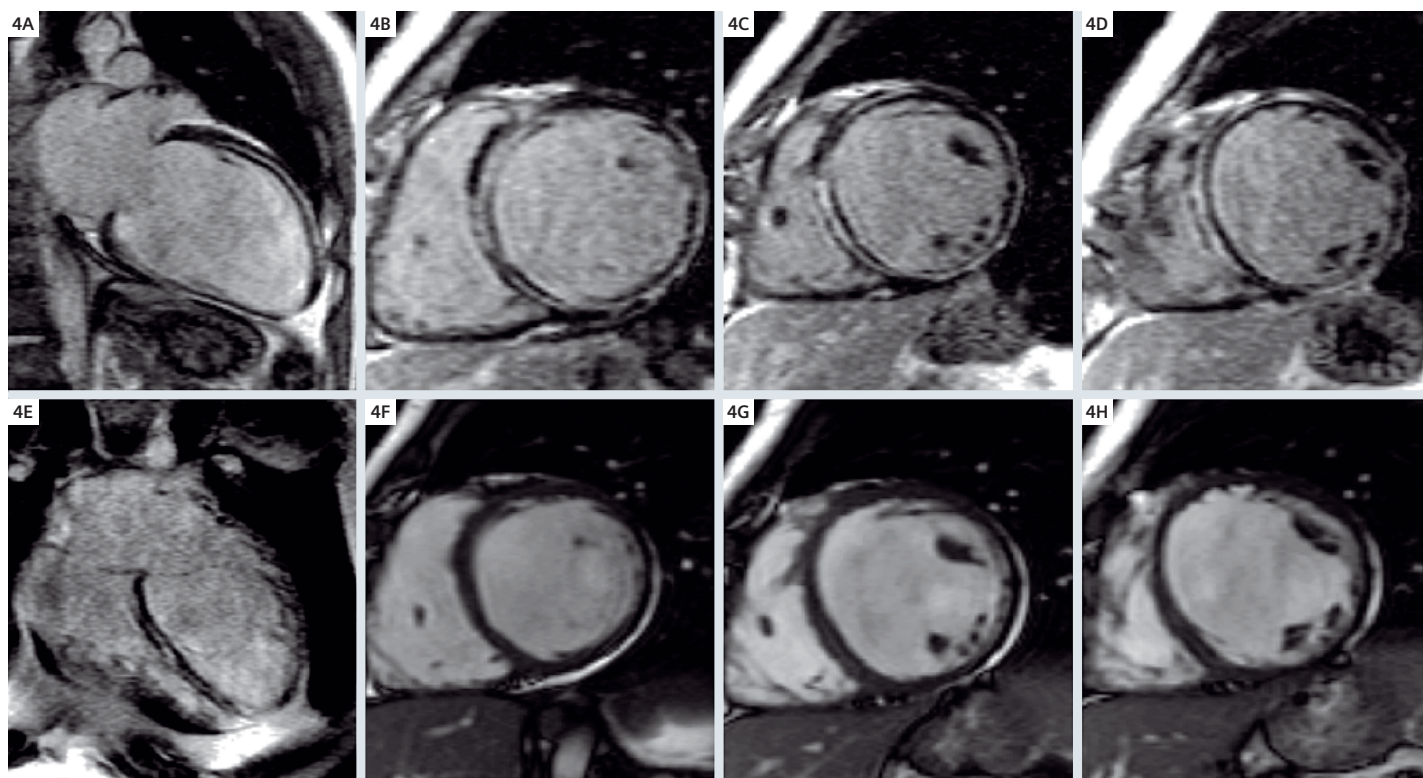
3 Semiautomated analysis of left and right ventricular mass, volume, and function. There are several software packages that can perform this assisted analysis and the one shown here is CMRtools® (Cardiovascular Imaging Solutions, London, UK; www.cmrtools.com). A 3-dimensional model of the epicardial and endocardial contours is generated, incorporating user-defined guide-points and shown in panel D. This model calculates the contours for all slices and is fully adjustable. The model is checked against a composite long axis image (panel C) and the time activity image (panel B) to ensure it is consistent through planes and time. Finally, thresholding of blood to account for papillary muscles is performed with an intensity based tool (LV blood orange with black arrow; RV blood blue with white arrow). The atrial contribution to volumes is excluded in diastole and systole by defining the mitral and tricuspid valve annuli from the long-axis cines.

Dilated Cardiomyopathy

CMR is superior to nuclear scintigraphic techniques to distinguish non-ischemic from ischemic etiologies of cardiomyopathy.

We use the term dilated cardiomyopathy to refer to patients with systolic dysfunction, a dilated heart and a cause from muscle dysfunction which has not resulted from the various manifestations of coronary artery disease. For many patients who present with systolic dysfunction and dilated heart, the ruling out of coronary artery disease as the etiology is of importance since this has a major impact on prognosis and treatment strategies [1-3]. There are studies using LGE as a novel non-invasive test to determine if LV dysfunction has an ischaemic etiology. In the absence of LGE in those with a dilated heart, an ischaemic etiology is extremely unlikely (97% negative predictive value), and in the presence of an ischaemic etiology, the amount of LGE correlates with the degree of severity of underlying CAD [4-7]. By contrast, patients with normal coronaries by angiography and LV dysfunction may still have an ischemic etiology for LV dysfunction (thrombosis on a non-stenotic plaque, or embolism in up to 13% of individuals),

and may have been inappropriately diagnosed as having a dilated cardiomyopathy [5]. The results of the LGE technique as a non-invasive method of differentiating ischaemic and dilated cardiomyopathy are superior to other techniques because the myocardial substrate can be interrogated with such high resolution. Additionally, CMR is superior to nuclear scintigraphic techniques to distinguish non-ischemic from ischemic etiologies. CMR is not limited by attenuation artefacts, which lead to false positive results for presence of myocardial infarction. Comparative studies between SPECT and CMR perfusion imaging have also demonstrated that CMR can better identify small myocardial infarctions than nuclear techniques [9]. Perfusion can also be assessed by both techniques to identify ischaemia, but CMR has superior spatial resolution and provides sensitivity and specificity values ranging between 83% and 95% and 53% and 95% respectively [10]. While the absence of LGE does not completely rule out an ischemic etiology in the rare setting of global myocardial hibernation in the absence of infarction, first-pass myocardial perfu-



4 Late gadolinium enhancement in dilated cardiomyopathy. There is mid-wall enhancement which is most marked in the septum. Vertical (A) and horizontal (E) long axis and three short axis (B, C, D) planes. Corresponding frames from the SSFP short axis cines are shown (F, G, H).

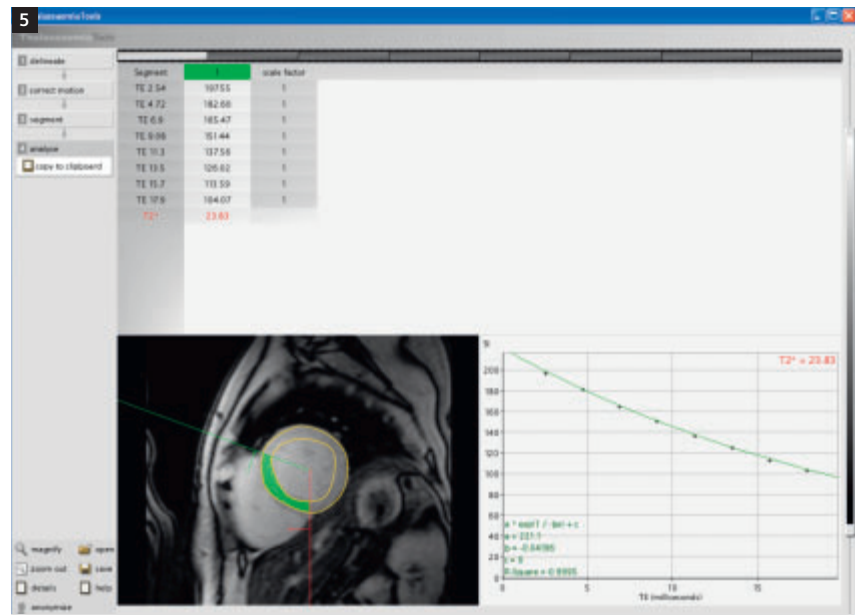
sion imaging or proximal coronary artery MR angiography can be performed.

Myocardial fibrosis, in a non-infarct pattern, is seen in up to 30% of patients with DCM, typically in a mid-wall septal distribution ("mid-wall striae", Fig. 4). The presence of fibrosis has important prognostic implications, with the presence of mid-wall fibrosis in DCM being associated with an increased risk of sudden cardiac death and ventricular tachycardia (VT), independent of other more traditional markers of increased risk [11]. These findings might also suggest the use of CMR for better identification of patients with need for an ICD implantation.

As highlighted above, CMR is the reference standard method of assessment of myocardial volumes and function. The interstudy and interindividual variability is less than 5%, thus making this technique accurate for picking up subtle reductions in ventricular function. This low variability also allows for accurate serial measurements over time to monitor for changes in function and monitor response to medical therapies. Furthermore, given the excellent interstudy reproducibility, smaller sample sizes are needed to detect true clinical differences between patient populations in research studies [12]. One example of this would be in a drug trial designed to detect a 10 g difference in LV mass with anti-hypertensive treatment, a sample size of 505 would be needed with 2D echo versus only 14 with CMR, for a power of 80% and P-value of 0.05 [13].

Thalassemia

Heart failure due to iron overload is the principle cause of death in patients with thalassemia, accounting for up to 71% of all deaths, with 50% of these patients dying before the age of 35, despite iron-chelating therapy [14-16]. This form of cardiomyopathy is reversible but intensive iron chelation is necessary to remove myocardial iron [17]. Unfortunately once heart failure symptoms occur in iron overload cardiomyopathy, the prognosis is poor. In the past, total body iron stores and approximation of myocardial iron loading were assessed by serum ferritin levels and liver biopsy, and indeed these parameters were also used to monitor success or failure of chelation therapy. It is now recognized that there can be marked discordance between liver and heart iron loading making early detection of myocardial iron chal-

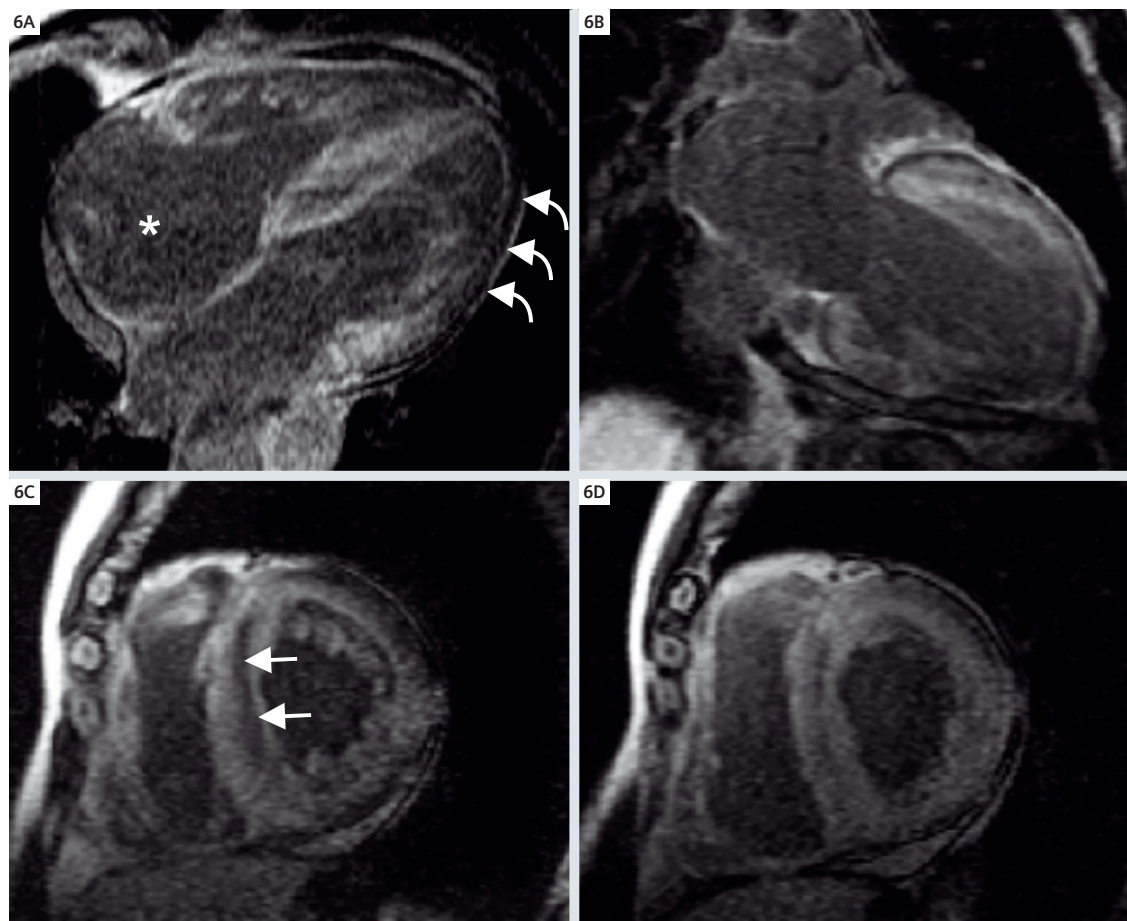


5 Myocardial T2* analysis using Thalassaemia-Tools® (plug-in of CMRtools®). The gradient echo images are loaded and the interventricular septum is defined. This area is least affected by variable susceptibility artefact commonly seen adjacent to the anterior and inferior walls (cardiac veins with deoxygenated blood) and the lateral wall (lungs). The software generates the signal against echo-time points and best fits the decay curve to estimate the T2* (in this case normal at 23.8 ms). When the myocardial T2* is very short (<10 ms), the latter points are comprised of noise rather than signal and the software can be instructed to discount such points to ensure the curve fits the "signal rich" initial decay points. This method is known as truncation. Other mathematical solutions for the data fitting exist including modeling of a constant for the baseline offset, and bi-exponential decay modeling. The truncation technique has been used for the major randomized controlled trials and its performance is well understood. The other techniques yield slightly different T2* values and therefore consistent analysis technique is important.

lenging using conventional techniques [18]. Since 2000 a new CMR technique has been able to address this problem. T2* is a relaxation parameter assessed by CMR arising principally from local magnetic field inhomogeneities that are increased with particulate storage iron deposition. This parameter is reproducible and correlates with liver and myocardial iron stores. It can be easily imaged and quantified in the heart using gradient echo techniques (Fig. 5). There is no better method of quantification of myocardial iron content than with this new CMR technique.

Using T2* it has been shown that there is no clinically useful correlation between myocardial iron and liver iron or ferritin levels confirming that reliance on these conventional parameters as a marker of cardiac iron loading is unreliable [18, 19]. The

CMR Thalassemia protocols are available with the Cardiac Suite (standard package) on all 1.5T MAGNETOM Tim systems.



6 Late gadolinium enhancement in cardiac amyloidosis. Horizontal (A) and vertical (B) long axis and two short axis (C, D) planes. Typical findings are shown including low intensity blood pool marked by * (LGE usually has high signal in the blood pool), and general enhancement favoring the subendocardium – the short curly white arrows show epicardial sparing. Mid-wall “sparing” is seen in the septum (zebra pattern – short white arrows).

The incidence of development of heart failure in those with a $T2^* < 6$ ms is very high, whereas it is uncommon in patients with a $T2^* > 10$ ms.

degree of myocardial iron is directly correlated with the severity of LV dysfunction. In a cross-sectional study, 89% of thalassemia patients with new onset cardiac failure had a $T2^*$ less than 10 ms. Therefore the threshold of <10 ms for myocardial $T2^*$ is now taken as indicating severe iron loading. Mild to moderate iron loading is indicated by a myocardial $T2^*$ of 10–20 ms, and >20 ms is normal (the median for the normal population is approximately 40 ms). In a prospective follow-up study, the incidence of development of heart failure in those with a $T2^* < 6$ ms is very high, whereas it is uncommon in patients with a $T2^* > 10$ ms. Arrhythmias however occur with a wider distribution of myocardial $T2^*$. $T2^*$ has been also used to monitor success of chelation therapy. Improvement in both cardiac function and myocardial $T2^*$

over a one-year period was found using 24-hour continuous intravenous deferoxamine for 12 months in heart failure [20]. A cross-sectional study showed that the oral chelator deferiprone was associated with superior ejection fraction and myocardial $T2^*$ than the standard treatment of injected subcutaneous deferoxamine [21]. Recently 2 prospective randomized controlled trials have confirmed that deferiprone has superior efficacy in removing cardiac iron. The first study indicated superiority of deferiprone as monotherapy over deferoxamine in reducing cardiac iron overload and improving ejection fraction [22]. In a second trial, the authors found that combination chelation therapy (deferiprone plus deferoxamine) improved both myocardial $T2^*$ and ejection fraction in comparison with deferoxamine monotherapy [23].

Since the introduction of the T2* technique to the management of thalassemia patients, with particular emphasis on intensification or alteration of chelation therapies, UK mortality rates in this condition have reduced by 80% [24]. This pattern has also been documented in Italy [15], and Cyprus [25]. This is a substantial health improvement for beta-thalassemia patients which has world-wide importance.

Myocardial inflammation: Viral Myocarditis, Sarcoidosis, SLE

Viral myocarditis is a common cause of dilated cardiomyopathy. In Europe, Parvovirus, Herpes virus and Coxsackie virus are most often found to be the culprit. Myocardial inflammation on the basis of systemic disease often determines the overall prognosis of the patient. However, based on autopsy studies, myocardial involvement is often clinically underdiagnosed, e.g. in sarcoidosis about 50% of cases are positive at autopsy [28]. Moreover, myocarditis can be of different origin including bacterial, viral, toxic or involvement in systemic diseases [29]. Focal and diffuse tissue changes on a histological level vary depending on the agents and the time course of the disease. Cellular infiltration with and without myocyte necrosis has been described [30, 31]. The broad clinical spectrum from subclinical disease to severe heart failure and a course of the disease from complete convalescence to dilated cardiomyopathy depends on the extent of the myocardial damage and its immediate detection. Therefore an early non-invasive differentiation is warranted.

Contrast-enhanced CMR (ceCMR) has been used to detect myocardial inflammation for several years [32]. A good correlation between ceCMR and endomyocardial biopsy including a relation to severity of disease was published recently [33,34]. Nevertheless, in our experience, some patients with inflammatory myocardial reaction may be overlooked by only applying LGE imaging. Exploiting the unique tissue characterization capabilities of CMR, a multi-sequential approach was introduced, which was shown to increase the diagnostic accuracy of magnetic resonance imaging to detect myocarditis [35]. This includes

- T2-weighted fast spin echo for oedema detection,
- T1-weighted spin echo imaging before and early after contrast to delineate increased interstitial space and

- LGE imaging to visualize necrotic areas.

The combined approach differentiates between reversible and irreversible damage and allows to a certain extent to assess the acuity of inflammation.

Applying a similar approach, we were able to detect myocardial involvement in sarcoidosis even when left-ventricular function was still preserved [36]. Different CMR techniques have proven useful during follow-up including steroid therapy in sarcoidosis [37, 38]. The extent of LGE may indicate the risk of the patients, but larger prospective trials are needed to address this issue. Interestingly, there is also first evidence that in systemic lupus erythematosus quantification of T2 is helpful in characterizing myocardial involvement [39]. Currently we recommend the combination of T1 and T2-weighted sequences. The proposed approach is published and is meanwhile optimized for different types of scanners. Nevertheless, we expect further technical improvement including more robust techniques.

T2-weighted imaging

For T2 we use a short T1 fast spin-echo sequence with triple inversion (STIR). More recent approaches (works in progress) include T2-weighted gradient echo attempting to overcome some of the drawbacks of the spin-echo approach: Insufficient blood suppression in areas of slow flow and posterolateral signal loss due to mistriggering, but they have not been proven in that setting yet.

Used parameters are as follows: TR = 2RR, TE 65 ms, TI 140 ms, slice thickness 15 mm, gap 5 mm, FoV 340–380 mm, matrix 256 x 256. Global instead of regional myocardial signal is measured. Skeletal muscle is used as a reference structure to minimize heart rate effects.

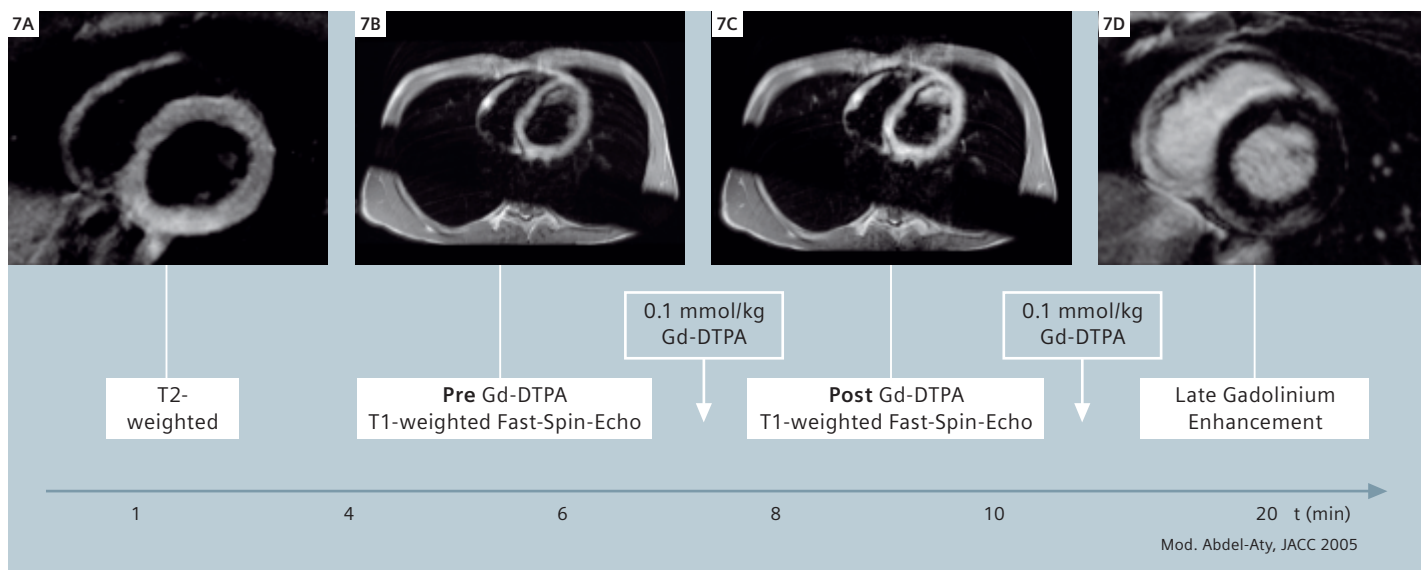
Contrast-enhanced T1-weighted imaging

For contrast enhanced T1-weighted imaging we recommend differentiating an early from a late phase. The early phase encloses the first 4 minutes after contrast administration, encompasses the steady-state during the whole period (non-breath-hold sequence). Hyperemia, increased distribution volume in the intercellular space and capillary leakage result in increased contrast enhancement in this phase. Here, we recommend a continuous non-breathhold interleaved multislice T1-weighted fast spin-echo sequence.

Since the introduction of the CMR T2* technique, mortality rates in thalassemia patients could be reduced by 80% in the UK.

There is a good correlation between ceCMR and endomyocardial biopsy including a relation to severity of myocardial inflammation.

TSE T1 & T2, 2D IR/PSIR sequences are provided in the Cardiac Suite (standard) on all MAGNETOM Tim systems.



7 Myocarditis CMR Protocol. Multi-sequential approach for assessment of myocardial inflammation. After assessment of left-ventricular function, T2- and T1-weighted sequences are acquired. See text for more details.

Quantitative analysis of the T1-weighted sequences for the assessment of the „relative enhancement“ takes ~5-10 minutes.

It is prone to flow artifacts, so saturation bands across the atria and the aorta might be helpful.

Typical parameters:

TR 475–480 ms, TE 30 ms, matrix 256 x 256; slice thickness 6 mm, number of acquisitions 4–6.

We compare signal intensity before and after contrast and calculate a ratio of myocardial over skeletal muscle enhancement (a number we have called “relative enhancement”) to control for heart rate effects. In addition to optimization for different scanners, normal values for the quantification of signal enhancement were established. The complete quantitative analysis of all sequences takes ~5–10 minutes.

LGE imaging

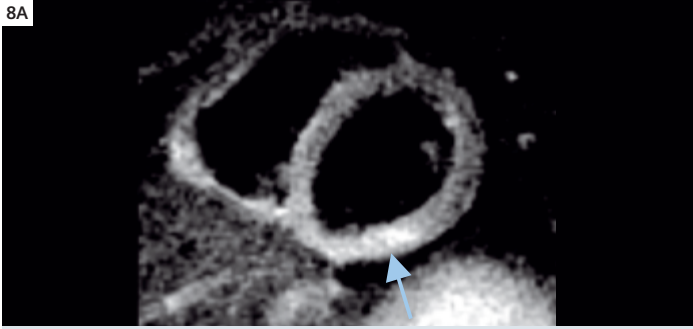
The third part of the protocol includes the assessment of late Gd enhancement images. The interpretation for clinical use is usually done qualitatively. In contrary to the “ischemic pattern”, LGE in patients with myocarditis is usually not located at myocardial segments consistent with coronary territories and can be located subepicardially or intramyocardially. According to recent studies there is even suspicion of a predominant localization of certain viruses in particular myocardial segments. LGE may appear grayish (instead of white) in myocarditis and have a patchy or solid appearance. LGE may reduce in size over the course of myocarditis – however, it is still unknown,

whether shrinkage of disseminated fibrotic areas, reduction of interstitial space (e.g. after oedema), or both cause this phenomenon (Figs. 7-9). CMR has been accepted, meanwhile, as clinically helpful in the diagnosis of myocarditis even if certain technical questions remain under discussion. Accordingly the recent conjoint report of the American College of Cardiology and the SCMR has classified its use as “appropriate” or “Class A Indication” in inflammatory cardiomyopathy [31].

Hypertrophic Cardiomyopathy (HCM)

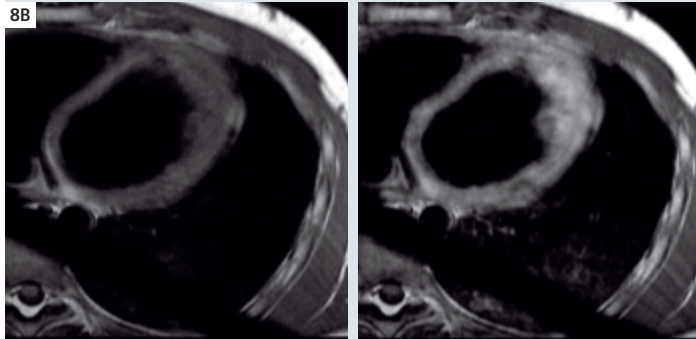
As a screening tool, echocardiography is used but it was recently shown that localized apical and anterolateral hypertrophies are under-diagnosed when applying echo [40]. This is of potential impact for risk stratification and screening of relatives. In CMR, the detection and quantification of hypertrophy can be easily done by application of cine-images (state of the art: steady-state free precession sequences, e.g. TrueFISP). The combination with parallel imaging (iPAT) allows a fast and robust coverage of the heart. The routinely used protocol includes standard long-axis and full coverage short-axis slices (Fig. 10). The localization of obstruction can be visualized by a signal loss due to the turbulent flow, the dimension of the left ventricular outflow tract can be measured applying cine-images of the LVOT [41]. This approach is not only helpful for the differentiation

ACC & SCMR classified the use of CMR in inflammatory CMP as a „Class A Indication“.

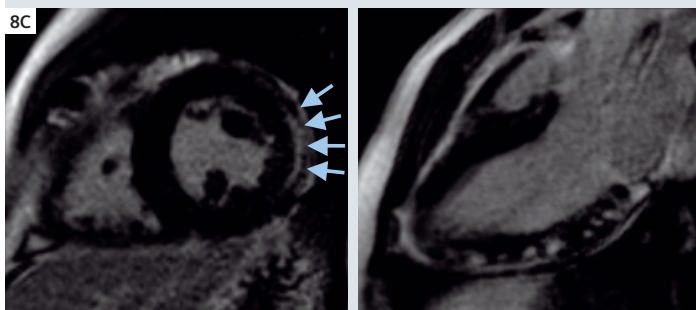


8 Myocarditis. 24-year-old male patient, admitted to our emergency unit with severe chest pain, history of respiratory infection, no known risk factors for coronary artery disease. ECG: left bundle branch block. Laboratory: Increased cardiac markers.

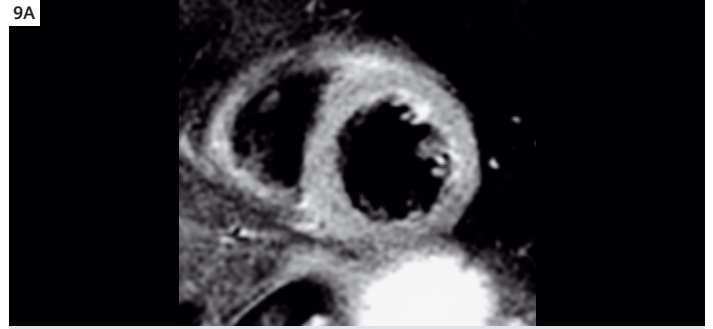
A) Oedema imaging: T2-weighted (T2w) images, increased global signal (ratio = 2.5), inferiorly a focal oedema can be visualized (arrow). Recovery during follow-up.



B) Early enhancement: T1w FSE before and after contrast application. Quantification of signal increase showed an increased value (ratio = 4.9) Normalization could be verified during follow-up.

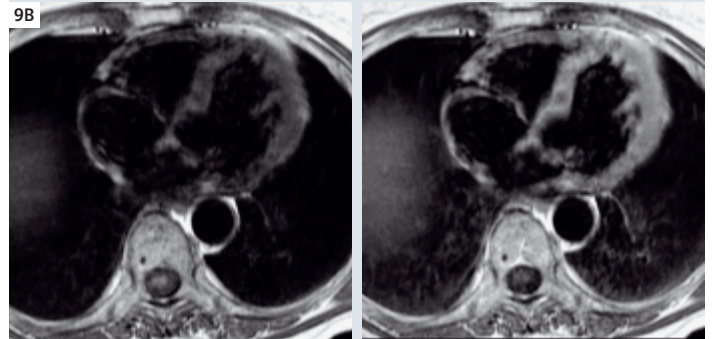


C) Late gadolinium enhancement (LGE): Typical subepicardial enhancement in the lateral wall as seen in the mid-cavity short axis orientation (left, arrows) and patchy enhancement in the inferolateral wall from base to apex as seen in the LVOT orientation (bright spots, right), indicative of fibrotic areas – persistent during follow-up. Note the saturation bands on both images, placed to prevent artefacts due to flow in atria or aorta. Diagnosis: active myocarditis.

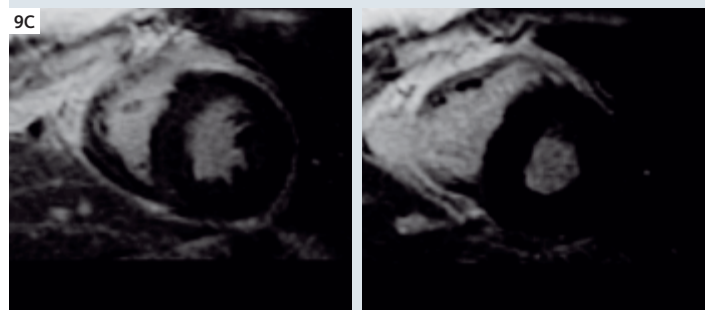


9 Myocarditis. 64-year-old female patient, admitted to the emergency room with severe chest pain, history of diarrhea. ECG: ST-Elevation in leads I, II, aVL, V5-6; T-wave inversion in lead II. Laboratory findings: CK two-fold elevated, Troponin highly elevated, leucocytes 16 Gpt/l, CRP 28 mg/dl (normal <5 mg/dl). Transthoracic echo: wall motion abnormalities in anteroseptal and anterolateral segments, LV ejection fraction 28%. Coronary angiography: exclusion of significant coronary artery disease (CAD). CMR-findings:

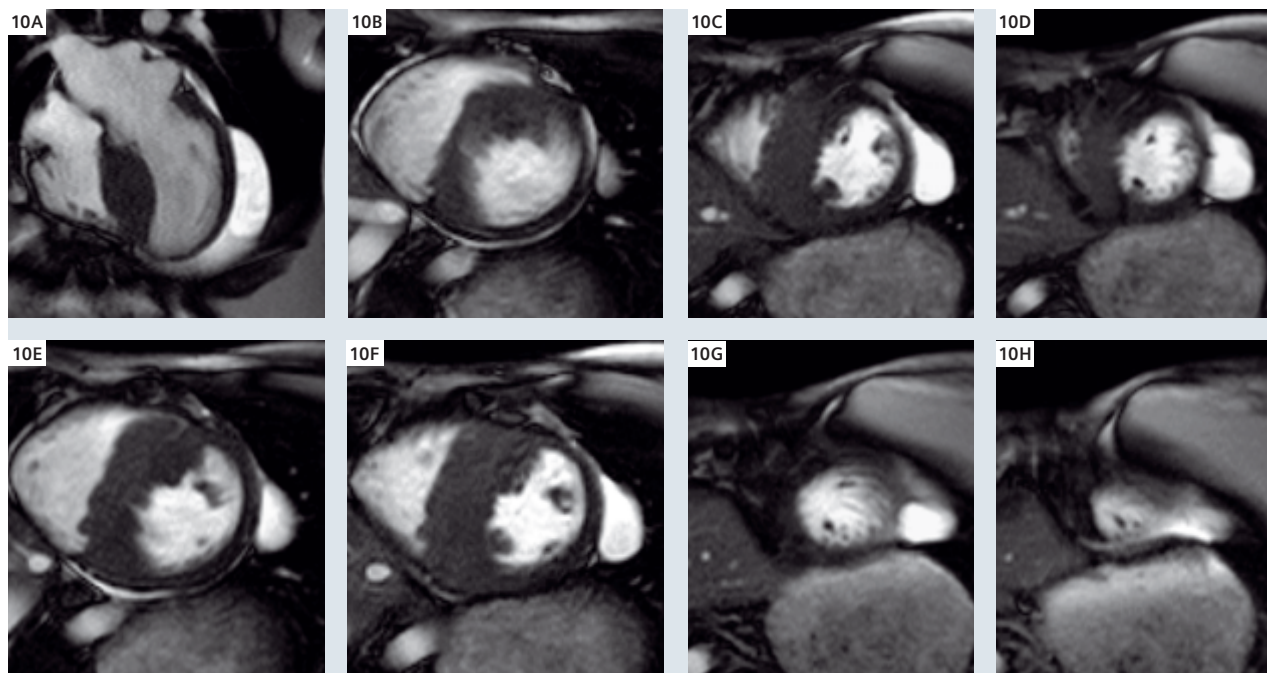
A) Oedema imaging: T2-weighted images, increased global signal (ratio = 2.3) – normalization during follow up.



B) Early enhancement: Showing T1w FSE before and after contrast application. Quantification of signal-increase showed a significant increase (ratio = 5.6) – normalization during follow up.



C) Late gadolinium enhancement (LGE): no evidence for LGE
Diagnosis: active myocarditis.



10 Hypertrophic Obstructive Cardiomyopathy. TrueFISP cine-images. Long-axis (4-chamber view) showing septal hypertrophy (A). Complete coverage of the left ventricle in short-axis orientation (B–H).

There is initial evidence for a correlation of LGE to higher risk regarding development of heart failure and sudden cardiac death in HOCM.

CMR is a reliable method for diagnosing cardiac amyloid by the presence of a typical LGE pattern, which is not seen in other LVH pathologies.

between obstructive and non-obstructive forms, but also allows us to understand the relationship between the evolution of obstruction and post-interventional tissue changes, e.g. following septal embolisation [42] (Fig. 11). The verification of new therapeutic approaches like septal ablation can be improved using ce CMR which is also useful during follow-up [43, 44].

We believe that the application of LGE is promising for further risk stratification in HOCM. There is initial evidence for a correlation to higher risk regarding development of heart failure and sudden cardiac death [45] (Fig. 12). LGE in HOCM usually appears as intramyocardial spots in the ventricular septum at the junction of RV and LV, and may extend as patchy areas throughout the hypertrophic myocardium. CMR is unique in simultaneously correlating the morphological abnormalities in HCM to their underlying tissue injury, thus providing a comprehensive characterization of the disease phenotype and elucidating the cause of LVH. Those data are not available by use of other non-invasive modalities free of ionizing radiation.

Amyloidosis

Cardiac involvement is frequent in AL amyloidosis, and is a key determinant of treatment options and

prognosis. Unfortunately, cardiac involvement remains the principle cause of death in approximately half of patients with AL amyloidosis. In general, the diagnosis of cardiac amyloidosis is made by echocardiography, demonstrating left ventricular hypertrophy and variable degrees of diastolic dysfunction in the setting of a histological diagnosis of amyloidosis (usually from outside the heart). In the presence of concurrent risk factors for LVH, however, the diagnosis can be difficult to make. By contrast, CMR is a reliable method for diagnosing cardiac amyloid by the presence of a typical LGE pattern, which is not seen in other LVH pathologies, with widespread enhancement preferentially affecting the subendocardium (Fig. 6). The wash-in and wash-out kinetics of gadolinium are markedly abnormal. LGE imaging therefore typically shows a dark blood pool. Since the mid-wall is relatively spared in the ventricular septum, there may be a characteristic zebra pattern with subendocardial enhancement of the LV and RV endocardium (for optimal LGE imaging in patients with suspicion of cardiac amyloidosis, see article of Voros et al., p. 86). Other features which are characteristic of cardiac amyloidosis include a thickened inter-atrial septum and RA free wall hypertrophy. Significant-

ly, the LGE in amyloidosis is not representative of fibrosis but instead of interstitial expansion by amyloid fibrils (protein). Most recently the gadolinium kinetics has been shown to predict prognosis. This CMR technique allows for more robust diagnosis of cardiac amyloid without the need for cardiac biopsy, and may also prove useful for monitoring serial changes over time with new treatments.

Arrhythmogenic Right Ventricular Dysplasia/Cardiomyopathy

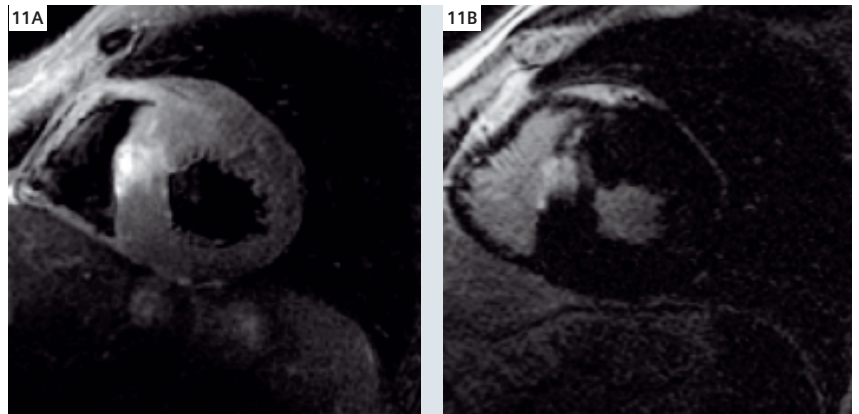
ARVD/ARVC is a genetically determined disease with the risk of malignant arrhythmias and sudden cardiac death (SCD) even in young patients. Current guidelines require a composite of clinical, functional and morphologic criteria to diagnose ARVC.

For years, CMR has been presented in the textbooks as particularly suitable for diagnosing ARVC especially through detection of right ventricular (RV) fatty infiltration. In daily practise, however, it is a lot more cumbersome.

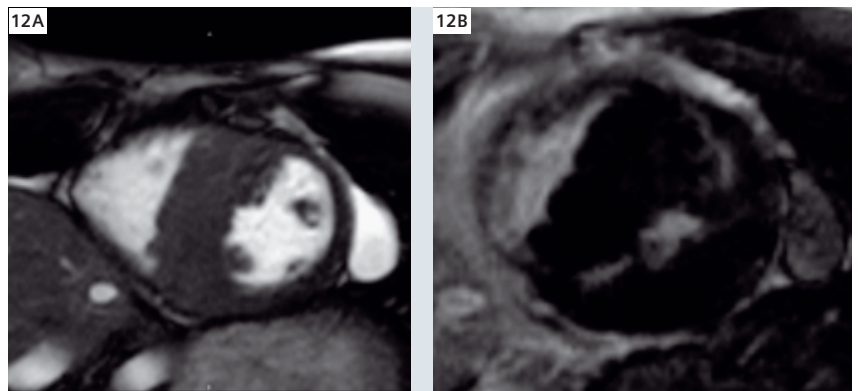
It is indeed easier to visualize and quantify the right ventricle by applying CMR than by use of echocardiography. We prefer the axial and sagittal orientation to a classical short axis approach for better delineation of the tricuspid valve plane and the outflow tract area. Due to the thinner RV walls, reproducibility of volume and functional measurements is still lower than for the left ventricle. Slice thickness should be reduced to 5 or 6 mm as a maximum; contiguous slice acquisition is warranted [46].

The literature has suggested the use of fast spin-echo T1-weighted images with and without fat saturation technique to detect fatty infiltration in the RV wall. In the "real world", sensitivity, specificity and reproducibility of this approach have been disappointing [47]. Indeed, pathologists have described fibro-fatty infiltration instead of pure fatty infiltration. This matches the first reports describing delayed enhancement in the RV wall [48] which nevertheless await verification from other groups. Newer sequence developments allow fat suppression in LGE images which offers the opportunity to investigate the fibro-fatty infiltration and may bring us closer to the proposed criteria of ARVC.

In agreement with other groups we found the detection of global and regional wall motion ab-



11 Hypertrophic Obstructive Cardiomyopathy. 57-year-old patient, scan was done seven days after interventional septal ablation. **Left:** Bright signal in the septal wall showing the oedema (STIR sequence). The oedema was resolved after 6 weeks. **Right:** After contrast application bright signal in the septal wall showing scar tissue (late gadolinium enhancement imaging). Lesion persists.



12 Fibrosis in hypertrophic cardiomyopathy. **Left:** Short-axis image showing septal hypertrophy. **Right:** Same short-axis view with LGE imaging: Bright signal shows fibrosis. The primary location of the enhancement at the insertion points of RV is a typical finding in HCM.

normalities the most helpful criterion in daily practise. Micro-aneurysms and bulging are highly suggestive of ARVC. However, one has to be familiar with the typical regional RV contraction patterns (e.g. around the moderator band or RVOT) to avoid false positive reports (Fig. 13).

Conclusion

CMR allows not only to differentiate ischemic from non-ischemic cardiomyopathic origins but also allows to establish the etiology within the non-ischemic category such as myocarditis, amyloidosis, thalassaemia or ARVD. CMR enables this by providing multiple different sequences that allow for visualization (and sometimes also quantification)

T1-weighted TSE and delayed enhancement sequences can be used to detect fibro-fatty infiltrations in ARVD.

There is an incremental value of CMR in the risk assessment of certain cardiomyopathies (e.g. HOCM, DCM).

All 2D sequences needed for cardiomyopathy evaluation are provided in the Cardiac Suite as standard on all MAGNETOM Tim systems.

of tissue alterations such as iron deposition, oedema, fibrosis etc. with high diagnostic accuracy. Since recent studies showed an incremental value of CMR in the risk assessment of certain cardiomyopathies (e.g. for sudden cardiac death and VT in HOCM and DCM), CMR has been increasingly used to ensure the best treatment for the right patient at the right time.

Acknowledgement

The whole Cardiac MR working group of the Franz Volhard-Klinik, Charité Campus Buch is engaged in all topics discussed in the Berlin sub-chapters of this manuscript. I want to acknowledge especially the work of Anja Zagrosek and André Rudolph who provided the case examples, and also to thank Hassan Abdel-Aty for his excellent and critical review.

Contacts

Prof. Dudley Pennell, M.D.
CMR Unit
Royal Brompton Hospital
Sydney Street
London SW3 6NP, UK
d.pennell@ic.ac.uk
+44 20 7351 8802
+44 207 351 8816

Assoc. Prof. Jeanette Schulz-Menger, M.D.
Franz-Volhard-Klinik
Charité Universitätsmedizin Berlin
Helios-Klinikum Berlin
Schwanebecker Chaussee 50
13125 Berlin, Germany
jeanette.schulz-menger@charite.de
+49 30 940152903
<http://www.charite-buch.de/fvkweb/CMR>

References

- 1 Likoff MJ, Chandler SL, Kay HR. Clinical determinants of mortality in chronic congestive heart failure secondary to idiopathic dilated or to ischemic cardiomyopathy. *Am J Cardiol* 1987;59:634–8.
- 2 Bart BA, Shaw LK, McCants Jr CB, et al. Clinical determinants of mortality in patients with angiographically diagnosed ischemic or nonischemic cardiomyopathy. *J Am Coll Cardiol* 1997;30: 1002–8.
- 3 Allman KC, Shaw LJ, Hachamovitch R, et al. Myocardial viability testing and impact of revascularization on prognosis in patients with coronary artery disease and left ventricular dysfunction: a meta-analysis. *J Am Coll Cardiol* 2002;39:1151–8.
- 4 Casolo G, Minneci S, Manta R, et al. Identification of the ischaemic etiology of heart failure by cardiovascular magnetic resonance imaging: diagnostic accuracy of late gadolinium enhancement. *Am Heart J* 2006;151:101–108.
- 5 McCrohon JA, Moon JC, Prasad SK, et al. Differentiation of heart failure related to dilated cardiomyopathy and coronary artery disease using gadolinium-enhanced cardiovascular magnetic resonance. *Circulation* 2003;108:54–9.
- 6 Bello D, Shah DJ, Farah GM, et al. Gadolinium cardiovascular magnetic resonance predicts reversible myocardial dysfunction and remodeling in patients with heart failure undergoing beta-blocker therapy. *Circulation* 2003;108:1945–53.
- 7 Soriano CJ, Ridocci F, Estornell J, et al. Late gadolinium-enhanced cardiovascular magnetic resonance identifies patients with standardized definition of ischemic cardiomyopathy: a single centre experience. *Int J Cardiol* 2007;116:167–173.
- 8 Bulkley BH, Hutchins GM, Bailey I, et al. Thallium 201 imaging and gated cardiac blood pool scans in patients with ischemic and idiopathic congestive cardiomyopathy: a clinical and pathological study. *Circulation* 1977;55:753–760.
- 9 Wagner A, Mahrholdt H, Holly TA, Elliott M.D., Regenfus M, Parker M, Klocke FJ, Bonow RO, Kim RJ, Judd RM. Contrast-enhanced MRI and routine single photon emission computed tomography (SPECT) perfusion imaging for detection of sub-endocardial myocardial infarcts: an imaging study. *Lancet* 2003; 361: 374–9.
- 10 Barkhausen J, Hunold P, Jochims M, et al. Imaging of myocardial perfusion with magnetic resonance. *J Magn Reson Imaging* 2004;19:750–7.
- 11 Assomull RG, Prasad SK, Lyne J, et al. Cardiovascular magnetic resonance, fibrosis, and prognosis in dilated cardiomyopathy. *J Am Coll Cardiol* 2006;48:1977–1985.
- 12 Keenan NG, Pennell DJ. CMR of ventricular function. *Echocardiography* 2007;24:185–193.
- 13 Bottini PB, Carr AA, Prisant M, et al: Magnetic resonance imaging compared to echocardiography to assess left ventricular mass in the hypertensive patient. *Am J Hypertens* 1995;8:221–228.
- 14 Olivieri NF, Nathan DG, MacMillan JH, Wayne AS, Liu PP, McGee A, Martin M, Koren G, Cohen AR. Survival in medically treated patients with homozygous beta-thalassemia. *N Engl J Med*. 1994;331: 574 –578.
- 15 Borgna-Pignatti C, Rugolotto S, De Stefano P, Zhao H, Cappellini M.D., Del Vecchio GC, Romeo MA, Forni GL, Gamberini MR, Ghilardi R, Piga A, Cnaan A. Survival and complications in patients with thalassemia major treated with transfusion and deferoxamine. *Haematologica*. 2004;89:1187–1193.
- 16 Modell B, Khan M, Darlison M. Survival in beta thalassaemia major in the UK: data from the UK Thalassaemia Register.

- Lancet. 2000; 355:2051–2052.
- 17 Wacker Ph.D., Balmer-Ruedin D, Oberhansli I, Wyss M. Regression of cardiac insufficiency after ambulatory intravenous deferoxamine in thalassaemia major. *Chest* 1993; 103: 1276–8.
 - 18 Anderson LJ, Holden S, Davis B, et al. Cardiovascular T2-star (*) magnetic resonance for the early diagnosis of myocardial iron overload. *Eur Heart J* 2001;21:2171–2179.
 - 19 Tanner MA, Galanello R, Dessi C, et al. Myocardial iron loading in patients with thalassemia major on deferoxamine chelation. *J Cardiovasc Magn Reson* 2006;8:543–547.
 - 20 Anderson LJ, Westwood MA, Holden S, et al. Myocardial iron clearance during reversal of siderotic cardiomyopathy with intravenous desferrioxamine: a prospective study using T2* cardiovascular magnetic resonance. *Br J Haematol* 2004;127:348–355.
 - 21 Anderson LJ, Wonke B, Prescott E, et al. Comparison of effects of oral deferiprone and subcutaneous desferrioxamine on myocardial iron concentrations and ventricular function in beta-thalassemia. *Lancet* 2002;360:516–520.
 - 22 Pennell DJ, Berdoukas V, Karagiorga M, et al. Randomised controlled trial of deferiprone or deferoxamine in beta-thalassemia major in patients with asymptomatic myocardial siderosis. *Blood* 2006;107:3738–3744.
 - 23 Tanner MA, Galanello R, Dessi C, et al. A randomized, placebo-controlled, double-blind trial of the effect of combined therapy with deferoxamine and deferiprone on myocardial iron in thalassemia major using cardiovascular magnetic resonance. *Circulation* 2007;115:1876–1884.
 - 24 Modell B, Khan M, Darlison M, Westwood MA, Pennell DJ, David Ingram D. Falling mortality and changing causes of death in thalassaemia major: data from the UK thalassaemia register and possible contribution from T2* cardiovascular magnetic resonance. *J Cardiovasc Magn Reson* In review.
 - 25 Telfer P, Coen PG, Christou S, Hadjigavriel M, Kolnakou A, Pangalou E, Pavlides N, Psiloinis M, Simamonian K, Skordos G, Sitarou M, Angastiniotis M. Survival of medically treated thalassemia patients in Cyprus. *Trends and risk factors over the period 1980–2004. Haematologica* 2006; 91: 1187–92.
 - 26 Falk RH, Skinner M. The systemic amyloidoses: an overview. *Adv Intern Med*. 2000;45:107–137.
 - 27 Maceira AM, Joshi J, Prasad SK, et al. Cardiovascular magnetic resonance in cardiac amyloidosis. *Circulation* 2005;111: 186–193.
 - 28 Iwai K, Tachibana T, Takemura T, et al. Pathological studies on sarcoidosis autopsy. I. Epidemiological features of 320 cases in Japan. *Acta Pathol Jpn*. Jul–Aug 1993;43(7–8):372–376.
 - 29 Feldman AM, McNamara D. Myocarditis. *N Engl J Med*. Nov 9 2000;343(19):1388–1398.
 - 30 Kawai C. From myocarditis to cardiomyopathy: mechanisms of inflammation and cell death: learning from the past for the future. *Circulation*. Mar 2 1999;99(8):1091–1100.
 - 31 Magnani JW, Dec GW. Myocarditis: current trends in diagnosis and treatment. *Circulation*. Feb 14 2006;113(6):876–890.
 - 32 Friedrich MG, Strohm O, Schulz-Menger J, et al. Contrast media-enhanced magnetic resonance imaging visualizes myocardial changes in the course of viral myocarditis. *Circulation*. May 12 1998;97(18):1802–1809.
 - 33 Mahrholdt H, Goedecke C, Wagner A, et al. Cardiovascular magnetic resonance assessment of human myocarditis: a comparison to histology and molecular pathology. *Circulation*. Mar 16 2004;109(10):1250–1258.
 - 34 Mahrholdt H, Wagner A, Deluigi CC, et al. Presentation, patterns of myocardial damage, and clinical course of viral myocarditis. *Circulation*. Oct 10 2006;114(15):1581–1590.
 - 35 Abdel-Aty H, Boye P, Zagrosek A, et al. Diagnostic performance of cardiovascular magnetic resonance in patients with suspected acute myocarditis: comparison of different approaches. *J Am Coll Cardiol*. Jun 7 2005;45(11): 1815–1822.
 - 36 Schulz-Menger J, Wassmuth R, Abdel-Aty H, et al. Patterns of myocardial inflammation and scarring in sarcoidosis as assessed by cardiovascular magnetic resonance. *Heart*. Mar 2006;92(3):399–400.
 - 37 Smedema JP, Snoep G, van Kroonenburgh MP, et al. Cardiac involvement in patients with pulmonary sarcoidosis assessed at two university medical centers in the Netherlands. *Chest*. Jul 2005;128(1):30–35.
 - 38 Vignaux O, Dhote R, Duboc D, et al. Detection of myocardial involvement in patients with sarcoidosis applying T2-weighted, contrast-enhanced, and cine magnetic resonance imaging: initial results of a prospective study. *J Comput Assist Tomogr*. Sep–Oct 2002;26(5):762–767.
 - 39 Singh JA, Woodard PK, Davila-Roman VG, et al. Cardiac magnetic resonance imaging abnormalities in systemic lupus erythematosus: a preliminary report. *Lupus*. 2005;14(2):137–144.
 - 40 Rickers C, Wilke NM, Jerosch-Herold M, et al. Utility of cardiac magnetic resonance imaging in the diagnosis of hypertrophic cardiomyopathy. *Circulation*. Aug 9 2005;112(6):855–861.
 - 41 Schulz-Menger J, Abdel-Aty H, Busjahn A, et al. Left ventricular outflow tract planimetry by cardiovascular magnetic resonance differentiates obstructive from non-obstructive hypertrophic cardiomyopathy. *J Cardiovasc Magn Reson*. 2006;8(5):741–746.
 - 42 Schulz-Menger J, Gross M, Messroghli D, et al. Cardiovascular magnetic resonance of acute myocardial infarction at a very early stage. *J Am Coll Cardiol*. Aug 6 2003;42(3):513–518.
 - 43 van Dockum WG, ten Cate FJ, ten Berg JM, et al. Myocardial infarction after percutaneous transluminal septal myocardial ablation in hypertrophic obstructive cardiomyopathy: evaluation by contrast-enhanced magnetic resonance imaging. *J Am Coll Cardiol*. Jan 7 2004;43(1):27–34.
 - 44 van Dockum WG, Beek AM, ten Cate FJ, et al. Early onset and progression of left ventricular remodeling after alcohol septal ablation in hypertrophic obstructive cardiomyopathy. *Circulation*. May 17 2005;111(19):2503–2508.
 - 45 Moon JC, McKenna WJ, McCrohon JA, et al. Toward clinical risk assessment in hypertrophic cardiomyopathy with gadolinium cardiovascular magnetic resonance. *J Am Coll Cardiol*. May 7 2003;41(9):1561–1567.
 - 46 Tandri H, Friedrich MG, Calkins H, et al. MRI of arrhythmogenic right ventricular cardiomyopathy/dysplasia. *J Cardiovasc Magn Reson*. 2004;6(2):557–563.
 - 47 Bluemke DA, Krupinski EA, Ovitt T, et al. MR Imaging of arrhythmogenic right ventricular cardiomyopathy: morphologic findings and interobserver reliability. *Cardiology*. 2003;99(3):153–162.
 - 48 Tandri H, Saranathan M, Rodriguez ER, et al. Noninvasive detection of myocardial fibrosis in arrhythmogenic right ventricular cardiomyopathy using delayed-enhancement magnetic resonance imaging. *J Am Coll Cardiol*. Jan 4 2005;45(1):98–103.

Myocardial Stress Perfusion Imaging using CMR

Andrew E. Arai, M.D.

National Heart, Lung and Blood Institute, National Institutes of Health, Bethesda, M.D., USA

Clinical role

Adult cardiology and medicine focuses tremendous emphasis on the evaluation of patients with known or suspected coronary artery disease since this is one of the leading causes of death in industrialized nations. There are three major clinical presentations of coronary artery disease: chest pain syndromes, acute coronary syndromes (including acute myocardial infarction) and sudden death. Since relatively few patients suffering from coronary artery disease can be resuscitated from sudden death, most efforts are aimed at detecting coronary artery disease at earlier stages of the disease and at preventing permanent myocardial damage. Stress testing is one of the most powerful diagnostic approaches to detecting coronary artery disease. In general terms, it is necessary to understand why it is necessary to perform stress testing to detect physiologically significant coronary artery disease when using technologies that do not directly image the coronary arteries.

Coronary artery disease causes symptoms of chest discomfort in two major presentations: acute coronary syndromes or in chronic stable angina. In acute coronary syndromes, a thrombus developed on an unstable coronary plaque resulting in intermittent or complete obstruction of a coronary artery. In the most extreme cases this will cause an ST elevation myocardial infarction. In patients with unstable angina, no permanent myocardial damage may have occurred and further testing with either coronary angiography or stress testing may be needed to determine whether coronary disease could explain the symptoms or needs intervention.

Outside of the setting of acute myocardial infarction or the most severe rest perfusion defects associated with hibernating myocardium, perfusion of the heart is generally normal at rest. Even

in the presence of a severe coronary stenosis, autoregulation of the heart's blood vessels maintains normal perfusion to the heart muscle. Thus, at rest, a patient can feel normal and have no chest pain. Likewise, images of rest perfusion can look quite normal and uniform in the heart. A stress test uncovers the coronary stenosis by challenging the adequacy of the heart's ability to regulate blood flow. As the patient exercises or vasodilator medicines are administered, blood flow increases in the heart muscle served by a normal coronary artery. However, blood flow cannot increase as much downstream from a significantly stenosed coronary artery. Thus, high levels of exercise may induce chest pain and ST segment abnormalities. During a stress perfusion study, a relative defect in blood flow to some regions of the heart may be imaged by nuclear methods (SPECT) or by CMR. Alternatively, imaging can be performed during stress to detect a new or worsening wall motion abnormality. Such testing can be performed by echocardiography (during exercise or dobutamine) or by CMR (during dobutamine).

Stress imaging tests are generally indicated when a patient has an equivocal stress ECG or uninterpretable ECG due, for example, to baseline ST segment abnormalities. Pharmacological stress testing is generally required in patients that cannot adequately exercise. For an exercise stress test to be diagnostic, peak heart rate must be at least 85% maximal predicted for age. Such high heart rates can be difficult to attain if a patient has problems such as arthritis.

Directly imaging the coronary arteries is an alternative approach to detecting coronary artery disease. However, the consensus of medical experts indicates that coronary interventions should primarily be performed in clinical situations where

Stress testing is one of the most powerful diagnostic approaches to detecting coronary artery disease.

Coronary interventions should primarily be performed when there is clinical evidence of myocardial ischemia associated with the coronary stenosis.

Table 1: Non-CMR stress tests used for the detection of coronary artery disease

	# of patients	Sensitivity	Specificity
Exercise ECG	2456	52	71
Exercise SPECT	4480	87	73
Stress Echocardiography	2637	85	77

Adapted from Fleischmann et al. and Klocke et al. [1, 2]

Among stress tests, exercise ECG has the lowest sensitivity and specificity for detecting coronary artery disease.

Table 2: Sensitivity and specificity of stress perfusion CMR for detecting coronary artery disease

Reference	N	Stress	Sensitivity (%)	Specificity (%)
Klem et al. [3]	92	adenosine	89	87
Ingkanisorn et al. [4]	135	adenosine	100	93
Okuda et al. [5]	33	dipyridamole	84	87
Sakuma et al. [6]	40	dipyridamole	81	68
Plein et al. [7]	92	adenosine	88	82
Takase et al. [8]	102	dipyridamole	93	85
Paetsch et al. [9]	49	adenosine	79	75
Paetsch et al. [10]	79	adenosine	91	62
Wolff et al. [11]	99	adenosine	93	75
Thiele et al. [12]	32	adenosine	75	97
			80	91
Plein et al. [13]	72	adenosine	88	83
Bunce et al. [14]	35	adenosine	74	71
Nagel et al. [15]	84	adenosine	88	90
Ishida et al. [16]	104	dipyridamole	84	82
Doyle et al. [17]	184	dipyridamole	57	78
			52	82
Kinoshita et al. [18]	27	dipyridamole	55	77
			77	81
Ibrahim et al. [19]	25	adenosine	69	89
Schwitzer et al. [20]	48	dipyridamole	87	85
			91	94
Panting et al. [21]	26	adenosine	79, 72, 60	83, 83, 43
			77	83
Al-Saadi et al. [22]	34	dipyridamole	90	83
Totals	1392		~83%	~80%

Taking all studies into account, the sensitivity and specificity of stress perfusion CMR is around 83% and 80% respectively.

there is clinical evidence of myocardial ischemia associated with the coronary stenosis. Thus, even in patients with known intermediate stenosis of a coronary artery, there is frequently a need for

stress testing to define whether the stenosis is physiologically significant in that individual. Now that non-invasive coronary CT angiography has progressed to a point where it can detect high-

Table 3: Image acquisition parameters for different perfusion pulse sequences

Method	SR-SSFP	SR-FLASH	SR-GRE-EPI (research WIP)
TE (ms)	1.1	1.3	1.1 (TE1)
TR (ms)	2.3	2.2	6.1
BW (Hz/pixel)	1400	780	1630
Echotrain length	1	1	4
Readout Flip Angle	50	12	25
Matrix	128 × 80	128 × 80	128 × 80
Parallel Imaging Factor	R = 2	R = 2	R = 2
TD (ms) (to 1st line)	39	41	54
TI (ms) (to center)	85	85	85
Tslice (ms) (total)	132	130	117
Slices per RR @ 60/90/120 bpm	7/5/3	7/5/3	8/5/4

The diagnostic accuracy of stress perfusion CMR is comparable to the other stress imaging modalities.

grade coronary artery stenosis in asymptomatic patients, there will be increasing need to define the physiological significance of these abnormalities. There is also a need to define the physiological significance of possible stenosis associated with highly calcified coronary arteries or in smaller coronary stents that cannot be adequately resolved with current generation CT scanners.

Cardiac risk factors are widely used clinically to help guide preventive treatments and to delay the onset of clinically overt coronary artery disease. The common risk factors for coronary disease include age, male gender, family history of premature coronary disease, diabetes, hypertension, hyperlipidemia, smoking, obesity, and physical inactivity. In addition, coronary calcium as detected and quantified by a CT scan has independent and additive risk as well as prognostic significance. Of the coronary risk factors identified, diabetes, hypertension, hyperlipidemia, smoking, obesity, and activity can all be modified through medical or individual intervention.

However, risk factors have a relatively weak short-term predictive value for coronary artery disease. For example, the Framingham risk score is commonly used to assess the likelihood that a patient has coronary artery disease but reports risk in probability of disease occurring over a 10-year period. For example, a non-smoking 55-year-old male patient with a cholesterol of 240 mg/dL, an HDL of 40 mg/dL, hypertension with a systolic blood pressure of 130 mmHg has a 10% risk of developing coronary artery disease over the next 10

years. That level of risk warrants intervention if the LDL cholesterol is high enough (130 mg/dL) per the ATP III guidelines [National Cholesterol Education Program, National Heart, Lung, and Blood Institute, National Institutes of Health, NIH Publication No. 01-3670, May 2001] but remains a low enough risk for direct detection of asymptomatic disease to be controversial.

In summary, stress testing and risk factor analysis or preventive cardiology perform complementary approaches to detecting and managing patients with coronary artery disease. At the current time, the primary role of stress testing is in detection of coronary disease or physiological assessment of coronary disease. Risk factor analysis focuses on optimizing management of medically modifiable risk factors either in the prevention of disease or in more aggressive management of patients with known disease.

Diagnostic accuracy

There are many forms of stress tests and significant differences in the sensitivity, specificity, and accuracy of these tests. Table 1 summarizes the sensitivity and specificity of non-CMR stress tests used for the detection of coronary artery disease. Table 2 presents similar statistics for stress perfusion CMR. The diagnostic accuracy of stress perfusion CMR is clearly comparable to the other stress imaging modalities and all stress imaging modalities have clinically significant increased sensitivity relative to stress ECG.

Sequences and protocols

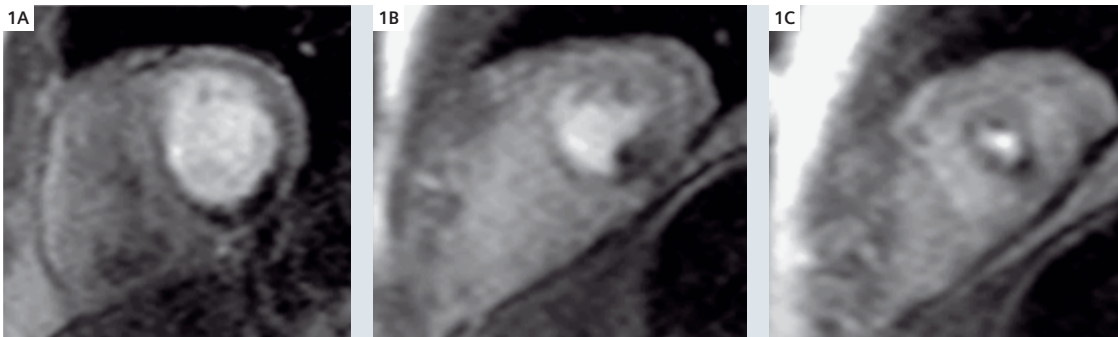
To perform first pass perfusion imaging, a series of T1 weighted images must be obtained every heartbeat or every other heart beat while a bolus of contrast passes through the heart and myocardium. As with many aspects of diagnostic testing, choices need to be made with regard to balance between anatomic coverage, spatial resolution within each imaging plane, temporal resolution, and image quality. We generally image 3 slices of the heart in a short axis orientation to assess at least 16 segments of the heart. In general, this allows acquiring all three slices every cardiac cycle. However, this choice was made since our group has focused much effort on developing fully quantitative analysis methods. It would be equally reasonable to image a total of 6 slices every other heartbeat to improve the anatomic coverage of the heart. Three main sequences have been used to acquire stress perfusion images: TurboFLASH (GRE), TrueFISP (SSFP), and hybrid echoplanar methods (GRE-EPI or hybrid EPI). Of these, TurboFLASH and TrueFISP are available as product level software and the hybrid echoplanar method is under

evaluation as a research “work-in-progress.” The main advantages of TurboFLASH are its simplicity and the minimal image artifacts. The main consideration for using the TrueFISP sequence is the higher signal-to-noise ratio and improved contrast-to-noise ratio. Either sequence produces high quality perfusion images. Examples of stress perfusion defects obtained with TurboFLASH, TrueFISP, and the hybrid echoplanar methods are shown in figures 1–4.

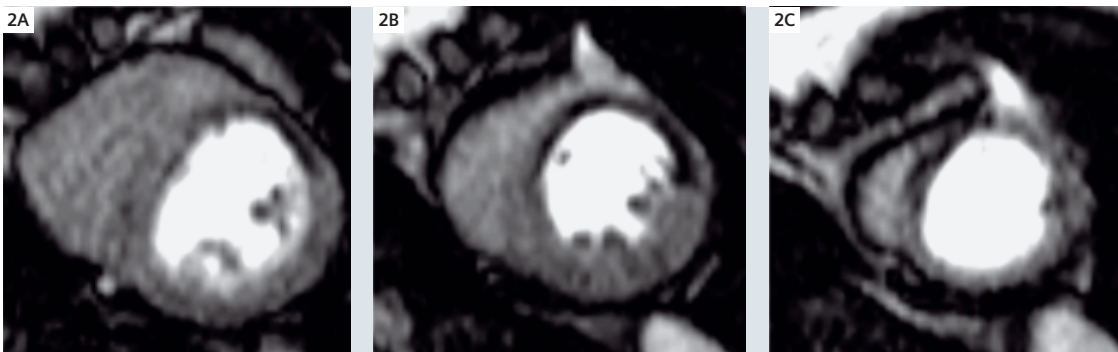
Table 3 summarizes recommended starting parameters for first pass perfusion studies. These are parameter sets that we have studied at the National Institutes of Health. Many groups push for higher spatial resolution but one must recognize that the time used to acquire more lines of k-space will lengthen the duration of the readout during the cardiac cycle opening the possibility of artifacts due to motion and will reduce the number of images per heartbeat (slices per RR). We have tried to aim for short imaging time during the cardiac cycle to minimize dark rim artifacts at the endocardial-blood interface. Parallel imaging factors (iPAT factors) are quite effective at im-

SR TrueFISP (SSFP) and SR TurboFLASH (GRE) sequences are available for CMR myocardial perfusion imaging.

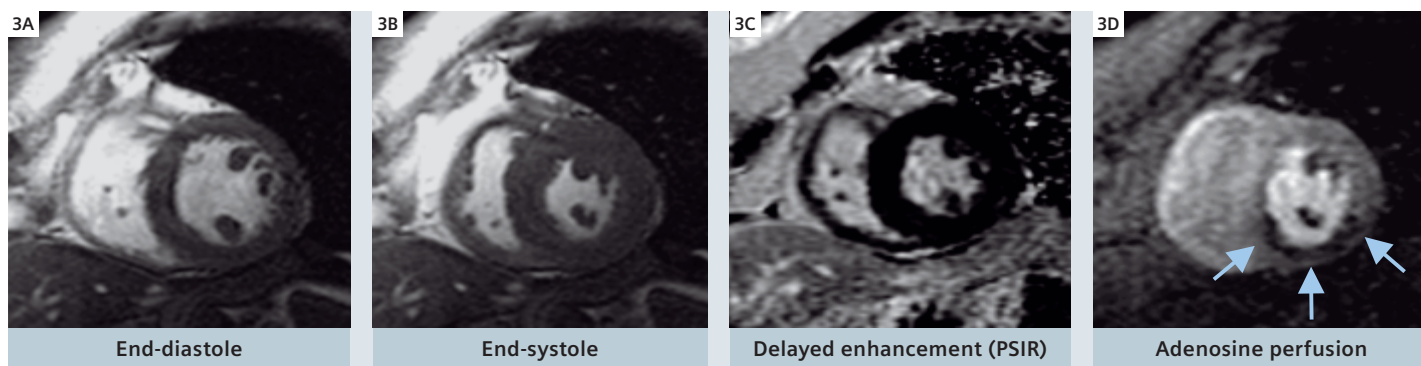
Up to 8 slices can be acquired in one or more orientations during the CMR first-pass perfusion imaging.



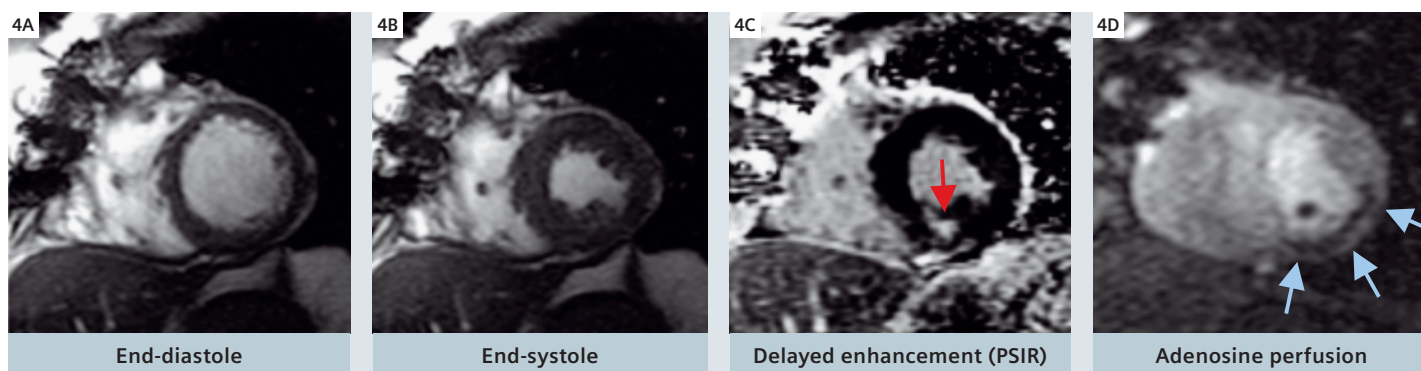
1 Inferior perfusion defect during stress using the SR TurboFLASH perfusion sequence.



2 Example of stress perfusion defect using SR TrueFISP.



3 Patient with stress induced perfusion defects but no myocardial scar.



4 Patient with prior bypass surgery, small inferior myocardial infarction, larger wall motion abnormality and perfusion defect. Findings consistent with stunned myocardium and inducible ischemia. PSIR is used as a fast technique for Delayed Enhancement MRI.

proving temporal resolution and well worth the tradeoff in signal-to-noise ratio. In our general experience, artifacts are a much larger issue than signal-to-noise ratio for perfusion images.

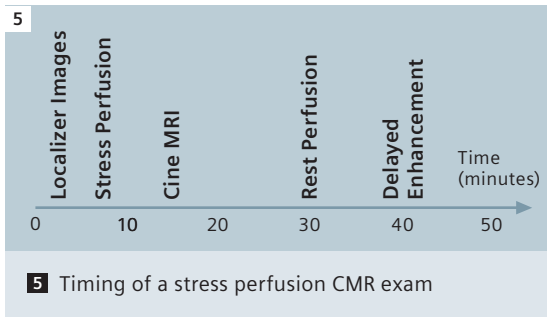
Typical protocol for CMR stress perfusion imaging

Figure 5 shows the typical timing of a stress perfusion protocol. After localizer images, the vasodilator stress agent is started. In the case of adenosine, we recommend mixing enough adenosine to provide a 6 minute infusion at 140 micrograms/kg/min. By 3 minutes into the infusion, adequate vasodilation should be achieved to allow performing the stress perfusion imaging. Once the stress perfusion images are acquired, the adenosine infusion can be stopped. When using dipyridamole, we recommend a net dose of 0.56 mg/kg infused over 4 minutes. Peak vasodilation with dipyridamole may not be achieved until several minutes after completing the infusion. We usually do the stress perfusion imaging 4 minutes after finishing the dipyridamole unless severe symptoms require

us to image earlier. Aminophylline 100 mg IV is sometimes needed to reverse the effects of dipyridamole symptoms due to the significantly longer half-time. When carrying out a rest perfusion study after the stress perfusion, it is generally a good idea to reverse the dipyridamole since it may have lingering effects that alter the rest perfusion.

After stabilizing the patient following the stress test, cine CMR can be performed to assess anatomy, ejection fraction, and regional wall motion. Some centers acquire rest cine images prior to the injection of adenosine and additionally during adenosine stress. A rest perfusion study is then performed using identical parameters to the stress test to facilitate comparisons. Finally, delayed enhancement imaging of myocardial infarction can be performed. If additional imaging is required one could do velocity encoded phase contrast before or after the rest perfusion study. Turbo spin echo (black blood imaging) should be completed prior to the stress perfusion imaging to avoid poor blood suppression related to having contrast in the circulation. A contrast-enhanced MRA could

Due to the very short half-life time (< 30 s), adenosine is mostly used as a vasodilator for stress tests.



be performed in place of the rest perfusion study if desired. Coronary MRA can generally be performed at any point along the time line since most of the sequences are not too severely affected by the presence of contrast. As regards the dosage of contrast, several factors have to be considered in the main decision. In general, for a given set of parameters, the signal-to-noise ratio will be better for higher doses of contrast but the linearity between gadolinium concentration and signal intensity may become an issue. The dual bolus and dual sequence methods were introduced by researchers attempting to benefit from higher doses of contrast for the myocardium but to preserve the linearity in the blood pool necessary to quantify perfusion [23, 24]. If one is not performing quantitative analysis, it is reasonable to use a dose of gadolinium contrast of 0.5 mmol/kg.

Pitfalls with CMR first-pass perfusion imaging

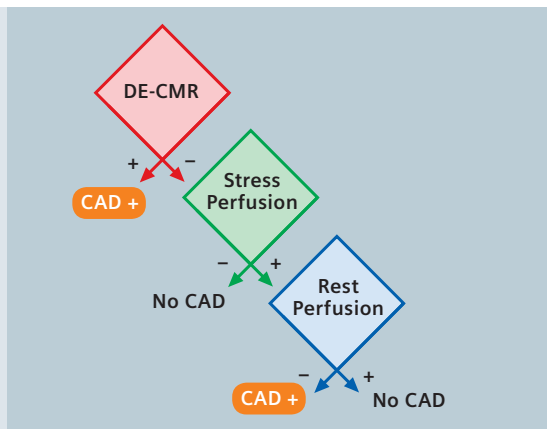
The pitfall in CMR first pass perfusion imaging is making a reasonable balance between sensitivity and specificity when interpreting images. There is no substitute for experience that includes correlation with invasive coronary angiography. Even as a center with experience in over 1000 stress perfusion cases, we found it extremely helpful to go back to correlation with cardiac catheterization when we switched imaging methods to the True-FISP perfusion sequence. You learn the most from cases with an unequivocal normal angiogram and also from true defects in patients with a significant stenosis in the absence of a myocardial infarction. When we project a perfusion study to a group of physicians, it is inevitable that one or more physicians will have a question about a gray rim near the endocardial border on one or more slices of a perfusion scan. There are many tricks that can be used to help determine the likelihood that these defects may or may not be real perfusion defects:

- Perfusion defects tend to follow the typical perfusion territories of the coronary artery.
- Perfusion defects tend to affect distal segments first depending on how distal or proximal the location of the stenosis is.
 - Exception: Patients with coronary artery bypass surgery.
 - Exception: Branch vessel disease such as diagonal or septal perforators.
- True perfusion defects tend to last several heartbeats beyond the initial rapid upslope of myocardial enhancement. Susceptibility artifacts tend to be worst during peak concentration of gadolinium during the intracavity RV and LV phases of enhancement and tend to disappear rapidly.
 - Corollary: If a dark rim disappears by the time most segments have reached about 90% maximal enhancement, then the rim is probably an artifact.
- Perfusion defects tend to be subendocardial except in the most severe cases. This allows using differences between endocardial and epicardial enhancement as another way to control for issues like surface-coil intensity drop off. It also makes it possible to detect balanced ischemia associated with multi-vessel disease.
- True perfusion defects usually have significantly lower enhancement than normal segments. If in doubt, place a small region of interest on the questionable dark rim artifact and a region of normal heart (close proximity to avoid surface coil intensity issues). Many of the things people list as possible defects are within 3–4% of the signal intensity of neighboring myocardium. A 15 or 20% difference in signal intensity is more likely to be a real defect.
- Use all information available to you when interpreting images. The delayed enhancement is a very specific tool for diagnosing coronary artery disease (see figure 6). The group at Duke University tested a simple interpretation algorithm that they find helps improve the specificity of reading perfusion scans [3]. Essentially, if the patient has a myocardial infarction on delayed enhancement imaging, it is very likely he has significant coronary disease. If an apparent perfusion defect is seen at rest and at stress in the absence of an MI on delayed enhancement imaging, it must be an artifact (only in the absence of wall motion abnormalities!). A defect

A typical stress MRI exam consists of function, perfusion and delayed enhancement imaging.

Low doses of Gadolinium are used for quantitative perfusion analysis, in order to preserve linearity between gadolinium concentration and signal intensity.

6 Duke method for using delayed enhancement and rest perfusion to improve the accuracy of interpreting stress perfusion images (Adapted from Klem et al.).



seen at stress but not at rest is most likely to represent a true defect.

- An unequivocal regional wall motion abnormality on cine CMR can also be very informative. However, do not put too much weight on marginal variations in wall motion.
- Also look for artifacts associated with sternal wires, vascular clips, and coronary stents. These findings increase the pretest likelihood of disease considerably.
- Time-intensity curves can also help distinguish true defects from false positive defects. It is not uncommon that one or more segments of the heart appears delayed by 1–2 heartbeats relative to the other segments. This can create a region of the heart being 25% or more darker than all other segments and appear like a severe perfusion defect. Time-intensity curves show such a region enhances at a similar rate to the other segments but is simply delayed in time relative to the other segments.

Advantages and benefits of CMR stress perfusion imaging

The main advantages of CMR stress perfusion imaging relate to the completeness and quality of the information obtained during this single examination. Figure 4 shows the utility of a CMR stress perfusion exam in a patient with known coronary artery disease. Thus, the clinical question is not a simple binary presence or absence of coronary disease. This patient had prior bypass surgery and a prior myocardial infarction. She presented with chest pain that occurred at rest but remained troponin negative throughout her hospitalization. The clinically relevant question is whether there is myocardial ischemia beyond the infarct. Follow-

ing the principles listed in the section on “pitfalls,” there are many pieces of useful information. Starting with the delayed enhancement image, there is a small inferior myocardial infarction (red arrow). Interestingly, the wall motion abnormality is more extensive than the small infarct and includes the inferolateral segment. The cine CMR also shows the sternal wire artifacts in the chest wall. Finally, the stress perfusion defect is also more extensive than the infarct. This study thus shows a patient with known coronary disease with evidence of stunned myocardium (viable myocardium with a wall motion abnormality in the setting of recent clinical suspicion of ischemia) and a stress induced perfusion defect consistent with inducible ischemia.

There are also advantages of stress CMR in terms of diagnostic workflow. A high-quality exam can be accomplished within 45–60 minutes covering cine CMR, stress perfusion, rest perfusion, and delayed enhancement images. This exam allows assessment of ejection fraction, regional wall motion, the valves, evidence of inducible perfusion defects, and the extent of myocardial infarction. The fact that these imaging methods can be displayed side-by-side in the same imaging planes facilitates interpretation, particularly for subtle abnormalities. Thus, stress CMR studies can be performed with an efficiency that is significantly higher than most nuclear methods. The time of exams is comparable to echocardiographic stress tests but with significantly more diagnostic information about ischemia and viability. Thus, as a complete package, the rest-stress CMR study provides more information than either echocardiography or SPECT.

The image resolution of CMR perfusion studies is also unique and a distinct advantage. Compared with SPECT, the image resolution is at least 10 times higher on a volumetric basis. Considering the normal left ventricular wall is only about 10 mm thick, SPECT operates at an acquisition resolution incapable of resolving epicardial from endocardial perfusion. Typical resolution CMR perfusion scans operate at an acquisition resolution smaller than ~3 mm and thus routinely resolve endocardial from epicardial perfusion abnormalities. The greatest advantage of this comes in detecting multivessel disease, left main disease, or microvascular disease [16, 25]. Recent papers have documented that stress perfusion imaging has prog-

CMR and echo stress tests have comparable exam times, however, CMR comes with significantly more diagnostic information about ischemia and viability.

Compared to SPECT, CMR offers an at least 10 times higher volumetric image resolution.

nostic value. In a series of patients studied after presenting to the emergency department, adenosine stress CMR had excellent sensitivity and specificity for diagnosing coronary artery disease [4]. A negative adenosine stress CMR study had excellent prognosis. In another study, the prognosis of positive or negative stress tests was nearly identical if the stress agent was adenosine or dobutamine [26]. Last but not least, when compared to SPECT imaging, instead of 4-20 mSv, no ionizing radiation is needed to perform a CMR stress exam.

Conclusions

In a center with the equipment and expertise to perform stress CMR, vasodilator stress tests are a very powerful tool for diagnosing and managing ischemic heart disease. The stress perfusion information is an important step beyond viability imaging since the presence or absence of inducible perfusion defects can alter the management of a patient. The combined evaluation of function, perfusion, and viability provides the information needed for managing complicated patients with coronary artery disease.

References

- 1 Fleischmann, K.E., et al., Exercise echocardiography or exercise SPECT imaging? A meta-analysis of diagnostic test performance. *J Nucl Cardiol*, 2002. 9(1): p. 133–4.
- 2 Klocke, F.J., et al., ACC/AHA/ASNC guidelines for the clinical use of cardiac radionuclide imaging-executive summary: a report of the American College of Cardiology/American Heart Association Task Force on Practice Guidelines (ACC/AHA/ASNC Committee to Revise the 1995 Guidelines for the Clinical Use of Cardiac Radionuclide Imaging). *Circulation*, 2003. 108(11): p. 1404–18.
- 3 Klem, I., et al., Improved detection of coronary artery disease by stress perfusion cardiovascular magnetic resonance with the use of delayed enhancement infarction imaging. *J Am Coll Cardiol*, 2006. 47(8): p. 1630–8.
- 4 Ingkanisorn, W.P., et al., Prognosis of negative adenosine stress magnetic resonance in patients presenting to an emergency department with chest pain. *J Am Coll Cardiol*, 2006. 47(7): p. 1427–32.
- 5 Okuda, S., et al., Evaluation of ischemic heart disease on a 1.5 Tesla scanner: combined first-pass perfusion and viability study. *Radiat Med*, 2005. 23(4): p. 230–5.
- 6 Sakuma, H., et al., Diagnostic accuracy of stress first-pass contrast-enhanced myocardial perfusion MRI compared with stress myocardial perfusion scintigraphy. *AJR Am J Roentgenol*, 2005. 185(1): p. 95–102.
- 7 Plein, S., et al., Coronary artery disease: myocardial perfusion MR imaging with sensitivity encoding versus conventional angiography. *Radiology*, 2005. 235(2): p. 423–30.
- 8 Takase, B., et al., Whole-heart dipyridamole stress first-pass myocardial perfusion MRI for the detection of coronary artery disease. *Jpn Heart J*, 2004. 45(3): p. 475–86.
- 9 Paetsch, I., et al., Myocardial perfusion imaging using OMNISCAN: a dose finding study for visual assessment of stress-induced regional perfusion abnormalities. *J Cardiovasc Magn Reson*, 2004. 6(4): p. 803–9.
- 10 Paetsch, I., et al., Comparison of dobutamine stress magnetic resonance, adenosine stress magnetic resonance, and adenosine stress magnetic resonance perfusion. *Circulation*, 2004. 110(7): p. 835–42.
- 11 Wolff, S.D., et al., Myocardial first-pass perfusion magnetic resonance imaging: a multicenter dose-ranging study. *Circulation*, 2004. 110(6): p. 732–7.
- 12 Thiele, H., et al., Color-encoded semiautomatic analysis of multi-slice first-pass magnetic resonance perfusion: comparison to tetrofosmin single photon emission computed tomography perfusion and X-ray angiography. *Int J Cardiovasc Imaging*, 2004. 20(5): p. 371–84; discussion 385–7.
- 13 Plein, S., et al., Assessment of non-ST-segment elevation acute coronary syndromes with cardiac magnetic resonance imaging. *J Am Coll Cardiol*, 2004. 44(11): p. 2173–81.
- 14 Bunce, N.H., et al., Combined coronary and perfusion cardiovascular magnetic resonance for the assessment of coronary artery stenosis. *J Cardiovasc Magn Reson*, 2004. 6(2): p. 527–39.
- 15 Nagel, E., et al., Magnetic resonance perfusion measurements for the noninvasive detection of coronary artery disease. *Circulation*, 2003. 108(4): p. 432–437.
- 16 Ishida, N., et al., Noninfarcted myocardium: correlation between dynamic first-pass contrast-enhanced myocardial MR imaging and quantitative coronary angiography. *Radiology*, 2003. 229(1): p. 209–16.
- 17 Doyle, M., et al., The impact of myocardial flow reserve on the detection of coronary artery disease by perfusion imaging methods: an NHLBI WISE study. *J Cardiovasc Magn Reson*, 2003. 5(3): p. 475–85.
- 18 Kinoshita, M., et al., Myocardial perfusion magnetic resonance imaging for diagnosing coronary arterial stenosis. *Jpn Heart J*, 2003. 44(3): p. 323–34.
- 19 Ibrahim, T., et al., Assessment of coronary flow reserve: comparison between contrast-enhanced magnetic resonance imaging and positron emission tomography. *J Am Coll Cardiol*, 2002. 39(5): p. 864–70.
- 20 Schwitter, J., et al., Assessment of myocardial perfusion in coronary artery disease by magnetic resonance: a comparison with positron emission tomography and coronary angiography. *Circulation*, 2001. 103(18): p. 2230–2235.
- 21 Panting, J.R., et al., Echo-planar magnetic resonance myocardial perfusion imaging: parametric map analysis and comparison with thallium SPECT. *J Magn Reson Imaging*, 2001. 13(2): p. 192–200.
- 22 Al-Saadi, N., et al., Noninvasive detection of myocardial ischemia from perfusion reserve based on cardiovascular magnetic resonance. *Circulation*, 2000. 101(12): p. 1379–83.
- 23 Christian, T.F., et al., Absolute myocardial perfusion in canines measured by using dual-bolus first-pass MR imaging. *Radiology*, 2004. 232(3): p. 677–84.
- 24 Gatehouse, P.D., et al., Accurate assessment of the arterial input function during high-dose myocardial perfusion cardiovascular magnetic resonance. *J Magn Reson Imaging*, 2004. 20(1): p. 39–45.
- 25 Panting, J.R., et al., Abnormal subendocardial perfusion in cardiac syndrome X detected by cardiovascular magnetic resonance imaging. *N Engl J Med*, 2002. 346(25): p. 1948–53.
- 26 Jahnke, C., et al., Prognostic value of cardiac magnetic resonance stress tests: adenosine stress perfusion and dobutamine stress wall motion imaging. *Circulation*, 2007. 115(13): p. 1769–76.

Contact

Andrew E. Arai, MD
Senior Investigator
National Heart,
Lung and Blood Institute
National Institutes
of Health
Bethesda, MD, 20892
USA

High-Dose Dobutamine Stress Cardiac MR Imaging for Detection of Myocardial Ischemia

Markus Jochims M.D.; Oliver Bruder M.D.; Christoph Jensen M.D.; Georg V. Sabin M.D.

Department of Cardiology and Angiology, Elisabeth Hospital Essen, Germany

Introduction

Stress induced impairment of regional left ventricular function is a reliable indicator of transient myocardial ischemia [1, 13]. Therefore, the analysis of wall motion abnormalities by echocardiography in conjunction with a variety of different stress modalities has grown to a clinically established non-invasive test for the assessment of myocardial ischemia [2]. However, optimal echocardiographic image acquisition depends on the skill of the operator and the presence of an adequate acoustic window. Approximately 15% of patients admitted to stress-echo yield suboptimal or non-diagnostic images [3, 4, 5, 6]. Formerly these patients were referred to myocardial scintigraphy performed in single-photon emission computed tomography (SPECT) technique. High-dose dobutamine stress cardiac magnetic resonance imaging (CMR) emerged as an alternative high-resolution and noninvasive method for the detection of stress induced myocardial ischemia, which does not expose the patient to radiation and provides a diagnostic accuracy for the detection and localization of functional significant coronary artery disease (CAD) comparable to stress echocardiography and SPECT technique [6, 16]. Various studies have shown that CMR permits acquisition of images with high-spatial and improved temporal resolution in any tomographic plane [7] and allows accurate determination of left ventricular function in terms of wall motion and wall thickening at rest and during pharmacological stress [8, 9]. High dose dobutamine stress testing can be safely performed with a standard dobutamine/atropine stress proto-

col similar to stress echocardiography studies and proved to be a clinically feasible tool for the assessment of hemodynamically significant coronary artery stenoses [6, 10, 11, 12, 14, 22, 23, 26].

Dobutamine stress cardiac MR imaging

Due to its high spatial resolution and good tissue contrast, CMR has been shown to be the most accurate imaging modality for determination of wall thickening and volume measurements [13, 14, 15]. Recent technical developments, providing stronger gradient systems with new ultrafast sequences and fast data reconstruction procedures providing "near real-time" imaging facilitate clinically feasible cardiac MRI stress testing. Cine CMR with retrospective ECG-gating displays myocardial contractility of the entire cardiac cycle and permits evaluation of global and regional function [17].

MR sequence

The image quality of gradient echo techniques, which offer a shorter acquisition time as spin-echo sequences, depends on flow effects and may decrease depending on impaired regional or global ventricular function. Steady-state free precession sequences (e.g. TrueFISP) provide much higher signal intensity and signal-to-noise ratio (SNR) [18]. They enable rapid data acquisition and a high contrast between blood and myocardium without flow artifacts. Because of the distinguished delineation of anatomic structures steady-state free precession sequences are ideally suited for evalua-

The diagnostic accuracy of dobutamine stress MRI is comparable to stress echocardiography and SPECT.

TrueFISP cine sequences provide rapid image acquisition and high contrast between blood pool and myocardium.

tion of wall motion and wall thickening. Parallel imaging techniques reduce imaging time even more, but there is a partial loss of SNR depending on the accelerating factor. Currently, steady state free precession sequences in combination with parallel image acquisition and retrospective gating are state of the art. New real-time imaging sequences with improved spatial and temporal resolution will lead to further improvement in cardiac MR imaging especially during stress testing [17].

Image acquisition

Primary rapid multi-slice localizing images are acquired to define the cardiac axes. By means of single-angulated tomograms intersecting the mitral valve and the cardiac apex on a transverse view double-angulated long-axis tomograms that also intersect the mitral valve plane and the apex are planned. Based upon these images contiguous true short-axis cine scans are acquired to cover the whole left ventricle. In addition, three long-axis tomograms – two chamber view, four chamber view and three chamber view – are acquired according to the equatorial short axis orientation. Scanning by breath-holding in end-expiration reduces breathing artifacts. True short-axis and long-axis cine images are obtained at each stress level.

Standard high-dose dobutamine protocol

As a primarily beta1-adrenergic catecholamine with positive inotropic and positive chronotropic effect, dobutamine increases the myocardial oxygen consumption. Coronary arteries with severe stenosis do not allow adequate increase of blood flow to compensate elevated myocardial oxygen consumption under stress conditions. Myocardial ischemia leads to impairment of regional myocardial function, depressed systolic contractility and loss of systolic wall thickening. ECG changes and clinical symptoms manifest later and inconsistently in the “cascade of ischemia” [13].

For stress testing dobutamine is infused intravenously during 3-minute stages at doses of 10, 20, 30 and 40 µg per kilogram of body weight per minute under continuously monitoring of heart rhythm, blood pressure and symptoms. If the sub-maximal stress level described by a target heart rate of $((220 - \text{age}) \times 0.85)$ is not reached, additional fractionated atropine doses of 0.25 mg every 60 seconds up to a maximal dose of 1.0 mg are administered intravenously. The same true short-axis and long-axis cine images are obtained at each stress level as acquired at rest (Figure 1). Immediately after acquisition images are displayed

iPAT (Integrated Parallel Acquisition Techniques) allow fast acquisition of cine images in multiple orientations.

Dobutamine stress MRI is performed using the same incremental dobutamine protocol as known from stress echocardiography.

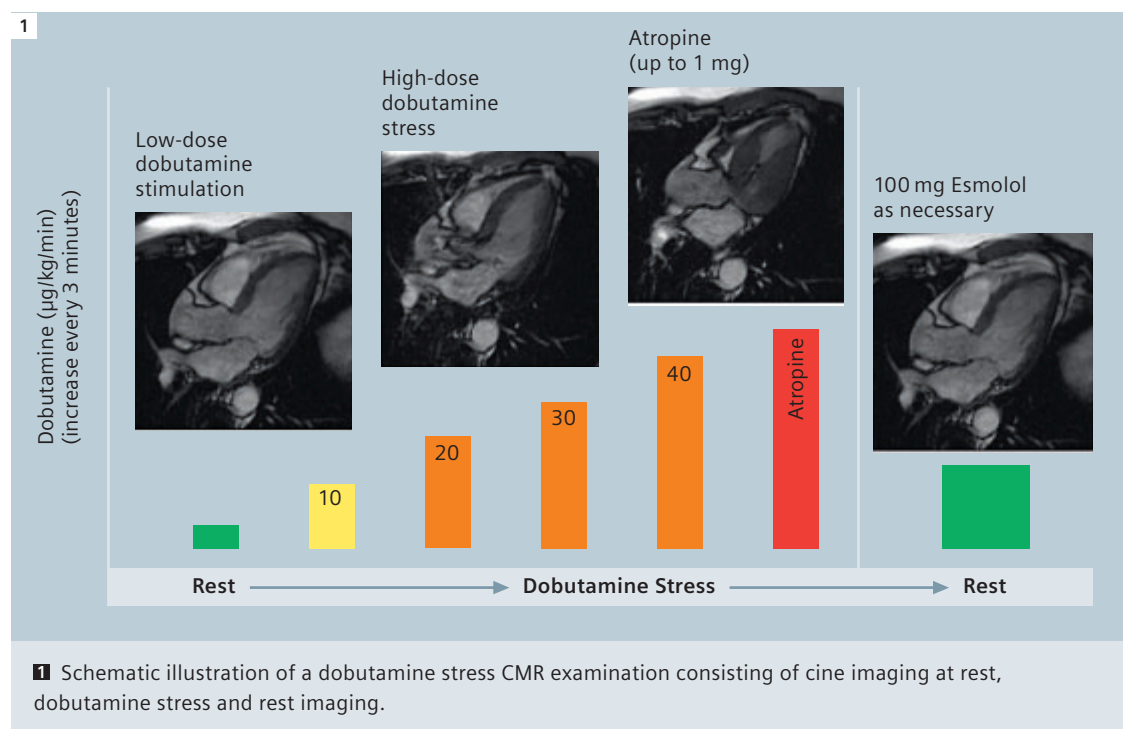


Table 1: Contraindications to dobutamine stress MRI

- Unstable angina pectoris
- Left main coronary artery disease
- Higher-grade aortic stenosis
- Hemodynamically relevant obstructive hypertrophic cardiomyopathy
- Myocarditis, endocarditis, pericarditis
- Aortic dissection / higher-grade aortic aneurysm
- Higher-grade complex ventricular arrhythmia
- History of sudden death
- Mobile left ventricular / left atrial thrombus
- Severe systemic hypertension (systolic blood pressure > 240 mmHg and/or diastolic blood pressure > 120 mmHg)
- Intractable anxiety / claustrophobia

Contraindications to atropine

- Advanced heart block
- Glaucoma
- Pyloric stenosis
- Prostatic hypertrophy

Table 2: Side effects during dobutamine / atropine stress:

- Mild complications (10–50%): Anxiety, nausea and vomiting, palpitations, heat sensations, tachypnoea, angina pectoris, hypertension, hypotension, premature ventricular beats, atrial and ventricular arrhythmia, atrial fibrillation, transient atrioventricular blocks
- Severe complications (0.1–0.3%): Sustained ventricular tachycardia, ventricular fibrillation and myocardial infarction

Table 3: Termination criteria for dobutamine stress MRI

- Target heart rate reached ($(220 - \text{age}) \times 0.85$)
- New or worsening wall-motion / thickening abnormalities
- Complex cardiac arrhythmias
- Systolic blood pressure increase > 240 mmHg and/or diastolic blood pressure > 120 mmHg
- Blood pressure decrease > 20 mmHg below baseline systolic blood pressure and/or decrease > 40 mmHg from a previous level
- Severe chest pain or other intractable symptoms

for observation of new wall motion abnormalities. If clinically relevant symptoms of arrhythmia or angina occurs or if the age predicted target heart rate or a systolic blood pressure over 240 mmHg or a diastolic blood pressure over 120 mmHg is reached, the dose of dobutamine must not be increased further. An advantage of dobutamine is its rapid onset of action and short half-life of about 120 seconds allowing for gradual drug titration. After stress termination, dobutamine side effects can be reversed by administration of a beta-blocker. To increase the sensitivity of the test, it is recommended to stop beta-blocker treatment 24–48 h prior to the examination [20].

Contraindications to dobutamine stress CMR, side effects, and termination criteria are listed in Tables 1, 2 and 3, respectively.

Due to the risk of severe side effects of stress testing, patients have to be closely monitored for their safety. Resuscitation equipment and trained personnel must be available.

Diagnostic criteria and image analysis

For standardized assessment and documentation of CMR the use of the 17-segment model of the American Heart Association is recommended [21]. It is generally accepted and enables comparability to other imaging modalities. The left ventricle will be divided into a

- basal,
- mid-cavity and
- apical short axis section.

With regard to the circumferential location, the basal and mid-cavity slices are further subdivided into six segments of 60° each, named

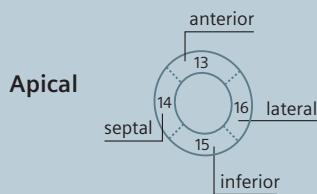
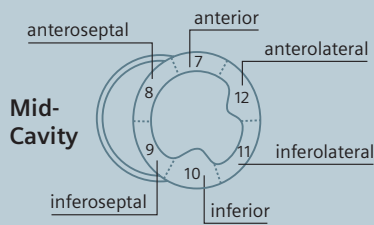
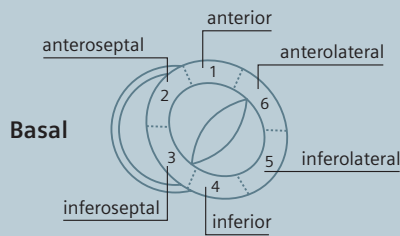
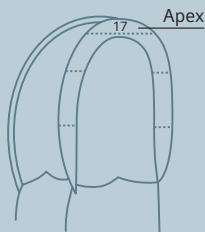
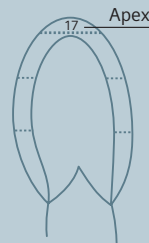
- anterior,
- anteroseptal,
- inferoseptal,
- inferior,
- inferolateral,
- anterolateral

and numbered anticlockwise from 1 (basal anterior) to 6 (basal anterolateral) respectively from 7 (mid anterior) to 12 (mid anterolateral). The apical slice is subdivided into four segments, named

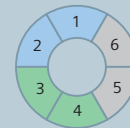
- anterior,
- septal,
- inferior and
- lateral

and numbered anticlockwise from 13 (apical ante-

2A

Short Axis (SA)**Horizontal Long Axis (HLA) (4 Chamber)****Vertical Long Axis (VLA) (2 Chamber)**

2B

Coronary Artery Territories**Short Axis (SA)****Basal****Mid****Apical****Vertical Long Axis****Mid**

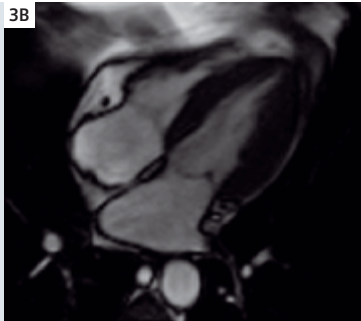
■ LAD
 ■ RCA
 ■ LCX

2 Recommendation of the American Heart Association for standardized myocardial segmentation and nomenclature in cardiac imaging. (Adapted from Cerqueira et al. [21])

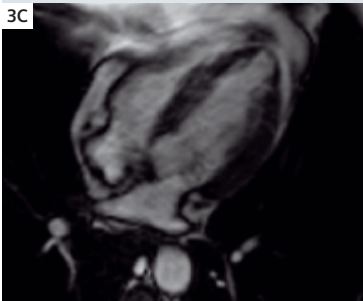
3A



3B



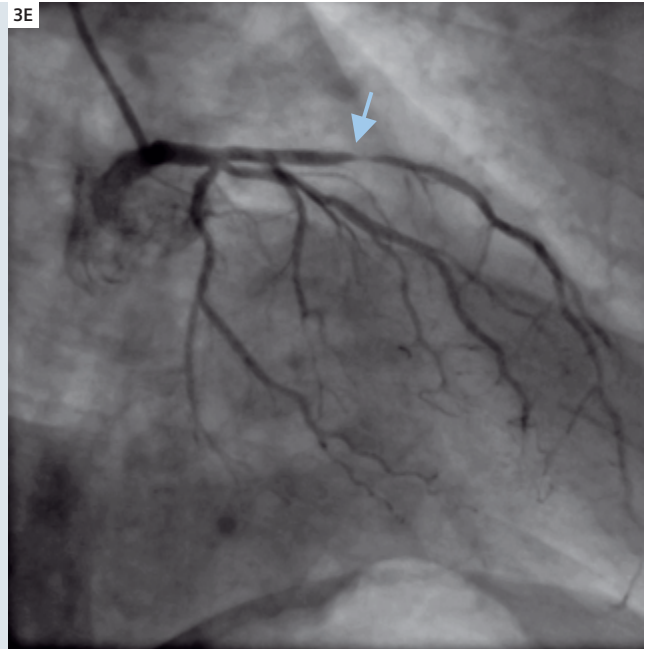
3C



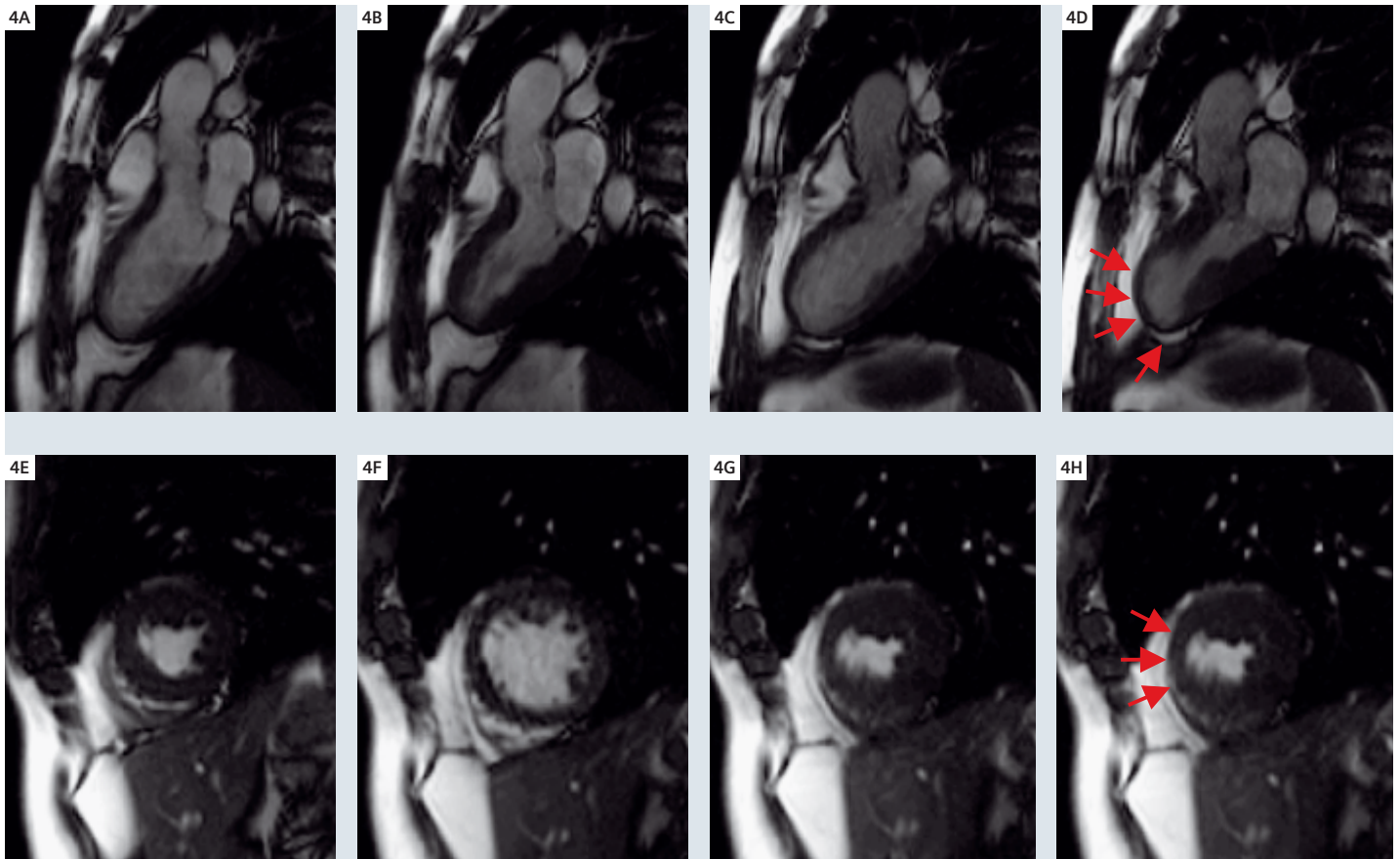
3D



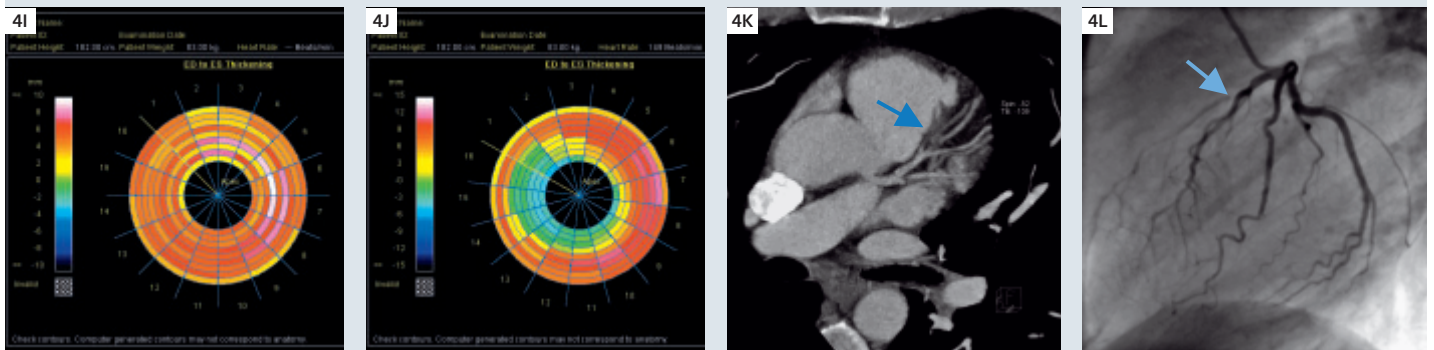
3E



3 (A–D): CMR images at rest (top) and at peak dobutamine stress (bottom) showing LV end-diastolic (l.), and end-systolic (r.) frames from a four-chamber view in a patient with normal contraction at rest and with inducible ischemia clearly visible as hypokinesia apical (red arrows). (E): Corresponding angiogram of the left coronary artery showing a high-grade LAD stenosis (blue arrow) in the same patient.



4 (A–D): End-diastolic and end-systolic frames from an apical long-axis view of the left ventricle (three chamber view) and **(E–H):** midventricular shortaxis view at rest (left) and at peak dobutamine stress (right) in a patient with inducible ischemia. Red arrows mark the region from anteroseptal midventricular to the apex that shows an impaired contractile response with pronounced wall motion abnormality and reduced thickening.



4 (I–J): Bulls eye plots of enddiastolic to endsystolic thickening at rest (left) and at peak dobutamine stress (right) in the same patient.

4 (K–L): Dual source computed tomography (DSCT) coronary angiography (left) and conventionally coronary angiography (right) reveal a subtotal stenosis of the LAD (blue arrows).

rior) to 16 (apical lateral). The apical cap represents the muscle at the tip of the ventricle and is defined as segment 17, called the apex (Figure 2). During high-dose dobutamine stress CMR all 17 left ventricular segments should be analyzed. Therefore, the acquisition of not less than three short-axis slices (basal, mid-cavity, apical) and at least one additional long-axis plane (two-, four- or three-chamber view) is recommended for evaluation of the apical region. At all stress levels an assessment of regional myocardial contractility is performed, including rest and post-stress phase. A **normal** wall motion response at dobutamine stress CMR is defined as development of hyperkinetic wall motion or preservation of the resting contraction pattern during dobutamine infusion. A pathologic response is characterized by transient wall motion abnormalities in at least one segment that was graded normal at rest (Figure 3). Segmental wall motion is graded **hypokinetic**, if endocardial inward movement and systolic wall thickening appeared decreased but not absent. A segment is graded **akinetic** if it shows lack of inward endocardial motion and absence of systolic wall thickening. A segment is graded **dyskinetic**

if it demonstrated paradoxical systolic outward movement of the endocardial border or systolic wall thinning [2].

The location of segments with normal and pathologic wall motion are compared to the perfusion territory of the main epicardial coronary arteries which are defined by the AHA recommendations [21]. Wall motion abnormalities in anterior, antero-septal, and septal segments are usually attributed to the left anterior descending artery (LAD), those in inferior and inferoseptal segments to the right coronary artery (RCA), and those in lateral segments to the circumflex artery (RCX). A coronary artery is considered as significantly stenosed if at least one of the segments located in its territory was abnormal at dobutamine stress CMR (Figure 4). If no segment was abnormal, the corresponding coronary artery is graded to have no relevant stenosis.

A coronary artery is considered as significantly stenosed if at least one of the segments located in its territory was abnormal at dobutamine stress CMR.

Discussion

High-dose dobutamine stress CMR is currently an established method for the assessment of stress inducible regional left ventricular wall motion abnormalities due to its high diagnostic accuracy, feasibility and versatility (Table 4).

Table 4: Dobutamine stress MRI for detection of significant CAD compared with conventional coronary angiography.

Author	Year	Sensitivity	Specificity	Number of patients
Pennell et al.	1992	91%	–	25
van Rugge et al.	1993	81%	100%	45
Baer et al.	1994	84%	–	35
van Rugge et al.	1994	91%	80%	39
Nagel et al.	1999	86%	86%	172
Hundley et al.	1999	83%	83%	41
Kuijpers et al.	2003	96%	95%	68
Paetsch et al.	2004	89%	80%	79
Wahl et al.	2004	89%	84%	160
Syed et al.	2005	89%	100%	19

Dobutamine stress MRI is a reliable, clinically safe and robust method to evaluate the functional significance of coronary lesions with high diagnostic accuracy.

Previous studies have demonstrated the clinical feasibility of CMR in conjunction with pharmacological stress testing for the detecting of relevant CAD [6, 10, 12, 14]. Pennell et al. [10] reported the first use of dobutamine stress in conjunction with CMR in 25 patients with chest pain by using an intermediate dose of dobutamine (up to 20 µg/kg/min). He found a 91% incidence of dobutamine-induced reversible wall motion abnormalities in patients with CAD.

Baer et al. [11] and van Rugge et al. [12] have shown that dobutamine MRI detects overall CAD with a sensitivity of 85% and 91%, respectively by using moderate doses of dobutamine up to 20 µg/kg/min.

Nagel et al. provided the first report on the efficacy and safety of high-dose dobutamine (up to 40 µg/kg/min and additional use of atropine as needed) combined with CMR for the detection of CAD in a larger patient population. In this study dobutamine stress CMR proved to be superior to dobutamine stress echocardiography in terms of sensitivity (86% vs. 74%) and specificity (86% vs. 70%) in 172 patients. The superior results of CMR were attributed to its better overall image quality, which was graded good or very good in 82%, but only in 51% of echocardiography studies [6]. Hundley et al. performed high-dose dobutamine CMR for the detection of ischemia in 41 patients who were not well suited for second harmonic stress echocardiography because of poor acoustic windows and reported a sensitivity and specificity of 83% for the detection of a coronary stenosis > 50% luminal diameter [22].

Wahl et al. performed high-dose dobutamine-atropine stress CMR after coronary revascularization in 160 consecutive patients with pre-existing wall motion abnormalities at rest. CMR displayed good results, with sensitivity of 89% and specificity of 84% for detection of significant CAD [23].

Using TrueFISP or SSFP cine sequences Paetsch et al. found high-dose dobutamine stress CMR to be superior to adenosine stress perfusion MR for detection of significant CAD, with sensitivities and specificities of 89% and 80% and 91% and 62%, respectively in 79 patients without history of prior infarction [26].

Syed et al. had shown a high interstudy reproducibility ($p = 0.91$) and a low interobserver variability ($\kappa = 0.81$) of dobutamine stress MRI in 19 patients with severe coronary disease [27].

The overall sensitivity and specificity for the assessment of ischemia induced wall motion abnormalities for detecting CAD achieved with dobutamine stress CMR is in good agreement with stress echocardiography studies yielding sensitivities of 78% to 96% and specificities of 66% to 85% [28–32].

Conclusion

Dobutamine stress CMR using a state of the art fast imaging sequence is a reliable and clinically safe and robust method to evaluate the functional significance of coronary lesions by detecting ischemic induced wall motion abnormalities.

Contact

Markus Jochims, M.D.
Department of Cardiology and Angiology
Elisabeth Hospital
Klara-Kopp-Weg 1
45138 Essen
Germany
m.jochims@elisabeth-essen.de

References and recommended reading

- 1 Sugishita J, et al. Dissociation between regional myocardial dysfunction and ECG changes during myocardial ischemia induced by exercise in patients with angina pectoris. *Am Heart J* 1983;106:1–8.
- 2 Geleijnse ML, et al. Methodology, feasibility, safety and diagnostic accuracy of dobutamine stress echocardiography. *J Am Coll Cardiol* 1997;30(3):595–606.
- 3 La Canna G, et al. Echocardiography during infusion of dobutamine for identification of reversibly dysfunction in patients with chronic coronary artery disease. *J Am Coll Cardiol* 1994;23:617–26.
- 4 Hoffmann R, et al. Analysis of interinstitutional observer agreement in interpretation of dobutamine stress echocardiograms. *J Am Coll Cardiol* 1996;27:330–6.
- 5 Zoghbi AW, Barasch E. Dobutamine MRI: A serious contender in pharmacological stress imaging? *Circulation* 1999;99:730–2.
- 6 Nagel E, et al. Noninvasive diagnosis of ischemia-induced wall motion abnormalities with the use of high-dose Dobutamine Stress MRI: Comparison with dobutamine stress echocardiography. *Circulation* 1999;99:763–70.
- 7 Sechtem U, et al. Cine MR imaging: potential for the evaluation of cardiovascular function. *AJR* 1987;148:239–46.
- 8 Pflugfelder PW, et al. Quantification of regional myocardial function by rapid cine MR imaging. *AJR* 1988;150:523–9.
- 9 Reichek N. Magnetic resonance imaging for assessment of myocardial function. *Magn Reson* 1991;Q 7:255–74.
- 10 Penell DJ, et al. Magnetic resonance imaging during dobutamine stress in coronary artery disease. *Am J Cardiol* 1992;70:34–40.
- 11 Baer FM, et al. Coronary artery disease: Findings with GRE MR Imaging and Tc-99m-Methoxyisobutyl-Isonitrile SPECT during simultaneous dobutamine stress. *Radiology* 1994;193:203–9.
- 12 Van Ruge FP, et al. Magnetic resonance imaging during dobutamine stress for detection and localization of coronary artery disease: quantitative wall motion analysis using a modification of centerline method. *Circulation* 1994;90:127–38.
- 13 Pennell DJ, et al. Dipyridamole magnetic resonance imaging: a comparison with thallium-201 emission tomography. *Br Heart J* 1990;64(6):362–9.
- 14 Pennell DJ, et al. Magnetic resonance imaging during dobutamine stress in coronary artery disease. *Am J Cardiol* 1992;70(1):34–40.
- 15 Baer FM, et al. Feasibility of high-dose dipyridamole-magnetic resonance imaging for detection of coronary artery disease and comparison with coronary angiography. *Am J Cardiol* 1992;69(1):51–6.
- 16 Jochims, et al. Dobutamine stress magnetic resonance imaging: a reliable alternative to stress echocardiography in patients with insufficient image quality? *Eur Heart J* 1999;20:678 (abstract).
- 17 Finn, et al. Cardiac MR Imaging: State of the Technology. *Radiology* 2006;241(2):338–54.
- 18 Barkhausen J, et al. MR evaluation of ventricular function: true fast imaging with steady-state precession versus fast low-angle shot cine MR imaging—feasibility study. *Radiology* 2001;219:264–9.
- 19 Nesto RW, et al. The ischemic cascade: temporal sequence of hemodynamic, electrocardiographic and symptomatic expressions of ischemia. *Am J Cardiol* 1987;59(7):23C–30C.
- 20 Nagel E, et al. Stress cardiovascular magnetic resonance: consensus panel report. *J Cardiovasc Magn Reson* 2001;3(3):267–81.
- 21 Cerqueira, et al. Standardized myocardial segmentation and nomenclature for tomographic imaging of the heart. A statement for healthcare professionals from the Cardiac Imaging Committee of the Council on Clinical Cardiology of the American Heart Association. *Int J Cardiovasc Imaging* 2002;18(1):539–42.
- 22 Hundley WG, et al. Utility of fast cine magnetic resonance imaging and display for the detection of myocardial ischemia in patients not well suited for second harmonic stress echocardiography. *Circulation* 1999;100(16):1697–702.
- 23 Wahl A, et al. High-dose dobutamine-atropine stress cardiovascular MR imaging after coronary revascularization in patients with wall motion abnormalities at rest. *Radiology* 2004;233(1):210–6.
- 24 Secknus MA, et al. Evolution of dobutamine echocardiography protocols and indications: safety and side effects in 3,011 studies over 5 years. *J Am Coll Cardiol* 1997;29(6):1234–40.
- 25 Wahl A, et al. Safety and feasibility of high-dose dobutamine-atropine stress cardiovascular magnetic resonance for diagnosis of myocardial ischaemia: experience in 1000 consecutive cases. *Eur Heart J* 2004;25(14):1230–6.
- 26 Paetsch I, et al. Comparison of dobutamine stress magnetic resonance, adenosine stress magnetic resonance, and adenosine stress magnetic resonance perfusion. *Circulation* 2004;110(7):835–42.
- 27 Syed MA, et al. Reproducibility and inter-observer variability of dobutamine stress CMR in patients with severe coronary disease: implications for clinical research. *J Cardiovasc Magn Reson* 2005;7(5):763–8.
- 28 Marcowitz PA, Armstrong WF. Accuracy of dobutamine stress echocardiography in detecting coronary artery disease. *Am J Cardiol* 1992;69:1269–73.
- 29 Mazeika PK, et al. Dobutamine stress echocardiography for detection and assessment of coronary artery disease. *J Am Coll Cardiol* 1990;19:1203–11.
- 30 Sawada SG, et al. Echocardiographic detection of coronary artery disease during dobutamine infusion. *Circulation* 1991;83:1605–14.
- 31 Segar DS, et al. Dobutamine stress echocardiography: Correlation with coronary lesion severity as determined by quantitative angiography. *J Am Coll Cardiol* 1992;19:1197–202.
- 32 Takeuchi M, et al. Comparison of dobutamine stress echocardiography and stress thallium-201 single-photon emission computed tomography for detecting coronary artery disease. *J Am Soc Echocardiogr* 1993;6:539–602.
- 33 Kuijpers D, et al. Dobutamine cardiovascular magnetic resonance for the detection of myocardial ischemia with the use of myocardial tagging. *Circulation* 2003;107(12):1592–7.
- 34 Strach K, et al. Cardiac stress MR imaging with dobutamine. *Eur Radiol* 2006;16: 2728–38.
- 35 Mandapaka S, et al. Dobutamine Cardiovascular Magnetic Resonance: A Review. *J. Magn. Reson. Imaging* 2006;24:499–

CMR for Assessment of Valvular Disease

Brett Cowan¹, Alistair Young¹, Chris Occleshaw², Andrew Kerr³

¹Centre for Advanced MRI, University of Auckland, Auckland, New Zealand

²Department of Cardiology, Auckland City Hospital, Auckland, New Zealand

³Department of Cardiology, Middlemore Hospital, Auckland, New Zealand

Introduction

Surgical treatment of valvular heart disease (VHD) has the potential to revolutionize the lives of affected patients. Unfortunately, surgery carries the peri-operative risks of stroke, myocardial infarction and occasionally death. Longer term risks include anticoagulation for mechanical valves and the need for re-operation particularly in patients receiving bio-prosthetic valves. In patients presenting or being followed with VHD, decisions need to be made regarding appropriate medical therapy and when this should give way to surgical management. In addition to clinical factors, these decisions are dependent on the type and severity of the lesion, the presence of cardiac decompensation, and also in part on the type of operation required. Cardiac magnetic resonance (CMR) is able to provide accurate quantitative and qualitative data to inform this decision-making process. We review typical applications of CMR in the assessment of VHD, focusing on common indications, case reviews and current limitations, and concluding with exciting new applications in the area of valve mapping.

Background

The majority of stenotic and regurgitant VHD affects the mitral and aortic valves and is either congenital in origin, or acquired as a result of degenerative processes, rheumatic fever, infective endocarditis or ischaemic heart disease. This article overviews practical methodologies which can be used to investigate aortic regurgitation (AR), aortic stenosis (AS) and mitral regurgitation (MR), accompanied by general comments on velocity and flow imaging. The decision to proceed with medical or surgical

treatment is currently typically based on clinical symptoms and an echocardiographic study. Echocardiography is readily available, portable, inexpensive and achieves high temporal and spatial resolution and is therefore well established in the evaluation of VHD. It is particularly well suited to the visualization of small valvular vegetations in endocarditis. It has the disadvantages of limited acoustic windows, poor image quality in obese patients or those with pulmonary disease, difficulties with consistently aligning a Doppler beam along the direction of blood flow and variability due in part to operator dependence. Doppler techniques are able to measure velocity with precision, but this is not always reflected in flow volumes.

The advantages of CMR for the evaluation of VHD include –

- flexibility to acquire flow or anatomical studies in any arbitrary plane,
- high-quality images (without requiring acoustic windows) in virtually all patients,
- accurate and reproducible measurements of velocity and flow, and
- the ability to consistently perform a full valvular study including ventricular volumes, hemodynamic evaluation and anatomical morphology.

The CMR assessment of stenotic, regurgitant or mixed VHD can be divided into three main components:

- (1) An assessment of the consequences of the valve lesion on left and right ventricular function and mass (see article on ventricular function) and effect on aortic and atrial size,
- (2) haemodynamic evaluation of lesion severity by measurement of stenotic velocities or

CMR is able to provide accurate quantitative and qualitative data to support the decision-making process of therapy in valvular disease.

CMR allows a comprehensive evaluation of valvular disease by imaging morphology, hemodynamics and ventricular volumes.

regurgitant volumes, and
(3) anatomical imaging including planimetry of the valve orifice, and direct visualization of the valve and leaflet morphology.

Many previous difficulties with valvular MR such as dealing with arrhythmias, difficulty with direct visualization of leaflet morphology and time required to perform quantitative post-processing have improved significantly over the last few years. CMR is now complementary to echocardiography and can offer precise additional important information on regurgitant volume, valve geometry and lesion severity.

Indications for CMR in valvular disease

In 2006 the American College of Cardiology Foundation [1] (in conjunction with other professional bodies including the Society for Cardiovascular Magnetic Resonance) gave CMR an appropriateness rating for "Characterization of native and prosthetic cardiac valves – including planimetry of stenotic disease and quantification of regurgitant disease" and "Patients with technically limited images from echocardiogram or TEE" of 'A' with a score of 8/9. An appropriate imaging study was defined as one "in which the expected incremental information, combined with clinical judgment, exceeded the expected negative consequences (defined as procedural risks, and the impact of false negatives or false positives) by a sufficiently wide margin that the procedure was generally considered acceptable care and a reasonable approach for the indication". CMR therefore plays an important role where echocardiographic windows are poor, there are contraindications to TEE, where a high degree of accuracy

is desirable or where the study forms part of a broader investigation already being performed by MR (for example in congenital heart disease). Standard contraindications to MR apply including pacemakers, ventricular assist devices and implanted defibrillators but prosthetic valves are safe in field strengths up to 1.5 Tesla. Although magnetic forces and heating in the valves are not a cause for concern, the presence of metal may unfortunately produce problematic sequence-dependent local image artifacts.

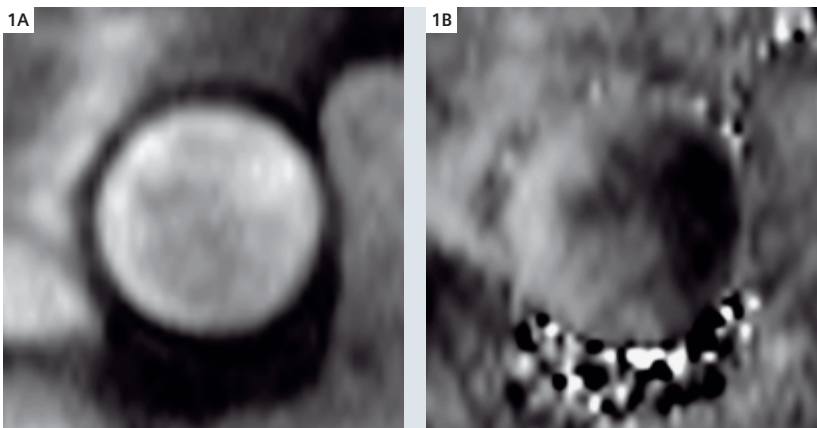
Phase contrast imaging

The mainstay of haemodynamic evaluation is phase contrast (PC) imaging. In a standard MR image, each small image element (known as a pixel) contains a single grey-scale value. In a PC study there are two images as each pixel contains two values, one for the signal intensity (magnitude) and the second for the velocity of blood flowing through the image plane (phase). In the velocity image, mid-grey represents stationary tissue, white the maximum velocity in the through-plane direction, and black the maximum velocity in the reverse direction (Figure 1).

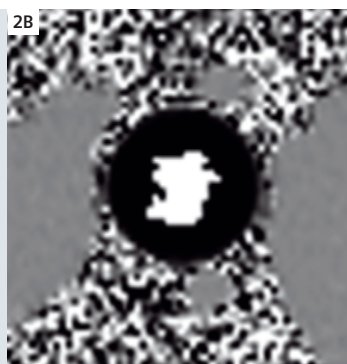
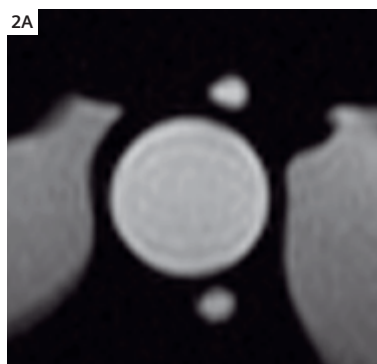
This maximum velocity that can be measured is known as the 'Velocity ENCoding' (VENC) value and this may be set by the user depending on the anticipated peak velocity in the vessel of interest. Typical VENC's for normal aortic flow are in the region of 150 cm/sec, increasing to 400 cm/sec or more for aortic stenosis. If the VENC is set too low, a problem known as 'aliasing' occurs where the blood velocity exceeds the VENC. In this case aliased pixels which should appear black, appear white (Figure 2), or vice versa, and this prevents quantitative analysis. Aliasing is typically seen on the systolic

CMR is complementary to echocardiography and offers precise information on regurgitant volume, valve geometry and lesion severity.

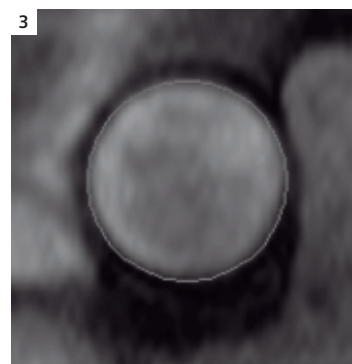
In a phase-contrast study there are two images as each pixel contains two values, one for the signal intensity (magnitude) and the second for the velocity of blood flowing through the image plane (phase).



1 (A) Standard magnitude image of an aorta, and (B) its corresponding velocity or phase image (both at 424 msec after the R-wave). On the phase image, white represents flow through the image plane in one direction and black in the opposite direction. Mid-grey represents stationary tissue. Some diastolic-phase regurgitation is accompanied by forward flow as shown by the presence of black and white regions in the velocity image. "Salt and pepper" or "checker board" noise in the velocity image under the aorta is caused by air in lung tissue where there are insufficient protons to return a reliable signal.



2 (A) Magnitude image of water flowing through a pipe, with (B) its velocity or phase image showing aliasing due to the VENC being set too low. The peripheral slower moving water is correct, but once the velocity reaches and then exceeds the VENC, there is an abrupt transition from black to white where the velocities are no longer correct.



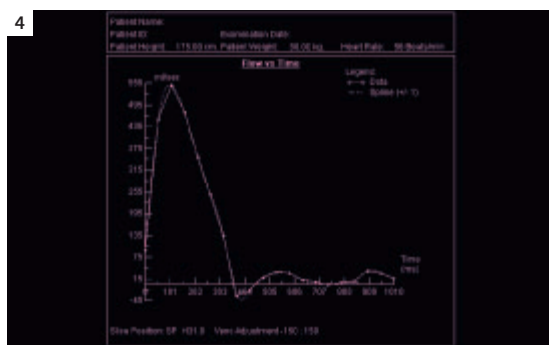
3 Argus contour outlining the region of interest in the aorta. Contouring is performed semi-automatically for each frame through the cardiac cycle cine using both the magnitude and phase images.

frame because this contains the highest velocities and if this occurs, the sequence should be repeated. If the VENC is set too high, accuracy and signal-to-noise ratio (SNR) is compromised because only a small subset of the available grey scale is utilized. Where the peak velocity is unknown or difficult to estimate, it may be useful to acquire a few velocity scouts to enable the VENC to be chosen with more certainty. The VENC should be set comfortably above (125–150%) the highest velocity expected to be measured.

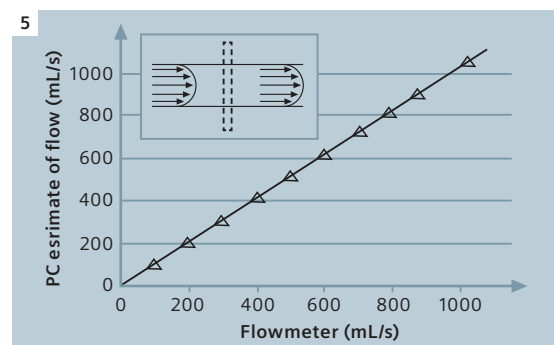
The main PC planning issues to be considered are to position the imaging slice at approximately right angles to the vessel of interest (small and even

moderate errors in angulation have little or no effect on the flow results but definition of the border of the vessel may be more difficult), choice of the number of frames for the cine (typically 20–30), selection of the VENC, and to select either a breath-hold or free-breathing approach (breath-hold is faster but has lower temporal and spatial resolution).

Once a cine flow series has been acquired, the vessel(s) of interest are outlined semiautomatically on all frames through the cardiac cycle using the Argus Flow analysis software (Figure 3), and the velocity in each pixel within this contour multiplied by its area, and summed to determine the total



4 Argus flow-versus-time graph for the aorta. The systolic phase with a peak flow rate of 555 ml/s is followed by very low levels of flow in diastole demonstrating normal valvular function.



5 Validation of phase contrast on a Siemens MAGNETOM Avanto scanner. Water was pumped through a straight pipe (internal diameter 17 mm) and compared to an electromagnetic flowmeter which acted as the gold standard. The maximum error was 2.9% (average error $1.9 \pm 0.7\%$, $r=0.99$).

The Flow Package contains a Flow Scout which enables fast assessment of up to 5 VENCs.

flow for each frame (Figure 4). Peak and average velocities, net flow and other parameters are then calculated automatically.

The high accuracy of PC imaging during non-pulsatile flow of water through a pipe with a diameter equal to the adult aorta on an Siemens MAGNETOM Avanto system is demonstrated in Figure 5.

Aortic regurgitation

Case 1: A 25-year-old man presented with dyspnoea and clinical evidence of aortic regurgitation. An initial trans-thoracic echo reported severe aortic regurgitation but was technically limited for left ventricular (LV) and aortic measurements. CMR was requested to better quantify LV size and function, lesion aetiology and severity, and aortic dilatation.

After establishing a good quality ECG signal, the patient was positioned with the phased-array body coil anteriorly and standard cardiac scouts performed followed by breath-hold short and long axis TrueFISP (SSFP) cines for ventricular function. Three parallel oblique coronal slices were planned along the long axis of the aortic root from an axial scout, and the one showing the best view of the aortic root selected to plan the aortic flow study (Figure 6 shows slice planning in a normal volunteer including a three-chamber view). A PC study was acquired using a segmented k-space breath-hold sequence with 24 frames, VENC=150 cm/s, slice thickness 8 mm, pixel size 1.5 x 1.5 mm, and with an acquisition matrix of 192 x 256.

The analysis produced forward and regurgitant volumes of 223 and 90 ml/s respectively from which a regurgitant fraction of 40% was calculated. With an LV end-diastolic volume of 503 ml and end-systolic volume of 280 ml the LV ejection fraction (EF) was reduced at 44%. The aortic root was assessed using standard aortic imaging techniques and showed maximum dilatation at the level of the aortic sinuses of 5.8 cm.

In order to visualize the leaflet morphology, True FISP cine images were obtained in the long and short axes of the aortic valve. The short axis (Figure 7) demonstrated an unusual congenital quadricuspid aortic valve with four unequal cusps and sinuses instead of the normal three. Interestingly each of the two pairs of leaflets were fused, resulting in a functionally bicuspid valve and there was central AR secondary to the leaflet abnormalities. On the basis of this information and the aortic imaging



6 Planning of an aortic flow study in a normal volunteer using (A) an aortic scout and, (B) a three-chamber view.

Argus Flow® allows for automatic calculation of peak and average velocities, flow, net flow and other parameters needed for accurate assessment of valvular disease.



7 Case 1: Quadricuspid aortic valve (arrowed).

Valvular regurgitant fraction can be assessed accurately using PC CMR. Cine images can be used for the evaluation of leaflet morphology.

showing a dilated root and proximal ascending aorta, the patient was referred for aortic valve and root replacement.

Background phase correction

It is common for eddy currents to be induced in the frame of the magnet by the gradients and these can produce a background phase (and hence velocity) signal in stationary tissue. A 'background phase correction' may be applied in Argus Flow by selecting a region of stationary tissue and subtracting this from the results in the vessel of interest.

Although this may provide some correction, unfortunately the background phase is not always constant across the entire FoV and may vary linearly [2], so that the selection of a region of stationary tissue relatively remote from the vessel of interest may introduce additional errors. More recent magnet designs such as the Siemens MAGNETOM Avanto have significantly lower eddy currents compared to older generation magnets and this has significantly reduced this problem. In the future, automated algorithms that calculate the true background phase distribution in all regions of the image are likely to provide a better solution.

Aortic stenosis

Case 2: A 70-year-old man presented with shortness of breath and clinical evidence of aortic stenosis, but had an equivocal echocardiographic study and MRI was requested to image the valve. The peak velocity in the stenotic jet is an important determinant of lesion severity and may be used as part of a calculation of effective valve area. Stenotic jets may be eccentric and the exact position of the maximum velocity may not always be readily apparent. It is possible to acquire multiple PC images transverse to the aortic root and to check each for their maximum velocity, or to acquire a longitudinal view of the aorta using in-plane (as opposed to through-plane) velocity encoding. In this case, three PC slices with a VENC of 400 cm/sec were acquired transverse to the aorta with a peak velocity of 245 cm/sec found in the jet. Valve area was calculated with the continuity equation using PC data obtained from both below the valve in the left ventricular outflow tract and at valve level. Ventricular function was good and in the presence of moderate hypertrophy the criteria for valvular replacement was not met and he was managed medically with regular follow-up.

Accurate assessment of velocity in the jet is essential for reliable diagnosis. Recent data from our laboratory has demonstrated that in the most severe cases of aortic stenosis, where jet velocities can exceed 400 cm/sec with very high levels of turbulence, there can be significant loss of signal due to intra-voxel dephasing and other effects. In order to minimize these effects, it is helpful to keep the TE as short as possible. When signal loss is severe, the PC images may develop evidence of 'salt and pepper' noise (as opposed to aliasing) indicating that the results are likely to be unreliable. When evaluating very high velocity jets, it is important to check the magnitude image in the vessel of interest for dark areas indicative of signal loss and low SNR. The velocity results may be unreliable in these regions, especially if the phase images also contain salt and pepper noise in the same region.

It is common to see flow artifacts in cines which can give a useful subjective impression of any jets or regurgitant flow that may be present. Although correlation with echocardiography has been shown, some caution must be exercised when attempting to accurately quantify or grade the severity of the lesion based on these subjective impressions. These techniques can be useful to quickly determine if there are likely to be solitary or multiple orifices in the valve as can sometimes be seen in mitral regurgitation.

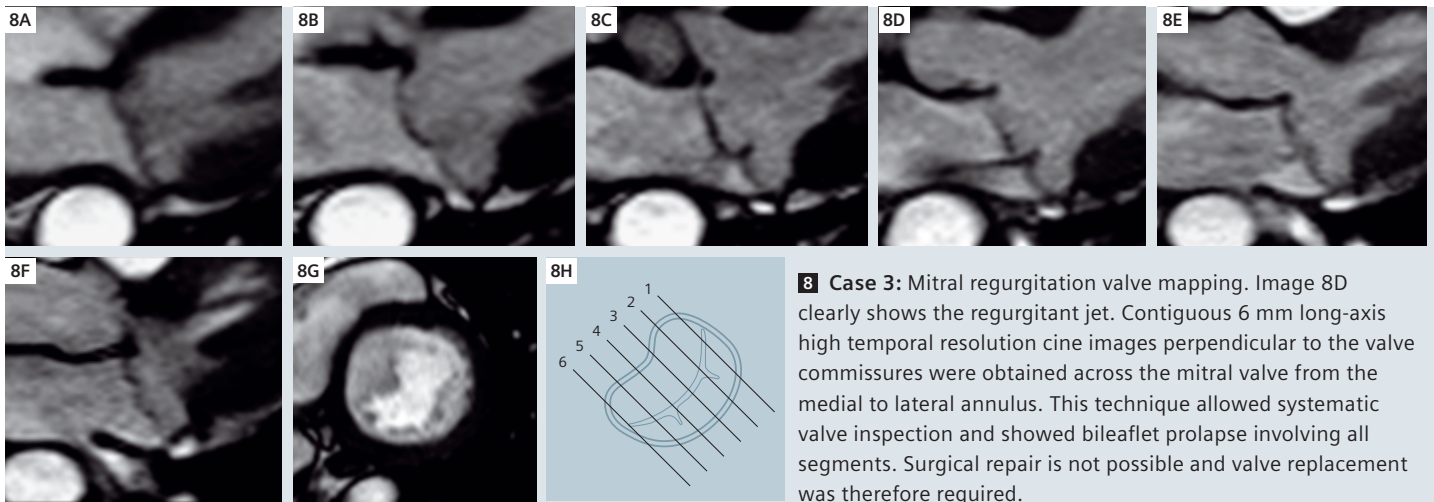
True-FISP cines in the plane of the aortic valve may be used to visualize and directly planimeter the area of the systolic opening providing a valve area independent of velocity or flow measurements, pressure gradients or formulae. These have been shown to be correlated with catheterization data and reasonably well correlated to echocardiographic results in aortic stenosis [3].

Mitral regurgitation

Case 3: A 55-year-old woman with a history of rheumatic fever had been followed for mitral regurgitation for 15 years. Her clinical status had deteriorated and there was uncertainty as to whether this was due to her rheumatic valvular disease or other significant co-morbidities including ischaemic heart disease. She was high risk for surgery and was referred for a detailed quantitative evaluation of her valve as part of a delayed enhancement and ventricular function CMR workup. The mitral valve descends by approximately 12 mm

MAGNETOM Avanto has significantly lower eddy currents than older generation magnets, enabling highly reliable flow measurements.

Maximum velocity assessment in stenotic jets can be done using longitudinal in-plane phase-contrast imaging.



8 Case 3: Mitral regurgitation valve mapping. Image 8D clearly shows the regurgitant jet. Contiguous 6 mm long-axis high temporal resolution cine images perpendicular to the valve commissures were obtained across the mitral valve from the medial to lateral annulus. This technique allowed systematic valve inspection and showed bileaflet prolapse involving all segments. Surgical repair is not possible and valve replacement was therefore required.

during systole, and this movement through a fixed imaging plane makes flow measurement at the mitral annulus challenging. In addition, direct measurement of a regurgitant jet is technically difficult because of jet eccentricity, possible multiple jets, and jet turbulence. It is therefore usual to measure mitral regurgitant volume indirectly by measuring the antegrade flow in the aorta with PC imaging, and comparing this to the ventricular stroke volume calculated from EDV – ESV with the difference representing the mitral regurgitant flow.

The PC flow results from the aorta showed a SV of 65 ml/m², and the ventricular function an EDV of 345 ml/m², ESV of 197 ml/m², SV of 148 ml/m², and ejection fraction of 43%. This equated to a regurgitant fraction of 56% (mitral valve regurgitant volume = LV ventricular SV – aortic SV) at the mitral valve in a dilated and de-compensating ventricle and the patient was referred for surgery. The delayed enhancement scan showed no evidence of previous myocardial infarction. With improvements in hardware and software, it is now possible to acquire high quality images of the mitral valve leaflets in a similar way to those shown for the aortic valve. Generally a thinner slice (5 mm) and increased in-plane and temporal resolution (within the limits of maintaining adequate SNR) are helpful in improving leaflet definition. Leaflets are best appreciated in cine mode, but representative images from across the regurgitant valve are shown in Figure 8. The slices were acquired serially across the valve and are especially useful for mapping leaflet prolapse or defining detailed valve morphology for surgical planning where repair is being contemplated. Left atrial measurements are an important part of

the evaluation and may be made from long axis cine views and volume estimated using standard echocardiographic formulae. If serial short axis slices are acquired through the left atrium, left atrial volume can be measured with more sophisticated software without geometric assumptions. In order to overcome the issues associated with mitral movement, newer research sequences are able to define the motion of the valve annulus and move the imaging slice with the valve through the cardiac cycle to ensure the acquisition remains aligned with the annulus. This technique may make the direct measurement of mitral regurgitant fraction clinically feasible.

Hardware

Most new generation magnets with cardiac gating and post-processing software are capable of performing valvular assessments without additional special equipment. In terms of maintaining flow measurement accuracy, low eddy currents are an important consideration and some older generation magnets with higher eddy currents may not be as well suited to flow studies.

Summary

CMR assessment of valvular disease is an appropriate indication and feasible on current equipment.

References

- 1 Hendel RC et al. ACCF/ACR/SCCT/SCMR/ASNC/NASCI/SCAI/SIR 2006 Appropriateness criteria for cardiac computed tomography and cardiac magnetic resonance imaging. *J Am Coll Cardiol* 2006;48:1475–97.
- 2 Lankhaar J et al. Correction of phase offset errors in main pulmonary artery flow quantification. *J Mag Res Img* 2005;22:73–79.
- 3 Friedrich MG. Quantification of valvular aortic stenosis by magnetic resonance imaging. *Am Heart J* 2002;144(2):329–34.

Using CMR, high-resolution images of the mitral valve leaflets can be acquired for defining detailed valve morphology.

The Flow Package for image acquisition and Argus Flow* for post-processing are available for all 1.5 and 3T systems.

Contact

Associate Professor
Brett Cowan
Centre for Advanced MRI
c/o University of Auckland
Private Bag 92019
Auckland, New Zealand
b.cowan@auckland.ac.nz

Evaluation of Cardiac Masses by CMR

Oliver Bruder, M.D.; Markus Jochims, M.D.; Christoph Jensen, M.D.; Georg V. Sabin, M.D.

Department of Cardiology and Angiology, Elisabeth Hospital Essen, Germany

Introduction

The prevalence of primary tumors of the heart is less than 0.3%, making them a relatively rare cardiac disease compared to other cardiovascular disease entities [1].

Secondary cardiac tumors are approximately 20 times more common according to post mortem studies [2]. Secondary tumors are the result of local invasion of cancer or metastatic involvement of the myocardium and/or pericardium.

Although cardiac tumors are rare, the clinical relevance is high as primary tumors can be malignant, and therefore lethal if left untreated, but curable if excised in time.

Ventricular thrombi are an important differential diagnosis of cardiac masses. Thrombi are in most cases related to prior myocardial infarction with extensive left ventricular aneurysm formation, and carry a high risk of embolic complications. Apart from thrombi, there is a wide variety of diseases that can be confused with primary cardiac tumors such as:

- vegetations,
- atypical focal variants of hypertrophic cardiomyopathies,
- abscesses,
- anatomic variants,
- pericardial cysts, or
- juxtacardiac findings such as diaphragmatic hernia.

Cardiac tumors can be classified by histopathology (malignant, benign), location (pericardial, intracavitary, paracardial, intramyocardial), morphology (sessile, pedunculated, or by the effect on blood flow (obstructive, non-obstructive).

In pre-MRI times diagnosis of cardiac tumors was,

due to insufficient imaging techniques, mainly confined to autopsy, leaving the majority of tumors undiagnosed during life time.

With the rapid development of CMR, cardiac tumors are diagnosed more frequently.

Benign cardiac tumors

75% of all primary tumors of the heart are benign, including myxomas, rhabdomyomas, fibromas, papillary fibroelastomas, lipomas, hemangiomas and teratomas.

Myxomas account for 50% of all cardiac tumors. They are typically located within the left atrium, although left ventricular, or right atrial involvement occurs. The morphology is rather polypoid than round-shaped, and they are often pedunculated-prolapsing into the mitral valve apparatus or even the left ventricle during diastole [3].

On CMR, myxomas are diagnosed by the typical location close to the interatrial septum, high signal intensity on T2-weighted spin-echo sequences, and heterogeneous enhancement following contrast administration [4]. Myxomas can grow rather large, and may be complicated by mitral valve obstruction, endocarditis or thrombotic embolism.

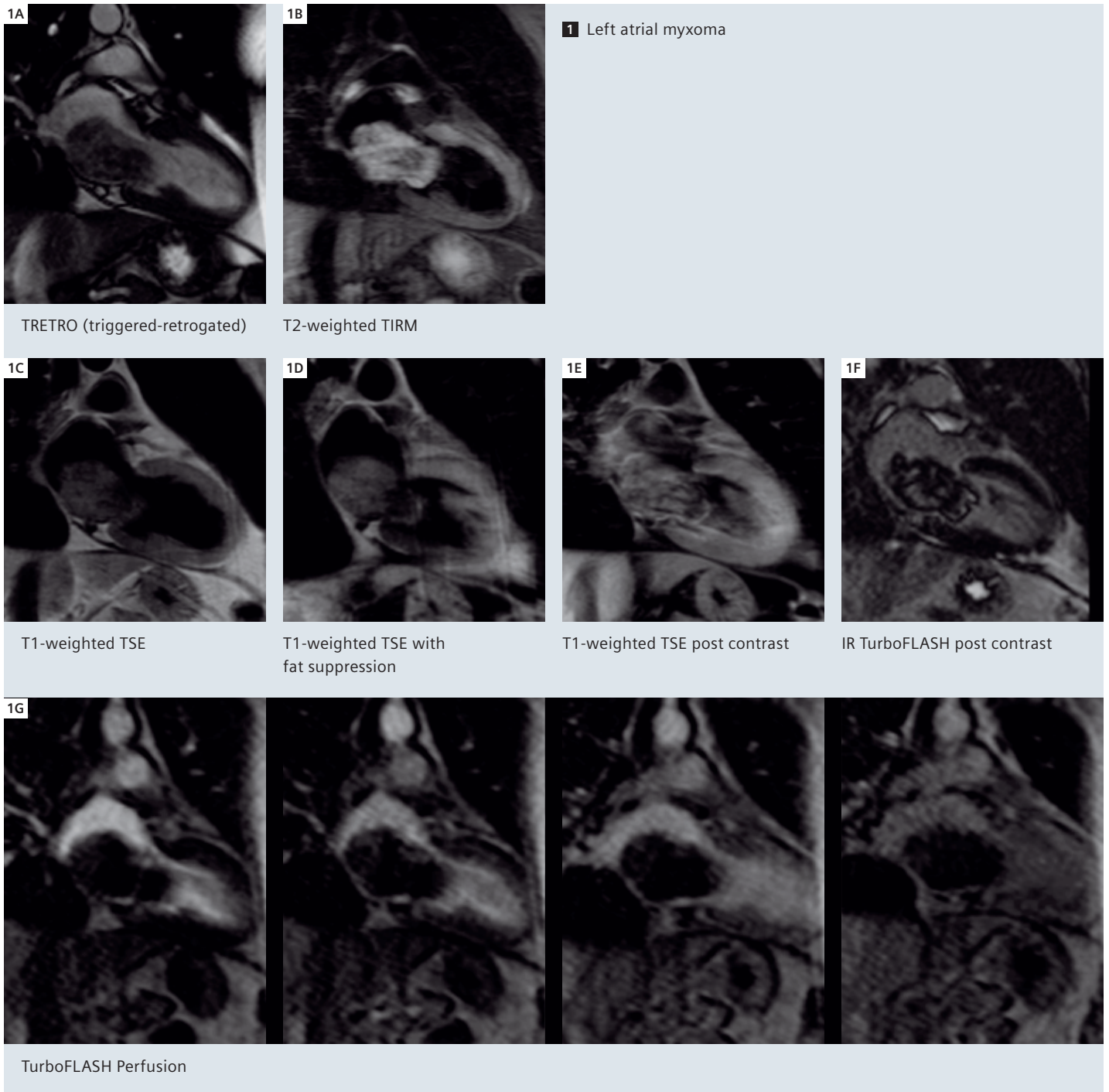
Rhabdomyomas present as several small tumors in the interventricular septum myocardium. Rhabdomyomas are most frequently found in young children.

Fibroelastomas are very small, mobile tumors that are fixed to the aortic or mitral valve leaflets.

Malignant cardiac tumors

25% of all primary cardiac tumors exhibit local tissue invasion and metastasize, and are therefore classified as malignant.

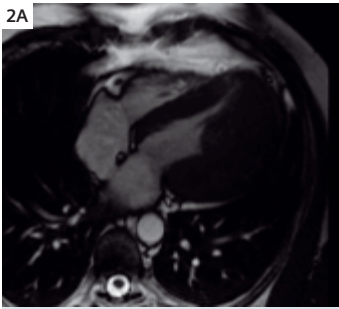
With the rapid development of CMR cardiac tumors are diagnosed more frequently. Secondary cardiac tumors are twenty times more common than primary tumors.



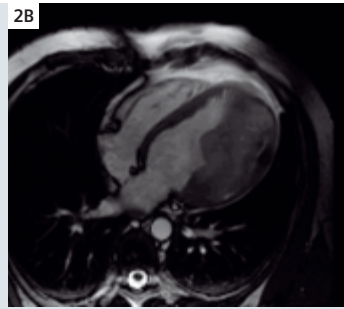
Sarcomas constitute the majority of malignant primary cardiac tumors (95%) including – in order of descending frequency – angiosarcomas (50%), leiomyosarcomas, rhabdomyosarcomas, and liposarcomas [5].

On CMR, malignant tumors are characterized by heterogeneous tissue characterization on T1-

weighted, T2-weighted, and contrast-enhanced pulse sequences, a sessile morphology with broad invasive attachment to the myocardium, large size, central necrosis, and invasion into more than one cardiac chamber [6]. They are often, especially with angiosarcomas, complicated by cardiac tamponade and tend to metastasize into the spine.

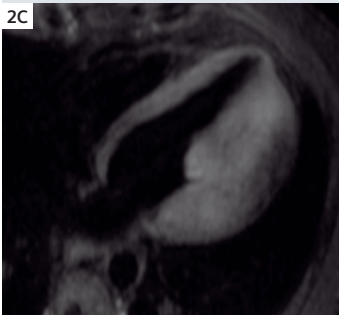


TRETRO (triggered-retrogated)

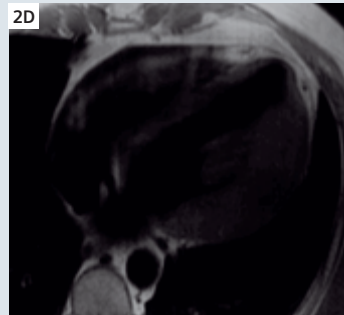


TRETRO post contrast

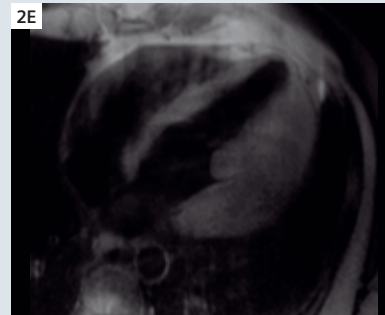
2 Left ventricular sarcoma.



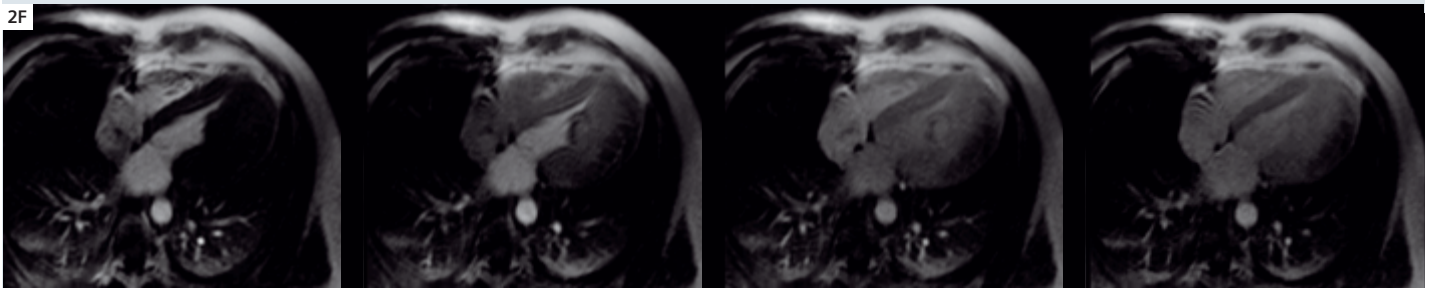
T2-weighted TIRM



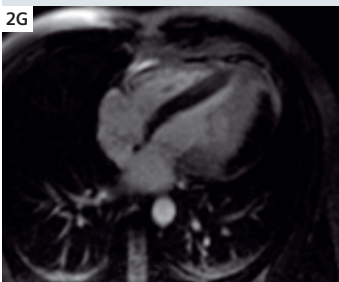
T1-weighted TSE



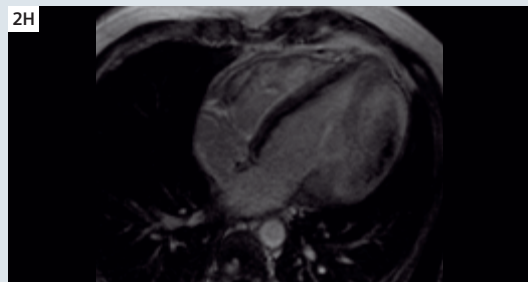
T1-weighted TSE with fat suppression



Perfusion



TI Scout TT 227 ms

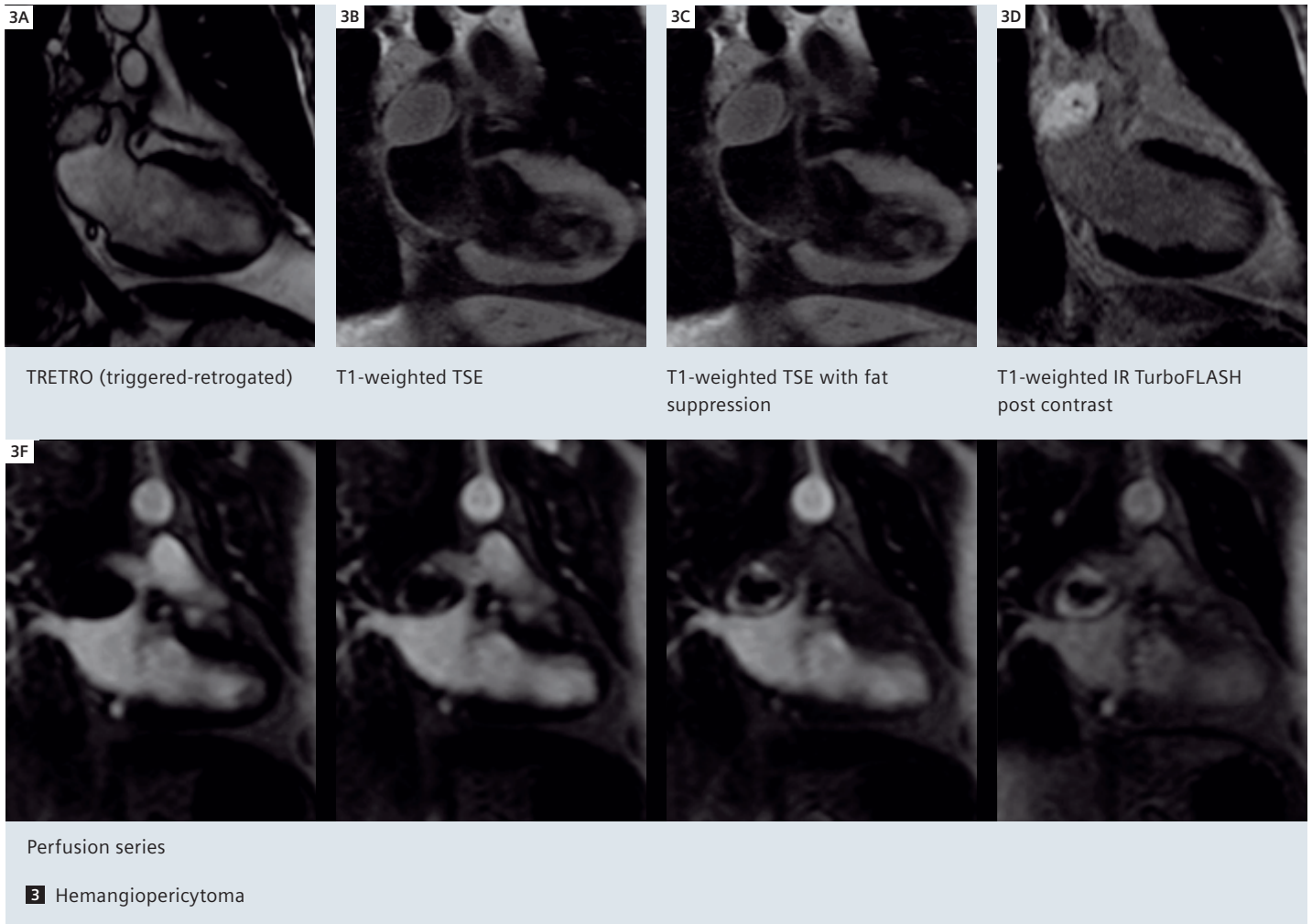


T1-weighted 3D IR TurboFLASH post contrast, TI 300

CMR protocol for cardiac tumors

A typical protocol consists of anatomic images in sagittal, coronal and axial orientation (e.g. fast low-angle shot gradient echo, FLASH), cine-imaging for function (steady-state free precession, TrueFISP), tissue characterization with various

T1-weighted and T2-weighted spin-echo sequences with and without fat suppression, and finally contrast-enhanced T1-weighted imaging for vascularisation. Apart from those general recommendations CMR protocols for cardiac tumors should be adapted to the specific needs of the individual patient.

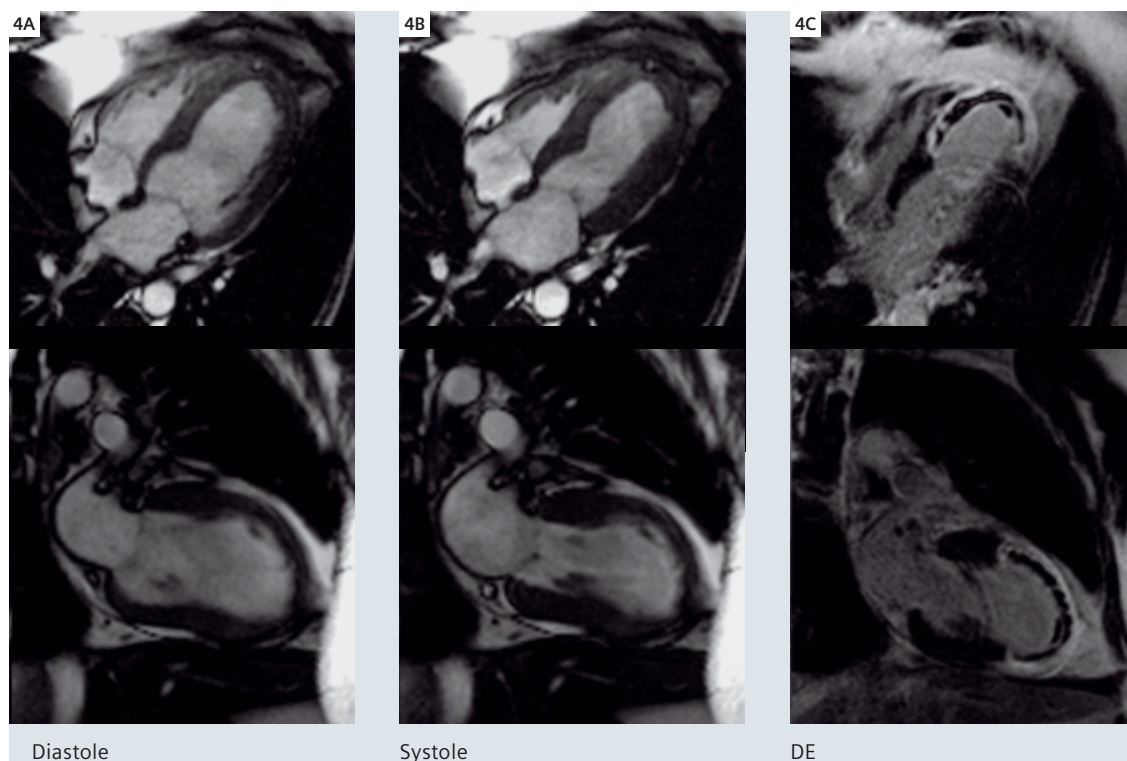


Cardiac thrombi

Left ventricular thrombus formation is a frequent complication following myocardial infarction in approximately 15% of patients [7]. Patients with left ventricular thrombi are treated with oral anti-coagulation to reduce the risk of embolization. In clinical practice LV thrombi are diagnosed by transthoracic echocardiography. The diagnosis of thrombi by echocardiography, however, is challenging due to insufficient acoustic windows, problematic apical segment imaging, and reduced endocardial border delineation. With contrast-enhanced CMR, LV function and LV tissue characterization are combined in one examination with a single imaging modality. Steady-state cine imaging further improves delineation of endocardial borders compared to ultrasound, allowing for a superior differentiation of thrombus and ventricular myocardium. In most cases thrombi are located at

the side of myocardial infarction, and are closely related to the extent of myocardial damage and impairment of segmental and global LV function. With the rare exception of large, old, and extensively vascularized thrombi, cardiac thrombi do not show enhancement following contrast application. On contrast-enhanced CMR using segmented gradient-echo sequences with an inversion-recovery prepulse (e.g. IR TurboFLASH) thrombi are visualized as dark areas between enhanced left ventricular cavity and infarct delayed enhancement. A 3D gradient echo sequence with a short inversion time early after contrast administration further improves cavity-to-thrombus contrast [8]. The “optimal TI” of a thrombus is different than the one for optimal myocardial suppression in delayed enhancement. Therefore, a brighter appearance of a thrombus when visualizing the myocardium for delayed enhancement imaging should not be

Contrast-enhanced CMR detects more thrombi than echocardiography in chronic myocardial infarction.



4 CMR in a patient with acute myocardial infarction. Note the black (nulled) subendocardial zone surrounded by delayed enhancement. This corresponds to a no-reflow zone. Additionally, a small apical thrombus can be seen in DE imaging.

In a pulmonary embolism protocol, MRA of the pulmonary arteries can be combined with cine and DE imaging of the right ventricle to detect RV thrombi.

mixed with a vascularisation of the thrombus. Not surprisingly, contrast-enhanced CMR detects more thrombi than echocardiography in chronic myocardial infarction [9]. In the setting of acute myocardial infarction, however, it can be difficult to differentiate thrombus and no-reflow zones, since microvascular obstruction (no-reflow) is predominantly located in the subendocardial layer of the left ventricular myocardium with no, or a very small rim of signal enhancement separating cavity from infarct no-reflow.

In pulmonary embolism right ventricular thrombi are frequently missed by echocardiography. In this setting MR angiography of the pulmonary arteries can be easily combined with delayed enhancement and cine imaging of the right ventricle [10].

Contact
Oliver Bruder, M.D.
Department of
Cardiology and
Angiology
Elisabeth Hospital
Klara-Kopp-Weg 1
45138 Essen
Germany
o.bruder@
elisabeth-essen.de

References

- 1 Reynen K. Frequency of primary tumors of the heart. *Am J Cardiol* 1996;77(1):107.
- 2 Hanfling SM. Metastatic cancer to the heart. Review of the literature and report of 127 cases. *Circulation* 1960;22: 474–83.
- 3 Reynen K. Cardiac myxomas. *N Engl J Med* 1995;333(24): 1610–7.
- 4 Grebenc ML, et al. Cardiac myxoma: imaging features in 83 patients. *Radiographics* 2002;22(3):673–89.
- 5 Herrmann MA, et al. Primary cardiac angiosarcoma: a clinico-pathologic study of six cases. *J Thorac Cardiovasc Surg* 1992; 103(4):655–64.
- 6 Siripornpitak S, Higgins CB. MRI of primary malignant cardiovascular tumors. *J Comput Assist Tomogr* 1997;21(3): p. 462–6.
- 7 Greaves SC, et al. Incidence and natural history of left ventricular thrombus following anterior wall acute myocardial infarction. *Am J Cardiol* 1997;80(4):442–8.
- 8 Bruder O, et al. [Detection and characterization of left ventricular thrombi by MRI compared to transthoracic echocardiography]. *Rofo* 2005;177(3):344–9.
- 9 Mollet NR, et al. Visualization of ventricular thrombi with contrast-enhanced magnetic resonance imaging in patients with ischemic heart disease. *Circulation* 2002;106(23): 2873–6.
- 10 Barkhausen J, et al. Detection and characterization of intracardiac thrombi on MR imaging. *AJR Am J Roentgenol* 2002; 179(6):1539–44.

Clinical Application of 3D/4D MR Angiography in Cardiovascular Diseases

Jörg Barkhausen, M.D.; Florian M. Vogt, M.D.; Stefan Maderwald, MSc; Harald H. Quick, Ph.D.

Department of Diagnostic and Interventional Radiology and Neuroradiology
University Hospital Essen, Germany

Introduction

Less than a decade following its first description, contrast-enhanced MR angiography (MRA) has replaced invasive catheter angiography as the diagnostic procedure of first choice for most vascular diseases. MRA provides high-spatial resolution 3D data sets with excellent image contrast and allows visualization of almost all vascular territories. Motivated by the clinical success of MRA, the technical developments have even gained speed within the last years. Latest hardware and software developments aim to move from static imaging of a single vascular territory towards dynamic data acquisition schemes.

For a standard MRA examination 10 to 30 ml of a Gadolinium-based contrast agent followed by a saline bolus are typically injected into the antecubital vein with a flow rate of 1 to 3 ml/s. The transit time is defined using a test bolus or care bolus technique and during peak arterial enhancement in the vascular territory of interest a 3D data set is collected within 10 to 30 seconds. This technique provides a stack of 60 to more than 100 cross-sectional images of the contrast filled arteries which can be post processed using maximum intensity projection (MIP), multi-planar reformats (MPR) or volume rendering. However, compared to DSA standard MRA techniques only provide morphologic information, whereas digital subtraction angiography as the standard of reference collects several images during the first-pass of the contrast agent providing additional information on flow dynamics. The lack of functional information has been considered one of the major limitations of MRA by some clinicians familiarized with DSA examinations. The recently introduced **syngo TWIST** dynamic MRA application provides **sub-millimeter 3D data sets** with a high temporal resolution of about 1 to 5 seconds depending on the sequence parameters

and the spatial resolution. Incorporating parallel acquisition techniques (iPAT) even a **subsecond temporal resolution** can be obtained while maintaining a reasonable spatial resolution. Additionally, MRA with perfect arterial enhancement can be performed **without bolus-timing**, and only **very low doses of contrast** are required for excellent arterial enhancement using TWIST.

Another exciting recent development is **syngo TimCT**, a technique for continuous moving table data acquisition providing seamless volume coverage for large body parts. The craniocaudal field-of-view (FoV) for a conventional single station MRA examination is limited to typically 40–50 cm. Therefore, MRA examinations of the run-off system covering the abdominal aorta down to the pedal arteries have to be performed using multi-station protocols. Following a single contrast bolus the different vascular territories are covered step by step in rapid succession using three to four 3D-data sets. This approach results in several steps which have to be performed by the technician at the right time and in the correct order, making peripheral MRA examinations difficult to perform for inexperienced staff. TimCT (Continuous Table move acquisitions using Tim – Total imaging matrix – coils) introduces a completely new approach since a single high-resolution large-FoV 3D data set covering the entire run-off system can be collected “on the move”.

High-quality MRA requires a 1.5 or 3 Tesla MR scanner equipped with high-performance gradients, dedicated surface coils that can cover the different regions of interest and an automatic injector for the contrast agent. The typical in-room time for an MRA examination is about 15 to 20 minutes, however additional sequences for functional information or parenchymal imaging may

syngo TWIST: dynamic MRA with subsecond temporal or submillimeter spatial resolution in all body regions.

syngo TimCT Angiography allows MRA image acquisition „on the move“.

need some extra time. In this article we would like to give an overview of techniques, scan protocols and the impact on patient management for five of the most common indications for MRA with regard to cardiovascular diseases.

Carotid artery stenosis

Background: Arterial steno-occlusive disease of the carotid arteries can frequently be found in elderly patients with the potential risk of ischemic cerebral infarctions and fatal stroke.

MRA versus other imaging modalities: Imaging of the carotid arteries is feasible using several different imaging modalities including ultrasound (US), computed tomography angiography (CTA), digital subtraction angiography (DSA) and magnetic resonance imaging (MRI). Ultrasound can easily be performed as a bed-side test and allows reliable measurements of wall thickness and the degree of stenoses especially in the carotid bifurcation. However, the ability to provide information on vascular morphology from the aortic arch up to the small intracranial arteries combined with information on parenchymal brain lesion related to carotid artery stenoses and microvascular diseases is a unique feature of magnetic resonance imaging.

Protocol recommendation: The basic protocol should include a diffusion-weighted sequence for the detection of acute ischemic lesions, a T2*-weighted sequence for the detection of intraparenchymal hemorrhage and a FLAIR / DarkFluid sequence for the morphologic evaluation of brain lesions. The MRA should preferably be performed

using the care-bolus technique for timing of the data acquisition. The voxel size should be below 1 mm³ and the scan time should not exceed 20 seconds to avoid venous overlay (Figure 1).

Conclusion: MRA is the diagnostic test of first choice for a comprehensive evaluation of the carotid arteries and the brain.

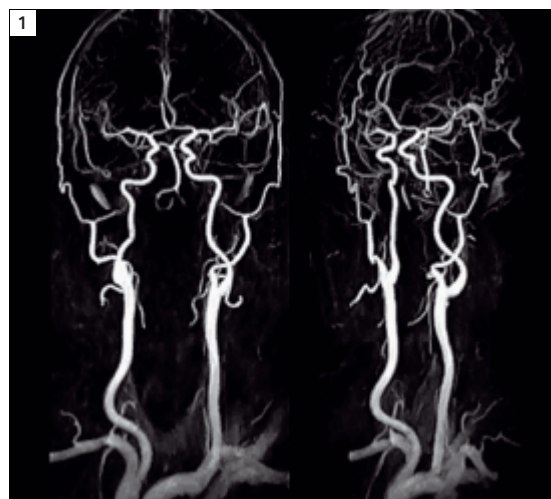
Congenital heart disease and vascular variants

Background: The most frequent congenital heart diseases (CHD) are frequently associated with vascular variants and malformations. Therefore in patients with known or suspected CHD cardiac MRI examinations including dark-blood TSE sequences, steady-state free precession sequences (e.g. TrueFISP) for the assessment of right and left ventricular function and phase velocity encoded cine MRI for flow measurements are typically combined with an MRA examination of the thoracic vessels. This comprehensive protocol provides all clinically relevant information on morphology and function that cannot be obtained with any other single imaging modality.

MRA versus other imaging modalities: Echocardiography, which is typically the first diagnostic test in CHD patients cannot visualize the entire vascular system and is of limited value for the assessment of right ventricular function. Additionally, a poor acoustic window may hamper a comprehensive cardiac exam especially in grown-up patients with CHD. ECG-triggered computed tomography (CT) provides excellent information on cardiac and vascular morphology but lacks functional information, e.g. quantification of shunt volumes and flow. Additionally, due to the need of routine follow-up examinations and the fact that mainly children and young adults are affected, radiation exposure must be considered a major limitation. Compared to all other imaging modalities catheter angiography still provides an unbeaten spatial and temporal resolution, however the lack of 3D information inherent to a projection technique and the invasiveness have to be taken into account.

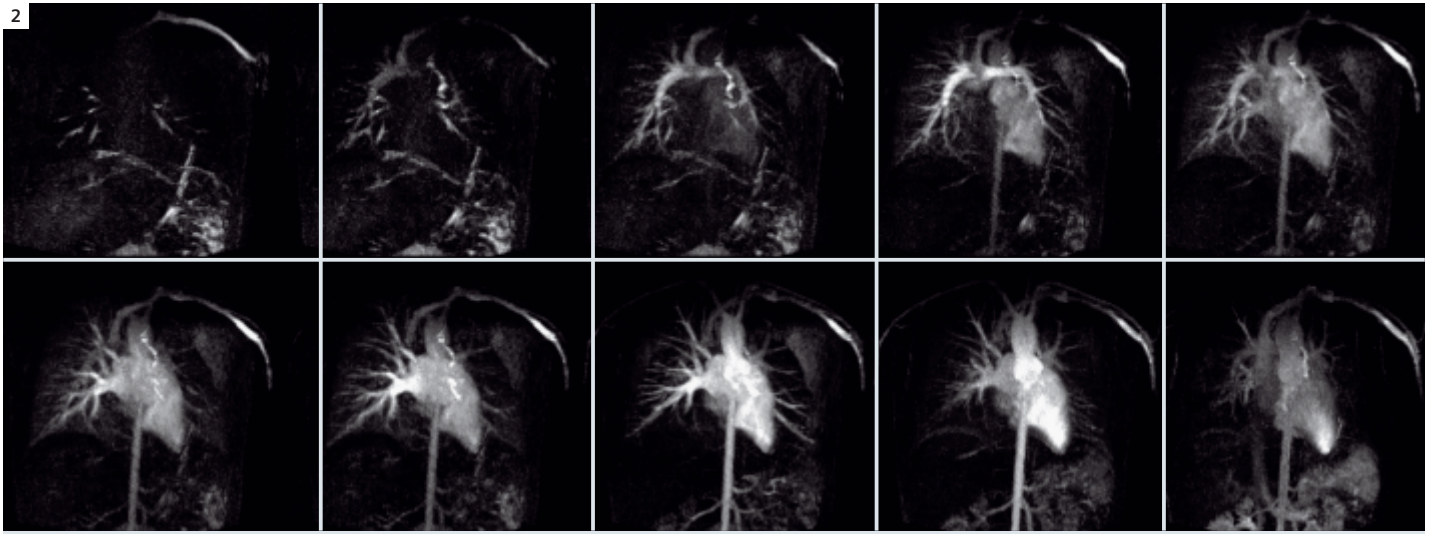
Protocol recommendation: For a comprehensive assessment of cardiac and vascular abnormalities in CHD patients we perform a time-resolved 3D (= 4D) MRA with subsecond temporal resolution using *syngo* TWIST and a small amount of contrast (5–8 ml) injected at a high flow rate (≥ 3 ml/s)

MRA is the diagnostic test of first choice for a comprehensive evaluation of the carotid arteries and the brain.



1 High-resolution MRA of the carotid arteries.

2



2 Subsecond 4D MRA using *syngo* TWIST in a patient with cavopulmonary anastomosis and hypoperfusion of the left lung.

(Figure 2). Due to the very high temporal resolution required for the assessment of shunts, spatial resolution has to be sacrificed to some degree. Therefore, the dynamic MRA is combined with a standard high-resolution MRA. The dynamic information from the TWIST sequence can be used for bolus timing and according to our experience the injected contrast does not reduce the image quality of the high resolution scan even if performed immediately following the dynamic MRA scan.

Conclusion: The combination of time-resolved and high-resolution MRA allows a comprehensive and fast evaluation of vascular abnormalities and shunts in patients with known or suspected congenital heart disease.

Aortic diseases

Background: Acute aortic syndromes are an important differential diagnosis in chest pain patients which are frequently missed or delayed diagnosed. Especially in Type A dissections this may have fatal consequences due to the high mortality rate if left untreated.

MRA versus other modalities: In patients with suspected acute aortic syndrome transesophageal echocardiography (TEE) is a fast and reliable bedside test that can be performed in the emergency room or the intensive care unit. However, TEE cannot display entire aorta including the side branches. Therefore, additional cross-sectional imaging is routinely performed prior to treatment. Due to the short scan time and the excellent patient access

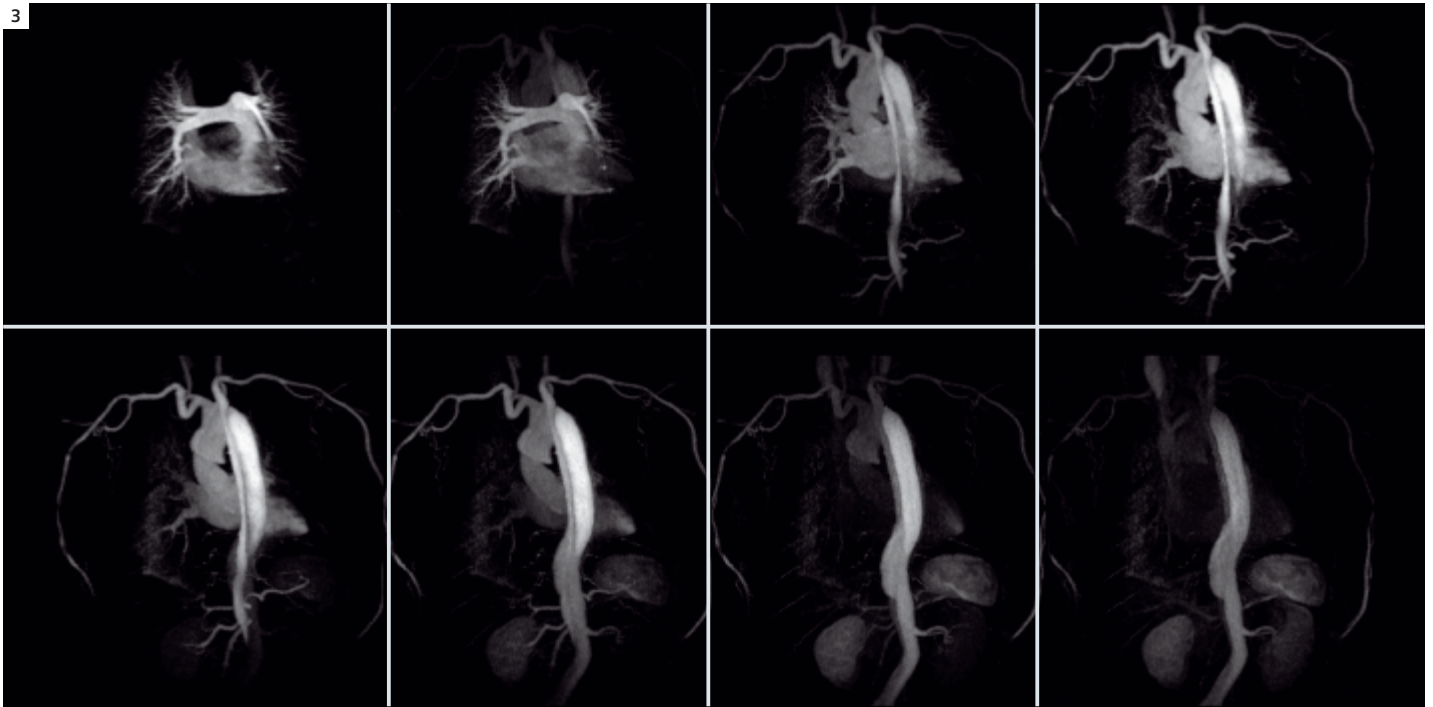
during the examination computed tomography is the imaging modality of first choice in case of an emergency. However, in stable patients, for follow-up examinations or for treatment planning MRA is an attractive alternative. Major advantages of MRA compared to CTA include the additional functional information (flow direction, tissue perfusion) that can be obtained from time-resolved MRA and the higher sensitivity of MRA for the detection of slow filling endoleaks after interventional treatment. Due to the invasive nature, the low sensitivity for the detection of small penetrating atherosclerotic ulcer, and the inability to detect intramural hemorrhage, catheter angiography can no longer be considered as a first line diagnostic test in patients with acute aortic syndromes.

Protocol recommendations: Our standard protocol comprises a timeresolved MRA in patients with suspicion of aortic syndromes. *syngo* TWIST combined with Parallel Acquisition Techniques (iPAT) provides a temporal resolution of about 2 seconds allowing the assessment of flow dynamics and organ perfusion combined with a sufficient spatial resolution for the assessment of vascular morphology (Figure 3). The time-resolved MRA allows a reliable detection and exclusion of aortic dissections and aneurysms. For the detection of intramural hemorrhage and small penetrating atherosclerotic ulcer, however, additional morphologic sequences (dark-blood turbo spin echo, steady-state free precession cine) and a high resolution stan-

syngo TWIST as a 4D MRA solution can be used either as a standalone technique or in addition to 3D MRA.

Time-resolved MRA with *syngo* TWIST allows reliable detection and exclusion of aortic dissections and aneurysms.

3



3 4D MRA using syngo TWIST in a patient with acute aortic dissection and delayed perfusion of the left kidney, which is supplied by the false lumen.

dard MRA sequence may be added to the protocol. **Conclusion:** MRA allows a complete evaluation of acute aortic syndromes in clinically stable patients and for follow-up examinations. Due to the limited patient access during the examination and the longer scan time, multi-slice CT should preferably be used in emergency patients.

Renal artery stenosis

Background: Arterial hypertension is a common clinical finding and must be considered an important risk factor for several potentially fatal events including stroke and myocardial infarction. Although arterial hypertension is only rarely caused by renal artery stenoses it has to be excluded to avoid missing of treatment options e.g. stent placement.

MRA versus other modalities: Digital subtraction angiography is still considered the standard of reference for detecting renal artery stenosis. However, DSA has several important disadvantages including risk of death, arterial dissection and renal failure. Therefore non-invasive imaging techniques such as ultrasound, CTA and MRA have been introduced for the diagnostic work-up of renal artery stenosis. Ultrasound of the renal arteries is challenging es-

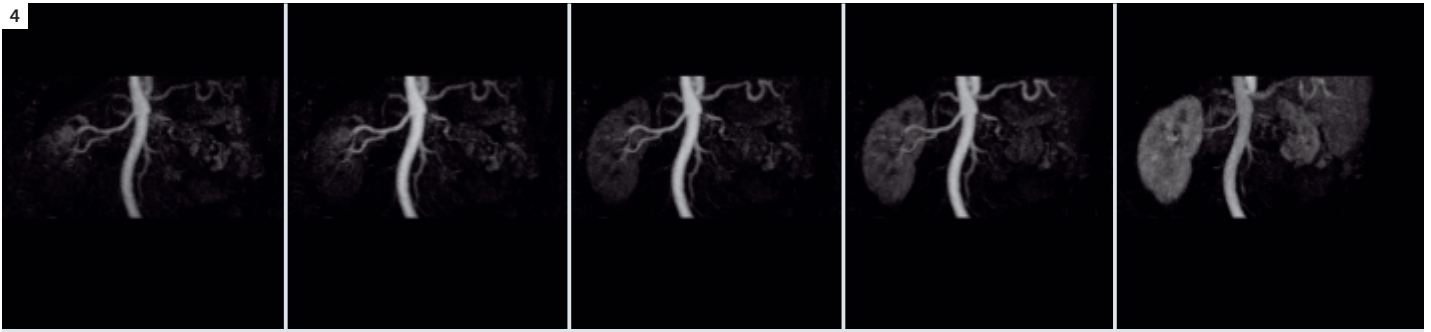
pecially in obese patients and the results strongly depend on the experience of the investigator.

MRA and CTA developed rapidly within the last five years and both modalities provide a high negative predictive value in patients with suspected atherosclerotic renal artery stenosis, whereas the diagnosis of fibromuscular dysplasia is more challenging. However, MRA can be combined with flow measurements and measurements of tissue perfusion providing additional functional information (Figure 4) which must be considered an important advantage of MRA compared to CTA.

Protocol recommendation: For the visualization of the renal arteries spatial resolution is crucial. We perform a multiphase standard MRA examination using the test bolus or care bolus approach for the timing of the data acquisition. The scan duration must be adapted to breath-hold capabilities of the patients to avoid motion artifacts. Most patients can hold their breath for about 20 seconds and within that scan time a spatial resolution below 1 mm³ can be obtained. To assess the hemodynamic significance of stenoses and to detect concomitant renoparenchymal disorders, flow measurements using the phase-contrast technique and first-pass perfusion mea-

MRA can be combined with flow and tissue perfusion measurements providing additional functional information in renal artery stenosis.

4



4 MRA of the renal arteries using *syngo* TWIST. High-grade stenosis of the left renal artery with delayed contrast enhancement of the hypoplastic left kidney.

surements following contrast administration can be added to the protocol.

Conclusion: A comprehensive examination combining high-resolution MRA with flow and perfusion measurements is a unique feature of magnetic resonance imaging and allows accurate characterization of renovascular and parenchymal disease.

Peripheral arterial disease

Background: Peripheral arterial disease (PAD) affecting the limb arteries is a frequent clinical problem being mostly caused by atherosclerosis. The leading feature is arterial narrowing with subsequent reduction of blood flow to the limbs resulting in intermittent claudication, which is estimated to occur in about 5% of people over 55 years old, but PAD is frequently under-diagnosed. Visualization of the entire limb arteries is a prerequisite to make the correct diagnosis and for treatment planning.

MRA versus other modalities: Duplex ultrasound providing high sensitivity and specificity for the detection of stenoses is an excellent first line test but exhibits a couple of disadvantages: it strongly depends on the experience of the physician and the acoustic window can be limited especially for the iliac arteries in obese patients. Additionally, ultrasound cannot display the entire vascular system in a single image to provide a comprehensive overview of the vascular system. The highly accurate digital subtraction angiography is still regarded as the gold standard for the diagnosis of atherosclerotic changes in peripheral vessels. However, important disadvantages including invasiveness, procedure related mortality and morbidity, costs, availability and the use of ionizing radiation as well as potentially nephrotoxic

contrast agents must be taken into account.

CT angiography can be performed to visualize the peripheral arteries but radiation exposure, potentially nephrotoxic contrast agents, time-consuming postprocessing and problems evaluating severely calcified vessels must be considered as important limitations. Therefore bolus-chase MRA protocols collecting multiple high resolution data sets covering the arterial vessels from the renal arteries down to the pedal arteries can be considered as the state of the art technique and imaging modality of first choice for a fast and comprehensive evaluation of patients suffering from peripheral arterial disease.

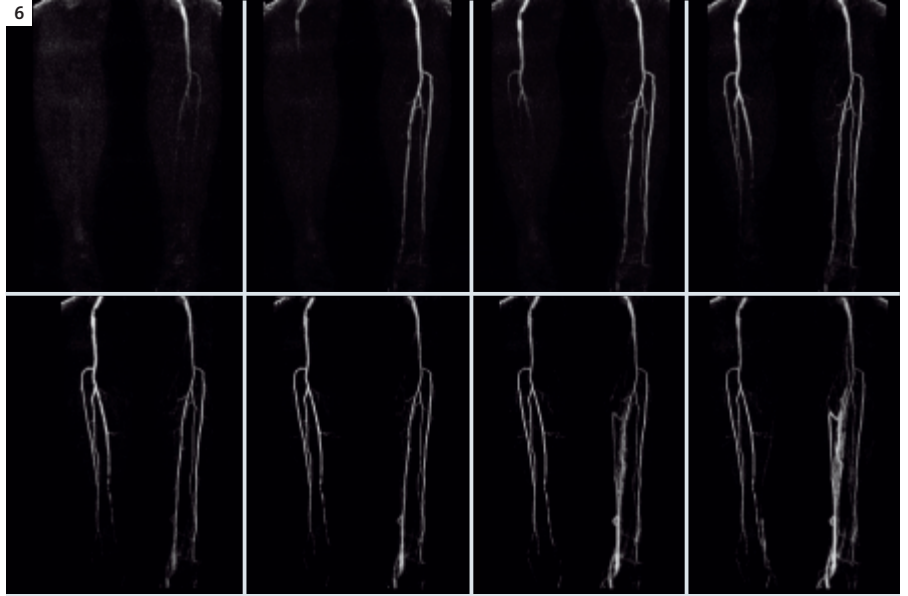
Protocol recommendation: Although the technique has been used in clinical routine for about 10 years, MRA of the run-off vessels can be still be challenging. Optimal timing of the contrast injection is crucial because inadequate timing may result in poor arterial opacification or venous overlay. Additionally, several data sets requiring user interaction have to be collected in rapid succession, making the procedure difficult to perform for inexperienced users. To overcome these limitations several new techniques have been developed. To simplify the procedure and to improve the workflow, *syngo* TimCT (Tim Continuous Table move) has recently been introduced. Instead of collecting several overlapping 3D data sets in rapid succession, a single high resolution 3D data set covering the arterial system from the abdominal aorta down to the pedal arteries, is collected during continuous table movement. This technique is revolutionary because motion, which was considered one of the major obstacles for MR imaging is now used to extend the field-of-view in cranio-caudal direction. TimCT is a robust and easy to

MRI allows accurate characterization of renovascular and parenchymal disease.

With *syngo* TimCT, table motion is used to extend the field-of-view in z-direction.



5 MRA acquired with *syngo* TimCT in a patient with PAD.



6 Dynamic MRA of the calf arteries using *syngo* TWIST.

MRA provides different imaging protocols for peripheral MRA and has replaced diagnostic DSA in PAD patients.

perform protocol for patients with PAD (Figure 5). In patients with diabetes or pedal ulcer which are prone to early venous filling, however, TimCT might not be the ideal tool. To avoid venous overlay for the infrapopliteal arteries hybrid MRA techniques combining time-resolved MRA of the lower legs using TWIST followed by bolus chase MRA for the pelvis and upper legs may be advantageous. Combining TWIST and Parallel Acquisition Techniques, a dynamic MRA can be obtained with a temporal resolution of about 2 seconds and a voxel size below 1 mm³ which reliably avoids venous overlay and adds functional information comparable to DSA (Figure 6).

Conclusion: MRA provides different imaging protocols for peripheral MRA and has replaced diagnostic DSA in PAD patients.

Discussion

MRA is a robust and reliable technique that can be applied to visualize all different vascular territories in daily clinical routine. The only vascular territory that remains challenging is MR angiography of the coronary arteries (MRCA). Reliable compensation of cardiac and respiratory motion cannot be achieved in all patients resulting in motion artifacts and reduced image quality. Therefore, MRCA must still be considered as a field of active research and is not ready for routine clinical

application in coronary artery disease patients. However, MRA is still developing rapidly and the new techniques will definitively change our scan protocols and further improve the diagnostic impact of MRA. The various MRA techniques mentioned above cover different parts of the vascular system. Using recent hard and software developments the examination can easily be extended to wholebody MRA without increasing the dose of contrast. The investment in increased scan times, the inroom time as well as the time required for post-processing and reading of the examination are, however, justified by, for example, the high prevalence of concomitant atherosclerotic findings in the carotids and thoracic aorta in PAD patients, and may improve patient care. Additionally, this might be a completely new approach for risk assessment in atherosclerotic disease because the total plaque burden within the arterial system can easily be assessed in a single examination taking only 15 to 20 minutes.

Contact

Prof. Joerg Barkhausen, M.D.
Department of Diagnostic and Interventional Radiology and Neuroradiology
University Hospital Essen
Hufelandstraße 55
45122 Essen
Germany

CME-Accredited CD Set – Order your free copy!

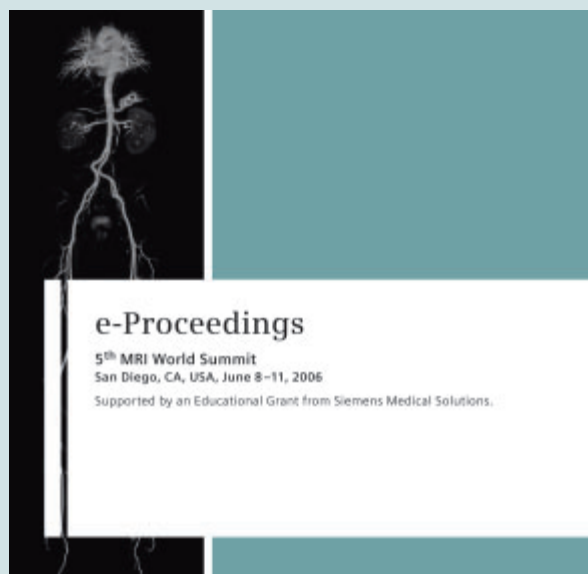
The **Johns Hopkins University Medical School** in Baltimore, Maryland, USA has captured 17 talks from the 5th MRI World Summit held in San Diego, California, USA. The talks of experienced and renowned experts cover a broad range of MR imaging:

- MR Imaging in Neurology (e.g. SWI, fMRI, DTI)
- Body MRI (e.g. MRI in cystic fibrosis lung, REVEAL, body MRI @ 3T)
- Cardiovascular MRI (e.g. MRI in cardiomyopathies)
- Orthopedic MRI (cartilage imaging @ 3T)
- MRI in Women's Health (e.g. pelvic MRI, breast MRI, MR biopsy)
- Tim (e.g. MR prostate cancer assessment, molecular imaging)

For Cardiovascular MRI, the following speakers contributed to the session:

- Dudley J. Pennell, M.D., Royal Brompton Hospital, London, UK; MRI in Ischemic vs Nonischemic Cardiomyopathies
- Bhavin Jankharia, M.D., Jankharia Imaging, Mumbai, India; CMR – a tool in today's clinical routine
- James C. Carr, M.D., Northwestern University, Chicago, IL, USA; MR angiography. New approaches with NATIVE and time resolved MRA

The set of 3 CDs is approved for AMA PAR Category 1 credit (in total 7.75). In order to obtain CME credits, please order the CDs free of charge directly at: The Johns Hopkins School of Medicine Office of Funded Programs/CME Ms. Jennifer Schutz 720 Rutland Ave, Turner 20 Baltimore, M.D. 21205-195 USA e-mail: fundedcme@jhmi.edu ph: +1 (410) 614-6211; fax: +1 (410) 614-7315



Dudley J. Pennell, M.D.



Bhavin Jankharia, M.D.

MR Imaging of Congenital Heart Disease

Vivek Muthurangu, M.D.; Michael Hansen, M.D.; Andrew M. Taylor, M.D.

UCL Institute of Child Health & Great Ormond Street Hospital for Children, London, UK



1 3D volume-rendered image of the normal heart and great vessels, recreated from a 3D navigator and ECG-gated TrueFISP dataset viewed from left anterior oblique.

Introduction

Congenital heart disease (CHD) has an incidence of 6–8 per 1000 at birth with prevalence increasing due to improvements in diagnosis and treatment. Management of patients with CHD relies heavily on imaging. Echocardiography is the first line investigation. However, echocardiography provides poor images of the peripheral vasculature, is user dependant and can be limited by difficult acoustic windows. These problems are exacerbated in patients with CHD as they often have restricted acoustic window access due to multiple previous operations and furthermore the structures that must be visualized in CHD are difficult to assess at echocardiography (i.e. right ventricle and pulmonary arteries).

CMR imaging allows accurate description of cardiac and vascular anatomy and provides accurate quantification of cardiac function and vascular flow.

Conventionally, more detailed anatomical and functional assessment has been acquired with x-ray cardiac catheterization. Cardiac catheterization gives good definition of vascular anatomy and enables assessment of haemodynamics (vascular stenosis, quantification of cardiac shunting, and pulmonary vascular resistance), but is associated with risks due to the invasive nature of the procedure and the exposure to ionizing radiation. In addition, x-ray fluoroscopy provides a projection image and has only limited three-dimensional (3D) capabilities.

More recently, cross-sectional cardiovascular imaging (MR and CT) has become a very important tool for diagnosis and follow-up of children and adults with CHD. Not only does cross-sectional imaging allow accurate description of cardiac and vascular anatomy in relation to the other structures of the chest, but MR imaging, in particular, can provide accurate quantification of cardiac function and vascular flow.

MR imaging

The majority of cardiovascular MR images are acquired using cardiac (ECG) gating during a breath-hold, to reduce the artifacts associated with cardiac and respiratory motion. For a complex case, MR imaging is performed over approximately 1 hour, though this can be considerably reduced if a focused question is addressed.

Imaging sequences can be broadly divided into:

- **'Black-blood'** spin-echo images, where signal from blood is nulled and thus not seen – for accurate anatomical imaging
- **'White-blood'** gradient echo or steady-state free precession (TrueFISP) images, where a positive signal from blood is returned – for anatomi-

cal, cine imaging, and quantification of ventricular volumes, mass and function

- **Phase-contrast imaging**, where velocity information is encoded – for quantification of vascular flow, and
- **Contrast-enhanced MR angiography**, where non-ECG gated 3D data is acquired after Gadolinium contrast medium has been administered – for thoracic vasculature imaging.

Imaging should be performed in the presence of a cardiovascular MR expert in conjunction with an MR technician to ensure that the appropriate clinical questions are answered. Currently, our own practice is to perform all cardiovascular MR in children less than 8 years of age under general anesthesia, as this enables the safe acquisition of accurate data (reduced movement and respiratory artifact). With the development of even faster sequences, breath holding may become less of a necessity, and MR data may then be acquired more easily during sedation.

There are many CHD's that lend themselves to cardiovascular MR. However; it is beyond the scope of this brief review to cover all these conditions. We will therefore discuss some of the most common lesions referred for cardiovascular MR: Aortic coarctation, tetralogy of Fallot, transposition of the great arteries (TGA), and the assessment of the functional single ventricle.

MR imaging of common conditions

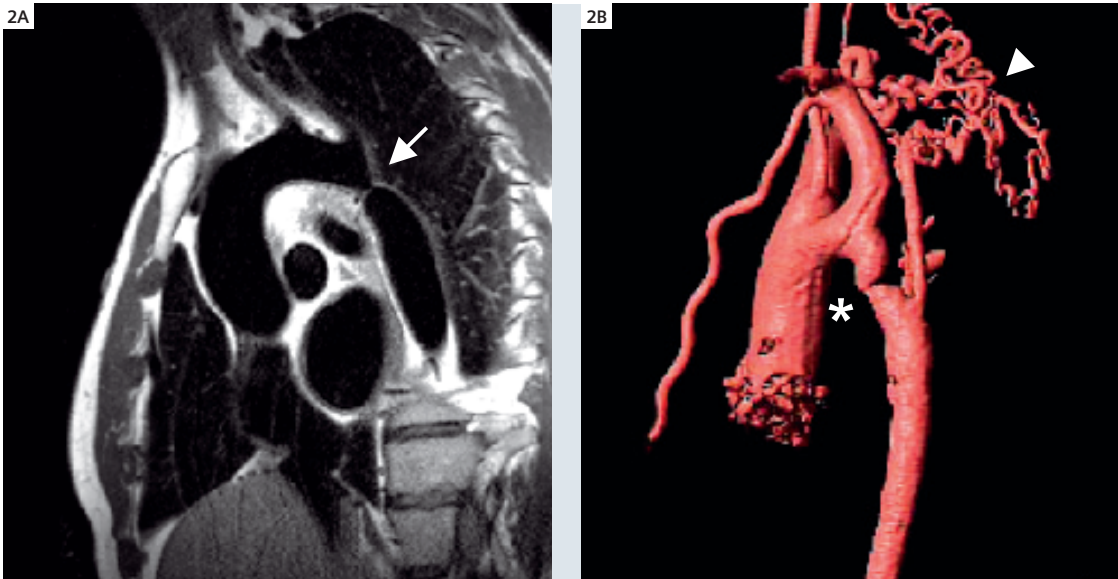
Aortic coarctation

Coarctation occurs in 6–8% of live CHD births with a predominance of males. There is an area of narrowing in the thoracic aorta in the region of insertion of the arterial duct (aortic isthmus, Fig. 2). There is a risk of hypertension, atherosclerosis and end organ damage, even in patients who have undergone surgical repair. Treatment in infancy with surgical excision of the narrowing is usually performed, though in older subjects balloon angioplasty may be undertaken, and following re-coarctation, aortic stenting can be used. In the neonatal population, echocardiography is used in the initial diagnosis. Echocardiography can also be used in follow up, but as children grow this becomes more difficult and imaging with MR is required in later life to establish if there is re-coarctation after repair (3–35% of patients), aneurysmal dilatation, or left ventricular hypertrophy secondary to hypertension. MR imaging is preferred if there are no contraindications, as this reduces population radiation.

Imaging is crucial for management decisions to establish the location and degree of stenosis, length of coarctation segment, associated aortic arch involvement (such as tubular hypoplasia), the collateral pathways (internal mammary and posterior mediastinal arteries), relationship to

The most common CHD referred for cardiovascular MR are aortic coarctation, tetralogy of Fallot, TGA, and the assessment of the functional single ventricle.

Multiple follow-up imaging exams are needed in CHD patients. Increasing utilization of CMR helps reducing population radiation.



2 Aortic coarctation. (2A) Oblique sagittal, 'black-blood' TSE image through a severe, discrete aortic coarctation (arrow). (2B) 3D, volume-rendered MRA image of another severe aortic coarctation (*), with multiple collaterals (arrowhead).

aberrant subclavian artery, post-stenotic dilatation and left ventricular hypertrophy.

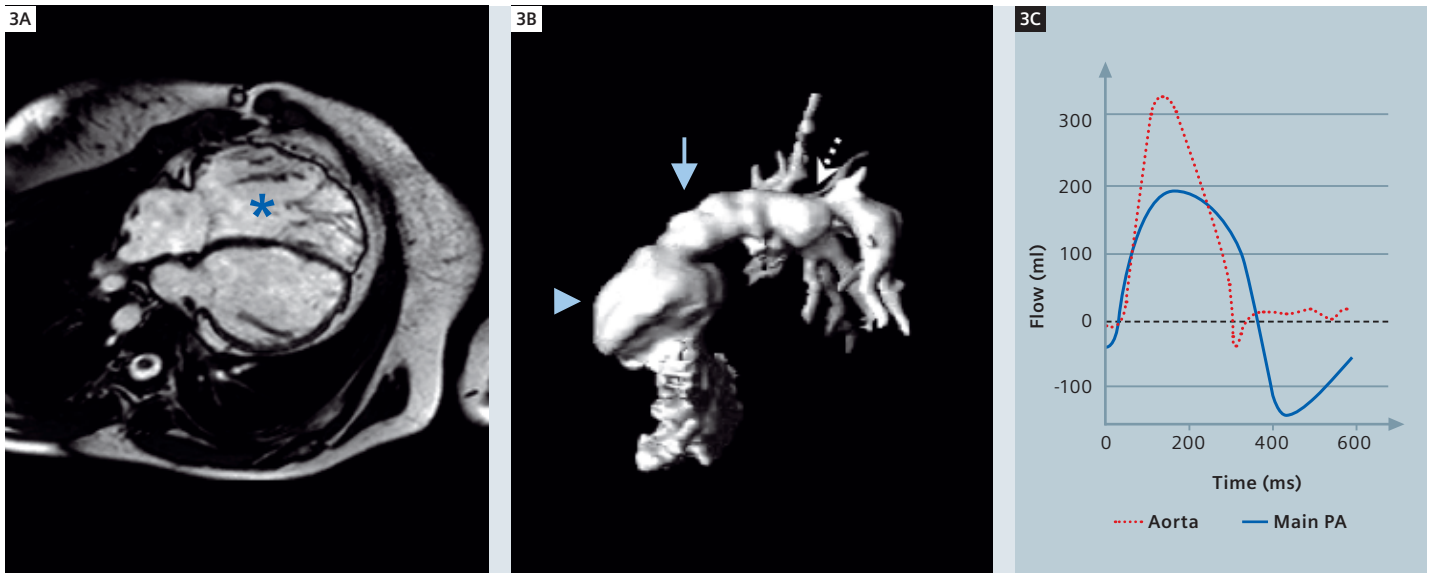
Tetralogy of Fallot

Tetralogy of Fallot is the most common cyanotic congenital heart defect with an incidence of approximately 420 per million live births. It is caused by malalignment of the infundibular septum, which leads to right ventricular outflow (RVOT) obstruction, a sub-aortic ventricular septal defect (VSD) with aortic override, and right ventricular hypertrophy. Current management consists of early single stage reconstructive surgery, with closure of the VSD, and relief of the RVOT obstruction, with possible placement of a trans-annular patch. Staged reconstruction is still required if there is significant hypoplasia of the central pulmonary arteries, with placement of a modified Blalock and Tausig (BT) shunt – a systemic to pulmonary anastomosis, usually between the innominate artery and the right pulmonary artery. This shunt is then taken down during subsequent definitive repair. Pre-operatively, cross sectional imaging has a role in delineating pulmonary artery anatomy, which helps decide between a single stage or multi-stage repair. However, the main role of imaging patients with tetralogy of Fallot is in the assess-

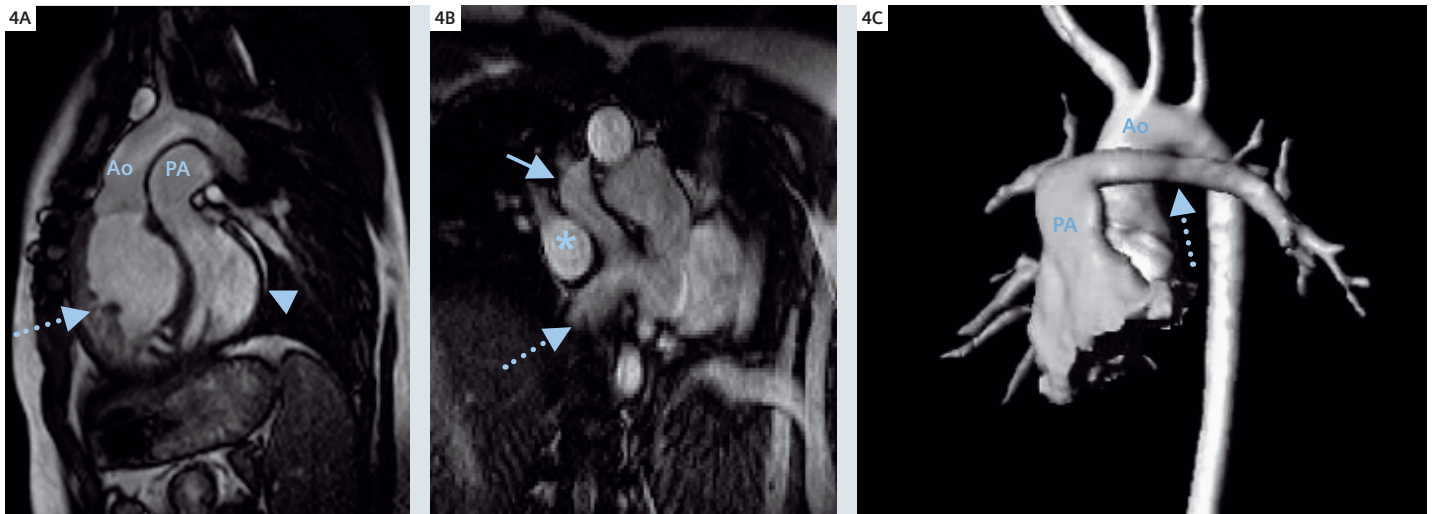
ment of post-operative complications (Figure 3). The most common late post-operative complication is pulmonary regurgitation secondary to trans-annular patch reconstruction of the RVOT/pulmonary annulus. This is often associated with aneurysmal dilatation of the RVOT. Surgical or trans-catheter valve replacement is the current method of managing patients with severe pulmonary regurgitation. Accurate quantification of regurgitation and assessment of RVOT anatomy and right ventricular (RV) function are particularly important in deciding the type and timing of procedures.

Branch pulmonary stenosis may also be present in this patient group and are best imaged by MR angiography. These can contribute to RV dysfunction, and significant obstructions should be repaired at the same time as valve replacement. The final role of MR is in evaluating RV function. This is important for timing of invasive therapeutic measures and evaluating the effect of any invasive procedure. It has been shown that, using a combination of MR ventricular volumetry and tricuspid and pulmonary flow maps, precise information about global and diastolic ventricular function can be assessed in patients with repaired tetralogy of Fallot.

Using a combination of CMR ventricular volumetry and tricuspid and pulmonary flow maps, global and diastolic RV function can be assessed precisely.



3 Repaired tetralogy of Fallot. (3A) TrueFISP 4-chamber image showing RV dilation (*). **(3B)** 3D, volume-rendered MRA image of the right ventricular outflow tract (RVOT) and proximal pulmonary arteries – lateral view. Note the large RVOT aneurysm is seen at the site of previous transannular patch repair (arrowhead), the pulmonary trunk (arrow), and the narrowed proximal left pulmonary artery (dashed arrow). **(3C)** Flow plotted against time for the aorta and pulmonary artery demonstrating pulmonary incompetence (regurgitant fraction = 33%) from phase contrast velocity maps.



4 Transposition of the great arteries. (4A) TrueFISP sagittal image; the aorta (Ao) arises anteriorly from the hypertrophied right ventricle (arrow); the posterior pulmonary artery (PA) arises from the left ventricle (arrowhead). **(4B)** TrueFISP images of intra atrial baffles in a patient who has undergone the atrial switch Senning operation –pulmonary venous blood into the right atrium (*), systemic venous blood into the left atrium, superior pathway (arrow), inferior pathway (dashed arrow). **(4C)** 3D volume-rendered MRA of the aorta (Ao) after the arterial switch operation. Anterior pulmonary arteries: pulmonary trunk (PA), left pulmonary artery (dashed arrow).

Transposition of the great arteries

Transposition of the great arteries (TGA) is the second most common cyanotic congenital heart disease in the first year of life with an incidence of 315 per million live births. It is defined as ventriculo-arterial discordance with an anterior aorta arising from the anterior RV, and the pulmonary artery arising from the posterior left ventricle (LV) (Fig. 4). Surgical therapy for this condition was revolutionized during the 1960's with the introduction of the Senning and Mustard procedure, in which blood is diverted from the right atrium to the left ventricle, and from the left atrium to the right ventricle. Both procedures produce a physiologically normal, but an anatomically very abnormal circulation (systemic venous return to the left atrium to LV and then to pulmonary artery; pulmonary venous return to the right atrium to RV and then to aorta). In 1975, the first arterial switch operation was performed. In this operation, the aorta and main pulmonary artery are transected, switched and re-anastomosed to the correct ventricle. This results in both a physiological and anatomically normal circulation, and for this reason, the arterial switch operation has become the procedure of choice for TGA. The arterial switch operation is performed in the first few days of life, and currently trans-thoracic

echocardiography is the imaging modality of choice for pre-operative diagnosis and assessment. The role of cross-sectional imaging is mainly in diagnosis of post-operative complications, particularly those that develop, as the child grows older. The main complications of the arterial switch operation are RVOT or branch pulmonary artery obstruction. Due to the unusual position of the pulmonary arteries immediately behind the sternum, trans-thoracic echocardiography is poor at detecting these lesions. Cardiovascular MR is ideal for imaging the RVOT and branch pulmonary arteries in this group of patients. Contrast enhanced MR angiography can be used to visualize the relationship between the pulmonary arteries and the aorta, while spin-echo sequences are used to assess accurately the degree of stenosis. A less common complication of the arterial switch operation is coronary stenosis secondary to the re-implantation procedure. Although the majority of coronary complications cause early post-operative mortality, a sub-set of patients suffer from late coronary events. In this group, coronary catheter angiography probably represents the modality of choice for investigation. However, coronary MR angiography or MDCT angiography are useful non-invasive methods for investigating the coronary arteries, particularly the proximal segments.

CMR is ideal for the detection of the main complications of the arterial switch operation: RVOT or branch pulmonary artery obstruction.

Anatomy, morphology, function and flow: CMR allows a comprehensive assessment of congenital heart diseases.

Although intra-atrial repair has been superseded by the arterial switch operation there is a sizeable population who have undergone either a Senning or Mustard operation. The most common complications of intra-atrial repair are baffle obstruction or leak, arrhythmias, and RV dysfunction. A combination of contrast MR angiography, spin-echo and phase contrast MR techniques allows comprehensive assessment of intra-atrial baffles.

The single ventricle

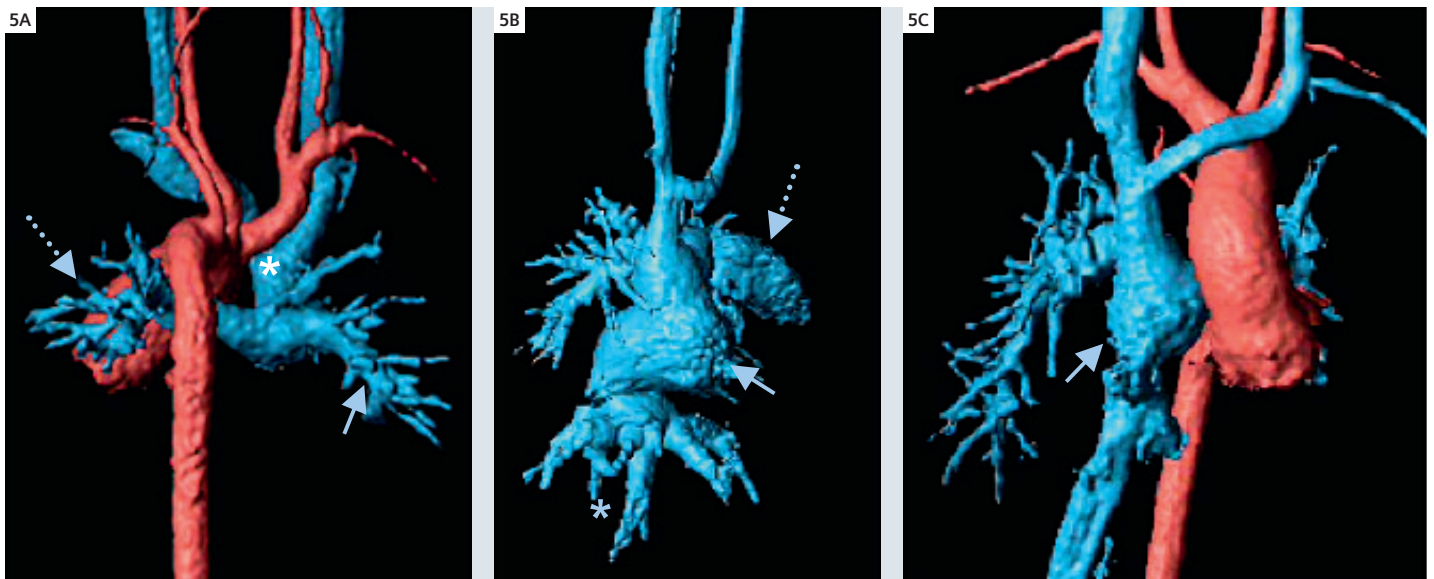
The single ventricle can be either an anatomical entity, for example in tricuspid atresia (single left ventricle) or hypoplastic left heart syndrome (single right ventricle), or a functional entity, where there are two ventricles connecting by a large VSD (Fig. 5). Even when there is anatomically a single ventricle, there is usually a vestigial remnant of the other ventricle. Depending on the size of the ventricles, and the great vessel anatomy, it may be possible to surgically 'septate' the ventricles to create a bi-ventricular circuit. If the ventricular sizes are not potentially equal, separation of the pulmonary and aortic circulations is required (the Fontan circulation), such that the single ventricle pumps blood into the systemic circulation, and systemic venous return is directed in to the pulmonary circulation.

Bi-directional Glenn circulation

The first stage in the creation of a single ventricular circulation is the bi-directional Glenn operation (or hemi-Fontan operation). In this procedure, a side-to-side anastomosis is created between the superior caval vein (SVC) and pulmonary arteries, and a patch is inserted to divide the SVC from the right atrium. Any systemic to pulmonary artery shunts are also taken down at this time. MR can be used to assess branch pulmonary artery narrowing and pulmonary venous obstruction prior to completion of the Fontan circulation otherwise the circulation may fail.

Fontan circulation

The Fontan circulation is completed by either anastomosis of the right atrium to the Glenn shunt (classical Fontan operation) or creation of a lateral or extra-cardiac tunnel between the inferior caval vein and the Glenn shunt (total caval pulmonary connection – TCPC). The latter procedure is now the preferred option; there remains however, a sizeable population with a standard Fontan circulation who require diagnostic assessment.



5 **Fontan circulation.** (5A) 3D volume-rendered MR angiogram of a bi-directional Glenn shunt (blue), posterior view – right pulmonary artery (arrow), left pulmonary artery (dashed arrow) superior caval vein (*), and descending aorta (red). (5B) 3D volume-rendered MR angiogram of a classical Fontan circulation showing severe right atrial dilation (arrow) – right atrial appendage (dashed arrow) and IVC drainage (*). (5C) 3D volume-rendered MR angiogram of a total caval pulmonary connection (TCPC) lateral tunnel Fontan circulation – lateral tunnel (arrow).

Conclusion

Cardiovascular imaging is important for the diagnosis and follow-up of children and adults with CHD. In young patients, echocardiography is the first line imaging modality; however, when echocardiography cannot provide a complete diagnosis, cross-sectional imaging with MR is rapidly becoming the next line of investigation, with interventional catheter angiography reserved for problem solving, for the assessment of the coronary arteries, and for the assessment of pulmonary vascular resistance.

In older children and adults, where echocardiography is less easy (poor acoustic windows and multiple operations), cross-sectional imaging is essential. MR in particular is important in this setting, as

there is no radiation burden, and both anatomy and function can be assessed to enable optimal follow-up and timing of future interventions.

Contact

Andrew M. Taylor, M.D., MRCP, FRCR
Reader in Cardiovascular Imaging
Director – Centre for Cardiovascular MR
Cardiothoracic Unit
UCL Institute of Child Health & Great Ormond Street
Hospital for Children
Great Ormond Street
London WC1N 3JH
United Kingdom
Tel: +44 (0) 207 404 9200 (ext. 5616)
Fax: +44 (0) 207 813 8263
E-mail: a.taylor@ich.ucl.ac.uk

The Advanced Cardiac Package includes the navigator and ECG gated 3D TrueFISP protocol for whole-heart imaging.

MR imaging protocol for congenital heart disease

The protocol below is a general protocol for imaging of CHD. It should be altered to answer clinical questions depending on patient anatomy.

1. Scouts and reference (parallel imaging) scans
2. HASTE black-blood axial imaging
3. Navigator-echo gated TrueFISP 3D volume of whole heart and great vessels
4. 2D single-slice TrueFISP cine images
 - a. Vertical long axis
 - b. Four-chamber view
 - c. RVOT in two planes
 - d. LVOT in two planes
 - e. Both branch pulmonary arteries
5. 2D multi-slice TrueFISP cine images – entirety of both ventricles in short-axis
6. 2D single-slice black-blood TSE imaging
 - a. Branch pulmonary arteries
 - b. Aortic arch
 - c. Vascular stenoses
7. Phase-contrast velocity mapping
 - a. Main pulmonary artery through-plane
 - b. Ascending aorta through-plane
 - c. Vascular stenoses in-plane
8. 3D contrast-enhanced MR angiography of the thoracic great vessels

Recommended reading

Paediatric Cardiology 2nd Edition. Eds: Anderson RH, Baker EJ, Macartney FJ, Rigby ML, Shinebourne EA, Tynan M. Churchill Livingstone, London, 2002. ISBN 0 443 07990 0

Hoffman JL, Kaplan S. The incidence of congenital heart disease. J Am Coll Cardiol 2002; 39:1890–1900

Anderson RH, Razavi R, Taylor AM. Cardiac anatomy revisited. Journal of Anatomy 2004; 205:159–77

Echocardiography in Pediatric Heart Disease. Snider AR, Serwer GA, Ritter SB. Mosby, 1997. ISBN 0 815 17851 4

Diagnosis and Management of Adult Congenital Heart Disease. Eds: Gatzoulis MA, Webb GA, Piers Daudeney P. Churchill Livingstone, London, 2003. ISBN 0 443 07103 9

Clinical Cardiac MRI. Eds: Bogaert J, Dymarkowski S, Taylor AM. Springer, Berlin, Heidelberg, New York, 2005. ISBN 3 540 40170 9

Coats L, Khambadkone S, Derrick G, et al. Physiological and clinical consequences of relief of right ventricular outflow tract obstruction late after repair of congenital heart defects. Circulation 2006; 113(17):2037–44

Schievano S, Migliavacca F, Coats L, et al. Planning of percutaneous pulmonary valve implantation based on rapid prototyping of the right ventricular outflow tract and pulmonary trunk from magnetic resonance imaging data. Radiology 2007; 242(2):490–7

MR Imaging in the Electrophysiology (EP) Laboratory

A Novel Method to Facilitate Treatment of Atrial Fibrillation

Robert S. Oakes¹, M.D.; Rob S. MacLeod^{2,3}; Christopher J. McGann¹; Eugene G. Kholmovski⁴; Edward V. R. Di Bella⁴; Nassir F. Marrouche¹, M.D.

¹*Division of Cardiology, Internal Medicine, University of Utah School of Medicine, Salt Lake City, Utah, USA*

²*Scientific Computing and Imaging Institute, School of Engineering, University of Utah, Salt Lake City, Utah, USA*

³*Nora Eccles Harrison Cardiovascular Research and Training Institute, University of Utah, Salt Lake City, Utah, USA*

⁴*Utah Center for Advanced Imaging Research, University of Utah, Salt Lake City, Utah, USA*

Background

Since the pulmonary veins were identified as one of the primary sources of atrial fibrillation (AF), a variety of treatment strategies have been developed to minimize the electrical effects of the pulmonary veins in AF [1]. These procedures often utilize a mapping catheter under fluoroscopic guidance to electrically isolate the pulmonary veins (PV) from the rest of the left atrium (LA). One technique in particular, Circumferential Pulmonary Vein Isolation (CPVI), has been reported to be highly effective for both the paroxysmal and persistent forms of AF [2–6]. CPVI has been reported to help return the majority of patients to normal sinus rhythm independent of the effects of antiarrhythmic-drug therapy, cardioversion or both [7]. There are other positive effects from successful CPVI including decreased size of the LA and improvement of left ventricular ejection fraction (LVEF) in patients who remain in sinus rhythm following the procedure [8].

However, despite the success of the CPVI procedure, the overall curative rate and complication rate for AF treatment is the same as it was at the turn of the millennium, despite years of investment and extensive study. Current challenges include efforts to maximize efficacy and safety, improve operator skills, better characterize left atrial anatomy and improve navigation within the cardiac chambers. In moving forward, integrating

three-dimensional (3D) imaging along with other accepted modalities shows promise in improving both the overall curative rate and for decreasing the complication rate.

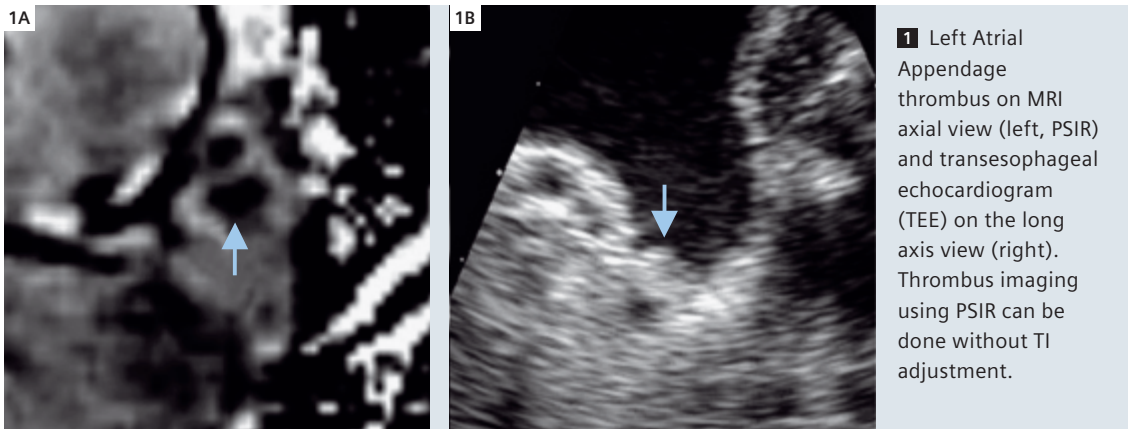
Of all the imaging modalities, MRI offers the most detailed anatomic and physiologic information about normal and damaged myocardial tissue. It has vastly superior soft tissue contrast when compared to fluoroscopy and CAT scans and does not expose the patient to ionizing radiation. In current practice, MRI has several important roles in patient screening and procedure planning, improved navigation in procedures requiring substrate based ablation, and important roles in follow-up and localizing causes of post-procedural complications.

MRI and treatment of atrial fibrillation – pre-procedure

Visualization of thrombus

Identification of left atrial thrombi is a critical component in preparing patients for a successful RF procedure. In AF, there is a very high age-dependent incidence of left atrial thrombus which may range between 3% and 21% [9]. One primary location for thrombus formation is within the left atrial appendage due to altered blood flow when the arrhythmia is present [10]. The current accepted clinical diagnostic test of choice to screen

CMR offers the most detailed anatomic and physiologic information about normal and damaged myocardial tissue.



1 Left Atrial Appendage thrombus on MRI axial view (left, PSIR) and transesophageal echocardiogram (TEE) on the long axis view (right). Thrombus imaging using PSIR can be done without TI adjustment.

for left atrial thrombi is transesophageal echocardiogram (TEE) [11, 12]. Firstly, despite very high accuracy, TEE is still semi-invasive which may lead some patients to forego the procedure. Secondly, the complex morphology of the left atrial appendage may make estimation/localization of a thrombus difficult and may result in underestimation of the thrombus [13]. In contrast, cardiac MRI allows for a convenient and useful alternative to TEE. It is non-invasive, allows evaluation of cardiac morphology without any assumptions in regard to cardiac geometry, and can be taken at the same time as other studies that are necessary for planning of the RF ablation procedure.

In recent studies, MRI successfully detected thrombus with 100% sensitivity (verified utilizing TEE) [14, 15]. The thrombus was imaged utilizing a delayed contrast-enhanced T1-weighted inversion (IR) recovery sequence timed to null thrombus. The images were acquired in axial and longitudinal planes through the left atrium with additional TrueFISP cine imaging in matched slices (Figure 1). By imaging the thrombus using multiple adjacent slices it is possible to provide a better estimation of its overall size and volume. Successful localization of the thrombus prior to ablative procedures allows for aggressive anti-coagulative therapy to be pursued which has been shown to be very effective in resolving the clot [14]. MRI shows promise as a future alternative to TEE for the detection of thrombus.

Segmentation and anatomy posterior to the left atrium

Radiofrequency ablation in the LA has the potential to damage adjacent structures with potentially deadly side effects. For this reason, MRI serves an

essential point in the planning of the procedure. In patients with permanent atrial fibrillation, the left atrium often dilates. This may result in changes to the morphology of the structures posterior to the left atrium. In one study of 42 patients about to undergo catheter treatment in the LA for AF, the larger LA size resulted in the spine and aorta impressing on the LA frequently. The esophagus was also a persistent feature running directly posterior to the LA and contacting it in all of the patients imaged. These findings are important as the topology of the posterior wall of the LA may be altered by the presence of the aorta or the spine [16]. There have also been reports of the LA wall and the pulmonary veins being compressed by the aorta. This has resulted in narrowing of the pulmonary veins and increased concern for aortic injury. Segmentation and volume rendering of structures and their relationship to the LA anatomy allows the physician performing the procedure to take care when performing ablation in points of concern.

MRI utilization in the cath lab – periprocedure

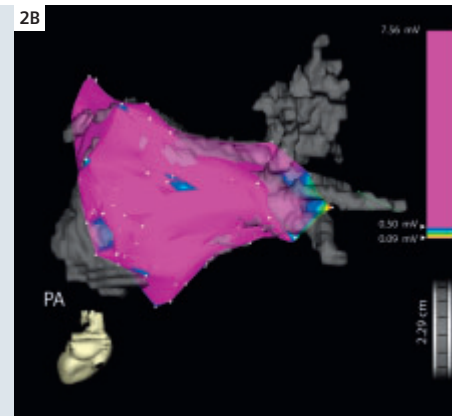
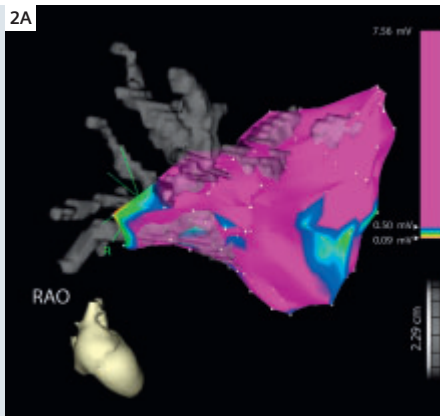
Merged image navigation – MRI and electro-anatomic mapping systems (CARTOMERGE)

Electroanatomic mapping systems which allow for high-resolution MRI images to be merged with electrophysiological data acquired during the ablation procedure help to alleviate some of the potential complications (Figure 2). The electroanatomic model also helps the physician performing the procedure to guide the catheter manipulation near pulmonary vein ostia and other complex structures while helping to ascertain complications which may involve other structures of concern such as the esophagus or aorta (Figure 3).

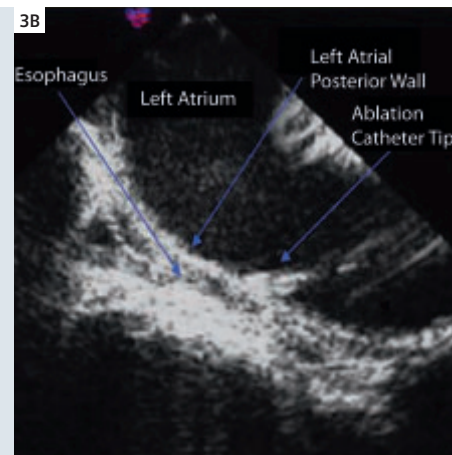
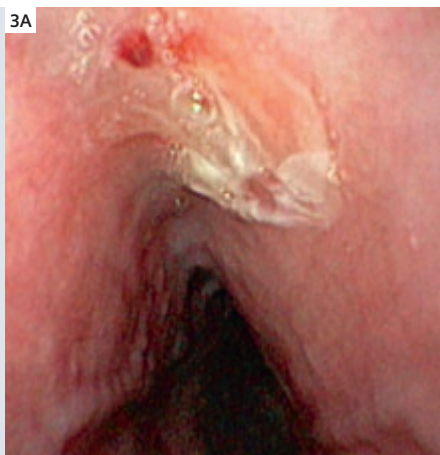
Cardiac MRI is a convenient and useful alternative to TEE for left atrial thrombus detection.

Inspace EP® facilitates merging of MRI and electroanatomic mapping data.

2 3D computed tomographic reconstruction of the left atrium (LA) aligned with 3D LA voltage map (solid contour map). The 3D images are acquired from high resolution MRI contrast scans obtained after injecting the patient with gadolinium. Purple areas represent normal myocardium with green and blue spots corresponding to areas of low voltage/fibrotic tissue.



3 (A) Necrotic and ulcer changes within the anterior aspect of the esophagus. These changes were seen in the esophageal wall in close proximity to the left atrial posterior walls. The image shown was taken 24 hours after circumferential pulmonary vein isolation (CVPI) utilizing RF energy.
(B) Intracardiac echocardiogram image demonstrating radiofrequency lesion delivery at the left atrial posterior wall (LA). The esophagus is often within close proximity of the posterior wall of the LA making it a likely candidate for injury.



Although merging with MRI data allows for navigation models to be substantially refined, the overall accuracy of the model still remains controversial [17, 18]. Image integration may be affected by a variety of factors including differences in the heart size because of changes in rhythm and rate, contractility or fluid status. In various studies, operators utilizing other real-time imaging modalities (e.g. fluoroscopy and intracardiac echocardiography [ICE]) were blinded to merged electroanatomic/MRI images created utilizing a CARTOMERGE® system (BioSense Webster; Denver, Colorado, USA). Despite careful attempts to optimize registration, the CARTOMERGE guided catheter positioning was subject to spatial errors in all studies from 0.5 to 1.0 cm when compared to mapping of the positions in ICE [17–19]. Such a misregistration is of significant clinical importance as it casts serious doubt on the location of lesion formation. This may result in complications such as the inappropriate ablation of the pulmonary veins resulting in PV stenosis. Accuracy can be improved through the addition of an appropriate two-dimensional image modality

including fluoroscopy or ICE though these solutions are imperfect. As real-time 3D MRI becomes available, it will become more important in providing real-time information regarding structure and function during RF procedures.

RF energy delivery and posterior mediastinal injury

An additional component of successful pulmonary vein isolation involves delivering an effective amount of energy for an appropriate duration. Both the choice of catheter and the mode of energy titration during RF ablation are likely to have important influences on the operator's success in accomplishing permanent changes to the electrical signal propagation within the LA. This is particularly important regarding the recognition of left atrial-esophageal fistula as a potentially fatal complication of the AF ablation procedure [20]. Striking a balance between effective lesion formation in the LA and preventing damage to the adjacent structures can be difficult. In one recent study comparing catheter types and imaging modalities,

esophageal wall changes (including edema/erythema and necrosis) were seen in 35.7% of the patients which were ablated using an open irrigation tip catheter and changes were seen in 57.1% of patients where power delivery was monitored using ICE (Figure 4) [21]. The high rate of injury highlights the need to effectively titrate and monitor tissue response to RF energy. MRI scans which utilize techniques such as delayed enhancement will play an important role in helping to determine appropriate power delivery settings which result in effect lesion formation without causing unnecessary damage to other structures.

MRI use in post-procedure care and follow-up

Delayed Enhancement MRI imaging – imaging RF ablation scar

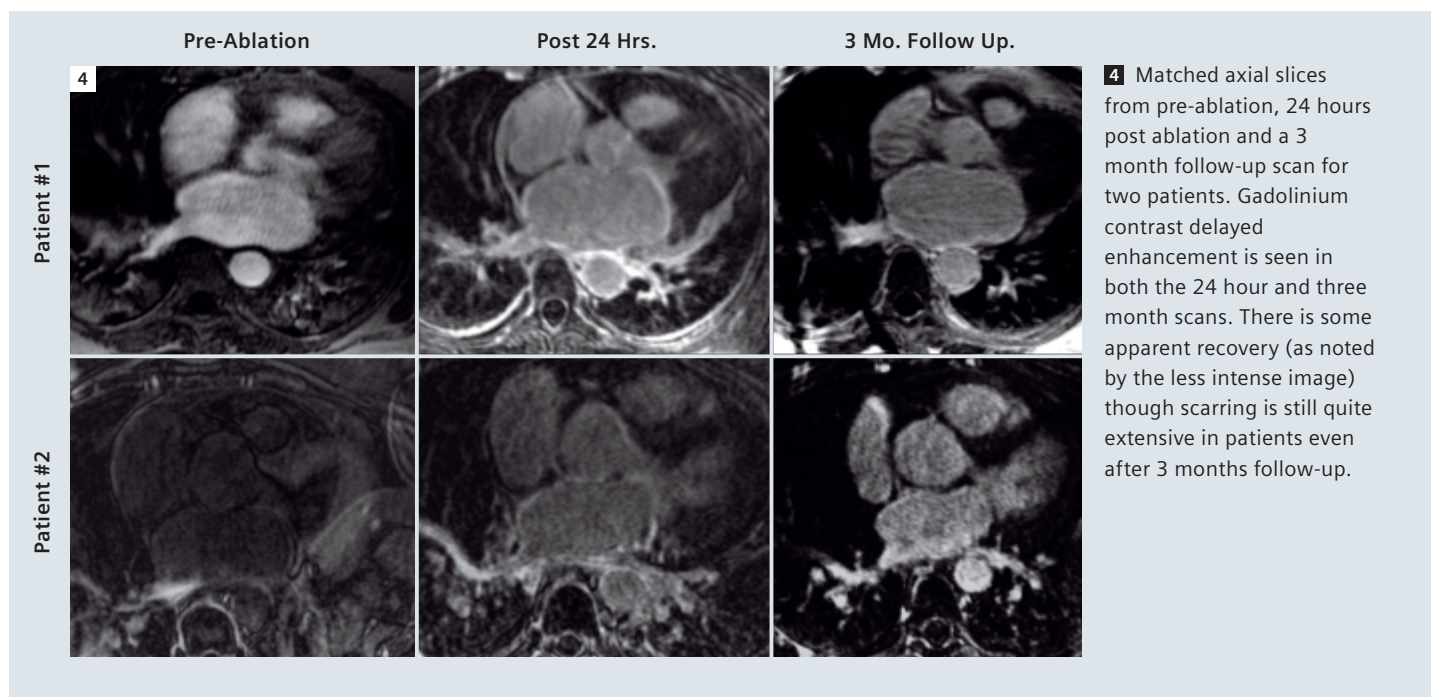
Given concerns about energy delivery and potential injury to other structures, MRI provides a powerful tool for investigation into the injury of tissues near the posterior LA wall. Delayed enhancement cardiovascular magnetic resonance imaging (DE-MRI) is an established clinical method for visualizing tissue necrosis in a variety of cardiac disease processes. These include visualizing myocardial infarction and injury due to myocarditis. This imaging method also has uses in determining the health of atrial tissue following ablation. Contrast en-

hancement in injured tissue observed by MRI occurs due to altered washout kinetics of gadolinium relative to the normal surrounding tissue. RF injury to the right ventricle has been shown on MRI using an intrathoracic high resolution coil [22]. Visualization of RF ablation lesions within the LA using MRI have also recently been reported and imaging modalities developed so that these scans may be run on clinical scanners [23, 24]. The typical imaging protocol includes contrast enhanced pulmonary vein angiography, 2D cine imaging and delayed enhancement imaging. Pulmonary vein MR angiography is acquired during injection of gadolinium-based contrast agent (0.2 mmol/kg). 20 minutes following the injection, an additional three dimensional (3D) DE-MRI scan of the atria and PVs is acquired with navigator tracking during free breathing [23, 25, 26].

Figure 4 shows typical images acquired using 3D DE-MRI sequence prior to the ablation procedure, 24 hours after the procedure and a follow-up scan at 3 months. Delayed enhancement is readily seen in both the 24 hour and 3 month follow-up images near the pulmonary vein ostia and along the posterior wall in all patients for whom imaging data was taken [23, 24]. In addition to the delayed enhancement seen at the site of the LA posterior wall, septum and roof of the LA it is possible to see significant enhancement in por-

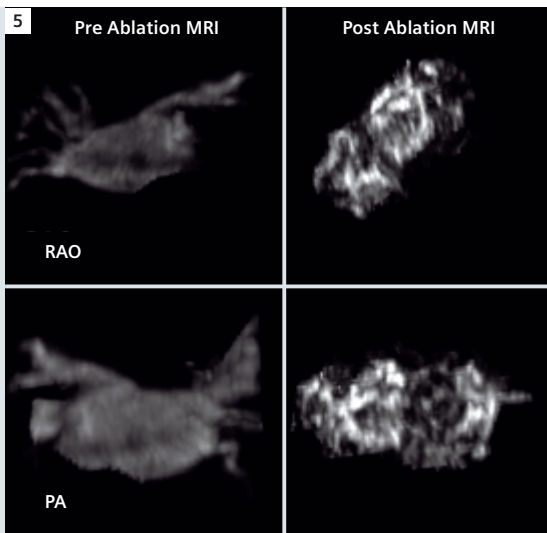
With delayed enhancement (DE) imaging, CMR provides a powerful tool for investigation into the injury of tissues after RF ablation.

A typical imaging protocol for post-procedure care includes contrast enhanced PV angiography, 2D cine and DE imaging.



4 Matched axial slices from pre-ablation, 24 hours post ablation and a 3 month follow-up scan for two patients. Gadolinium contrast delayed enhancement is seen in both the 24 hour and three month scans. There is some apparent recovery (as noted by the less intense image) though scarring is still quite extensive in patients even after 3 months follow-up.

5 Maximal Intensity Projection (MIP) of 3D reconstruction of Delayed Enhancement MRI (DE-MRI) images and scar formation as a result from RF ablation in a single patient.



2D and 3D PSIR and TurboFLASH/TrueFISP IR sequences are provided for delayed enhancement imaging in the Advanced Cardiac Package.

tions of the aorta and the pulmonary tree. It is probable that while some enhancement is due to injury and inflammation, it is also likely that some delayed enhancement in the aorta is also due to the increased fibrous nature of the tissue in this location. 3D visualization and segmentation of the image volume acquired by the DE-MRI sequence allow for the overall extent of scarring to be evaluated (Figure 5). This image analysis offers evidence of the extent of atrial scarring and its relationship to the original ablation scar created during the RF procedure (CARTOMERGE model). The DE-MRI scan may be used to analyze patients with post-procedural complications and determine how they might be related to initial RF procedure or other factors related to their inpatient-hospital care. This new imaging method also allows patient outcome studies to be performed which might assess how atrial scarring is connected to the recurrence of AF.

Future work: MRI guided ablation procedures

One of the great advantages of MRI guidance for electrophysiology procedures is the excellent soft tissue contrast and adequate spatial resolution available without the need to expose a patient to ionizing radiation. Research groups have reported success in guiding the RF ablation catheter to the atrial wall and the right ventricle apex. By using low-pass RF filters, image acquisition was possible even during RF energy applications. Studies in animal models have also have also reported success in imaging lesion formation by T2-weighted FSE

imaging and T1-weighted contrast enhanced-gradient echo imaging [27]. Using pulse sequences such as the delayed enhancement sequence discussed and other novel imaging sequences, it may be possible to develop technology which allows for the imaging of scar formation in real-time. As MRI techniques for scar imaging become available, MRI will be an indispensable tool within the cath lab itself. Within a single display, it will become possible to show lesion size and location and how that relates to existing abnormal tissue. This is likely to greatly improve the success rate in complex patients.

Conclusion

MRI is an extremely important modality for the treatment of atrial fibrillation. It currently has important implications in preparing patients for the initial treatment by helping to localize left atrial thrombus and defining anatomy of pulmonary veins, left atria, and the surrounding structures. During the ablation procedure, MR angiograms help to improve anatomical maps which are used in conjunction with other imaging modalities to determine appropriate sites for ablation. MRI also has very important roles in post-procedural assessment and follow-up. Using delayed enhancement MRI, it is possible to visualize the scar utilizing clinical scanners. This will likely prove valuable in diagnosing post-procedural complications and determining how they may be related to the RF parameters. Additional research regarding patient outcome and its relation to the type and extent of post-procedure scar should be pursued. As interventional MRI scanners become available, MRI will become even more important than it now is in the treatment of atrial fibrillation patients. By building on the success of other groups which have successfully applied MRI technology to interventional procedures targeting the ventricle; it will be possible to assess lesion size and change in tissue pathology in real-time. These steps will serve to greatly increase the curative rate for AF while simultaneously decreasing the complication rate.

Acknowledgements

The authors gratefully acknowledge the assistance of Joshua E. Blauer, Troy J. Badger, and Eric Fish in the preparation and editing of this manuscript.

CMR is a highly valuable tool in preparation, performing and follow-up of RF ablation procedures in cardiac electrophysiology.

Contact

Nassir F. Marrouche, M.D.
 Director, Cardiac Electrophysiology Laboratories
 Director, Atrial Fibrillation Program
 Division of Cardiology
 University of Utah Health Sciences Center
 30 North 1900 East
 Room 4A100
 Salt Lake City, Utah 84132-2400
 USA
 Nassir.Marrouche@hsc.utah.edu
 Phone: +1-801-581-2572
 Fax: +1-801-581-7735

References and recommended reading

- Haissaguerre M, Jais P, Shah DC, et al. Spontaneous initiation of atrial fibrillation by ectopic beats originating in the pulmonary veins. *The New England Journal of Medicine*. 1998;339(10):659–66.
- Kottkamp H, Tanner H, Kobza R, et al. Time courses and quantitative analysis of atrial fibrillation episode number and duration after circular plus linear left atrial lesions: trigger elimination or substrate modification: early or delayed cure? *Journal of the American College of Cardiology*. 2004;44(4):869–77.
- Oral H, Scharf C, Chugh A, et al. Catheter ablation for paroxysmal atrial fibrillation: segmental pulmonary vein ostial ablation versus left atrial ablation. *Circulation*. 2003;108(19):2355–60.
- Pappone C, Manguso F, Vicedomini G, et al. Prevention of iatrogenic atrial tachycardia after ablation of atrial fibrillation: a prospective randomized study comparing circumferential pulmonary vein ablation with a modified approach. *Circulation*. 2004;110(19):3036–42.
- Pappone C, Oreto G, Rosanio S, et al. Atrial electroanatomic remodeling after circumferential radiofrequency pulmonary vein ablation: efficacy of an anatomic approach in a large cohort of patients with atrial fibrillation. *Circulation*. 2001;104(21):2539–44.
- Pappone C, Rosanio S, Augello G, et al. Mortality, morbidity, and quality of life after circumferential pulmonary vein ablation for atrial fibrillation: outcomes from a controlled non-randomized long-term study. *Journal of the American College of Cardiology*. 2003;42(2):185–97.
- Oral H, Pappone C, Chugh A, et al. Circumferential pulmonary vein ablation for chronic atrial fibrillation. *The New England Journal of Medicine*. 2006;354(9):934–41.
- Lemola K, Desjardins B, Sneider M, et al. Effect of left atrial circumferential ablation for atrial fibrillation on left atrial transport function. *Heart Rhythm*. 2005;2(9):923–8.
- Stollberger C, Chnupa P, Kronik G, et al. Transesophageal echocardiography to assess embolic risk in patients with atrial fibrillation. ELAT Study Group. *Embolism in Left Atrial Thrombi*. *Ann Intern Med*. 1998;128(8):630–8.
- Narumiya T, Sakamaki T, Sato Y, et al. Relationship between left atrial appendage function and left atrial thrombus in patients with nonvalvular chronic atrial fibrillation and atrial flutter. *Circ J*. 2003;67:68–72.
- Daniel WG, Mugge A. Transesophageal echocardiography. *The New England Journal of Medicine*. 1995;332(19):1268–79.
- Manning WJ, Weintraub RM, Waksmonski CA, et al. Accuracy of transesophageal echocardiography for identifying left atrial thrombi. A prospective, intraoperative study. *Ann Intern Med*. 1995;123(11):817–22.
- Stollberger C, Ernst G, Bonner E, et al. Left atrial appendage morphology: comparison of transesophageal images and postmortem casts. *Z Kardiol*. 2003;92(4):303–8.
- McGann C, Di Bella EVR, Wilson B, et al. MRI to Detect and Follow Regression of Left Atrial Appendage Thrombus. Paper presented at: Scientific Sessions - AHA 2007, 2007.
- Mohr OK, Nowak B, Petersen SE, et al. Thrombus detection in the left atrial appendage using contrast-enhanced MRI: a pilot study. *Am J Roentgenol*. 2006;186(1):198–205.
- Hoffmeister PS, Chaudhry GM, Mendel J, et al. Evaluation of left atrial and posterior mediastinal anatomy by multidetector helical computed tomography imaging: Relevance to ablation. *J Interv Card Electrophysiol*. 2007;18(3):217–23.
- Zhong H, Lacomis JM, Schwartzman D. On the accuracy of CartoMerge for guiding posterior left atrial ablation in man. *Heart Rhythm*. 2007;4(5):595–602.
- Malchano ZJ, Neuzil P, Cury RC, et al. Integration of cardiac CT/MR imaging with three-dimensional electroanatomical mapping to guide catheter manipulation in the left atrium: implications for catheter ablation of atrial fibrillation. *Journal of Cardiovascular Electrophysiology*. 2006;17(11):1221–9.
- Dacarcett M, Segerson NM, Gunther J, et al. Blinded Correlation Study of Three-Dimensional Electroanatomical Image Integration and Phased Array Intra-cardiac Echocardiography for Left Atrial Mapping. University of Utah 2007.
- Papone C, Oral H, Santinelli V, et al. Atrio-esophageal fistula as a complication of percutaneous transcatheter ablation of atrial fibrillation. *Circulation*. 2004;109:2724–6.
- Marrouche NF, Guenther J, Segerson NM, et al. Randomized comparison between open irrigation technology and intra-cardiac-echo-guided energy delivery for pulmonary vein antrum isolation: procedural parameters, outcomes, and the effect on esophageal injury. *Journal of Cardiovascular Electrophysiology*. 2007;18(6):583–8.
- Dickfeld T, Kato R, Zviman M, et al. Characterization of radiofrequency ablation lesions with gadolinium-enhanced cardiovascular magnetic resonance imaging. *Journal of the American College of Cardiology*. 2006;47(2):370–8.
- Peters DC, Wylie JV, Hauser TH, et al. Detection of pulmonary vein and left atrial scar after catheter ablation with three-dimensional navigator-gated delayed enhancement MR imaging: initial experience. *Radiology*. 2007;243(3):690–5.
- McGann C, Kholmovski EG, Oakes RS, et al. Magnetic Resonance Imaging Detects Chronic Left Atrial Wall Injury Post Ablation of Atrial Fibrillation. 2007, Scientific Sessions – AHA 2007, Orlando.
- Stuber M, Botnar RM, Danias PG, et al. Contrast agent-enhanced, free-breathing, three-dimensional coronary magnetic resonance angiography. *J Magn Reson Imaging*. 1999;10(5):790–9.
- Saranathan M, Rochitte CE, Foo TK. Fast, three-dimensional free-breathing MR imaging of myocardial infarction: a feasibility study. *Magn Reson Med*. 2004;51(5):1055–60.
- Lardo AC, McVeigh ER, Jumsirikul P, et al. Visualization and temporal/spatial characterization of cardiac radiofrequency ablation lesions using magnetic resonance imaging. *Circulation*. 2000;102(6):698–705.

Workflow Optimization for CMR Adenosine Stress Perfusion in Clinical Routine

Giso v. der Recke, M.D.; David Hardung, M.D.; Heyder Omran, M.D.

St.-Marien-Hospital, Dept. of Cardiology, Bonn, Germany

Introduction

Adenosine stress perfusion cardiac magnetic resonance (CMR) has been demonstrated to provide reliable information about relevant myocardial ischemia [1, 2, 3]. In stable patients with suspected coronary artery disease, this method offers high diagnostic accuracy for identifying patients that benefit from coronary revascularisation [4]. Furthermore it has been shown that the negative predictive value for an event free follow-up is excellent [5, 6, 7]. Cardiac adverse events are extremely rare during adenosine administration. Due to the very short half-life of adenosine, stress CMR can be performed without extended patient monitoring [8].

Besides academic considerations concerning diagnostic accuracy; patient acceptance, cost and time efficiency, as well as convenience for the investigator, are also important for routine clinical application. In this outline we provide tips and tricks for improving performance of a cardiac MR unit with a focus on stress perfusion MRI based on our experience.

Logistics and patient preparation

A team of two trained technologists and one physician can efficiently operate a CMR unit in a high volume setting.

24 hours prior to the investigation patients have to refrain from caffeine (e.g. coffee, tea, cacao, energy drinks) and drugs (e.g. xanthines/theophylline, nitrates) that could alter the response to adenosine. Thus, a checklist of precautions should be handed over to the patient together with the written informed consent as early as possible. Immediately prior to entering the magnet room,

the physician explains the procedure to the patient in detail. Special emphasis should be taken on possible side effects during adenosine infusion. The patient should be informed that thoracic oppression / chest pain, dyspnoea and increased anxiousness may occur in the first 3–4 minutes. This prevents discontinuation of the procedure during or right after the stress test.

Within the scanner room, the patient is prepared by one of the technologists. Two i.v. lines should be placed in each of the antecubital veins (fig. 1). A line for contrast agent and one for adenosine are connected **separately** to avoid a bolus injection of adenosine when the contrast agent is flushed with much higher flow rate. The blood pressure cuff should be placed on the arm of the contrast injection, to avoid interference with the administration of adenosine.

ECG electrodes are placed and checked for quality. An integrated ECG display at the scanner including a 5-star quality grading visualization (new with MR B15) supports the workflow. Exclusion of tachyarrhythmia or severe ventricular arrhythmias is mandatory. Additional application of a pulse clip as an alternative trigger acts as a backup in case of ECG impairment while the patient is in the scanner. The venous access should be tested via administration of saline solution to exclude paravasation or slow gadolinium flow. In case of claustrophobia, the short acting benzodiazepines (e.g. midazolam 1.0 to 1.5 mg i.v.) can be administered. Possible effects on driving fitness should be taken into account.

Parallel to the preparation of the patient in the scanner room, the second technologist prepares



1 Patient preparation for CMR Adenosine Stress Perfusion Imaging. ECG electrodes are attached to the chest. Signals are transferred via Bluetooth™ to the scanner. Two iv lines are placed allowing for independent injection of Adenosine and contrast media. For optional monitoring of blood pressure during the exam, a blood pressure cuff is placed on the contrast agent injection side.

the adenosine-infusion once contraindications (e.g. severe arrhythmia, AV blockade) are excluded. We use an automatic perfusion pump for injection, which is connected to the patient by the above mentioned 6 m i.v. line. The line itself contains 12 ml of volume. The perfusion pump is positioned outside the scanner room.

The total volume of fluid filled into the pump is 48 ml. The solution consists of adenosine 140 µg/kg BW/min for three minutes plus the amount of saline needed to fill up for 48 ml. The pump is then forwarded, so that the i.v. line is completely filled. Thus, 36 ml will be given to the patient; the remaining 12 ml will stay in the 6 m i.v. line after injection.

The purpose behind this kind of preparation is for the same total amount of fluid to be injected for each patient so that the settings of the perfusion pump do not have to be adjusted. Furthermore, the adenosine is diluted, so that negative side effects due to wrong infusion rates or bolus administration can be reduced.

The total preparation time for a patient from being undressed to entering the magnet takes an average of about 8 minutes.

After patient preparation, one of the technologists performs the MRI scan. The other technologist han-

dles the previous patient and the patient next in line. In the meantime, the physician can read the previous scan, write reports, or provide explanations for the patients.

Protocol optimization

Our protocol for adenosine stress perfusion MRI is based on study protocols used in larger trials and on our own experience. The protocol is established on a MAGNETOM Avanto 1.5 Tesla scanner (Siemens, Erlangen). For the routine indication of relevant ischemia this protocol is usually not altered. Each successive step is predefined on the scanner. This allows for a fast and standardized acquisition and reduces interobserver variability. For other indications (e.g. myocarditis, cardiomyopathies) different selectable protocols are provided.

Function

After localizer acquisition we perform functional imaging of the left and right ventricle for assessment of global and regional wall motion abnormalities and valve function. By standard, three long axes are planned along the left ventricle, including four-chamber view (4CV), two-chamber view (2CV) and a leftventricular outflow tract (LVOT or 3-ch) view. The Siemens *syngo* acquisition work-

2 A flexible, light-weight Tim Body Matrix coil is placed on the chest. A pulse clip can be used as an alternative way for triggering image acquisition. A headphone is connected for communication with the patient – due to the very low noise level on the MAGNETOM Avanto, there is no need for special noise protection.



place is configured in such a way that a short axis localizer image remains in the middle view segment. That way, the orientation of the image plane can easily be rotated into each of the long axis views and acquisition speed can be increased. Special care is taken for the left ventricular outflow tract to exclude severe aortic stenosis as a contraindication for stress testing. Next, 2 views along the long axis of the right ventricle and a stack of up to 12 short axis slices covering both ventricles are acquired.

Stress perfusion

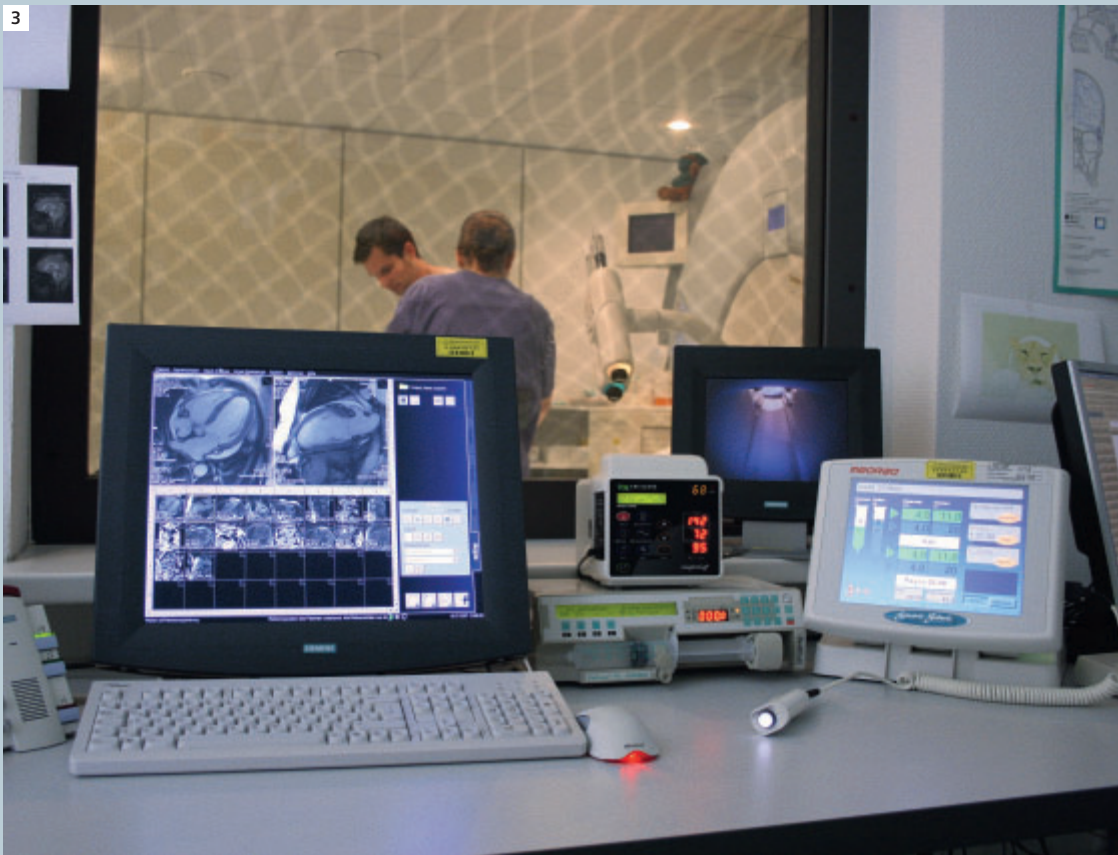
The module of stress perfusion consists of a test acquisition and the actual perfusion sequence. The test sequence is performed to guarantee correct slice position. Fold-over artifacts into the left ventricle should be avoided. Furthermore, care should be taken to exclude the left ventricular outflow tract from the most basal slice. The test sequence can be adjusted as often as necessary for an optimal acquisition. As soon as this is achieved, a "copy reference" is activated, which transfers all settings to the following sequences.

Accordingly, the set of short axes of the test perfusion is the reference for all following acquisitions including wall motion, perfusion, and late enhancement which enables easy comparison of the respective slices.

After informing the patient about the expected physiologic reactions, the perfusion pump for the adenosine is started. Usually, an increment in heart rate is expected within the first 30 seconds to one minute – the extent can differ from patient to patient and there is no maximum heart rate to be reached. The blood pressure is then checked [BP control is not mandatory]. For a successful study, it is important to keep talking to the patient and to reassure her/him that the changes she/he might experience are quite usual.

30 seconds prior to the end of the adenosine infusion (after 2.5 min), the perfusion sequence is started together with a 0.075 mmol / kg BW injection of Gd-DTPA at a rate of 4 ml / sec. (The applied dose of contrast is sufficient for visual analysis; it may differ from site to site, but is usually between 0.05 and 0.1 mmol/kg BW). An "online window" can give information on the correct appearance of

3



3 The CCTV screen, adenosine perfusion pump, injector control unit and the BP/sO₂ monitoring device are positioned next to the MR acquisition workplace to ensure optimal workflow and patient monitoring.

contrast in the heart and the “physio control window” identifies correct ECG triggering.

Afterwards, the patient is questioned again about condition. Usually, the heart rate starts to drop within 30 seconds after the end of the adenosine infusion and possible complaints disappear in parallel.

A possible amendment for this module is to include functional stress imaging during the plateau phase of heart rate increment. The plateau after reaching peak heart rate normally comprises the last minute before contrast agent injection. During this time, an SSFP (TrueFISP) cine sequence with real time acquisition can acquire three short axis slices in six heart beats. These then allow for wall motion analysis. This method has been demonstrated to have a very low sensitivity for relevant ischemia. However, the specificity of an observed wall motion abnormality for a high grade coronary artery stenosis is very high.

Break

To allow contrast wash-out from stress perfusion, a gap of ten minutes is planned between stress

and rest perfusion. During this time, the patient stays in the magnet. Either further functional studies (e.g. valve function, phase-contrast sequences) are acquired, or simply the radio is turned on for the entertainment of the patient, during which time the physician can review the stress perfusion and function.

Alternatively, using a Whole-Heart 3D sequence with motion – adaptive diaphragmatic triggering, an approach towards coronary MR angiography can be taken during this break. But since patients do experience a considerable drop in heart rate during the first minute after stress perfusion, the accurate planning of this sequence might be challenging.

Rest Perfusion

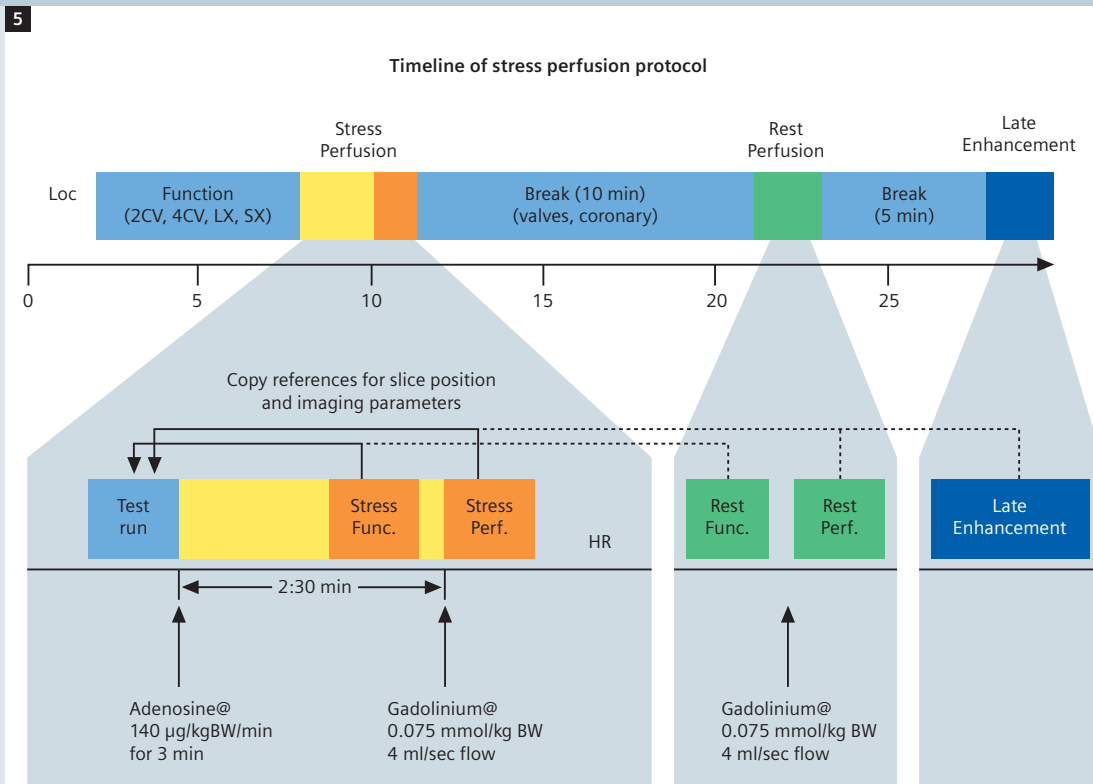
Rest perfusion is performed using exactly the same sequence parameters and amount of contrast agent as for stress perfusion. By implementation of a “copy reference” on the stress perfusion, the sequence can be run without any further planning or adjustment. In case of a completely normal stress perfusion, the rest perfusion could be skipped. In

4 The Cardiovascular MRI team of St. Marien-Krankenhaus, Bonn; from left to right: Ms Ilka Hees (RT), Dr. Carsten Pipp (volunteer), Dr. Giso von der Recke (head of CMR team), Dr. David Hardung (cardiology resident), Ms. Christine Bäumler (RT)



5 Timeline of stress perfusion protocol

Loc = Localizer Sequence
2CV = two-chamber view
4CV = four-chamber view
LX = long axis
SX = short axis
Func = function
Perf = perfusion
HR = heart rate
BW = body weight



that case a second bolus of contrast agent should be administered to reach the required 0.15 to 0.2 mmol / kg BW for optimal late enhancement imaging. However, we recommend including rest perfusion in every patient for retrospective evaluation.

Late Enhancement

At least five minutes after the second contrast agent has been administered, the sequences for late enhancement are run. Generally, we use a phase sensitive inversion recovery (PSIR) sequence. Therefore, no adjustment for correct "Time of Inversion" is needed. Otherwise, when using a IR-GRE (e.g. IR TurboFLASH), a TI-Scout sequence is performed first. However, if we stick to the time frame of 10 minutes between stress and rest, and an additional five minutes between rest and late enhancement, the time of inversion is relatively fixed at 300 ms with our scanner. Again, these sequences are planned using copy references. First, a high resolution IR-sequence with reference on the stress perfusion slices is planned. Afterwards, a single-shot sequence with a copy reference on the stack of short axes acquired for cine imaging is used cover the whole left ventricle. In case of pathologic findings on the late enhancement, additional long axis slices are planned manually to confirm this finding. Afterwards, the patient is taken out of the scanner.

As pointed out predefined protocols using copy references facilitate the investigation. Essentially, as soon as the first set of short axes for the test perfusion is adjusted to the optimal field of view, no further planning is needed for the standard adenosine stress perfusion protocol. However, this implies that the stack of short axes for test perfusion is planned with meticulous care. With this protocol the question of relevant myocardial ischemia is answered in less than 30 minutes scanning time.

Summary

Adenosine stress perfusion MR is a feasible and safe procedure for a high throughput setting. Inpatients as well as outpatients can easily be handled by two technologists and one physician. With the above mentioned protocol optimization and logistic guidelines, 40 minutes in the scanner room can be assigned for each patient. For optimal logistics it is essential to use trained personnel that routinely handle patients for stress

perfusion measurements and are accustomed to the specific preparation steps. Furthermore, a standardized and predefined protocol for adenosine stress perfusion guarantees time efficiency as well as low interobserver variability.

Contact

Giso v. der Recke, M.D.
St.-Marien-Hospital
Robert-Koch-Str. 1
53115 Bonn
Germany
Phone: +49-228-505-2577
recke@cardiomrt.net

References

- Schwittler J, Nanz D, Kneifel S, et al. Assessment of myocardial perfusion in coronary artery disease by magnetic resonance: a comparison with positron emission tomography and coronary angiography. *Circulation*. 2001;103(18):2230–5.
- Klem I, Heitner JF, Shah DJ, et al. Improved detection of coronary artery disease by stress perfusion cardiovascular magnetic resonance with the use of delayed enhancement infarction imaging. *J Am Coll Cardiol*. 2006;47(8):1630–8.
- Schwittler J. MR IMPACT: First-pass MR perfusion test superior to SPECT for detection of CAD. Oral presentation. Annual meeting of European Society of Cardiology 2005, Stockholm, Sweden.
- Pilz G, Bernhardt P, Klos M, et al. Clinical implication of adenosine-stress cardiac magnetic resonance imaging as potential gatekeeper prior to invasive examination in patients with AHA/ACC class II indication for coronary angiography. *Clin Res Cardiol*. 2006;95(10):531–8.
- Ingkanisorn WP, Kwong RY, Bohme NS, et al. Prognosis of negative adenosine stress magnetic resonance in patients presenting to an emergency department with chest pain. *J Am Coll Cardiol*. 2006;47(7):1427–32.
- Jahnke C, Nagel E, Gebker R, et al. Prognostic value of cardiac magnetic resonance stress tests: adenosine stress perfusion and dobutamine stress wall motion imaging. *Circulation*. 2007;115(13):1769–76.
- Hardung D, v. der Recke G. Event free survival in patients with suspected coronary artery disease and a negative test result in adenosine stress perfusion magnetic resonance imaging. Oral presentation. SCMR Ninth Annual Scientific Sessions 2006, Miami, USA.
- Miszalski K, v. der Recke G. A prospective study in 644 consecutive patients to assess safety and feasibility of adenosine stress magnetic resonance perfusion for diagnosis of myocardial ischemia. Oral presentation. SCMR Ninth Annual Scientific Sessions 2006, Miami, USA.

CMR Imaging of Myocardial Amyloidosis Using Late Contrast Enhanced Imaging: Challenges and Potential Solutions

Szilard Voros, M.D.¹; Gary McNeal²; Peter Weale²

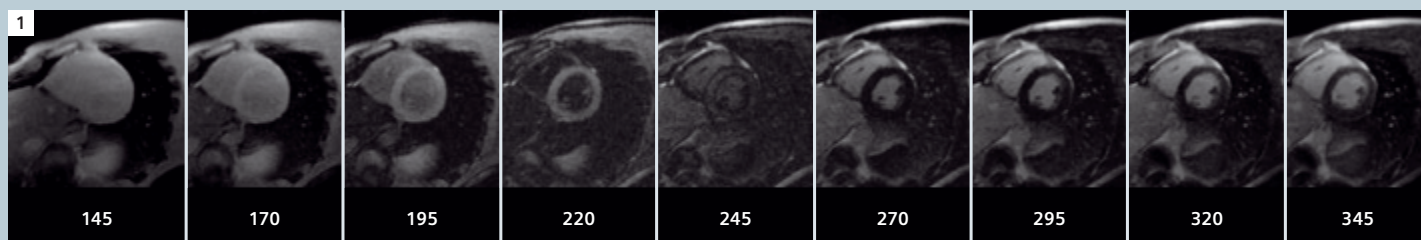
¹Medical Director Cardiovascular MRI and CT,
Fuqua Heart Center of Atlanta, Piedmont Hospital, Atlanta, NC, USA

²Advanced Cardiovascular MR Application Specialists,
Siemens Medical Solutions USA, Chicago, IL, USA

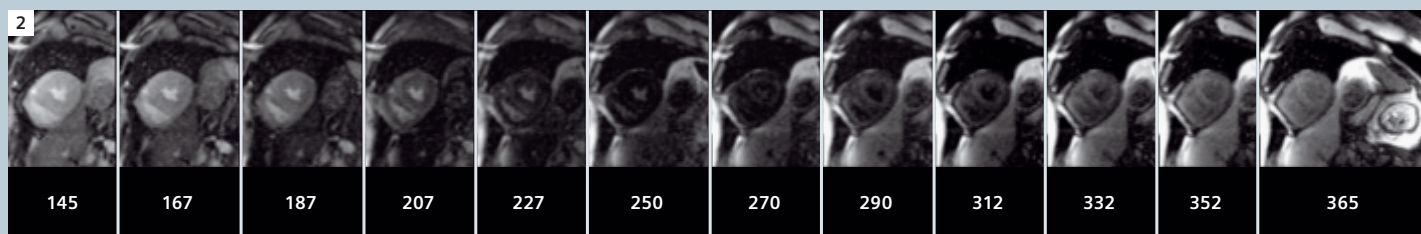
Late Contrast Enhancement (LCE, also known as Delayed Enhancement) is a CMR technique that was initially developed as a method for imaging the extent and transmural extent of myocardial infarction. However, since this technique detects gadolinium retention in tissue, it is useful for the detection of a variety of pathological conditions where gadolinium is retained in the heart due to fibrosis of ischemic or inflammatory etiology and infiltrative disorders. Therefore, this technique has proven to be useful in the evaluation of non-ischemic car-

diomyopathies, including evaluation of fibrosis in hypertrophic cardiomyopathies, myocarditis and infiltrative diseases (e.g. amyloidosis).

The technique is based on maximizing contrast between "abnormal" and "normal" myocardium by use of an inversion recovery magnetization preparation scheme where the inversion time (TI) is selected to eliminate signal from the "normal" myocardium and areas where there is abnormal accumulation of contrast agent and subsequent T1 shortening.



1 Individual frames from a TI-scout - the appropriate TI [in ms] where "normal" myocardium is completely nulled is easily seen to be 270 ms.



2 In this subject with amyloid the null point for myocardium is reached before the blood pool is nulled indicating that the T1 of myocardium is shorter than that of blood. Typically, for infarct imaging, with conventional contrast agents and scan timing the blood pool will have a T1 which is shorter than the T1 of "normal" myocardium.

Selection of TI

The required TI varies with the contrast agent, contrast dose, time after injection, heart rate and other physiological parameters such as the rate of elimination of the contrast agent from the blood pool via the kidneys or other mechanisms.

The traditional method of selecting the optimal TI is to use the "TI Scout" sequence where, in essence, each frame of a cine sequence is acquired after an initial inversion pulse and consequently has a different TI.

This strategy is effective when regional differences exist in gadolinium retention, such as in infarcted tissues, where these regions can be compared to a significant amount of "remote", non-infarcted myocardium. However, diseases that affect the entire myocardium without regional variation pose a challenge with this approach, since no "normal" myocardium can be detected to choose an optimal null-point. This is particularly true for cardiac amyloidosis, where typically the entire myocardium is involved in a circumferential manner and the contrast wash-in and wash-out kinetics are also significantly altered.

The pitfall of the traditional approach is that the operator determining the optimal null-point for the myocardium erroneously may choose an inversion time that nulls signal in the abnormal and not in the normal myocardium. This can result in false negative examinations. This typically does not occur in ischemic heart disease, since the infarcted myocardium is well-delineated and it can be clearly distinguished from normal myocardium.

In amyloid heart disease, the deposition of the abnormal protein occurs in a circumferential manner, starting in the endocardial layers and spreading through the myocardium in a transmural fashion, particularly in the most advanced cases. Therefore, choosing an optimal TI time is difficult, since the amount of normal myocardial tissue is quite minimal. Using the traditional TI-scout approach invariably will lead to incorrect TI selection – the TI chosen, when looking for the "black myocardium", will be significantly shorter than the TI which would have been selected if normal myocardium was in the TI scout slice.

Another important issue is that contrast wash-in and wash-out kinetics are significantly altered in cardiac amyloidosis. Due to the infiltration of tissues, gadolinium is extracted faster from the blood pool, compared to normal myocardial tissue.

Therefore, the optimal time to image after contrast injection is shorter than in typical cases of myocardial infarction.

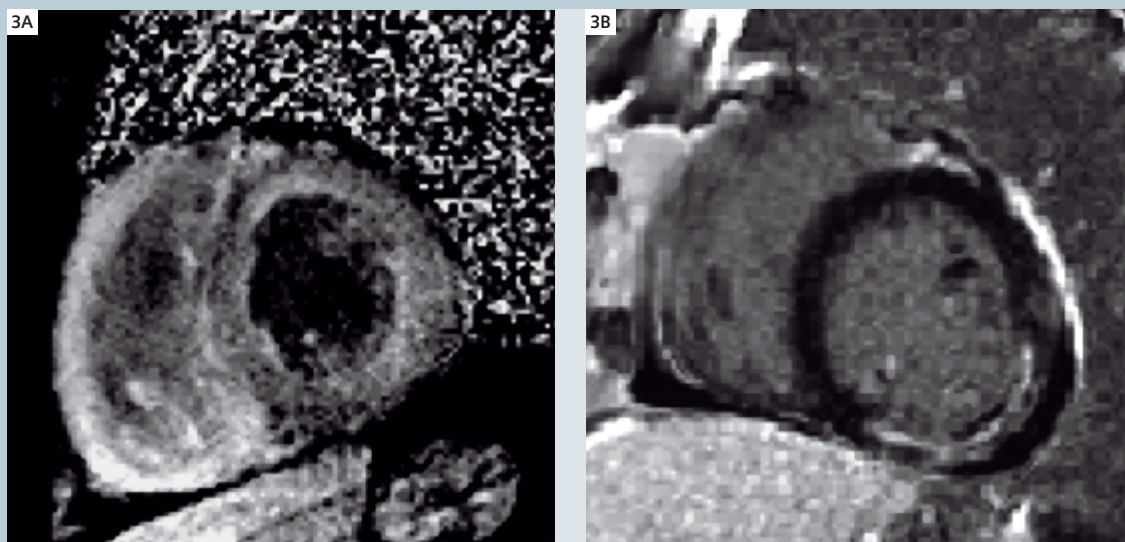
Therefore, timing is critical in patients with suspected cardiac amyloidosis. Both the time after injection as well as the inversion time needs to be modified when looking for this disease.

To identify when this is a problem there are a few indicators which can help:

- when identifying the optimal null point with the TI-scout is more challenging than in most cases, it should raise the suspicion of "global hyperenhancement" due to cardiac amyloidosis,
- when a TI-scout is performed, in the majority of cases the blood pool will reach its null point before the myocardium. If it appears that in a given patient the myocardium reaches the null point before the blood pool, it might also raise the possibility of cardiac amyloidosis,
- use of a Phase Sensitive Inversion Recovery (PSIR) sequence will reduce the need for a precise TI setting, however the lack of "normal" tissue still makes identification of "abnormal" difficult. Again, if the tissue contrast between the blood pool and myocardium is poor, it should raise the issue of cardiac amyloidosis,
- global hyperenhancement in cardiac amyloidosis typically spreads from the subendocardial layers to the subepicardium. Therefore, except in the most advanced cases, a rim of normal tissue might be seen in the epicardial layer.

The best way to make the diagnosis of cardiac amyloidosis is to adjust image acquisition in patients in whom there is sufficient suspicion. At our institution, referring physicians are asked to specifically note on the order sheet when there is any suspicion of cardiac amyloidosis, so the imaging protocol can be adjusted accordingly. We alter our usual "delayed hyperenhancement" imaging protocol as follows:

- Perform an SSFP-based TI-scout in a mid-ventricular short axis slice EARLY (approximately 5 minutes after gadolinium injection).
- Adjust the TI time for the PSIR sequence if needed.
- Perform the PSIR delayed enhancement coverage of the myocardium as usual (2-chamber, 4-chamber, 3-chamber and short axis stack).
- REPEAT the TI-scout in a mid-ventricular short



3 Cardiac amyloidosis (left) vs Ischemic heart disease illustrated by PSIR images - the amyloidosis patient shows „patchy“ enhancement pattern and the myocardium is brighter than the blood pool. In the ischemic patient the normal tissue is homogeneously dark.

(Images courtesy of Dr. Glenn Coates, Wake Radiology, Raleigh, NC, USA.)

axis slice 15 minutes after the injection of the contrast agent.

- Adjust the TI-time for the PSIR sequence again
- REPEAT the typical PSIR coverage of the heart as above

Summary

CMR is the most powerful non-invasive tool to detect cardiac amyloidosis, but it is critical that appropriate technique is utilized. The most important approach is to alter the image acquisition scheme upfront in order to follow the abnormal contrast wash-in and wash-out kinetics seen in this disease. Although some features described above can help to identify the disease with the usual approach, it is much easier if the imaging protocol is altered accordingly. The pointers and indicators

in the preceding text may help to identify these scenarios, both by the abnormal behavior of the TI-scout sequence (with reference to “normal” behavior in ischemic heart disease patients) and in the close examination

of the PSIR sequences to look for heterogeneity in the texture of hyperenhancement and the abnormal contrast of the myocardial signal with reference to the blood-pool.

It should be noted that many of these observations are based on the assumption of a certain contrast agent dose and timing of the scan at a certain time after contrast administration. Significant variation in contrast agent dose may invalidate some of these indicators outlined in this document.

Flow Measurements: Basics and the Application to the Main Pulmonary Artery

Nasreddin Abolmaali, M.D.

OncoRay – Center for Radiation Research in Oncology, Medical Faculty Carl Gustav Carus, TU Dresden, Germany

Introduction

In 1959, Jerome „Jay“ R. Singer published his fundamental work on the quantification of macroscopic flow and microscopic motion (diffusion) using magnetic resonance (MR) [1]. The introduction of MR flow measurements with velocity encoding to the clinical application in the mid-1980s made a new field of functional diagnosis accessible to radiologists [2]. Within the past 20 years, velocity encoded MR has been continuously improved [3] including correction for Maxwell terms [4]. The effective reduction of eddy current effects on flow quantification was established with recent scanners. Further developments include parallel imaging techniques in space and time [5, 6], but these techniques are not widely available. Among others [7], generally accepted clinical applications today include measurement of the cardiac output especially after cardiac surgery [8], quantification of shunt volumes in congenital heart disease [9], and evaluation of valvular anomalies after inconclusive echocardiography [10].

Technical Requirements

Over the last years, most research on and clinical application of flow measurements utilized 1.5 Tesla scanners. But as with other sequence techniques, 3 Tesla will provide a marked increase in signal-to-noise ratio, which was shown to be of up to 79% in MR flow measurements [11]. In every flow measurement, Maxwell-terms and eddy currents may degrade the quantitative results. Therefore it is highly advisable to perform accurate positioning of the target vessel in the center of the main field (B_0), especially along the z-axis. For quantification of vascular flow an appropriate ECG-triggering is mandatory. Triggering may be



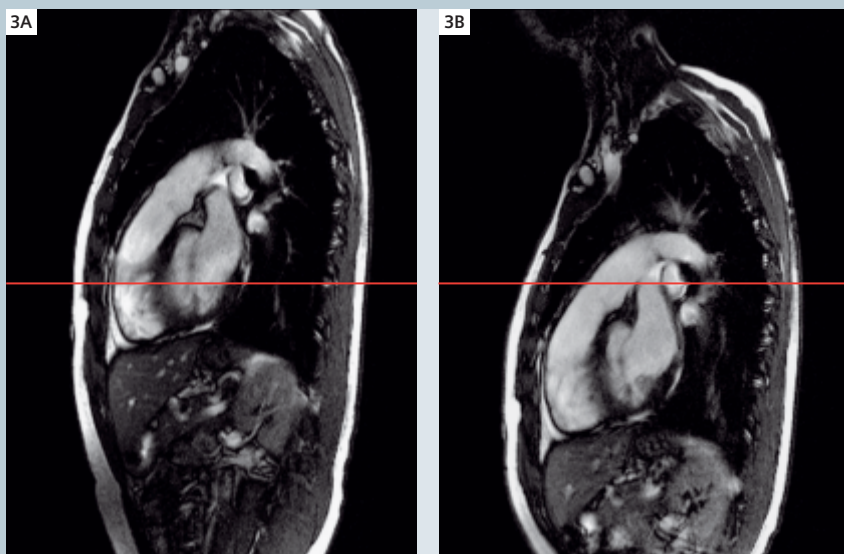
1 For flow measurements in the large vessels of adults, ventral and dorsal body coils are recommended. Small children may be investigated by a combination of the head coil and the large flex coil.



2 Infants are preferably examined in the knee coil.

done prospectively, if high temporal resolution is required, or retrospectively, in the case of most clinical examinations. Triggering should be done without any time delay, which is unavoidable if certain devices are used – some devices cause a delay of up to 40 ms! With prospective triggering, for example, 40 ms delay results in data loss of the first parts of systole.

All vendors supplied their scanners with flow measurement sequences, which are often referred to as phase contrast mapping measurements that



3 When the heart is centered in the B_0 field (red line in Fig. 3A) the main pulmonary artery (MPA) will be a few cm above the B_0 center. The next scout image at the isocenter verifies the centered position of the MPA (Fig. 3B) resulting in the highest accuracy for flow measurements in this vessel.

utilize simple gradient echo techniques. But new sequence designs for flow measurements receive increasing attention.

For flow measurements in the large vessels of adults, ventral and dorsal body coils are recommended. Small children may be investigated by a combination of the head coil and the large flex coil (Fig. 1). Infants are preferably examined in the knee coil (Fig. 2)! The temporal resolution of MR flow measurements cannot compete with echocardiography. Without application of parallel imaging techniques all available scanners should provide a best temporal resolution of about 10 ms with prospective triggering. But for most clinical applications in large vessels (e.g. main pulmonary artery [MPA]) 30 ms may be sufficient.

As a rule of thumb, the selected spatial resolution should at least provide four flow pixels within the acquired vessel to generate reliable flow quantification, but: the more, the better. While the large vessels and the renal arteries may be sufficiently analyzed [12], the flow quantification of the coronary arteries is challenging [13].

The size of the velocity encoding gradients has to be defined before image acquisition. This is usually done with the so-called VENC, which may be set to 150 cm/s in the ascending aorta and 130 cm/s in the main pulmonary artery. For flow data acquisition near valves it is mandatory not to include

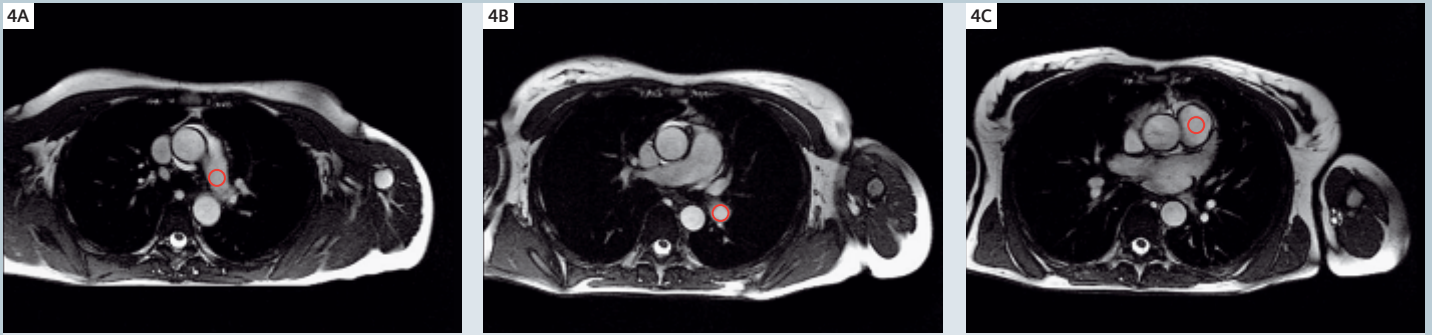
any parts of the leaflets into the quantification region of interest (ROI) during any part of the cardiac cycle. Therefore, the acquisition plane should be about 1–2 cm above the valves in diastole (cardiac contraction during systole will displace the valves caudally).

The last major prerequisite is sufficient flow analysis. Basic algorithms are provided by the vendors, but more comprehensive and comfortable software is available.

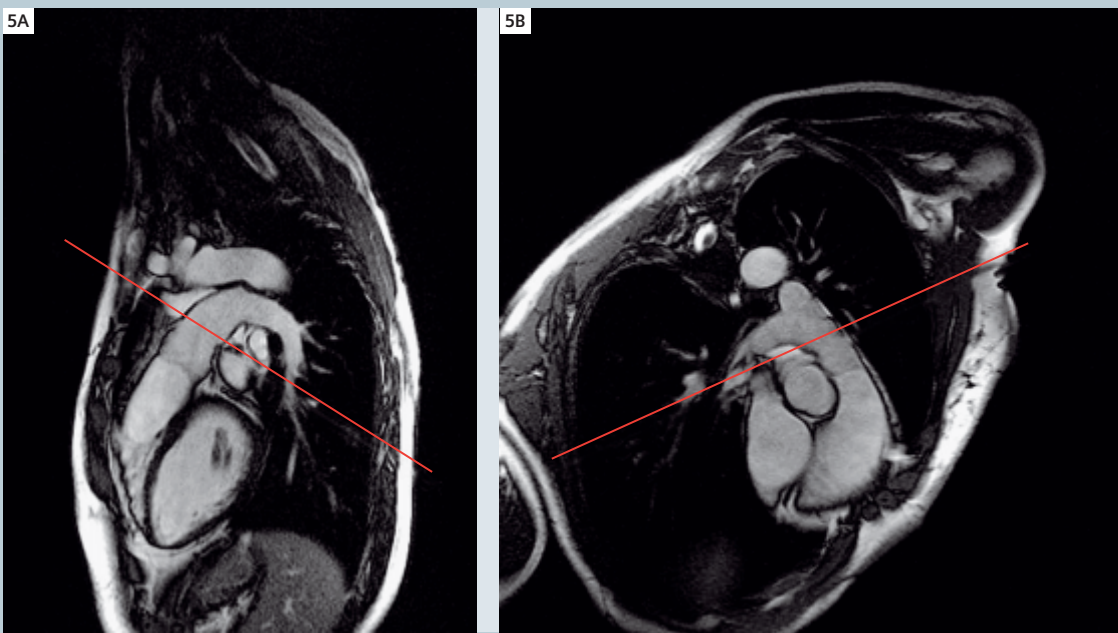
Optimized planning of the acquisition plane in the MPA

To optimize the accuracy of MR flow data, the analysis area ROI in the MPA should be centered in the B_0 -field, especially in the z-axis. For cardiac MR examinations, the technologist usually centers the heart in the B_0 -field. The resulting sagittal scout image (axial images are not useful) at the isocenter (red line in Fig. 3) shows the MPA approximately 5 cm above the B_0 center (Fig. 3A). Using the coordinate display available on the scout images loaded to the EXAM-card, the required repositioning distance (direction out with respect to standard cardiac examinations) of the scanner table can be measured. The correct acquisition position can be adjusted at any time point of any cardiac examination without repositioning the patient on the scanner table. The next scout image at the isocenter verifies the centered position of the MPA (Fig. 3B) resulting in the highest accuracy for flow measurements in this vessel. Subsequently, several axial images from the upper part of the left pulmonary artery down to the right ventricle clarify the double-oblique course of the MPA (Fig. 4).

The following oblique-sagittal image preferably is planned using the three-point-method (represented with red circles) at the following positions: (1) in the center of the right ventricular outflow tract (RVOT) just below the pulmonary valve (Fig. 4C), (2) in the center of the left pulmonary artery just downstream from the MPA bifurcation at its highest point (Fig. 4A), and (3) in the center of the lower left pulmonary artery (Fig. 4B). The resulting image (Fig. 5A) nicely displays the MPA from the pulmonary valve to the bifurcation and is used to generate an oblique coronal image (Fig. 5B) using the perpendicular tool (right mouse click). To perform flow quantification of the MPA, orthogonal “through plane” measurements are required.



4 The planning of the oblique-sagittal image (Fig. 5A) is preferably planned using the three-point method (represented with red circles) at the following positions: in the center of the left pulmonary artery just downstream from the MPA bifurcation at its highest point (Fig. 4A), in the center of the lower left pulmonary artery (Fig. 4B), and in the center of the right ventricular outflow tract (RVOT) just below the pulmonary valve (Fig. 4C).



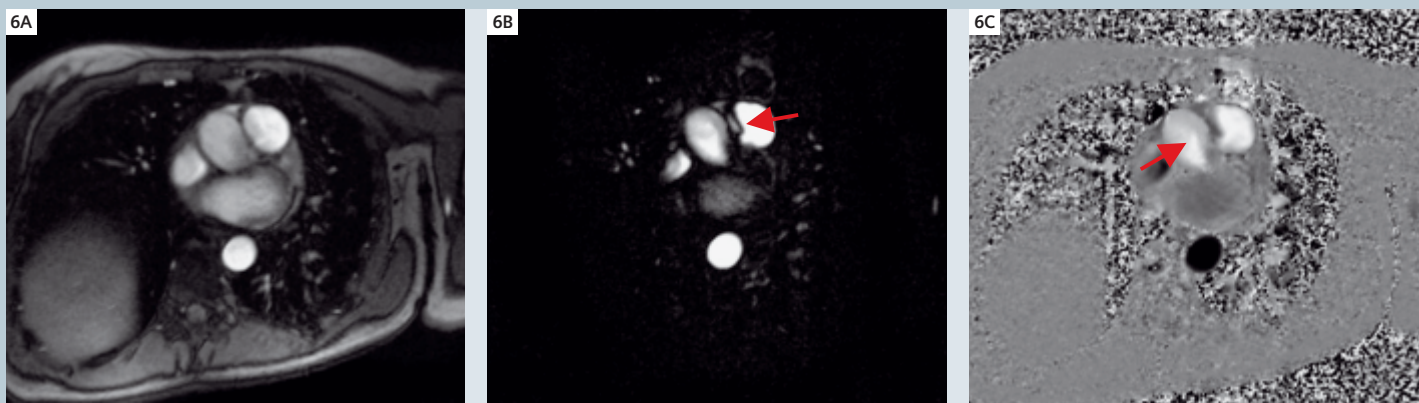
5 Figure 5A nicely displays the MPA from the pulmonary valve to the bifurcation and is used to generate an oblique coronal image (Fig. 5B) using the perpendicular tool (right mouse click). The desired acquisition plane for through-plane flow measurements in the MPA is delineated (red line) and must be perpendicular to both double-oblique scout images.

The desired acquisition plane for flow measurements in the MPA is delineated in Figure 5 (red line) and must be perpendicular to both double-oblique scout images. For highest accuracy, the flow acquisition should not deviate more than 15° from perpendicular to the flow in the MPA. Comprehensive reports on basic MR flow measurement techniques [14] and of MR flow measurements in the MPA have been published [15].

Data acquisition

To determine the true physiological situation of the patient lying in the scanner in supine position, flow measurements should be performed under free-breathing conditions. Scanning in inspiration will significantly reduce the true cardiac output [16] and expiratory breath-holding might not be

reproducible. Detectable breathing related motion artifacts are excluded by the use of long term averaging (sequence tab). Furthermore, three averages should be acquired. The resulting scanning time will be dependent from the number of cardiac cycles needed to acquire the data at a given temporal and spatial resolution. A further advantage of the longer acquisition time is the increase of averaging over the cardiac cycle during different breathing positions. Slice thickness is 5 mm in adults, 4 mm in children and 3 mm in infants. For many clinical applications, retrospective gating is favorable (fl_fq_retro). Using fast HF- and gradient settings, two segments and a bandwidth of 369 Hz/Px, a TE of 3 ms and a TR of 27 ms are possible. Arrhythmia-detection may be used for arrhythmic patients and children, but is not manda-



6 Images generated by the flow measurement: rephased (= anatomical; Fig. 6A), magnitude (motion is bright and no velocity information for quality control; Fig. 6B), and phase images (velocity information for quantification; Fig. 6C). All of them are visualized using the Siemens Argus Flow® software. Figure shows systolic images revealing the maximum flow; note that even during systole, some parts of the vessel lumen show very low flow (red arrows).

tory in most of the patients. In adults, the field of view is 320 mm, matrix is 256, phase resolution is 100% and FoV-phase is 87.5%. For optimized flow quantification, up to 40 phases along the cardiac cycle should be reconstructed.

For selected patients, prospective triggering may be favorable (fl_fq). Using fast HF- and gradient settings, one segment and a bandwidth of 1395 Hz/Px, a TE of 2.6 ms and a TR of 9.8 ms (equaling the true temporal resolution of this sequence) are possible. The acquisition window is set to 90% of the average cardiac cycle. In arrhythmic patients and children (respiratory arrhythmia) sometimes only 85% of the cardiac cycle is measurable. The disadvantage is small, since only small amounts of blood are moved through the MPA during late diastole. The major advantage is the possibility to acquire flow data from every 10 ms in the cardiac cycle, especially in early systole. In adults, the field of view is 320 mm, matrix is 256, phase resolution is 93% and FoV-phase is 75%.

It is recommended to reconstruct all available images generated by the flow measurement sequences, i.e. rephased (= anatomical; Fig. 6A), magnitude (motion is bright and no velocity information for quality control; Fig. 6B), and phase images (velocity information for quantification; Fig. 6C). All of them are visualized using the Siemens Argus Flow® software. The rephased images are used to draw the analysis ROI, quantification will be calculated by the phase images. In Figure 6, systolic images revealing the maximum flow are

displayed. Note that even during systole, some parts of the vessel lumen show very low flow (red arrows)!

Clinical application

Normal values of the pulmonary circulation in children [17] and adults [18] have been published. The major indication for pulmonary flow measurements in infants and children is the quantification of shunt volumes in ventricular septal defects [19], which is not accurately possible using other non-invasive methods. Furthermore, MR flow measurements can provide important information in many congenital cardiac anomalies [20]. Developing pulmonary arterial hypertension (PAH) in children and adults suffering from cystic fibrosis has been detected with MR flow measurements [21] and an experimental model for the quantification of PAH has been published [22]. In adults, the quantification of PAH using MR flow measurements has been investigated by several groups [23–33] and MRI with combined morphological and functional techniques has been developed to a major diagnostic tool in chronic thromboembolic pulmonary hypertension [34].

Conclusion

The expansion of morphological findings by functional data made achievable with flow measurements of the MPA adds valuable information to the clinical diagnostic algorithm in several cardio-pulmonary diseases.

Contact

PD Dr. med. habil. Nasreddin D. Abolmaali
 OncoRay – Center for Radiation Research in Oncology
 Medical Faculty Carl Gustav Carus, TU Dresden
 Fetscherstrasse 74, Haus 31, Pf 86
 01307 Dresden
 Germany
 Phone: +49 351 458 7414
 Fax: +49 351 458 7311
 Website: www.oncoray.de

References

- 1 Singer JR. Blood flow rates by nuclear magnetic resonance measurements. *Science* 1959;130:1652–3.
- 2 Nayler GL, Firmin DN, Longmore DB. Blood flow imaging by cine magnetic resonance. *J Comput Assist Tomogr* 1986;10:715–22.
- 3 Gatehouse PD, Keegan J, Crowe LA, et al. Applications of phase-contrast flow and velocity imaging in cardiovascular MRI. *Eur Radiol* 2005;15:2172–84.
- 4 Bernstein MA, Zhou XJ, Polzin JA, King KF, et al. Concomitant gradient terms in phase contrast MR: analysis and correction. *Magn Reson Med* 1998;39:300–8.
- 5 Tsao J, Boesiger P, Pruessmann KP. k-t BLAST and k-t SENSE: dynamic MRI with high frame rate exploiting spatiotemporal correlations. *Magn Reson Med* 2003;50:1031–42.
- 6 Tsao J, Kozerke S, Boesiger P, et al. Optimizing spatiotemporal sampling for k-t BLAST and k-t SENSE: application to high-resolution real-time cardiac steady-state free precession. *Magn Reson Med* 2005 53:1372–82.
- 7 Glockner JF, Johnston DL, McGee KP. Evaluation of cardiac valvular disease with MR imaging: qualitative and quantitative techniques. *Radiographics* 2003;23:e9.
- 8 van Straten A, Vliegen HW, Hazekamp MG, et al. Right ventricular function after pulmonary valve replacement in patients with tetralogy of Fallot. *Radiology* 2004;233:824–9.
- 9 Rees S, Firmin D, Mohiaddin R, et al. Application of flow measurements by magnetic resonance velocity mapping to congenital heart disease. *Am J Cardiol* 1989;64:953–56.
- 10 Kroft LJ, Simons P, van Laar JM, et al. Patients with pulmonary fibrosis: cardiac function assessed with MR imaging. *Radiology* 2000;216:464–71.
- 11 Gutberlet M, Noeske R, Schwinge K, et al. Comprehensive cardiac magnetic resonance imaging at 3.0 Tesla: feasibility and implications for clinical applications. *Invest Radiol* 2006;41:154–67.
- 12 Bax L, Bakker CJ, Klein WM, et al. Renal blood flow measurements with use of phase-contrast magnetic resonance imaging: normal values and reproducibility. *J Vasc Interv Radiol* 2005;16:807–14.
- 13 Schiemann M, Bakhtiary F, Hietschold V, et al. MR-based coronary artery blood velocity measurements in patients without coronary artery disease. *Eur Radiol* 2006;16:1124–30.
- 14 Lotz J, Meier C, Leppert A, et al. Cardiovascular flow measurement with phase-contrast MR imaging: basic facts and implementation. *Radiographics* 2002;22:651–71.
- 15 Abolmaali N. [Funktionelle Magnetresonanztomographie des Truncus pulmonalis], 1 edn. Lehmanns Media-Lob.de, Berlin 2006.
- 16 Sakuma H, Kawada N, Kubo H, et al. Effect of breath holding on blood flow measurement using fast velocity encoded cine MRI. *Magn Reson Med* 2001;45:346–8.
- 17 Abolmaali ND, Esmaeili A, Feist P, et al. [Reference values of MRI flow measurements of the pulmonary outflow tract in healthy children]. *Rofo* 2004;176:837–45.
- 18 Ley S, Mereles D, Puderbach M, et al. Value of MR phase-contrast flow measurements for functional assessment of pulmonary arterial hypertension. *Eur Radiol* 2007;17:1892–7.
- 19 Esmaeili A, Hohn R, Koch A, et al. Assessment of shunt volumes in children with ventricular septal defects: comparative quantification of MR flow measurements and invasive oximetry. *Clin Res Cardiol* 2006;95:523–30.
- 20 Varaprasathan GA, Araoz PA, Higgins CB, et al. Quantification of flow dynamics in congenital heart disease: applications of velocity-encoded cine MR imaging. *Radiographics* 2002;22:895–905.
- 21 Abolmaali ND, Smaczny C, Posselt HG, et al. Flow measurements in the main pulmonary artery of patients with cystic fibrosis (CF) using magnetic resonance imaging (MRI). *Journal of Cystic Fibrosis* 2003;2:50.
- 22 Abolmaali ND, Seitz U, Kock M, et al. Assessment of an experimentally induced pulmonary hypertension using high-resolution MR flow measurements in pigs. *Proc Intl Soc Mag Reson Med* 2003;11:407.
- 23 von Schulthess GK, Fisher MR, Higgins CB. Pathologic blood flow in pulmonary vascular disease as shown by gated magnetic resonance imaging. *Ann Intern Med* 1985;103:317–323.
- 24 Rooleveld RJ, Marcus JT, Boonstra A, et al. A comparison of noninvasive MRI-based methods of estimating pulmonary artery pressure in pulmonary hypertension. *J Magn Reson Imaging* 2005;22:67–72.
- 25 Murray TI, Box LM, Katz J, et al. Estimation of pulmonary artery pressure in patients with primary pulmonary hypertension by quantitative analysis of magnetic resonance images. *J Thorac Imaging* 1994;9:198–204.
- 26 Bouchard A, Higgins CB, Byrd BF, et al. Magnetic resonance imaging in pulmonary arterial hypertension. *Am J Cardiol* 1985;56:938–42.
- 27 Kondo C, Caputo GR, Masui T, et al. Pulmonary hypertension: pulmonary flow quantification and flow profile analysis with velocity-encoded cine MR imaging. *Radiology* 1992;183:751–8.
- 28 Bogren HG, Klipstein RH, Mohiaddin RH, et al. Pulmonary artery distensibility and blood flow patterns: a magnetic resonance study of normal subjects and of patients with pulmonary arterial hypertension. *Am Heart J* 1989;118:990–9.
- 29 Mohiaddin RH, Paz R, Theodoropoulos S, Firmin DN, et al. Magnetic resonance characterization of pulmonary arterial blood flow after single lung transplantation [see comments]. *J Thorac Cardiovasc Surg* 1991;101:1016–23.
- 30 Mousseaux E, Tasu JP, Jolivet O, et al. Pulmonary arterial resistance: noninvasive measurement with indexes of pulmonary flow estimated at velocity-encoded MR imaging-preliminary experience. *Radiology* 1999;212:896–902.
- 31 Henk CB, Schlechta B, Grapp S, et al. Pulmonary and aortic blood flow measurements in normal subjects and patients after single lung transplantation at 0.5 T using velocity encoded cine MRI. *Chest* 1998;114:771–9.
- 32 Paz R, Mohiaddin RH, Longmore DB. Magnetic resonance assessment of the pulmonary arterial trunk anatomy, flow, pulsatility and distensibility. *Eur Heart J* 1993;14:1524–30.
- 33 Tardivon AA, Mousseaux E, Brenot F, et al. Quantification of hemodynamics in primary pulmonary hypertension with magnetic resonance imaging. *Am J Respir Crit Care Med* 1994;150:1075–80.
- 34 Kreitner KF, Kunz RP, Ley S, et al. Chronic thromboembolic pulmonary hypertension – assessment by magnetic resonance imaging. *Eur Radiol* 2007;17:11–21.

Guidelines for Credentialing in CMR endorsed by the SCMR

Gerald M. Pohost, M.D., FACC, Chair; Raymond J. Kim, M.D., FACC;
Christopher M. Kramer, M.D., FACC; Warren J. Manning, M.D., FACC

Society for Cardiovascular Magnetic Resonance Representative

Printed with permission of SCMR.

Cardiovascular magnetic resonance (CMR), one of the newest cardiovascular imaging modalities, provides useful, often unique information with which all cardiologists should be conversant (Table 1). Training in CMR for cardiology fellows should be divided into three levels.

Training Levels

Level 1 General training (1 month) to provide the cardiovascular trainee with a working knowledge of CMR methods and diagnostic utility.

Level 2 Specialized training (at least 3 months) designed to provide fellows with the skills necessary to independently interpret CMR imaging studies.

Level 3 Advanced training for those who ultimately wish to be responsible for the operation of a CMR laboratory. Level 3 criteria must include appropriate levels of patient care, teaching, and research.

Overview of CMR Training

All cardiovascular medicine trainees should be taught the basic types of CMR studies and their in-

Table 1: Classification of CMR Procedures

1. Standard CMR procedures, including:

- a) Tomographic still-frame CMR for morphology using "bright" and/ or "dark blood" methods with and/or without a paramagnetic contrast agent
- b) Cine and other approaches to CMR for assessment of ventricular function
- c) Magnetic resonance angiography and cine CMR of the great vessels, anomalous coronary arteries, and coronary artery bypass grafts
- d) Delayed contrast-enhanced CMR imaging for myocardial infarction, scar, intraventricular thrombus and microvascular obstruction (associated with MI) and viability assessment and visualization of other causes of abnormal myocardial interstitium
- e) First-pass CMR imaging (with vasodilator infusion) or cine CMR imaging with stress (with inotropic agent) for myocardial perfusion evaluation and ischemia detection

- f) Phase-contrast velocity mapping for blood flow quantification for shunt sizing and determination of regurgitation and stenosis
- g) Peripheral MR angiography

2. Less common procedures, including:

- a) Myocardial tagging (approach unique to CMR that allows more detailed evaluation of intramural and transmural myocardial function than ventriculography alone and for evaluation of pericardial disease)
- b) MR angiography of the native coronary arteries
- c) MR spectroscopy using ³¹P (to assess "high-energy phosphate metabolism") or other nuclei

Abbreviations:

CMR = cardiovascular magnetic resonance;
MI = myocardial infarction;
MR = magnetic resonance.

dications. Mentored interpretation of CMR studies should be coupled with comparison and integration of test results with other relevant clinical and laboratory data. A mentor is an individual with the equivalent of Level 3 CMR training. This training generally should be acquired through the Accreditation Council for Graduate Medical Education – an approved cardiology or radiology program with expertise in CMR and under the aegis of a Level 3-qualified mentor in a laboratory accredited by an organization such as the Intersocietal Commission on the Accreditation of MR Laboratories (ICAMRL). Occasionally, a Level 3 qualified mentor will not be available in the institution housing the general fellowship program, but is available at a nearby nonacademic but medical center accredited for CMR by an organization such as the ICAMRL. Under these circumstances it is acceptable to place the trainee(s) at such a medical center for Level 1 to Level 3 training. The CMR training center and the trainee should maintain a logbook or other specific records to document the trainee's case review and the didactic hours in which the trainee has participated.

The depth of knowledge should increase with increasing levels of training. In the case of the Level 3 trainee, specialized training and, for academic trainees, research should be offered as a part of an established training program (Table 2).

Level 1: General Training (1-month Minimum)

The trainee should have exposure to the methods and the multiple applications of CMR for a period of not less than 1 month or its equivalent when interwoven with other training activities. This experience should provide basic background knowledge in CMR sufficient for the practice of adult cardiology and referral for CMR, but not for the practice/independent clinical interpretation of CMR. As a practical matter, many fellowship programs in cardiovascular medicine may not be able to fulfill CMR training. In these instances, fellows should be encouraged to obtain experience in an alternate program with appropriate training and accreditation in the performance of CMR studies.

Didactic Activities

Interpretation of CMR studies. During their 1-month of training, trainees should actively participate in daily CMR study interpretation under

Table 2: Components of CMR Training

1. Didactic activities
 - a) Lectures (it will be necessary in learning the physical principles and in case interpretation to derive such information from relevant lectures—no more than 5% of the cases)
 - b) Self-study (it is possible to use cases from teaching files, journals, textbooks, or electronic/on-line courses. Such self-study cases need to be well documented in the trainee's records and should not comprise any more than 50% of the cases studied)
2. Independent interpretation of CMR cases (performed in the mentoring CMR laboratory)
3. Participation in CMR case study interpretation
4. "Hands-on" CMR experience

Abbreviations: CMR = cardiovascular magnetic resonance.

the direction of a Level 2- or Level 3-trained CMR physician-mentor. For all studies in which angiographic, echocardiographic, radionuclide, computed tomography, or hemodynamic data are available, such information should be correlated with CMR studies. Studies should include the range of procedures listed in Table 1. Experience in interpretation (a minimum of 50 cases) may include studies from an established CMR teaching file.

Lectures and self-study in CMR. This component should consist of lectures on the basic aspects of CMR and parallel reading material of selected articles, digital training programs, or CMR text. The lectures and reading should provide the fellow with an understanding of CMR applications. Specificity, sensitivity, diagnostic accuracy, utility in assessing prognosis and use of interventions, costs, artifacts, indications, contraindications, and pitfalls must be included for each cardiovascular diagnostic subset. Such information could be effectively transmitted within a weekly non-invasive or clinical teaching conference during which CMR data are presented.

A basic understanding of magnetic resonance physics should be provided, including the following:

1. the physics of magnetic resonance as it relates to image intensity and contrast, including flow, T1 (spin-lattice relaxation time), T2 (spin-spin relaxation time) and contrast agents;
2. sources of artifacts, including motion, arrhythmias, and metal objects; contrast agent side effects;
3. safety of devices in the CMR environment; and
4. general post-processing tools and analyses.

Hands-On Experience

Hands-on experience is not necessary for Level 1.

Level 2: Specialized Training (At Least 3 Months)

Training for Level 2 should begin with the CMR experience outlined in Level 1. Level 2 is for those trainees who wish to practice the specialty of CMR, including independent interpretation of CMR studies. Level 2 trainees must have at least 3 months of dedicated CMR training (where 1 month is defined as 4 weeks and a week is defined as 35 h), including the basic elements listed in the following text. The trainee would be expected to become familiar with the CMR techniques listed in Table 1.

Background

In addition to Level 1 training, understanding of CMR physics should be more advanced (see the following text).

Didactic Activities

Interpretation of CMR studies. During their 3 or more months of experience, trainees should actively participate in daily CMR study interpretation under the direction of a Level 2 or Level 3 (preferred) CMR-qualified physician. For all studies in which other cardiac imaging data are available, such information should be correlated with CMR data. The trainee should interpret at least 150 CMR examinations during this training period, including 50 for which the trainee is present during the scan, ideally as the primary operator and is the primary interpreter. Up to 50 of the 100 examinations for which the trainee is not the primary interpreter can be derived from established teaching files, journals, and/or textbooks or electronic/online courses. Careful documentation of all case material and the details of the way in which the case was derived is essential.

Lectures and self-study in CMR. Course work would include the components for Level 1 training but also should include more advanced lectures and reading materials. This work, with parallel reading, should continue for the duration of the traineeship. Course work should include the following:

- 1. Physics:** trainees should receive didactic lectures from a CMR-trained physician and/or physicist on the basic physics of magnetic resonance in general and CMR in particular. The content should include the same materials as in Level 1 (basic) plus lectures

with supportive reading on the following topics:

- a) Image formation, including k-space, gradient echo, spin echo, fast spin echo, echo planar, spiral, steadystate free precession (SSFP), and parallel imaging.
- b) Specialized imaging sequences, including flow and motion, phase imaging, time of flight, contrast agents, and radiofrequency tagging.
- c) Hardware components, including the elements of gradient coil design, receiver coils, and digital sampling.

2. Applications, interpretation, indications, and contraindications:

Level 2 didactic activities should include an understanding of the sensitivity, specificity, accuracy, utility, costs, acquisition approaches, and disadvantages of all of the contemporary techniques in CMR. The following techniques should be covered in the didactic program:

- a) Imaging of structure and tissue characterization (T1, T2, spin echo, gradient echo, SSFP, and fat suppression).
- b) Imaging of function (cine and tagged cine magnetic resonance including SSFP imaging).
- c) Volumetric imaging of mass, biventricular volumes, and ejection fraction (using cine magnetic resonance imaging).
- d) Flow imaging (e.g., velocity-encoded techniques).
- e) Imaging of myocardial infarction, scarring, and viability assessment (delayed contrast-enhancement imaging).
- f) Pharmacologic stress-testing with evaluation of ventricular function and/or first-pass perfusion using a contrast agent.
- g) Magnetic resonance angiography (vascular).
- h) Electrocardiogram and peripheral pulse gating and triggering including timing of image acquisition within the R-R interval, motion artifacts and their effects on CMR images; respiratory motion suppression methods (e.g., breath-holding and navigators).
- i) Magnetic resonance spectroscopy methods (e.g., depth resolved surface coil spectroscopy or DRESS).
- j) Cardiovascular magnetic resonance image analysis and post-processing tools.
- k) Contraindications for CMR study.
- l) Incidental findings suggesting pathology outside of the cardiovascular system.

Evaluation

The person responsible for the CMR training program must be responsible for assessing the competence of the CMR trainee at the completion of the program. This is accomplished by examining the ability of the trainee in the understanding of the acquisition methods and the interactive role of the operator during the performance of studies and in the interpretation of the data acquired during daily reading sessions. This may be supplemented by formal testing.

Level 3: Advanced Training (12 Months or More for Those Interested in Running an Academic Program)

Level 3 CMR training represents the highest level of training and would enable the trainee to pursue a clinical or academic career in CMR and to direct a CMR laboratory. Level 3 training in CMR could be obtained as part of a 3- or 4-year cardiology fellowship. In addition to the recommendation for Level 2, the Level 3 academic program should include active participation in ongoing basic or clinical CMR research or both, with individual responsibility for a specific portion of that research.

Focused research work with publication of one or more manuscripts is an important part of Level 3 training. Level 3 training must be performed under the guidance of at least one Level 3-trained CMR physician. In parallel with research activities, the Level 3 trainee must participate in clinical imaging that should include supervised interpretation of at

least 300 CMR cases. The trainee must be physically present and involved in the acquisition and the primary interpretation of at least 100 CMR cases. In the remaining 200 cases, the trainee should review at least 100 of these with the Level 3 mentor at the training facility. The remaining cases can be derived from established teaching files, journals, and/or textbooks or electronic/on-line courses. Careful documentation of all case material and the details of the way in which the case was derived are essential.

Knowledge of magnetic resonance physics must be more advanced than Level 2 and include the following:

1. Analysis of why certain specialized imaging sequences are applicable for specific clinical protocols, including imaging of heart function, coronary arteries, perfusion, delayed enhancement, and peripheral arteries.
2. Basic understanding of the clinically applicable spectroscopic methods.
3. The essentials of data collection, including capturing of digital data, the maintenance of accurate databases and records, signal processing, and the approach for obtaining quantitative data.

Evaluation

Evaluation should be similar to that of Level 2.

Summary of Recommendations

The overall requirements for training in CMR are summarized in Table 3.

Table 3: Summary of Requirements for Each Level of CMR Training

Level	Duration (Months)	Number of Cases
1	1	50+ mentored interpretations (by a Level 2- or 3-trained physician)
2	3 to 6*	150+ mentored interpretations (by a certified Level 2- or Level 3- [preferred] qualified CMR physician) including at least 50 as primary interpreter (and operator, if possible)**
3	12+ months of training*	300+ mentored interpretations (by a Level 3-qualified CMR physician) including 100+ as primary interpreter (and operator, if possible)**

*This time represents the number of months spent reviewing cases, and interpreting, performing, and learning about CMR, and need not be a consecutive block of time, but at least 50% of the time should represent mentored laboratory experience.

**The case recommendations may include studies from an established teaching file, previous CMR cases, journals, and/or textbook or electronic/on-line courses/ continuing medical education. No less than 50% of the cases should be from those performed at the mentoring CMR laboratory.

Abbreviations: CMR = cardiovascular magnetic resonance.

Cardiovascular MR Courses and Fellowships for Physicians and Technologists

(Please contact the respective course director or – in case of Phase 1–3 courses taking place in the US, Ms M. Bieman, Phone (+1) 888-221-8010, margaret.bieman@siemens.com)

CMR Courses and Fellowships – USA

Phase 1 – Introductory Short Courses for Technologists

These 4-day introductory short courses consist of many hands-on scanning sessions, many technical discussions and demonstrations, with a few clinical discussions and demonstrations. Two days are dedicated to hands-on scanning volunteers, while two more days are dedicated to post-processing and observing clinical patient exams.

Every sponsoring institution that offers these courses presents the same agenda and syllabus so that each attending technologist receives the same “ASRT-accredited” training. Attendees should have good familiarity with Siemens’ latest MR conventions, nomenclature, and software in order that the principles of MR may be applied during the course and to facilitate the learning of basic Cardiovascular MR techniques.

Introduction to Cardiovascular MR

Northwestern Memorial Hospital,
Radiology Division, Chicago, IL

Registration:

Charles Fasanati, RT
+1-312-926-5685
cfasanat@nmh.org

Introduction to Cardiovascular MR

University of Virginia Health System,
Radiology Division, Charlottesville, VA

Registration:

John Christopher, RT
+1-434-243-6904
jmc2v@virginia.edu

Introduction to Cardiovascular MR

William Beaumont Hospital,
Cardiology Division, Royal Oak, MI

Registration:

Ralph Gentry, RT
+1-248-898-7258
rgentry@beaumont.edu

Introduction to Cardiovascular MR

The Ohio State University, Ross Heart
Hospital, Columbus, OH

Registration:

Beth McCarthy, RT
+1-614-247-7847
beth.mccarthy@osumc.edu

Phase 2 – Intermediate Short Courses for Physicians and Technologists

These 3- to 5-day intermediate short courses consist of numerous clinical discussions, clinical case reviews, and clinical exam observations, as well as some technical discussions and demonstrations, and a few hands-on scanning sessions. These courses are ideally suited for a physician and technologist team, but would be appropriate for either individually. Clinical concepts and practices are vendor non-specific, whereas Siemens Cardiovascular MR Courses & Fellowships equipment is demonstrated during practical hands-on sessions.

Cardiovascular MR Practicum

Duke University, Cardiovascular
MR Center, Durham, NC

Directors: Raymond Kim, M.D.,
& Robert Judd, Ph.D., Div. of Cardiology

Registration:

Michele Parker
+1-919-668-1671
michele.parker@duke.edu
<http://dcmrc.mc.duke.edu>

Cardiovascular MR Hands-on Experience and Cardiac MR Case Interpretation

Washington University, Mallinckrodt
Institute of Radiology, St. Louis, MO
Director: Pamela Woodard, M.D.,
Radiology Division

Registration:

Laura Schollmeyer
+1-314-362-7697
schollmeyerl@mir.wustl.edu
<http://www.cvil.wustl.edu/mr-course>

Cardiovascular CT/MR: Update and Case Review

The Ohio State University
Ross Heart Hospital, Columbus, OH
Directors: Orlando P. Simonetti, Ph.D.
and Subha V. Raman, M.D., MSEE,
Cardiovascular Medicine

Registration:

Ellen
+1-614-293-9992
<http://ccme.osu.edu>

MRI Basic Principles for Physicians

Siemens Training & Development, Center, Cary, NC
Director: Mark A. Brown, Ph.D.,
Siemens Training & Development
Center: 1-919-468-7445

Registration:

Denise Hardy
+1-800-888-7436, Opt. 4
<http://www.siemensmedical.com>
(US) → Education → Clinical Applications Training → MR

Experience in Clinical and Research

Cardiovascular Magnetic Resonance
Fuqua Heart Center of Atlanta,
Piedmont Hospital, Atlanta, GA
Director: Szilard Voros, M.D.,
Cardiology Division

Registration:

Kim Christian, RT
+1-404-605-4905
kim.christian@piedmont.org

Phase 3 – Observational Fellowships for Physicians and Technologists

These observational fellowships for physicians and technologists provide an opportunity to observe and participate in the clinical practice of Cardiovascular MR over the course of several weeks. Attendees may observe and participate in routine clinical exams and interpretations, review case files, discuss operational and technical issues, and learn important resources for setting up a practice. Typically, no classroom instruction is provided. All dates are ongoing, apply for availability. Many offer both MR and CT training.

William Beaumont Hospital,
Cardiovascular MRI Center, Royal Oak, MI
 Director: Gil Raff, M.D.
 Cardiology Division
Registration: Gil Raff, M.D.
 +1-248-898-0116
graff@beaumont.edu

Fuqua Heart Center of Atlanta,
Piedmont Hospital, Atlanta, GA
 Director: Szilard Voros, M.D.,
 Cardiology Division
Registration: Kim Christian, RT
 1-404-605-4905
kim.christian@piedmont.org

The Ohio State University
Ross Heart Hospital, Columbus, OH
 Directors: Orlando P. Simonetti, Ph.D.
 and Subha V. Raman, M.D., MSEE,
 Cardiovascular Medicine
Registration: Beth McCarthy, RT
 +1-614-247-7847
beth.mccarthy@osumc.edu

Phase 4 – Advanced Long Term Credentialing Fellowships for Physicians

These advanced long term fellowships for physicians meet the guidelines for CMR training established by the SCMR (Society for Cardiovascular MR). In general, 1 month meets Level 1 credentialing, 3 months meets Level 2 credentialing, and 1 year meets Level 3 credentialing, but these may vary. These fellowships teach the physician how to perform and interpret Cardiovascular MR exams. Some locations will require a minimum number of weeks or months of attendance, and most allow the education to be conducted in intervals that can meet individual practice needs (few weeks, few months, entire year). All dates are ongoing, apply for availability. Many offer both MR and CT training.

Duke University,
Cardiovascular MR Center, Durham, NC
 Director: Raymond Kim, M.D. & Robert Judd,
 Ph.D., Div. of Cardiology
Registration: Michele Parker
 +1-919-668-1671
mparker@dcmr.mc.duke.edu
<http://dcmr.mc.duke.edu>

University of Virginia Health System, Depart-
ments of Radiology & Medicine (Cardiology),
 Charlottesville, VA
 Director: Christopher Kramer, M.D.,
 Radiology/Cardiology
Registration: Christopher Kramer, M.D.
 +1-434-243-6060
ckramer@virginia.edu
<http://www.healthsystem.virginia.edu/internet/radiology/CardiacMRI/cardiaccmri.cfm>

William Beaumont Hospital, Royal Oak, MI
 Director: Gilbert Raff, M.D.; Cardiology Division
Registration: Gilbert Raff, M.D.
 +1-248-898-0116
 graff@beaumont.edu

**The Ohio State University,
 Ross Heart Hospital, Columbus, OH**
 Directors: Orlando P. Simonetti, Ph.D.,
 and Subha V. Raman, M.D., MSEE,
 Cardiovascular Medicine
Registration: Beth McCarthy, RT
 +1-614-247-7847
 beth.mccarthy@osumc.edu

**Fuqua Heart Center of Atlanta,
 Piedmont Hospital, Atlanta, GA**
 Director: Szilard Voros, M.D.; Cardiology Division
Registration: Kim Christian, RT
 +1-404-605-4905
 kim.christian@piedmont.org

CMR Courses and Fellowships – International (excluding USA)

Canada

**Stephenson Cardiovascular MR Centre Foothills
 Medical Centre University of Calgary, Canada**
 Director: Matthias Friedrich, M.D., FESC
Registration: Silke Friedrich, M.D.
 Tel. +403-944-8806
 cmr.centre@calgaryhealthregion.ca

**VU University Medical Center, Amsterdam,
 Netherlands**
 Hands-on Course Cardiovascular MRI
 Director: A.C. van Rossum, M.D.
Registration: Ankie Muller,
 Tel. +31-20-444 2244
 cardiol@VUmc.nl

Europe

**Charite Campus Buch, Franz-Volhard-Klinik,
 Dept. of Cardiology, Berlin, Germany**
 Director: Jeanette Schulz-Menger, M.D., FESC
Registration: Annette Köhler
 Tel. +49 30-94172353
 info@circle-institute.com

**Cardiovascular Magnetic Resonance Unit
 Royal Brompton Hospital, London, UK**
 Director: Dudley Pennell, M.D.
Registration: Dudley Pennell, M.D.
 Tel. +44 20 7351 8810
 d.pennell@ic.ac.uk

**Kerckhoff Heart Center
 Dept. of Cardiology, Bad Nauheim, Germany**
 Director: Thorsten Dill, M.D., FESC
Registration: Annegret Thomas,
 Siemens Medical Solutions
 Tel. +49 9131 84-7726
 annegret.thomas@siemens.com

**Leeds International Cardiac MR Course
 University of Leeds, UK**
 (5-days course, annually)
 Director: Mohan Sivananthan, M.D.
 Consultant Cardio-Radiologist
Registration: Margaret Green
 Tel. +44 (0)113 294 5702
 Mgreen@leedscmr.org

**St. Marien-Hospital,
 Dept. of Cardiology, Bonn, Germany**
 Director: Giso von der Recke, M.D.
Registration:
 Annegret Thomas, Siemens Medical Solutions
 Tel. +49 9131 84-7726
 annegret.thomas@siemens.com

**University of Queensland, Centre for Magnetic
 Resonance, Brisbane, Australia**
 Basic Cardiac MRI
Registration: Erica Maddock
 erica.maddock@cmr.uq.edu.au

CMR Site Accreditation Process

Robert C. Bremser, MSA BSM ASRT(R) (CT) (MR)

Senior MR Clinical Education Specialist, Siemens Medical Solutions, USA

Every year there is an increase of our customers that are utilizing cardiac imaging on a regular basis. This market trend shows us that the potential for cardiac imaging is about to explode. The American College of Radiology has stepped forward to establish the criteria necessary to set the standard in cardiac imaging. The purpose of this article is to familiarize the customers of the United States to the process, guidelines, and quality that is necessary to meet the ACR requirements which will allow them to collect more revenue from third party reimbursements. The MRI Clinical Education team at the Uptime Service Center in Cary, North Carolina is available to answer imaging questions at (+1) 1-800-888-7436. Additional information on the ACR and their guidelines can be located on the American College of Radiology web site, www.acr.org.

Quality assurance

Effective April 1, 2007, all sites initially applying for ACR accreditation or renewal must have active participation in a peer review program.

Phantom testing

The ACR phantom testing will remain the same as ACR whole-body evaluation. The site will use the ACR protocols for T1 and T2 as well as its own routine T1 and T2 brain sequences. Most likely in the future there will be an ACR cardiac phantom for which pro-

ocols and criteria will be developed for evaluation. Phantom image testing will remain the same and assess the following:

- Image artifacts
- Image ghosting ratio
- Limiting high-contrast spatial resolution
- Signal uniformity
- Slice positioning accuracy
- Distance measurement and accuracy
- Slice thickness accuracy
- Signal uniformity

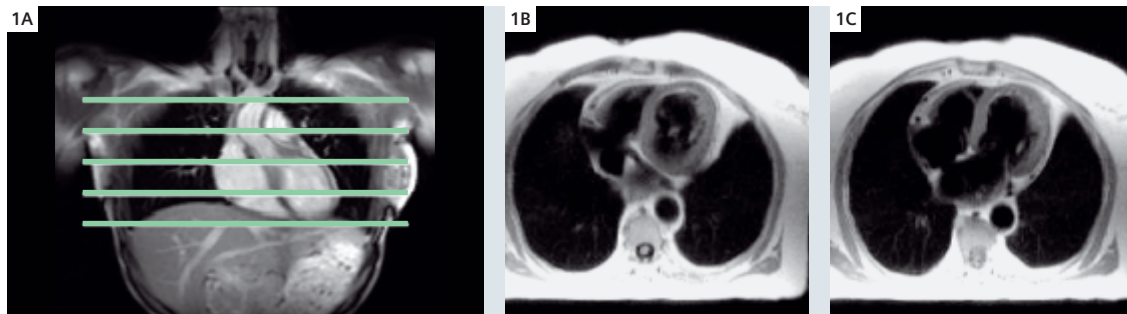
Quality control

The purpose of the QC program is to assess relative changes in system performance over time by the technologist, service engineer, medical physicist and physician.

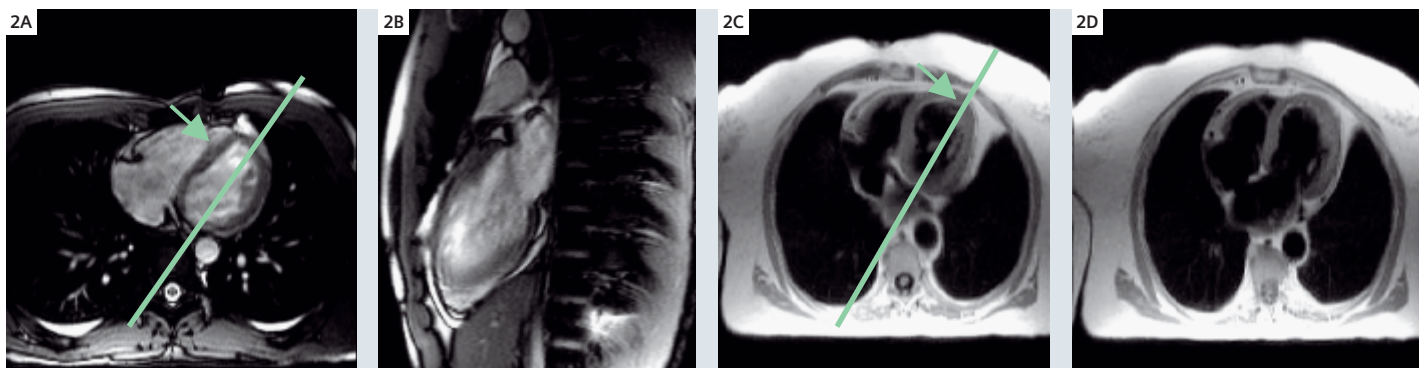
List of QC tests that must be performed:

Technologist's weekly QC tests

- Table positioning
- Setup and scanning
- Geometric accuracy
- Center frequency
- Visual checklist
- Low contrast resolution
- High contrast resolution
- Film quality control
- Artifact analysis



1 Black Blood Exam (e.g. SE or TSE): HASTE imaging technique is not allowed. Must be T1 (1 R-R/short TE) or PD (2 R-R/short TE). Axial plane or short axis plane and gated to the cardiac cycle. Anatomical coverage from aortic root to diaphragm or from base to apex.



2 Two-chamber vertical long axis (VLA): Position slice parallel to ventricular septum through the middle of left ventricle. Use axial image to verify slice passing through mitral valve and another axial view to ensure that slice goes through apex.

Medical physicist's annual QC tests

- Slice position accuracy
- Slice thickness accuracy
- Magnetic field homogeneity
- Soft copy displays (monitors)
- Inter-slice radiofrequency interference
- Radiofrequency coil checks

General recommendations for clinical imaging

- Images submitted to the ACR must be from clinical examinations. Exams performed on models or volunteers are not permitted.
- Clinical images must be obtained within one week (before or after) the acquisition of the phantom images.
- Clinical images for each region of anatomy to be submitted to the ACR must be from one patient only.
- Only images that are requested in the Full MRI Accreditation Application document should be submitted to the ACR. Include slice displays for each series. Submit on film only.
- Phantom clinical protocols done in the head coil must be used for the clinical patient head studies; if not, a letter of explanation must be included.

Required images for clinical Cardiac MRI accreditation:

Each scanner applying for Cardiac ACR MRI accreditation has to submit four complete patient exams.

- Black Blood SE or TSE (one exam) T1 or PD/axial or short axis/ cardiac gated (Figure 1).
- Delayed Enhanced Exams (two exams)
 - Short axis cines covers left ventricle base to apex (Figure 3).
 - Long axis cines 2-chamber VLA and 4-chamber HLA including LVOT (Figures 2, 4, 5).
 - Delayed enhanced IR prepared short axis with T1 optimized to suppress normal myocardium (Figure 6).
- Basic Cardiac Exam (one exam)
 - Short axis cines covers left ventricle base to apex (Figure 3).
 - Long axis cines 2-chamber VLA and 4-chamber HLA including LVOT (Figures 2, 4, 5).

Each set of clinical images will be evaluated for

- Cine display
- Anatomical coverage and imaging planes
- Artifacts
- Pulse sequence and image contrast
- Temporal resolution
- Spatial resolution
- Exam ID including all patient information annotated on clinical exams

Recommended clinical parameters Black Blood examination:

T1 (1R-R/short TE) or proton density (2 R-R/short TE) (Figure 1)				
Slice Thickness	Gap	Pixel Phase	Pixel Freq.	Temporal Res.
≤ 8.0	≤ 4 .0	≤ 2.5	≤ 1.6	NA

in mm

Anatomical coverage/tips

- Must cover from aortic root to diaphragm (axial)
- Or from the base to the apex (short axis)
- Position slices perpendicular to the long axis of left ventricle (short axis)
- Must cover the entire cardiac cycle
- Used to display the morphology of the heart
- Most effective for blood flow in the through-plane (perpendicular)

Potential artifacts

- Poor contrast between dark blood and myocardium
- Poor resolution, images are too grainy and/or blurry
- Ghosting, patient motion and/or aliasing
- Excessive inhomogeneities, susceptibility, and/or chemical shift

Delayed Enhanced examination: a) Short axis cine

Steady State Free Precession (TrueFISP) or Spoiled GRE (f12d) techniques (Figure 3)				
Slice Thickness	Gap	Pixel Phase	Pixel Freq.	Temporal Res.
≤ 8.0	≤ 2 .0	≤ 3.1	≤ 2.1	≤ 45 ms

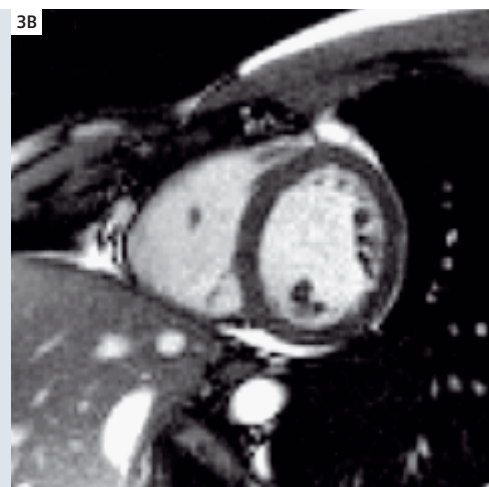
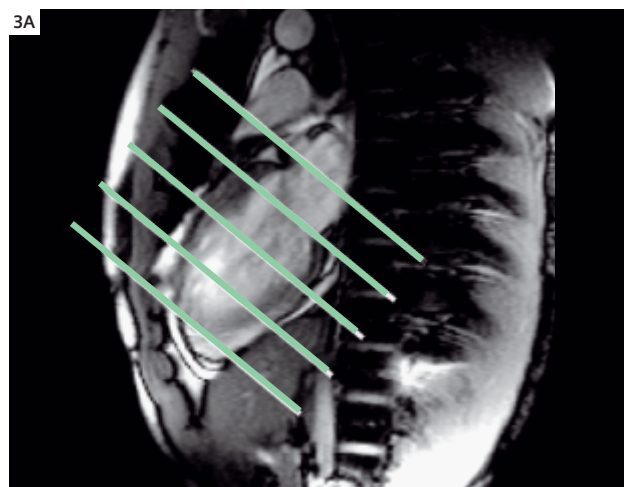
in mm

Anatomical coverage/tips

- Must cover the entire left ventricle from base to apex
- Optimal sequence cine_trufi_retro
- Must cover of the entire cardiac cycle
- Number of calculated phases are user defined
- Position slices perpendicular to the long axis of left ventricle

Potential artifacts

- Poor contrast between bright blood and dark myocardium
- Poor resolution, images are too grainy and/or blurry
- Ghosting, patient motion and/or aliasing
- Excessive inhomogeneities, susceptibility, and/or chemical shift



3 Short axis view apex to base (SA): Position slices perpendicular to the long axis of left ventricle. Slices need to cover entire left ventricle from the base to the apex.

b) Long axis cine

Steady State Free Precession (trufi) or Spoiled GRE (fl2d) techniques (Figure 2)

Slice Thickness	Gap	Pixel Phase	Pixel Freq.	Temporal Res.
≤ 8.0	NA	≤ 3.1	≤ 2.1	≤ 45 ms

in mm

Anatomical coverage / tips

- Two-chamber must be submitted (vertical)
- Four-chamber must be submitted (horizontal) (Figure 4)
- Left ventricle aortic outflow tract must be demonstrated (Figure 5)
- Optimal sequence cine_trufi_retro
- Must cover of the entire cardiac cycle
- Number of calculated phases are user defined

Potential artifacts

- Poor contrast between bright blood and dark myocardium
- Poor resolution, images are too grainy and/or blurry
- Ghosting, patient motion and/or aliasing
- Excessive inhomogeneities, susceptibility, and/or chemical shift

c) Delayed Enhancement

Inversion Recovery Prepared GRE (tfi psir or tfl psir) (Figure 6)

Slice Thickness	Gap	Pixel Phase	Pixel Freq.	Temporal Res.
≤ 8.0	≤ 2.0	≤ 1.8	≤ 1.4	< 200 ms

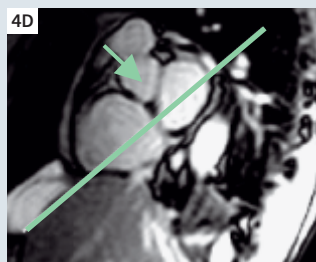
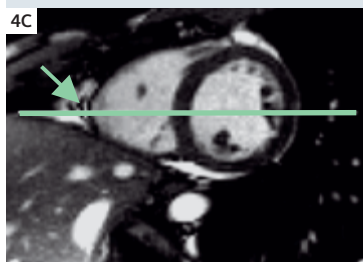
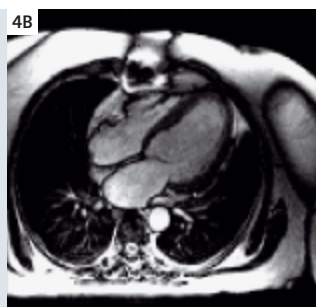
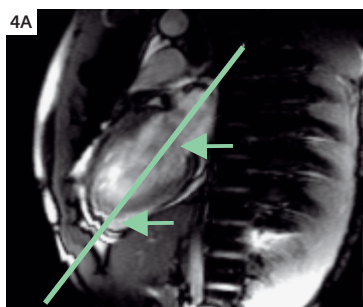
in mm

Anatomical coverage / tips

- Must be short axis plane in patients with prior myocardial infarction
- Must cover the entire cardiac cycle
- Good contrast between blood pool, enhancing infarction and normal myocardium
- Position slices perpendicular to the long axis of left ventricle

Potential artifacts

- Insufficient delay may not distinguish between blood pool and myocardial infarction
- Suboptimal TI may result in poor contrast between dark myocardium and bright infarction
- Poor resolution, images are too grainy and/or blurry
- Ghosting, patient motion and/or aliasing
- Excessive inhomogeneities, susceptibility, and/or chemical shift



4 Four-chamber horizontal long axis (HLA): Position slice off short axis view through right ventricle apex and midline to left ventricle. Use another short axis image to verify slice misses aortic root. Position slice on vertical long axis through mitral valve and apex of left ventricle.

Basic cardiac examination:**a) Short axis cine**

Steady State Free Precession (trufi) or Spoiled GRE (fl2d) techniques (Figure 3)				
Slice Thickness	Gap	Pixel Phase	Pixel Freq.	Temporal Res.
≤ 8.0	≤ 2.0	≤ 3.1	≤ 2.1	≤ 45 ms

in mm

Anatomical coverage/tips

- Must cover the entire left ventricle from base to apex
- Optimal sequence cine_trufl_retro
- Must cover of the entire cardiac cycle
- Number of calculated phases are user defined
- Position slices perpendicular to the long axis of left ventricle

Potential artifacts

- Poor contrast between bright blood and dark myocardium
- Poor resolution, images are too grainy and/or blurry
- Ghosting, patient motion and/or aliasing
- Excessive inhomogeneities, susceptibility, and/or chemical shift

b) Long axis cine

Steady State Free Precession (trufl) or Spoiled GRE (fl2d) technique (Figure 2)				
Slice Thickness	Gap	Pixel Phase	Pixel Freq.	Temporal Res.
≤ 8.0	NA	≤ 3.1	≤ 2.1	≤ 45 ms

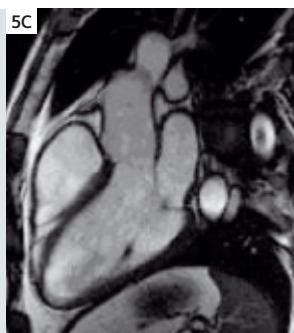
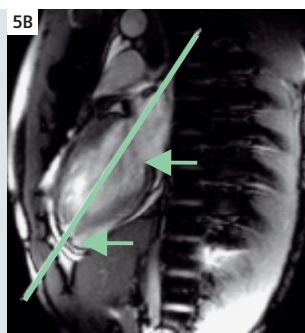
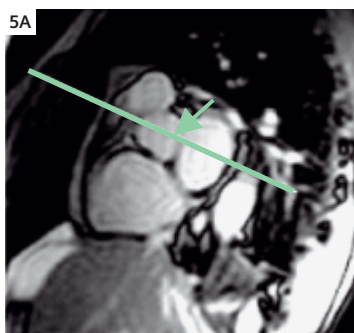
in mm

Anatomical coverage/tips

- Two-chamber must be submitted (vertical)
- Four-chamber must be submitted (horizontal) (Figure 4)
- Left ventricle aortic outflow tract must be demonstrated (Figure 5)
- Optimal sequence cine_trufl_retro
- Must cover of the entire cardiac cycle
- Number of calculated phases are user defined

Potential artifacts

- Poor contrast between bright blood and dark myocardium
- Poor resolution, images are too grainy and/or blurry
- Ghosting, patient motion and/or aliasing
- Excessive inhomogeneities, susceptibility, and/or chemical shift

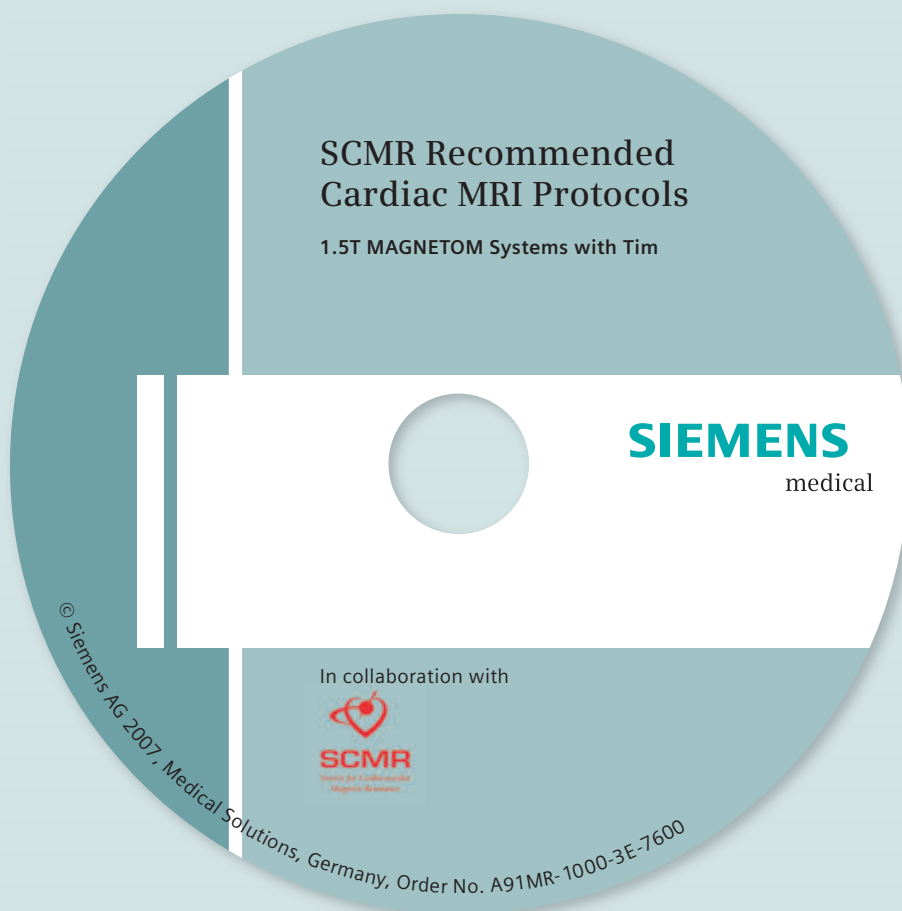


5 Left Ventricle Outflow Tract (LVOT): Position slice on vertical long axis through mitral valve and apex of left ventricle. Use short axis image to position slice through aortic root and left ventricular outflow tract.

6 Delayed Enhanced tfl_psr: Short axis plane with patients having prior myocardial infarction. Inversion prepared GRE sequence with inversion time (TI) optimized to suppress myocardium. Good contrast between blood pool, enhancing infarction, and normal myocardium.

SCMR recommended CMR protocols and CMR Users Guide – on CD!

To aid standardization of CMR, the Society for Cardiovascular Magnetic Resonance (SCMR) released early this year CMR exam protocol recommendations for the most frequent CMR procedures, from MR imaging of myocardial infarct and cardiomyopathies, stress MRI, coronary MRA to valvular disease, congenital heart disease and more. In a collaborative effort of Siemens Medical Solutions and the SCMR we were able to prepare clinically optimized exam protocols for Siemens 1.5T MAGNETOM Tim systems in accordance to the SCMR recommendations.



The protocols are available as downloadable EDX files on the attached CD for the following MAGNETOM systems:

- MAGNETOM Avanto 32-channel SQ engine
- MAGNETOM Avanto 18-channel SQ engine
- MAGNETOM Avanto 18-channel Q engine
- MAGNETOM Avanto 8-channel Q engine
- MAGNETOM Espree 18-channel DZ engine
- MAGNETOM Espree 18-channel Z engine
- MAGNETOM Espree 8-channel Z engine
- MAGNETOM Symphony, A Tim System

Please use the appropriate protocols optimized for your particular scanner type, number of receiver channels and gradient performance. For ease of use, the protocols are organized by exam modules or common cardiac diseases and sub-organized by the patient's cooperative abilities.

For example:

Acute Myocardial Infarct

- Recommended – Breathhold & Triggered Protocol
- Free Breathing & Triggered Protocol
- Extreme Arrhythmia – Free Breathing & Non-Triggered Protocol

The CD also contains a comprehensive CMR Users Guide (90+ pages) for the most frequent CMR indications including illustrations on how to plan the correct orientations. To enable the use in everyday routine, the chapters are closely linked to the EDX protocols provided on the CD.

Acknowledgement: We would like to thank Prof. Stefan Neubauer (University of Oxford, UK; President of SCMR), Prof. Christopher Kramer (University of Virginia, USA; Chair of the CMR Acquisition Protocol Committee at SCMR) and Gary McNeal (Advanced CMR Application Specialist; Siemens Medical Solutions USA) for their tremendous efforts and support.

Common Acronyms

AF	Atrial Fibrillation	MRA	Magnetic Resonance Angiography
B₀	Main (constant) magnetic field	PC	Phase Contrast
B₁	Radio-frequency magnetic field	PD	Proton Density
CA	Contrast Agent	PSIR	Phase-Sensitive Inversion Recovery
ce	Contrast Enhanced	RF	RadioFrequency
CMR	Cardiac / Cardiovascular Magnetic Resonance (Imaging)	RV	Right ventricle
CNR	Contrast-to-Noise Ratio	RVOT	Right-ventricular Outflow Tract
CO	Cardiac Output	SAR	Specific Absorption Rate
CP	Circular Polarization	SE	Spin-Echo
CTA	Computed Tomography Angiography	SENSE	Sensitivity Encoding
DCE	Delayed Contrast Enhancement, syn.: DE	SLT	SLice Thickness, syn.: SL
DE	Delayed Enhancement, delayed hyperenhancement	SNR	Signal-to-Noise Ratio
DESS	Dual Echo Steady State	SR	Saturation Recovery
DSA	Digital Subtraction Angiography	SSFP	Steady-State-Free-Precession
EPI	Echo Planar Imaging	STIR	Short T1 Inversion Recovery
EDV	End-diastolic Volume	SV	Stroke Volume
EF	Ejection Fraction	T	Tesla
ESV	End-systolic Volume	TA	Acquisition Time
FA	Flip Angle	TD	Trigger Delay
FLASH	Fast-Low-Angle-SHOT	TE	Echo time
FLAIR	Fluid Attenuated Inversion Recovery	TEE	Transesophageal Echocardiography
fMRI	Functional Magnetic Resonance Imaging	TFL	TurboFLASH
FoV	Field of View	TI	Inversion Time
GRAPPA	GeneRalized Autocalibrating Partially Parallel Acquisition (parallel imaging technique)	Tim	Total imaging matrix
GRE	GRAdient Echo	TimCT	Tim Continuous Table Move
HASTE	Half-Fourier Acquisition Single-shot TurboSE	TIRM	Turbo Inversion Recovery Magnitude
HLA	Horizontal Long Axis	TrueFISP	True Fast Imaging and Steady Precession
iPAT	integrated Parallel Acquisition Technique	TR	Repetition Time
IR	Inversion Recovery	TSE	Turbo Spin-Echo
LCE	Late Contrast Enhancement, syn.: DE	tSENSE	Time-adaptive SENSitivity Encoding (parallel imaging technique)
LE	Late Enhancement, syn.: DE	TTE	Transthoracic Echocardiography
LGE	Late Gadolinium Enhancement, syn.: DE	TTP	Time to Peak
LVOT	Left-ventricular Outflow Tract	TWIST	Time-resolved angiography With Interleaved Stochastic Trajectories
MEDIC	Multi-Echo Data Image Combination	venc	Velocity Encoding
MION	Monocrystalline Iron Oxide Nanoparticles	VIBE	Volume Interpolated Breathhold Examination
MIP	Maximum Intensity Projection	VLA	Vertical Long Axis
MNP	Magnetic (Iron Oxide) Nanoparticles	VRT	Volume Rendering Technique
MPR	Multiplanar Reconstruction/Reformation	VSD	Ventricular Septal Defect



We see a way to reduce retake examinations by up to 75%

Proven Outcomes

Helping cardiologists make 24 hours work like 48.

Proven Outcomes in Cardiology.

Caring for more patients, over a longer period of time, with fewer resources. Impossible? On the contrary: We can prove it. With integrated solutions that create a seamless cardiology workflow. Where images and data are retrieved instantaneously. Where cutting-edge technology enables absolute precision. Where clinicians are free to provide the best care possible. These are the Proven Outcomes that are transforming the delivery of health care. Today.

www.siemens.com/medical

SIEMENS
medical

Dark-Blood Delayed Enhancement Imaging: New Developments in the Imaging of Myocardial Viability

Wolfgang G. Rehwald, Ph.D.^{1,2}; Michael Salerno, M.D., Ph.D.²

¹Siemens Medical Solutions USA

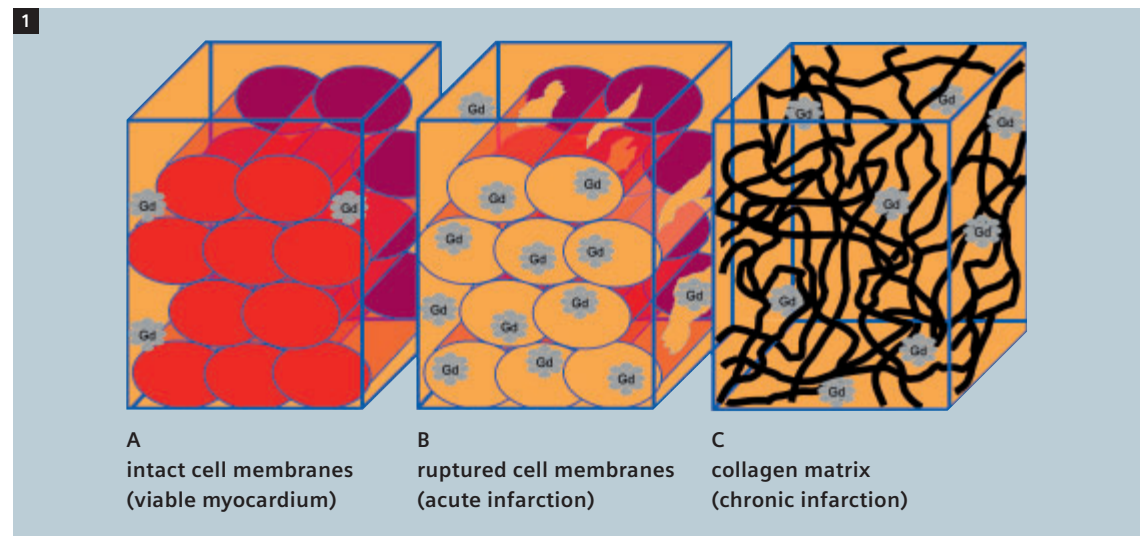
²Duke Cardiovascular MR Center, Durham, NC, USA

Introduction

The MR delayed enhancement technique allows the precise assessment of myocardial viability [1]. After intravenous injection, gadolinium-based contrast agents passively diffuse into viable (living) and infarcted (dead) myocardium (heart tissue). Dead myocardium, either chronically (scar) or acutely infarcted, appears bright in these MR images, whereas viable tissue appears dark. In viable myocardium, the contrast agent is confined to the extracellular space which makes up only ap-

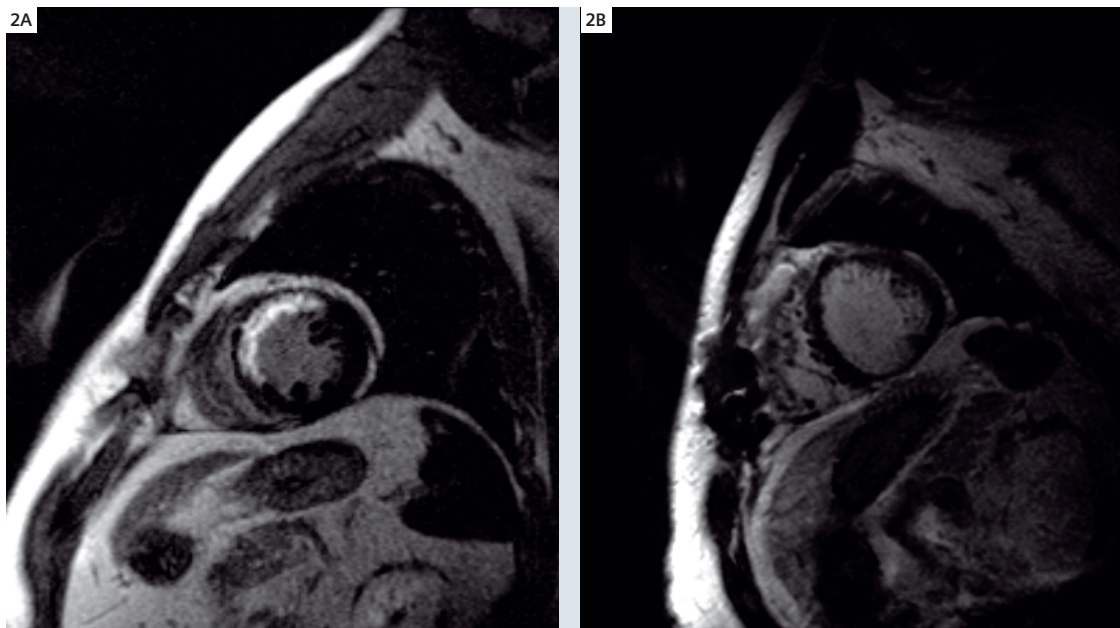
proximately 20% of the tissue volume (orange region of Fig. 1A). The volume available for contrast agent distribution ('distribution volume') is small. In acutely infarcted myocardium ruptured cell membranes allow the agent to enter the intracellular space (Fig. 1B). The distribution volume now includes both the intra- and extracellular space and is increased resulting in higher contrast agent concentrations as compared to viable myocardium [2]. In chronic infarction (scar) the contrast agent

CMR Delayed Enhancement imaging allows accurate assessment of myocardial viability.



1 **A:** Model of living myocardial cells: The Gadolinium-based (Gd) contrast agent is confined to the extracellular (orange) space. **B:** Acutely infarcted myocardial cells: The contrast agent can distribute in the extracellular (orange) space, but due to ruptured cell membranes also in the intracellular (red) space. The volume available for distribution is increased compared to A. **C:** Scar (chronic infarction): In this setting, the contrast agent can also distribute in a larger volume than in A.

(Modified from: Shah DJ, Judd RM, Kim RJ; "Assessment of Myocardial Viability"; Chapter 35 in "Edelman (Editor) et al.: Clinical Magnetic Resonance Imaging"; Vol 1, 3rd Edition, Saunders Elsevier, 2006.)



2 A: An MR image showing an anteroseptal myocardial infarction in a short axis view of a human heart acquired with the “gold standard” inversion-recovery TurboFLASH technique. B: A similar view in a different human heart where a thin subendocardial infarct is disguised by the isointense blood pool.

can distribute in the interstitial space between the collagen strands, and the distribution volume is also increased (Fig. 1C). Regions of myocardium with increased concentrations of gadolinium will have shorter T1 relaxation times. The T1-reduction in infarcted territory compared to healthy tissue can be visualized with a heavily T1-weighted pulse sequence such as inversion-recovery TurboFLASH [3]. Consequently, myocardial viability can be imaged. Due to the high spatial resolution of MRI the transmural extent and the location of ischemic injury are easily determined [4], and even tiny infarcted areas can be readily identified. This technique is now considered to be the gold standard for the assessment of myocardial viability. Figure 2A shows a delayed enhancement viability image of an anteroseptal infarct in a short-axis slice of a patient’s heart.

Limitations of the standard technique

In conventional delayed enhancement imaging, small subendocardial infarcts can sometimes be difficult to detect as they may have similar image intensities as the blood pool. A thin subendocardial infarct in figure 2B is disguised by the isointense blood pool. These types of infarcts can be difficult

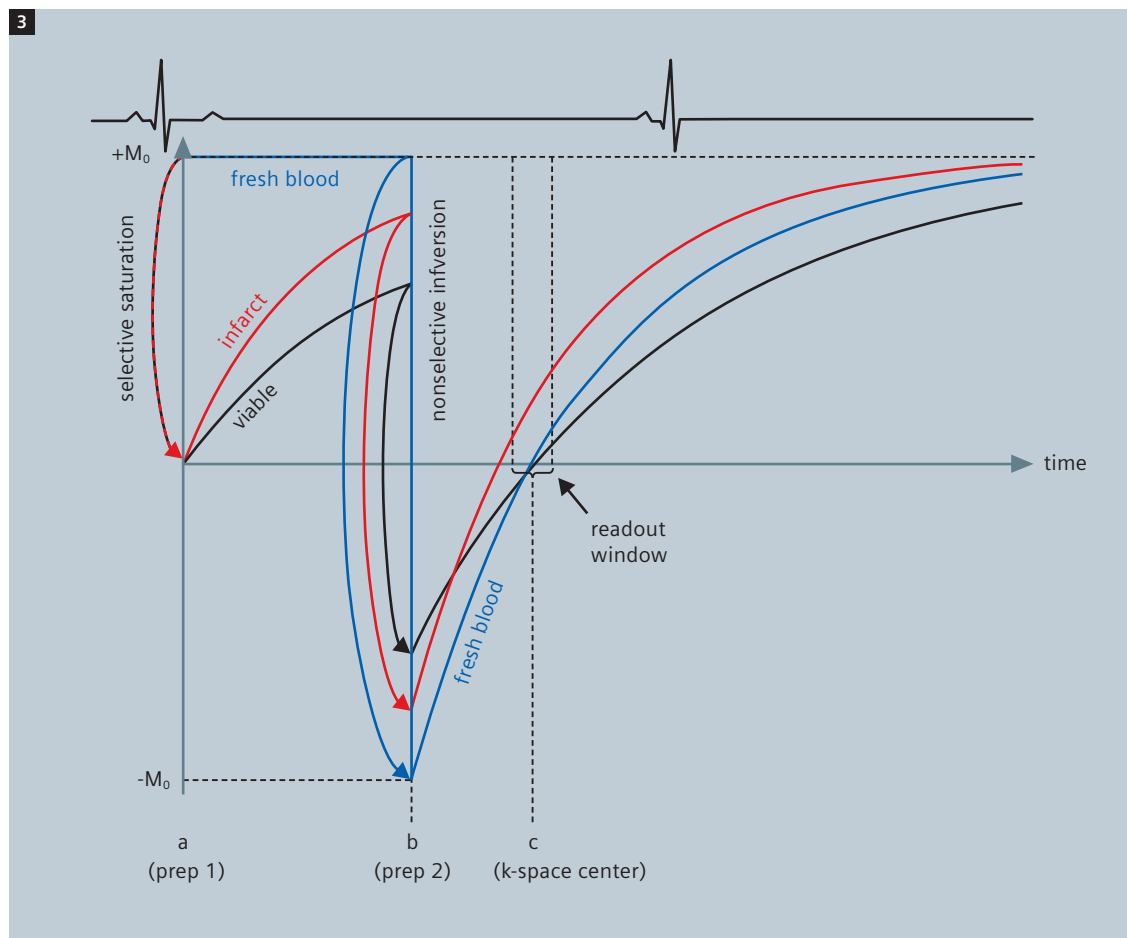
to detect especially if images are acquired early after contrast agent administration in order to increase patient throughput, or if the agent is only slowly cleared from the blood pool due to the patient’s cardiac and renal physiology. In these situations, the new dark-blood viability sequence described in this article can prove very useful. Image contrast between infarct and blood pool is much improved, and contrast between infarct and viable myocardium is slightly reduced, but remains sufficiently high.

Methods

The dark-blood viability sequence simultaneously nulls normal myocardium and blood (two different ‘T1-species’) after contrast agent administration. This goal is achieved through a double preparation scheme. It is different from the classic double IR black-blood preparation first described by Edelman et al. [5] where a non-selective inversion pulse is immediately followed by a slice-selective inversion pulse. This method is routinely employed by the black-blood HASTE sequence, but only works in the absence of a contrast agent. The dark-blood viability WIP overcomes this limitation by separating both preparation pulses in time. The first pulse usually occurs right after the R-wave

2D/3D PSIR and TurboFLASH/TrueFISP IR sequences are provided for delayed enhancement imaging in the Advanced Cardiac Package.

The works-in-progress dark-blood viability sequence simultaneously nulls myocardium and blood.



3 T1-relaxation curves of viable, infarcted myocardium, and blood when playing a selective SR pulse at time a and a non-selective IR pulse at time b. Due to the correctly chosen times between both preparations and the center of k-space at time c the curves of blood and viable myocardium cross zero simultaneously. Hence viable tissue and blood appear dark in the image. Magnetization in the infarct has recovered much more and appears bright. As fresh blood enters the imaging slice after the slice-selective preparation it only experiences the non-selective inversion pulse whereas myocardium experiences both.

For dark-blood viability imaging, myocardium and blood are prepared differently.

and is slice-selective. It is either a saturation-recovery (SR) [6, 7] or an inversion-recovery (IR) pulse [7, 8] as explained in the next section. The second preparation always is a non-selective inversion-recovery pulse. The time between the first and the second preparation and between the second preparation pulse and the readout (of the k-space center) are crucial for creating the desired dark-blood viability image contrast. Figure 3 shows the relaxation curves of viable (black line), infarcted myocardium (red line), and blood (blue line) when playing a selective SR (a – prep 1) and a later non-selective IR pulse (b – prep 2). Relaxation times in this simulation were chosen to mimic contrast agent concentrations that are

present 5 to 10 minutes after intravenous injection of a standard dose. Due to the correctly chosen times between preparations and readout the curves of blood and viable myocardium cross zero at the same time (c – k-space center) so that viable myocardium and blood appear dark in the image. Magnetization in the infarct has recovered much more and appears bright. Note that the technique works because myocardium and blood are prepared differently. Fresh blood enters the imaging slice after the slice-selective preparation. This fresh blood only experiences the non-selective inversion pulse whereas myocardium experiences both.

Using the sequence

TI parameters and image contrast

As it is impractical to manually determine the correct times between preparations and readout during a clinical exam, the sequence calculates these times automatically. Rather than specifying one inversion time TI as done in classic viability imaging (delayed enhancement) to null normal myocardium and user interface parameter TR to move the readout window to diastole, the user now provides two inversion times to simultaneously null normal myocardium and blood. The timing is then calculated by the sequence and the protocol parameters TR and TI are adjusted accordingly. TR and TI are still displayed, yet are no longer directly editable. Instead, the special card parameters "TI blood" and "TI norm myocard" are modified by the user leading to the correct setting of TR and TI. The Sequence/Special card with its TI input fields can be seen in figure 4. For completeness we note that nulling blood and normal myocardium at exactly the same time point as shown in figure 4 for reasons of simplicity will not provide the optimal diagnostic information. If both normal myocardium and blood are black it is difficult to make out the endocardial border and the myocardium. Therefore, it is advantageous to create an image where blood appears black, normal myocardium dark grey and infarct bright. This concept is already included in the WIP sequence and TI and TR are calculated accordingly.

Cardiac mechanics and timing parameters

Two conditions need to be fulfilled for the dark-blood viability sequence to work properly.

1) The slice-selective preparation and data

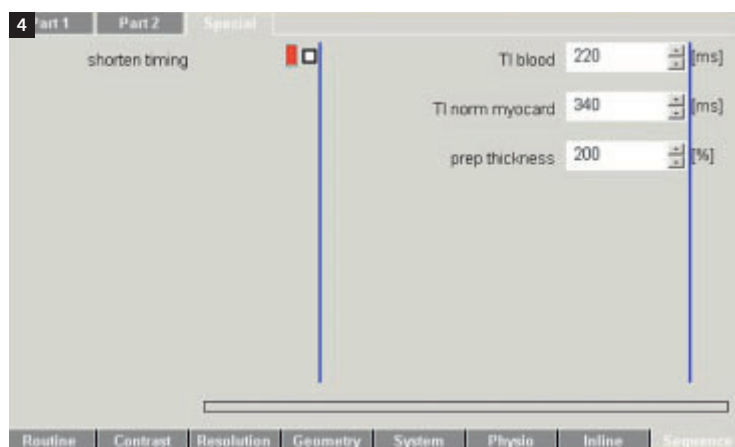
readout need to occur when the heart is in approximately the same position, see figures 5A and 5B. This ensures that the imaged slice is homogeneously prepared. In 5A the slice-selective preparation occurs immediately after the R-wave prior to the onset of systolic contraction and the readout occurs during mid to late diastole of the same heartbeat. In 5B the slice is prepared during mid to late diastole of one heartbeat, and the readout occurs during the same cardiac phase of the next beat. Also, the preparation thickness is usually twice as thick as the readout-slice to homogeneously prepare the readout slice even if it is not positioned exactly in the center of the preparation slice. The preparation slice thickness is a special card parameter and defaults to 200% of the imaging slice thickness. In case of insufficient blood exchange the user may reduce this number to e.g. 170%, but when reduced too much, the myocardium may no longer be homogeneously prepared.

2) In order to replace the selectively prepared blood by fresh blood a systolic contraction needs to occur between the slice-selective preparation and the readout. It is physically impossible to null blood and at the same time to not null infarcted tissue despite their similar T1 values, unless they are differently prepared. This can only be realized through fresh blood in the imaged slice.

Depending on a patient's heart rate, the timing approach of either figure 5A or 5B will work better. The "shorten timing" checkbox on the left side of the Sequence/Special card offers additional timing flexibility. When checked a selective SR pulse is played, otherwise a selective IR pulse is played. As signal recovers faster after a SR pulse than after

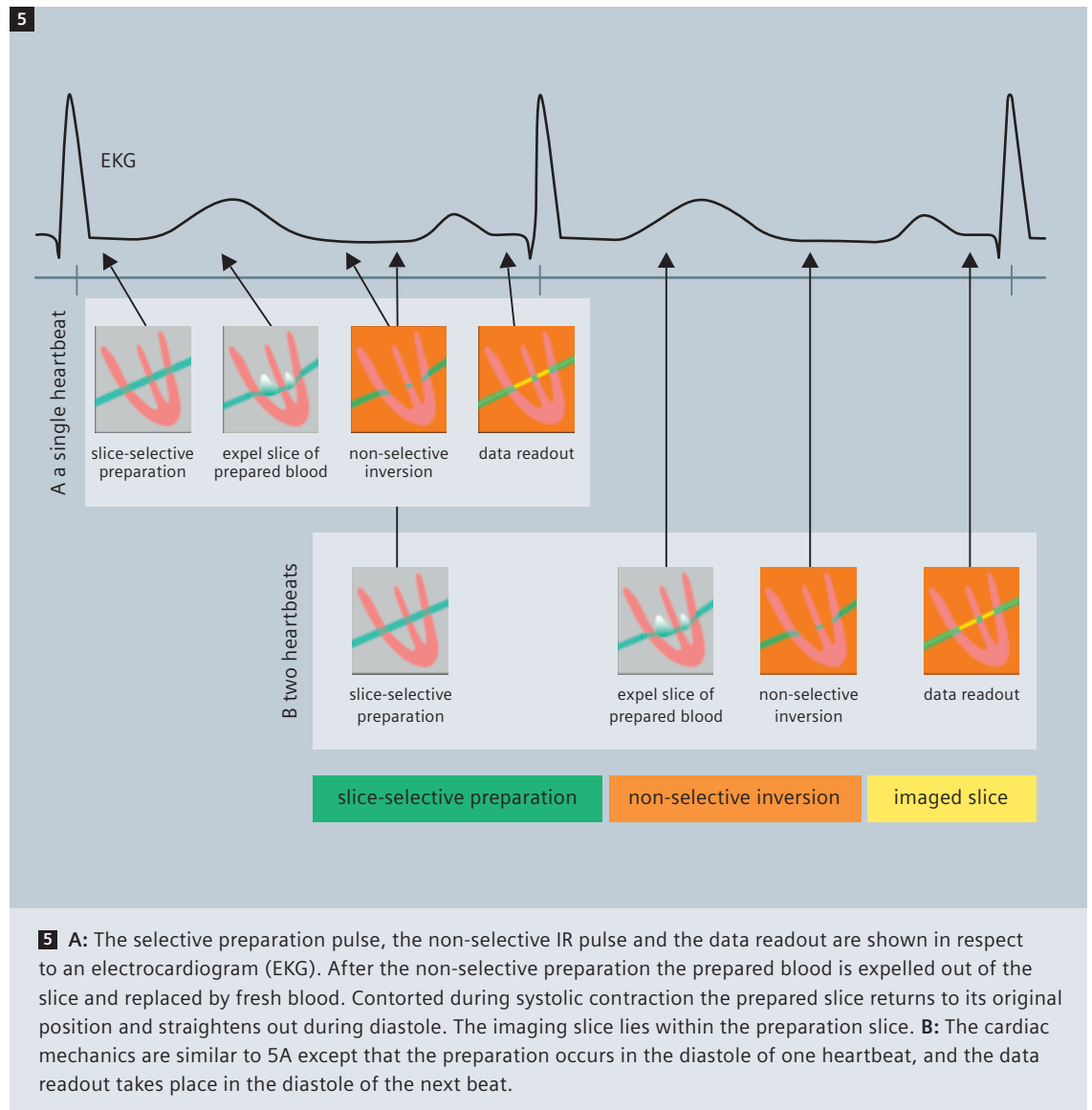
For delineation of endocardial border and myocardium, blood-pool will appear black, whereas the myocardium will appear dark grey.

For choosing between an IR or SR pulse a „shorten timing“ checkbox is provided.



4 The Sequence/Special card showing the "shorten timing" box on the left and the input boxes for inversion times of blood, normal (viable) myocardium, and relative preparation slice thickness on the right.

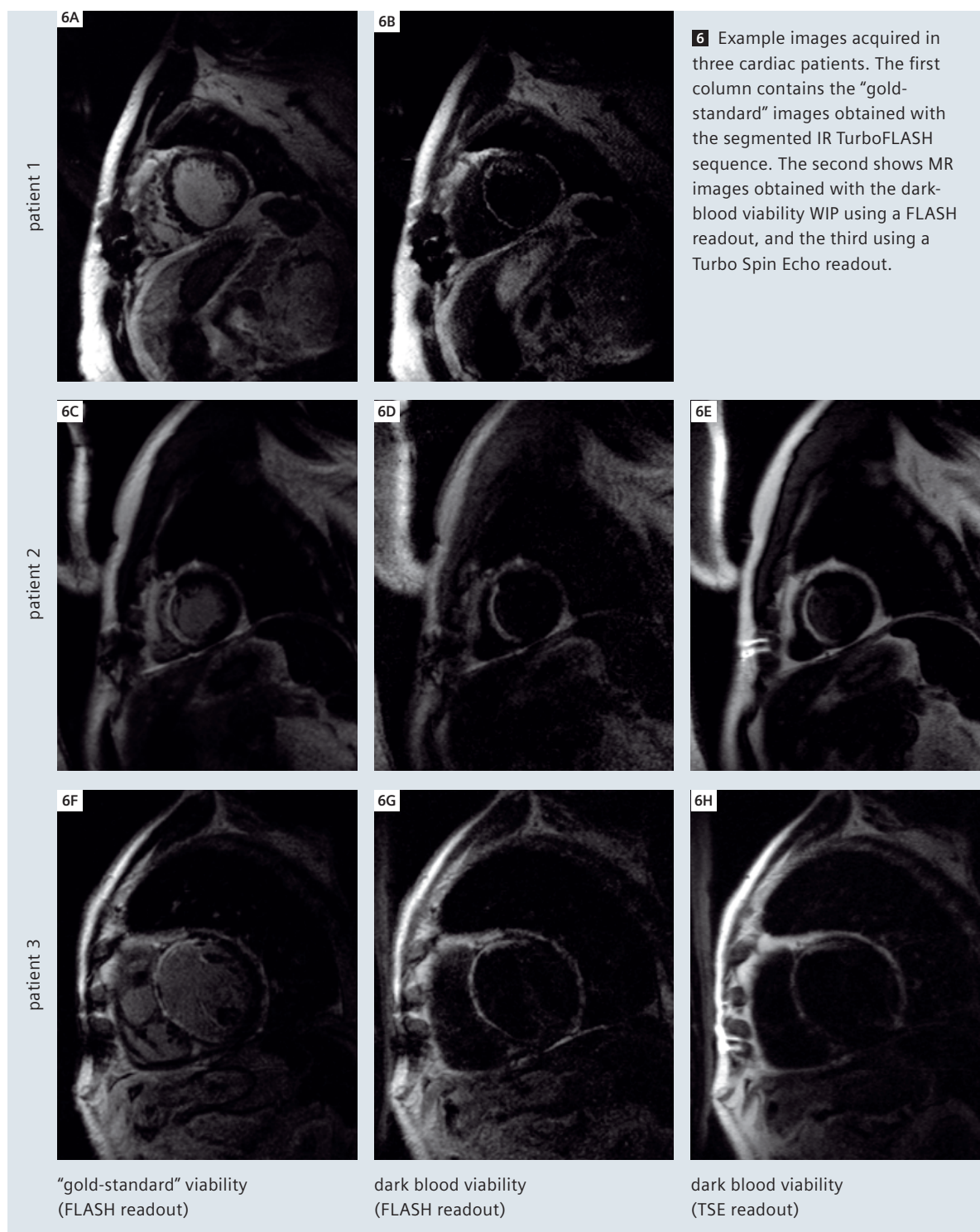
The dark blood viability works-in-progress sequence comes with a FLASH and a TSE readout.



an IR pulse, the time between preparation and readout is shortened, and higher heart rates can be accommodated. The combination of the “shorten timing” checkbox with the timing schemes of 5A or 5B gives the user sufficient options to accommodate any heart rate.

Instead of adjusting the user interface parameters TI and TR during the scan, the scanner operator

now adjusts one TI to null blood and a second TI to null normal myocardium. The scanner operator should possess a basic knowledge of cardiac mechanics as it is required to place slice-selective preparation and data readout in the correct cardiac phases. Only then a homogeneous imaging slice preparation and sufficient blood exchange can be ensured.



Available sequences

Whereas the preparation scheme is identical for all sequences included in the WIP package the data readout techniques vary. For software version *syngo* MR B13 (including MAGNETOM Avanto and MAGNETOM Trio, A Tim System) a segmented Flash, segmented TrueFISP, Turbo Spin Echo (TSE), single-shot Flash, and single-shot TrueFISP version are available. For *syngo* MR 2004A (including the MAGNETOM Sonata) a segmented Flash and Turbo Spin Echo version exists.

Results

Figure 6 shows representative example images acquired in three cardiac patients. The first column contains the “gold-standard” images obtained with the segmented IR TurboFLASH sequence. The second shows MR images obtained with the dark-blood viability WIP using a FLASH readout, and the third using a TSE readout. The images of patient 1 are of particular interest as the gold-standard does not reveal the thin infarcted subendocardial rim in the septum, but the dark-blood viability technique does. The images of patients 2 and 3 show that the infarcted regions in all dark-blood images match those of the gold-standard.

Conclusions

We have described a new dark-blood viability technique that employs a precisely timed double-preparation scheme to render blood black, normal myocardium dark-grey, and infarct bright. When care is taken to ensure that the preparations occur at the proper times in the cardiac cycle, homogeneous preparation with sufficient blood exchange occurs, resulting in high quality dark-blood delayed enhancement images.

The dark-blood viability sequence leads to a better delineation of thin subendocardial scars from the blood-pool.


References

- 1 Judd RM, Wagner A, Rehwald WG, Albert T, Kim RJ. Technology insight: assessment of myocardial viability by delayed-enhancement magnetic resonance imaging. *Nat Clin Pract Cardiovasc Med* 2005;2(3):150–158.
- 2 Rehwald WG, Fieno DS, Chen EL, Kim RJ, Judd RM. Myocardial magnetic resonance imaging contrast agent concentrations after reversible and irreversible ischemic injury. *Circulation* 2002;105(2):224–229.
- 3 Simonetti OP, Kim RJ, Fieno DS, Hillenbrand HB, Wu E, Bundy JM, Finn JP, Judd RM. An improved MR imaging technique for the visualization of myocardial infarction. *Radiology* 2001;218(1):215–223.
- 4 Wu E, Judd RM, Vargas JD, Klocke FJ, Bonow RO, Kim RJ. Visualisation of presence, location, and transmural extent of healed Q-wave and non-Q-wave myocardial infarction. *Lancet* 2001;357(9249):21–28.
- 5 Edelman RR, Chien D, Kim D. Fast selective black blood MR imaging. *Radiology* 1991;181(3):655–660.
- 6 Rehwald WG, Salerno M, Zuehlsdorff S, Kim RJ, Judd RM. Dark Blood Delayed Enhancement MRI for the Assessment of Subendocardial Infarcts (abstract 110). *Journal of Cardiovascular Magnetic Resonance* 2007:101.
- 7 Salerno M, Rehwald WG, Chen EL, Judd RM, Kim RJ. Contrast Optimization of Black-Blood Viability Imaging. *Proc Intl Soc Mag Reson Med* 2007.
- 8 Rehwald WG, Salerno M, Chen EL, Darty S, Aljaroudi W, Maier CS, Judd RM, Kim RJ. Dark Blood Delayed Enhancement in Humans By Double Preparation and Gradient-Echo or Turbo-Spin-Echo Readout. *Proc Intl Soc Mag Reson Med* 2007.

Contact

Wolfgang Rehwald, Ph.D.
Duke Cardiovascular MR Center
Duke South – Room 4226A
DUMC – Box 3934
Durham, NC 27710
USA
wolfgang.rehwald@siemens.com



 We see a way to deliver 99% uptime on diagnostic imaging and biomedical systems

Proven Outcomes

Recouping days of productivity and millions in revenue.

Proven Outcomes in Health Care.

Cutting costs. Optimizing workflow. Advancing the quality of care. Impossible? On the contrary: We can prove it. Across every clinical setting, we are helping health care become more efficient, more effective, and more profitable. With solutions that apply cutting-edge technology and strategic problem solving. So you can focus on essentials – and make the vision of the fully integrated hospital a reality. These are the Proven Outcomes that are transforming the delivery of health care. Today.

www.siemens.com/medical

SIEMENS
medical

The Promise of Molecular MRI in Cardiovascular Imaging

David E. Sosnovik, M.D. FACC^{1,2}

¹Center for Molecular Imaging Research, Massachusetts General Hospital, Harvard Medical School, Boston, MA, USA

²Department of Cardiology, Massachusetts General Hospital, Harvard Medical School, Boston, MA, USA

The term “Molecular Imaging” refers to the noninvasive imaging of certain cellular and subcellular events in vivo. The advantages of an MRI-based approach to cardiovascular molecular imaging include its high spatial resolution, excellent soft tissue contrast and ability to simultaneously image cardiovascular anatomy and physiology [1]. The role of molecular MRI in cardiovascular medicine has been extensively described in several recent reviews, and the interested reader is referred to these articles for a more comprehensive discussion of the field [1, 2]. In this article, the reader is provided with a brief introduction to cardiovascular molecular imaging. The opportunities and challenges pertaining to the use of gadolinium-based probes, magnetic (iron-oxide) nanoparticles, positive and negative contrast imaging, and the application of these contrast agents and techniques to cardiovascular disease are discussed.

Contrast agents and imaging techniques

The principal challenge of molecular MRI lies in its lower sensitivity, compared, for example, to nuclear imaging techniques. Conventional gadolinium chelates have a sensitivity in the micromolar range, which is usually inadequate for molecular MRI. Conventional extracellular gadolinium chelates also have extremely short intravascular half-lives and rapid renal excretion, which further limits their utility for most molecular imaging applications. Several novel gadolinium constructs have been developed to address these limitations including gadolinium-loaded liposomes, micelles and lipoproteins. These constructs are heavily loaded with paramagnetic gadolinium chelates and in general have longitudinal relaxivity (R1) values ranging from 10–20 s⁻¹ mM⁻¹ [3,4]. The relaxivity of

an MR contrast agent reflects its ability to interact with adjacent protons and strongly influences its detectability. The higher the longitudinal relaxivity (R1) of an agent, the brighter tissue in its vicinity becomes, while the higher the transverse relaxivity (R2), the darker the tissue becomes.

Gadolinium based probes are generally imaged with T1-weighted sequences at standard clinical field strengths, such as 1.5 and 3 Tesla. However, the R1 of these agents decreases rapidly at high field strengths, while the R2 of paramagnetic gadolinium-based probes increases with field strength. Increasing the dose of a gadolinium-based probe at higher field strengths may thus increase the dominance of the T2 effects and makes the generation of positive contrast even more difficult.

Although no acute toxic effects have been reported with most of the novel gadolinium constructs, the long-term effect of these agents remains less well understood. Prolonged tissue retention of low amounts of a targeted gadolinium-based probe may be safe, particularly in the absence of dechelation, but will require significant further study and testing. The recent description of a systemic fibrosis syndrome in those with renal dysfunction, and thus prolonged tissue retention of conventional gadolinium chelates, will likely require any new gadolinium construct to be extensively tested for similar types of chronic toxicity.

Magnetic iron oxide nanoparticles

Magnetic iron oxide nanoparticles (MNP) are typically superparamagnetic and can be imaged with T1, T2, T2* and steady state free precession techniques [5–7]. MNP agents typically have a central core of iron-oxide, measuring 3–5 nm in diameter, surrounded by a carbohydrate (for macrophage targeting) or polymer coat (often for targeting to

The advantages of cardiovascular molecular MRI include its high spatial resolution, excellent soft tissue contrast and ability to simultaneously image anatomy and physiology.

other cells) [8, 9]. A citrate coated iron-oxide nanoparticle has also recently been developed and used as a blood pool agent [10]. Selected MNP have been used extensively in the clinical arena to image the liver and lymphatic system [11], and their established safety record thus makes them a highly appealing platform for molecular MRI. MNP do not contain any inert or non-degradable moieties, and it has been shown that the iron-oxide core of these agents is metabolized within two weeks, after which the released iron is used in the synthesis of new red blood cells. However, the ability of the body to excrete excess iron is limited, which places a limit on the frequency with which these contrast agents can be given. It is thus likely that limitations will be imposed on the frequency of repeat dosing for most MNP.

The R2 values of the superparamagnetic MNP range from 50 to > 600 s⁻¹ mM⁻¹ [9,12], and remain constant over all field strengths > 0.5 Tesla. The R1 values of these agents, however, decrease with field strength much like paramagnetic gadolinium constructs. First generation MNP, such as Feridex™ (Advanced Magnetix, Cambridge, MA, USA), contain relatively thin dextran coats and have the propensity to form polycrystalline clusters, which are rapidly cleared from the blood stream by the reticulo-endothelial system. This agent can thus be used to detect the replacement of normal liver tissue by neoplasm and after intravenous injection, and has been FDA-approved for this since 1993. The metabolism, pharmacokinetics and toxicity of MNP taken up by cells in the reticulo-endothelial system have been well studied [13]. Histologic and serologic studies have not revealed any toxic effects related to MNP administration. Iron radiotracer (59Fe) and MR relaxivity studies have also shown that the iron-oxide core of the MNP is broken down into other forms of iron and then incorporated normally into hemoglobin in newly formed erythrocytes [13]. More recently, several groups have used Feridex™ and other iron oxide nanoparticles to label exogenous stem cells prior to their in vivo administration [14, 15]. The pharmacokinetics, metabolism and safety profile of Feridex™ when used for cell labeling, however, requires a separate and detailed evaluation.

MION

Second and third generation MNP have been synthesized with more extensive polymer coatings

and remain monodisperse in solution [8]. The term monocrystalline iron oxide or MION is thus often applied to these agents. Unlike Feridex™, these agents were designed to have a much longer blood half life (24 hours in humans, 11 hours in mice) and typically have a homogenous uniform size distribution in the 30 - 50 nm range [8, 9,16]. The small size, long blood half lives and high relaxivities of these MNP constitute a powerful combination that allows them to penetrate deep tissue spaces, such as the interior of atherosclerotic plaque and the myocardium [17, 18], and detect sparsely expressed targets in the low nanomolar range. The MNP Ferumoxtran (Combidex™ or Sinerem™), a preparation similar to the experimental MION-47, has been used to image lymph node micrometastases in several phase 3 clinical trials [11]. This agent has also been used to image inflamed vulnerable plaque in humans [19,20], although the experience in this regard is very preliminary.

CLIO

A highly stabilized and cross-linked derivative of MION-47, known as CLIO-47, has also recently been developed for targeted molecular imaging applications [9, 21]. CLIO contains amine groups on cross-linked dextran chains, allowing a large variety of ligands to be conjugated to the nanoparticle with a high degree of flexibility, stability and ease. Near infrared fluorochromes, for instance, can be attached to the amine groups on the probe to form a dual modality magnetofluorescent nanoparticle [22, 23]. In addition, many copies of the targeting ligand can be attached to the CLIO-fluorochrome conjugate to form a multivalent (> 1 targeting ligand) magnetofluorescent nanoparticle. Examples of two recently used such ligands include annexin for apoptosis imaging [6, 23], and a peptide specific for the adhesion molecule VCAM-1 [24, 25]. More recently an experimental MNP with even higher relaxivity (MION-48, CLIO-48, R2 > 180 s⁻¹ mM⁻¹) has been synthesized, and has the potential to enhance the sensitivity of these and other targeted probes even further.

Specificity of agents

The specificity of both gadolinium and iron oxide based probes is influenced by their size, potential for non-specific binding to extracellular proteins and other substances, and their degree of uptake

MNP do not contain any inert or nondegradable moieties – the iron-oxide core of these agents is metabolized within two weeks, after which the released iron is used in the synthesis of new red blood cells.

Multivalent magnetofluorescent nanoparticles can be used for molecular imaging of apoptosis or adhesion molecules like VCAM-1.

Table 1: Recognition of artifacts in cardiovascular molecular MRI. Potential solutions to these artifacts are shown in parenthesis.

Gadolinium Constructs	Comment
Incomplete fat suppression	Short T1 of fat may mimic probe uptake in the vascular wall. (Improve shim or use inversion recovery techniques.)
Incomplete suppression of signal from blood pool due to slow flow	Residual positive signal from blood may compromise evaluation of probe uptake by atherosclerotic plaque. (Use of diffusion encoded stimulated echo techniques to improve signal loss in blood pool.)
B ₁ inhomogeneity	Variable flip angle can produce inconsistent contrast in image. Problem in humans and larger animals at higher field strengths, such as 3 Tesla and higher. (Adiabatic excitation pulses or RF shimming with multiple transmit coils.)
Ghosting from chest wall fat into region of interest	(Parallel acquisition to reduce breathhold duration and/or use of fat suppression.)
Iron Oxide Nanoparticles	
Calcification	Low signal may mimic MNP uptake. (MNP produce bright signal with T1 or positive contrast techniques. Ultrashort echo or UTE techniques may also play a role.)
Air	Low signal may mimic MNP uptake. (MNP produce bright signal with T1 or positive contrast techniques. Ultrashort echo or UTE techniques may also play a role.)
Susceptibility Artifacts	Can produce either non-specific negative or positive contrast depending on whether on-resonance or off-resonance imaging is performed. (Compare to conventional spin echo image.)
Hemorrhage	Endogenous iron products may mimic exogenous MNP accumulation. Exceedingly rare in mouse heart and atheromatous plaque. Incidence in humans will require study. (Dual modality imaging combining MRI with Fluorescence or PET will resolve issue.)
Motion	Can produce spin dephasing and MR signal loss, particularly with the long echo times needed for T2*-weighting. (Reduce echo time, use gradient moment nulling, change to off-resonance technique with short echo time.)

by immune cells such as macrophages. Larger gadolinium-containing liposomes for instance, may become retained non-specifically in the interstitial space of the myocardium, and gadolinium-containing micelles may bind non-specifically to lipophilic or hydrophilic components of the extracellular matrix. MNP may be taken up non-specifically by macrophages in inflamed tissues, but high throughput chemical screens have recently revealed that minor surface modifications of the MNP may reduce this [26].

When T2, T2* or SSFP sequences are used the MNP is imaged through the generation of negative contrast or relative signal hypointensity. Concerns have been raised that this negative contrast could be non-specific and difficult to differentiate from signal hypointensity due to calcification, susceptibility artifacts, flow related signal loss or air (Table 1). Several off-resonance or positive contrast techniques have thus recently been developed by Cunningham, Mani, Stuber and others to potentially address these issues. The sensitivity of the positive contrast sequences for MNP may approach that of conventional T2* based techniques, (nanomolar) [27, 28], if performed under optimal conditions and with parameters producing low specificity. However, under most circumstances the sensitivity of the off-resonance techniques is lower than that of conventional gradient echo imaging. In addition, these techniques work less efficiently at higher field strengths and are fairly nonlinear, particularly if the echo time is not kept extremely short [28].

Artifacts in cardiovascular molecular MRI

Several important artifacts, likewise, need to be considered when using gadolinium based probes (Table 1). Fat has a high R1 value and appears bright on T1-weighted sequences. Incomplete suppression of the perivascular fat, for instance, can thus mimic uptake of the probe in the vessel wall. Slow flow within the vessel lumen can also result in incomplete suppression of the blood signal and thus mimic uptake of the probe within the endothelium [29]. Finally B1 inhomogeneity becomes a significant problem at higher field strengths and can produce significant variation in signal intensity due to inconsistent flip angles. This B1 inhomogeneity will need to be addressed with techniques such as adiabatic pulses or B1 shimming if T1-weighted sequences are to be used optimally in humans and large animals at higher field strengths [30].

A strong awareness of the sensitivity, specificity and artifacts produced by each imaging technique (T1, T2*, off-resonance) is thus needed (Table 1). Methods to recognize and potentially eliminate some of these possible artifacts are provided in the parentheses within Table 1. In extreme cases multi-modality imaging may be needed. However, one of the strengths of MRI lies in its ability to generate multiple forms of contrast, which can usually be used to differentiate any potential artifacts from a true molecular signal.

Cardiovascular applications

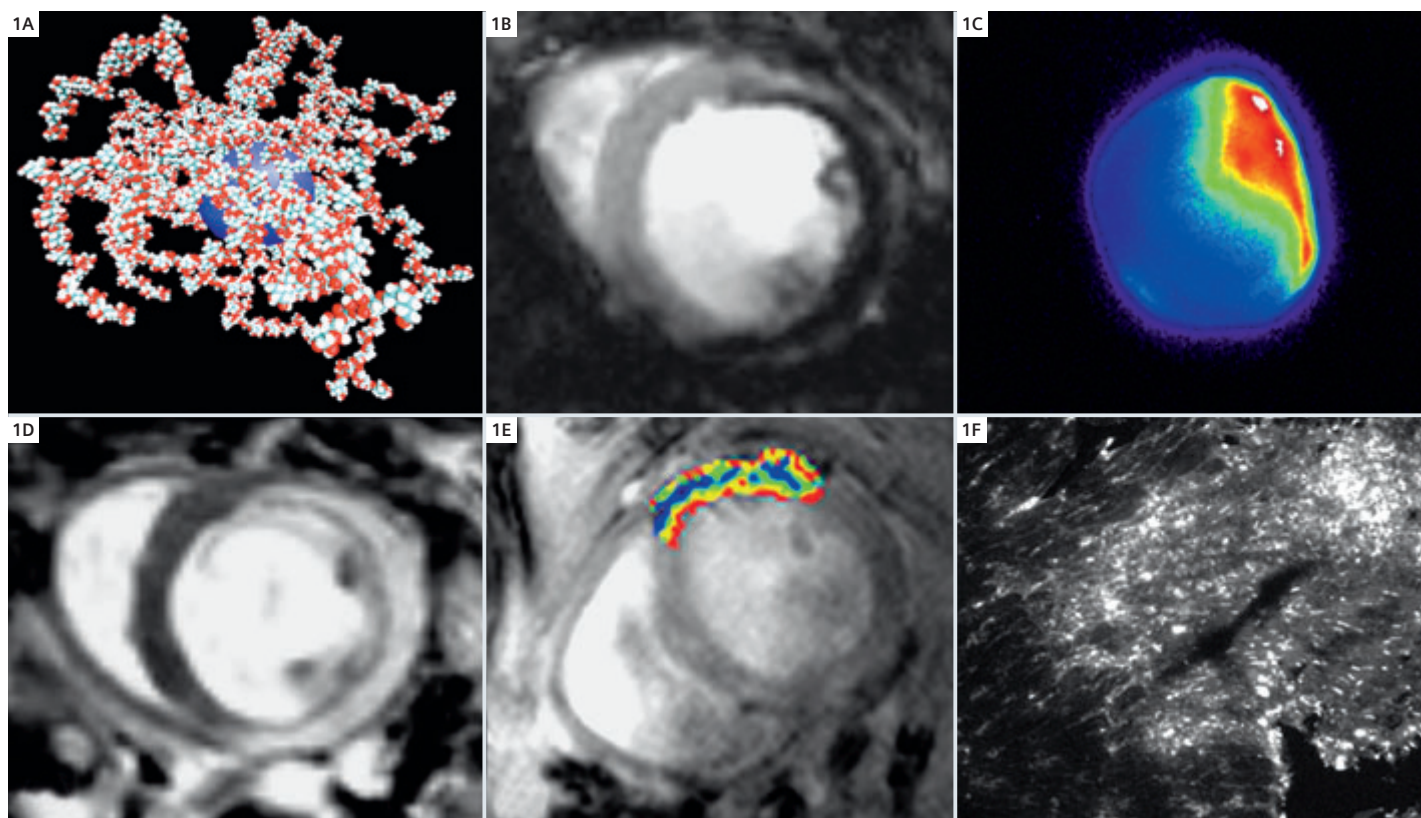
MNP have been used to image molecular targets in atherosclerosis [17, 25], myocardial injury [6, 18, 31], and stem cell therapy [14, 15]. The properties of MNP make them ideal agents with which to image myocardial macrophage infiltration in healing infarcts, transplant rejection and myocarditis [18, 31, 32]. This was recently demonstrated in a mouse model of post-infarction macrophage infiltration. The mice were injected intravenously with 3–20 mg Fe/kg of the MNP, CLIO-Cy5.5, 48 hours after the infarct and then imaged with conventional T2*-weighted MRI 48 hours later. Negative contrast, consistent with the uptake of the probe by infiltrating macrophages, was seen in the infarcted anterolateral myocardium of all mice and at all doses [18], as shown in Figure 1.

Targeted imaging of cardiomyocyte injury has been performed using apoptosis and necrosis detecting MNP probes. Cardiomyocyte apoptosis has been imaged in vivo by MRI in a mouse model of transient coronary ligation [6]. No significant changes were seen in myocardial signal intensity when mice were injected with an unlabeled control probe. However, injection of the annexin-labeled probe (AnxCLIO-Cy5.5) produced significant negative contrast enhancement [6]. As shown in Figure 1, T2* could be measured in the injured myocardium and was significantly lower in those mice injected with the annexin labeled probe [6]. Cardiomyocyte necrosis has been imaged by MRI in the rat heart ex-vivo with an antimyosin antibody conjugated to MION [33]. The use of this probe in conjunction with apoptosis detecting probes could thus provide powerful insights into the pathogenesis of cell death during acute myocardial injury.

The myocardium is highly suited to multimodal molecular imaging approaches. Fluorescence tomography of the myocardium, for instance, has recently

MNP have been used to image molecular targets in atherosclerosis, myocardial injury, and stem cell therapy.

The myocardium is highly suited to new multimodal imaging approaches such as fluorescence tomography or MR-PET.



1 Molecular MRI of myocardial injury in mouse models [1, 18].

(A) Schematic of a second-generation iron oxide magnetic nanoparticle (MNP), showing the iron oxide core and surrounding dextran coat. The composite size of the nanoparticle reaches 30-50 nm and remains monodisperse in solution.

(B) Accumulation of the MNP CLIO-Cy5.5 in macrophages infiltrating a healing myocardial infarct [18]. Negative contrast due to CLIO-Cy5.5 accumulation can be seen in injured anterolateral wall of the myocardium.

(C) Conjugation of a fluorochrome, such as Cy5.5, to the MNP allows fluorescence imaging to be performed to confirm the MRI findings [18]. The distribution of the MNP in panel (B), signifying macrophage infiltration, corresponds well to the area of delayed enhancement after gadolinium injection (D).

(E) T2* map of AnxCLIO-Cy5.5 accumulation in apoptotic myocardium following transient coronary artery ligation in a mouse [6]. The T2* values in the hypokinetic myocardium are significantly lower than in the remote myocardium, indicating the presence of cardiomyocyte apoptosis and uptake of the probe. The construction of T2* maps allows serial noninvasive quantification of the molecular process to be performed in-vivo [6].

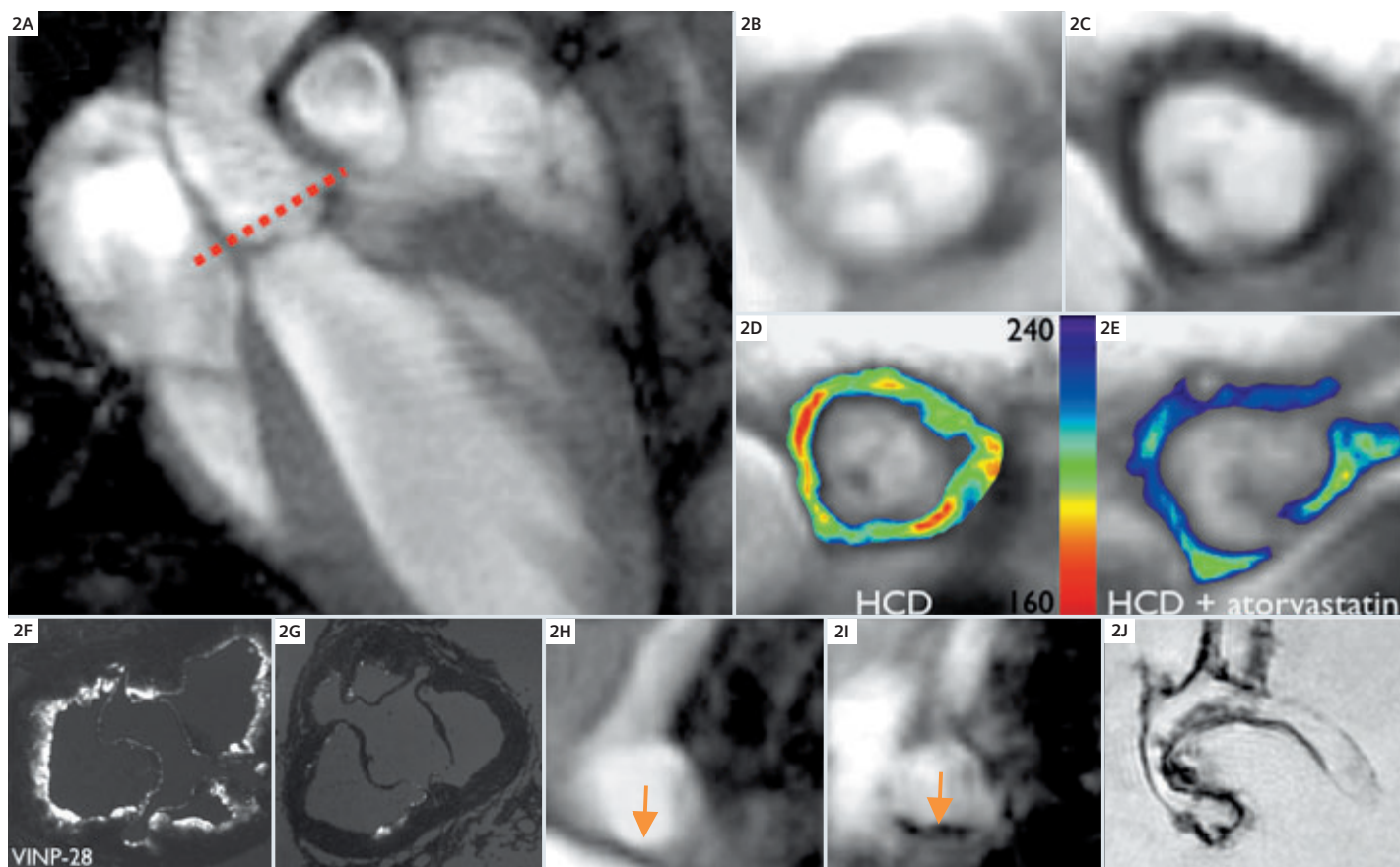
(F) Since the attachment of a fluorochrome to a MNP does not affect its pharmacokinetics, this can be used to evaluate the cellular localization of the MNP by fluorescence microscopy [1, 18]. This is a distinct advantage of molecular MRI with MNPs over radioisotope techniques, where cellular and microscopic localization of the probe is not possible.

Studies demonstrate the potential of targeted magnetic nanoparticles for diagnostic and therapeutic use.

been performed in the mouse heart in vivo [18, 31]. This is a completely non-invasive technique that is easily performed in conjunction with the MRI of magnetofluorescent MNP in small animals. In large animals and humans MRI can be combined with PET imaging either sequentially or simultaneously, using novel MR-PET systems.

Molecular MRI approaches to the imaging of atherosclerosis have focused on the detection of plaque lipid content, plaque inflammation, plaque thrombosis and plaque angiogenesis [2]. Gadofluorine is a novel chelate of gadolinium, which is more lipophilic and has a longer circulation half-life than con-

ventional chelates, and has been used to detect lipid rich plaques in rabbits [29, 34]. Labeled gadolinium-containing liposomes have been used in rabbits to target the v3 integrin and also used as a platform for the anti-angiogenic agent fumagillin [35]. This construct demonstrates the potential of using a targeted magnetic nanoparticle in both a diagnostic and therapeutic capacity. Gadolinium containing HDL-like nanoparticles have also been shown to accumulate in atherosclerotic plaques [4, 36]. Plaques rich in macrophages tend to take up these lipoprotein nanoparticles quicker than those with a low macrophage content [4]. Plaque macrophage



2 (A–G) Molecular MRI of VCAM-1 expression in apoE^{-/-} mice imaged with a VCAM-1 sensing probe [25].

(A) T2*-weighted gradient echo image of the long axis of the left ventricle and thoracic aorta. The short axis plane through the aortic root is shown by the dashed red line. The images were acquired on a 9.4T horizontal bore MR scanner (Biospec, Bruker, Billerica, MA, USA).

(B, C) Short axis images of the aortic root before (B) and after (C) the injection of the probe are shown. Significant accumulation of the probe, consistent with VCAM-1 expression, is seen in the aortic root, which is an area rich in plaque.

(D, E) VCAM-1 expression in the aortic root of a cholesterol fed apoE^{-/-} mouse (D) is shown by in vivo MRI to be significantly higher than in a statin treated apoE^{-/-} mouse (E). Ex-vivo fluorescence images of the aortic root confirm higher probe accumulation in the untreated mouse (F) than the statin treated mouse (G).

(H–J) MRI of macrophage infiltration in atherosclerotic plaque in vivo [17, 44]. A cross section of the aortic arch of an apoE^{-/-} mouse is imaged in (H, I) showing a smooth vessel outline when the mouse is injected with saline (H), but evidence of MNP accumulation in plaque when the mouse is injected with CLIO-Cy5.5 (I). The in vivo distribution of MNP in plaque can be confirmed by ex-vivo MRI (J).

content has also been imaged with a gadolinium containing micelle decorated with an antibody to the macrophage scavenger receptor [37].

A fibrin specific peptide has been conjugated to a conventional gadolinium-containing chelate to yield a small molecular weight probe. This probe has been used to image both acute and subacute thrombi in a variety of large animal models [38–41]. The low background uptake of this peptide and the very high levels of fibrin expression within thrombi allowed this agent to be conjugated to a low relaxivity conventional gadolinium chelate. This served both to make the agent potentially

safe in humans (initial results in 4 patients have been reported) but also required large amounts of the targeting peptide to be synthesized per dose, raising logistical concerns and barriers. At the present time further development of this agent has thus been stopped. Conjugation of a lower dose of the peptide ligand to a higher relaxivity contrast agent could potentially solve this issue.

The largest and perhaps most clinically applicable experience in the imaging of atherosclerotic plaque inflammation has been with MNPs [2]. Long circulating MNPs are able to penetrate an atherosclerotic plaque and are then taken up by its cellular compo-

Long circulating MNPs are able to penetrate an atherosclerotic plaque.

nents (Figure 2). Plaque inflammation has been imaged with MNPs in mice [17], large animal models [42], and in human carotid arteries in-vivo [19, 20]. Several generations of VCAM-1 targeted MNPs have also been developed. With the latest generation (linear peptide) of this probe, VCAM-1 expression could be successfully imaged in the aortic roots of apoE^{-/-} mice in-vivo (Figure 2) [25]. In addition, the effect of statin therapy on VCAM-1 expression could be imaged in-vivo with this probe (Figure 2) [25]. Molecular MRI of VCAM-1 expression was thus able to detect a sparsely expressed molecular marker early in a disease process and also demonstrate adequate dynamic range to detect a treatment effect. The use of stem cells for cardiac regeneration is highly promising and molecular MRI may play an important role in the development of this therapy. The MNP, Feridex™, has been used to label and image stem cells injected directly into the myocardium [14, 15]. Recently stem cells have been labeled with gadolinium and fluorine containing constructs too, allowing both proton and fluorine MRI to be performed. While MRI offers superior spatial resolution, its sensitivity for stem cells remains lower than SPECT [43]. MRI of labeled cells is also not able to determine cell viability or metabolic state. The advantage of MRI of labeled stem cells, therefore, lies in its ability to precisely delineate the infarct, guide the intramyocardial injection of the cells and track their movement over time [14, 15].

Conclusion

Molecular MRI is currently playing an increasing role in basic science research and pharmaceutical development. Examples showing the utility of molecular MRI in the imaging of biological processes in the myocardium and atherosclerotic plaque have been provided in this article. First generation polymer-coated MNP are already FDA approved and subsequent generations of MNP (Combidex™) have completed phase-3 clinical trials [11]. Molecular MRI in the cardiovascular system thus has the potential to become a powerful tool in both the basic science as well as the clinical settings.

Contact

David Sosnovik, M.D., FACC
Instructor in Medicine at Harvard Medical School
Director, Program in CMR
Martinos Center for Biomedical Imaging,
Department of Cardiology, MGH
sosnovik@nmr.mgh.harvard.edu

References

- 1 Sosnovik DE, Nahrendorf M, Weissleder R. Molecular magnetic resonance imaging in cardiovascular medicine. *Circulation* 2007;115(15):2076–2086.
- 2 Jaffer FA, Libby P, Weissleder R. Molecular and cellular imaging of atherosclerosis: emerging applications. *J Am Coll Cardiol* 2006;47(7):1328–1338.
- 3 Morawski AM, Winter PM, Crowder KC, Caruthers SD, Fuhrhop RW, Scott MJ, Robertson JD, Abendschein DR, Lanza GM, Wickline SA. Targeted nanoparticles for quantitative imaging of sparse molecular epitopes with MRI. *Magn Reson Med* 2004;51(3):480–486.
- 4 Frias JC, Ma Y, Williams KJ, Fayad ZA, Fisher EA. Properties of a versatile nanoparticle platform contrast agent to image and characterize atherosclerotic plaques by magnetic resonance imaging. *Nano Lett* 2006;6(10):2220–2224.
- 5 Li W, Salaniti J, Tutton S, Dunkle EE, Schneider JR, Caprini JA, Pierchala LN, Jacobs PM, Edelman RR. Lower extremity deep venous thrombosis: evaluation with ferumoxytol-enhanced MR imaging and dual-contrast mechanism-preliminary experience. *Radiology* 2007;242(3):873–881.
- 6 Sosnovik DE, Schellenberger EA, Nahrendorf M, Novikov MS, Matsui T, Dai G, Reynolds F, Grazette L, Rosenzweig A, Weissleder R, Josephson L. Magnetic resonance imaging of cardiomyocyte apoptosis with a novel magneto-optical nanoparticle. *Magn Reson Med* 2005;54(3):718–724.
- 7 Heyn C, Bowen CV, Rutt BK, Foster PJ. Detection threshold of single SPIO-labeled cells with FIESTA. *Magn Reson Med* 2005;53(2):312–320.
- 8 Shen T, Weissleder R, Papisov M, Bogdanov A, Jr., Brady TJ. Monocrystalline iron oxide nanocompounds (MION): physicochemical properties. *Magn Reson Med* 1993;29(5):599–604.
- 9 Wunderbaldinger P, Josephson L, Weissleder R. Crosslinked iron oxides (CLIO): a new platform for the development of targeted MR contrast agents. *Acad Radiol* 2002;9 Suppl 2:S304–306.
- 10 Wagner S, Schnorr J, Pilgrimm H, Hamm B, Taupitz M. Monomer-coated very small superparamagnetic iron oxide particles as contrast medium for magnetic resonance imaging: preclinical in vivo characterization. *Invest Radiol* 2002;37(4):167–177.
- 11 Harisinghani MG, Barentsz J, Hahn PF, Deserno WM, Tabatabaei S, van de Kaa CH, de la Rosette J, Weissleder R. Noninvasive detection of clinically occult lymph-node metastases in prostate cancer. *N Engl J Med* 2003;348(25):2491–2499.
- 12 Moffat BA, Reddy GR, McConville P, Hall DE, Chenevert TL, Kopelman RR, Philbert M, Weissleder R, Rehemtulla A, Ross BD. A novel polyacrylamide magnetic nanoparticle contrast agent for molecular imaging using MRI. *Mol Imaging* 2003;2(4):324–332.
- 13 Weissleder R, Stark DD, Engelstad BL, Bacon BR, Compton CC, White DL, Jacobs P, Lewis J. Superparamagnetic iron oxide: pharmacokinetics and toxicity. *AJR Am J Roentgenol* 1989;152(1):167–173.
- 14 Kraitchman DL, Heldman AW, Atalar E, Amado LC, Martin BJ, Pittenger MF, Hare JM, Bulte JW. In vivo magnetic resonance imaging of mesenchymal stem cells in myocardial infarction. *Circulation* 2003;107(18):2290–2293.
- 15 Hill JM, Dick AJ, Raman VK, Thompson RB, Yu ZX, Hinds KA, Pessanha BS, Guttman MA, Varney TR, Martin BJ, Dunbar CE, McVeigh ER, Lederman RJ. Serial cardiac magnetic resonance imaging of injected mesenchymal stem cells. *Circulation* 2003;108(8):1009–1014.
- 16 Wunderbaldinger P, Josephson L, Weissleder R. Tat peptide directs enhanced clearance and hepatic permeability of magnetic nanoparticles. *Bioconjug Chem* 2002;13(2):264–268.

- 17 Jaffer FA, Nahrendorf M, Sosnovik D, Kelly KA, Aikawa E, Weissleder R. Cellular imaging of inflammation in atherosclerosis using magnetofluorescent nanomaterials. *Mol Imaging* 2006;5(2):85–92.
- 18 Sosnovik DE, Nahrendorf M, Deliolanis N, Novikov M, Aikawa E, Josephson L, Rosenzweig A, Weissleder R, Ntziachristos V. Fluorescence tomography and magnetic resonance imaging of myocardial macrophage infiltration in infarcted myocardium in vivo. *Circulation* 2007;115(11):1384–1391.
- 19 Trivedi RA, JM UK-I, Graves MJ, Cross JJ, Horsley J, Goddard MJ, Skepper JN, Quartey G, Warburton E, Joubert I, Wang L, Kirkpatrick PJ, Brown J, Gillard JH. In vivo detection of macrophages in human carotid atheroma: temporal dependence of ultrasmall superparamagnetic particles of iron oxide-enhanced MRI. *Stroke* 2004;35(7):1631–1635.
- 20 Kooi ME, Cappendijk VC, Cleutjens KB, Kessels AG, Kitslaar PJ, Borgers M, Frederik PM, Daemen MJ, van Engelshoven JM. Accumulation of ultrasmall superparamagnetic particles of iron oxide in human atherosclerotic plaques can be detected by in vivo magnetic resonance imaging. *Circulation* 2003;107(19):2453–2458.
- 21 Lewin M, Carlesso N, Tung CH, Tang XW, Cory D, Scadden DT, Weissleder R. Tat peptide-derivatized magnetic nanoparticles allow in vivo tracking and recovery of progenitor cells. *Nat Biotechnol* 2000;18(4):410–414.
- 22 Kircher MF, Mahmood U, King RS, Weissleder R, Josephson L. A multimodal nanoparticle for preoperative magnetic resonance imaging and intraoperative optical brain tumor delineation. *Cancer Res* 2003;63(23):8122–8125.
- 23 Schellenberger EA, Sosnovik D, Weissleder R, Josephson L. Magneto/optical annexin V, a multimodal protein. *Bioconjug Chem* 2004;15(5):1062–1067.
- 24 Kelly KA, Nahrendorf M, Yu AM, Reynolds F, Weissleder R. In vivo phage display selection yields atherosclerotic plaque targeted peptides for imaging. *Mol Imaging Biol* 2006;8(4):201–207.
- 25 Nahrendorf M, Jaffer FA, Kelly KA, Sosnovik DE, Aikawa E, Libby P, Weissleder R. Noninvasive vascular cell adhesion molecule-1 imaging identifies inflammatory activation of cells in atherosclerosis. *Circulation* 2006;114(14):1504–1511.
- 26 Weissleder R, Kelly K, Sun EY, Shtatland T, Josephson L. Cell-specific targeting of nanoparticles by multivalent attachment of small molecules. *Nat Biotechnol* 2005;23(11):1418–1423.
- 27 Mani V, Briley-Saebo KC, Itskovich VV, Sember DD, Fayad ZA. Gradient echo acquisition for superparamagnetic particles with positive contrast (GRASP): sequence characterization in membrane and glass superparamagnetic iron oxide phantoms at 1.5T and 3T. *Magn Reson Med* 2006;55(1):126–135.
- 28 Farrar C, Dai G, Rosen B, Sosnovik D. Off Resonance Imaging of Superparamagnetic Iron Oxide Nanoparticles in Infarcted Mouse Myocardium at Dilute Concentrations and High Magnetic Field Strengths. *J Cardiovasc Magn Reson* 2007;9:444–445.
- 29 Sirol M, Itskovich VV, Mani V, Aguinaldo JG, Fallon JT, Misselwitz B, Weinmann HJ, Fuster V, Toussaint JF, Fayad ZA. Lipid-rich atherosclerotic plaques detected by gadofluorine-enhanced in vivo magnetic resonance imaging. *Circulation* 2004;109(23):2890–2896.
- 30 Vaughan T, DelaBarre L, Snyder C, Tian J, Akgun C, Shrivastava D, Liu W, Olson C, Adriany G, Strupp J, Andersen P, Gopinath A, van de Moortele PF, Garwood M, Ugurbil K. 9.4T human MRI: preliminary results. *Magn Reson Med* 2006;56(6):1274–1282.
- 31 Nahrendorf M, Sosnovik DE, Waterman P, Swirski FK, Pande AN, Aikawa E, Figueiredo JL, Pittet MJ, Weissleder R. Dual channel optical tomographic imaging of leukocyte recruitment and protease activity in the healing myocardial infarct. *Circ Res* 2007;100(8):1218–1225.
- 32 Kanno S, Wu YJ, Lee PC, Dodd SJ, Williams M, Griffith BP, Ho C. Macrophage accumulation associated with rat cardiac allograft rejection detected by magnetic resonance imaging with ultrasmall superparamagnetic iron oxide particles. *Circulation* 2001;104(8):934–938.
- 33 Weissleder R, Lee AS, Khaw BA, Shen T, Brady TJ. Antimyosin-labeled monocrySTALLINE iron oxide allows detection of myocardial infarct: MR antibody imaging. *Radiology* 1992;182(2):381–385.
- 34 Barkhausen J, Ebert W, Heyer C, Debatin JF, Weinmann HJ. Detection of atherosclerotic plaque with Gadofluorine-enhanced magnetic resonance imaging. *Circulation* 2003;108(5):605–609.
- 35 Winter PM, Neubauer AM, Caruthers SD, Harris TD, Robertson JD, Williams TA, Schmieder AH, Hu G, Allen JS, Lacy EK, Zhang H, Wickline SA, Lanza GM. Endothelial $\alpha(v)\beta_3$ integrin-targeted fumagillin nanoparticles inhibit angiogenesis in atherosclerosis. *Arterioscler Thromb Vasc Biol* 2006;26(9):2103–2109.
- 36 Frias JC, Williams KJ, Fisher EA, Fayad ZA. Recombinant HDL-like nanoparticles: a specific contrast agent for MRI of atherosclerotic plaques. *J Am Chem Soc* 2004;126(50):16316–16317.
- 37 Lipinski MJ, Amirbekian V, Frias JC, Aguinaldo JG, Mani V, Briley-Saebo KC, Fuster V, Fallon JT, Fisher EA, Fayad ZA. MRI to detect atherosclerosis with gadolinium-containing immunomicelles targeting the macrophage scavenger receptor. *Magn Reson Med* 2006;56(3):601–610.
- 38 Botnar RM, Perez AS, Witte S, Wiethoff AJ, Laredo J, Hamilton J, Quist W, Parsons EC, Jr., Vaidya A, Kolodziej A, Barrett JA, Graham PB, Weisskoff RM, Manning WJ, Johnstone MT. In vivo molecular imaging of acute and subacute thrombosis using a fibrin-binding magnetic resonance imaging contrast agent. *Circulation* 2004;109(16):2023–2029.
- 39 Spuentrup E, Buecker A, Katoh M, Wiethoff AJ, Parsons EC, Jr., Botnar RM, Weisskoff RM, Graham PB, Manning WJ, Gunther RW. Molecular magnetic resonance imaging of coronary thrombosis and pulmonary emboli with a novel fibrin-targeted contrast agent. *Circulation* 2005;111(11):1377–1382.
- 40 Sirol M, Aguinaldo JG, Graham PB, Weisskoff R, Lauffer R, Mizsei G, Cheresnev I, Fallon JT, Reis E, Fuster V, Toussaint JF, Fayad ZA. Fibrin-targeted contrast agent for improvement of in vivo acute thrombus detection with magnetic resonance imaging. *Atherosclerosis* 2005;182(1):79–85.
- 41 Sirol M, Fuster V, Badimon JJ, Fallon JT, Moreno PR, Toussaint JF, Fayad ZA. Chronic thrombus detection with in vivo magnetic resonance imaging and a fibrin-targeted contrast agent. *Circulation* 2005;112(11):1594–1600.
- 42 Schmitz SA, Taupitz M, Wagner S, Coupland SE, Gust R, Nikolova A, Wolf KJ. Iron-oxide-enhanced magnetic resonance imaging of atherosclerotic plaques: postmortem analysis of accuracy, inter-observer agreement, and pitfalls. *Invest Radiol* 2002;37(7):405–411.
- 43 Kraitchman DL, Tatsumi M, Gilson WD, Ishimori T, Kedziorrek D, Walczak P, Segars WP, Chen HH, Fritzges D, Izbudak I, Young RG, Marcelino M, Pittenger MF, Solaiyappan M, Boston RC, Tsui BM, Wahl RL, Bulte JW. Dynamic imaging of allogeneic mesenchymal stem cells trafficking to myocardial infarction. *Circulation* 2005;112(10):1451–1461.
- 44 Aikawa E, Nahrendorf M, Sosnovik D, Lok VM, Jaffer FA, Aikawa M, Weissleder R. Multimodality molecular imaging identifies proteolytic and osteogenic activities in early aortic valve disease. *Circulation* 2007;115(3):377–386.

mMRI[®] (molecular MRI) for the Detection of Vulnerable Plaques

Joerg Schnorr DVM¹; Arne Hengerer, Ph.D.²; Carsten Warmuth, Ph.D.²

¹Radiology, Charité, Berlin, Germany

²Siemens Medical Solutions Erlangen, Germany

The aim of the „Nano_AG“ project is to develop a new class of targeted, electrostatically stabilized iron-oxide contrast agents.

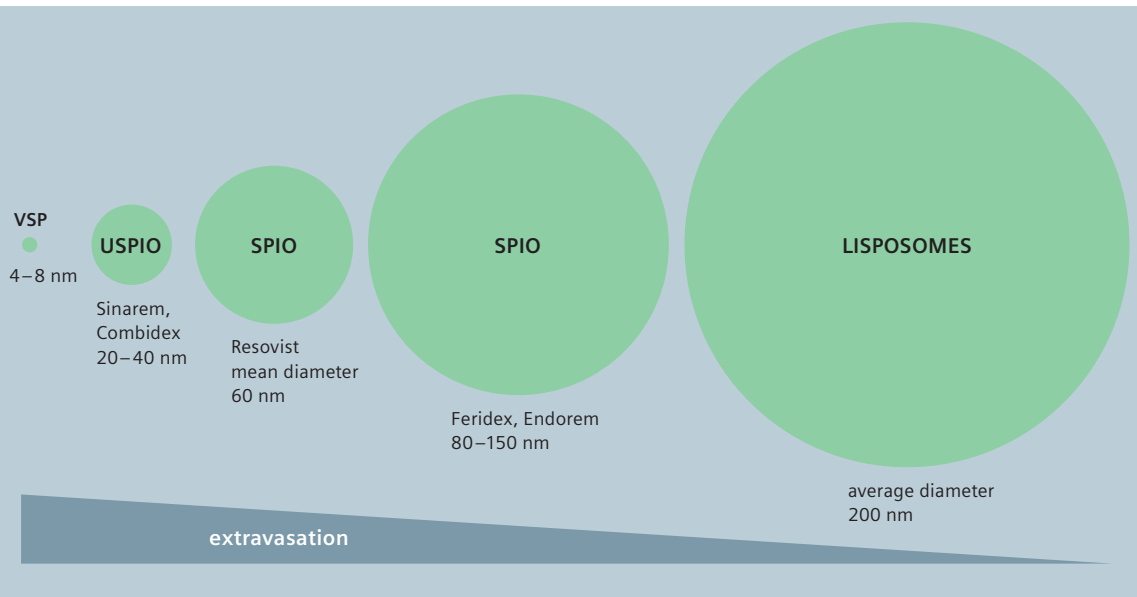
There is evidence that sudden coronary events or stroke are caused by vulnerable atherosclerotic plaques. Vulnerable plaques are atherosclerotic lesions due to endothelial inflammations, that may rupture and induce thrombus formation. Subsequent myocardial ischemia and acute myocardial infarction is considered to be responsible for approximately 60–70% of cardiac deaths. Determining the degree of stenosis by angiogram, currently the routine method relied on for clinical decision making, is unreliable for risk stratification. Thus a differentiation of stable or unstable atherosclerotic plaque burden is currently not possible with non-invasive imaging methods, although techniques like contrast enhanced CT can visualize plaque composition to some degree.

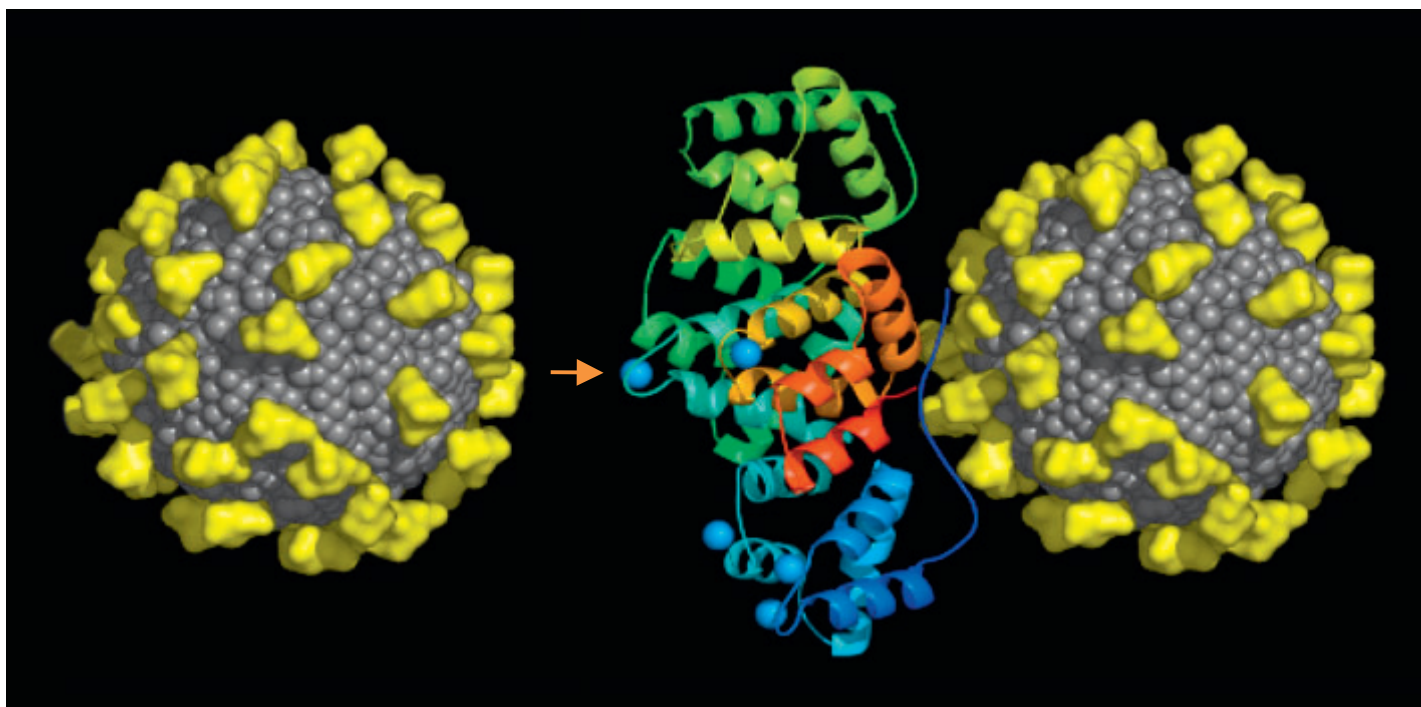
Major pathomorphologic characteristics of plaque vulnerability are the thickness of the fibrous cap, increased vessel wall angiogenesis, migration of inflammatory cells like macrophages, and degra-

dation of connective tissue along with a decrease in smooth muscle cells. Several molecular biomarkers are associated with vulnerable plaque formation such as adhesion molecules, matrix metalloproteases, cathepsins and integrins.

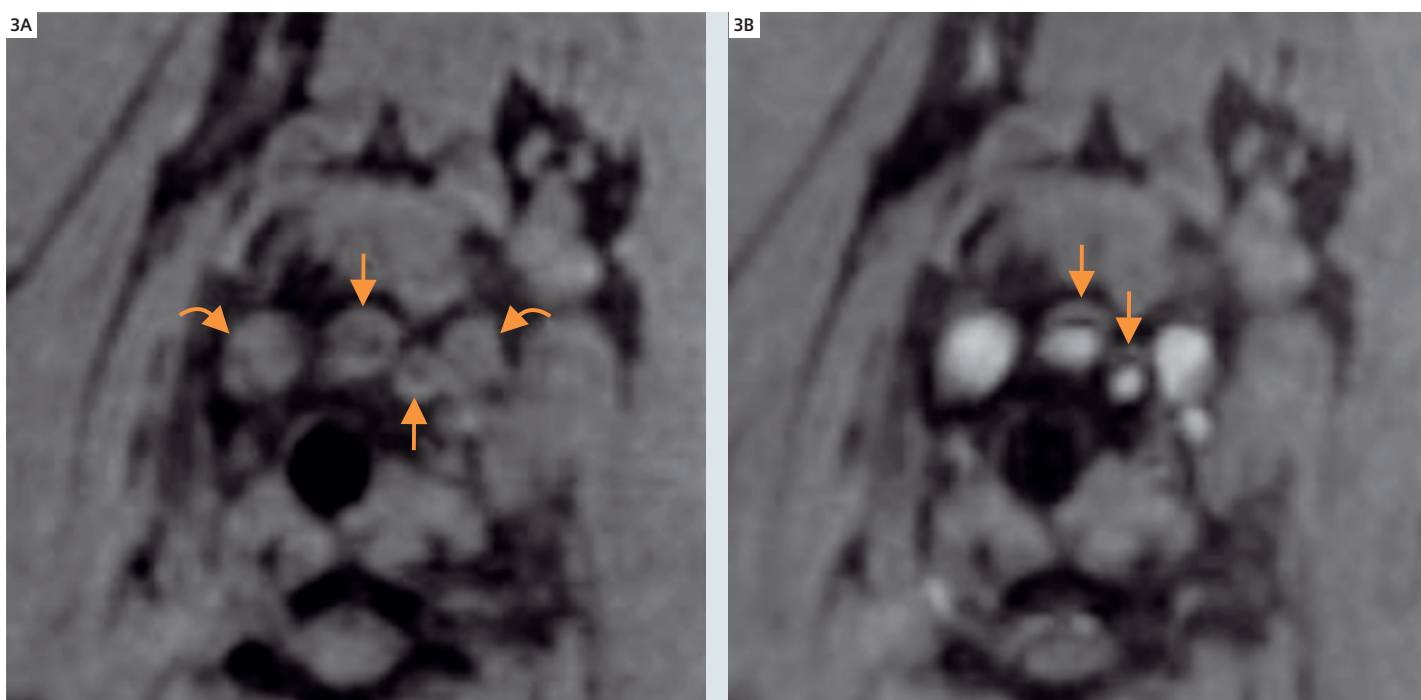
The aim of the „Nano_AG“ project is to develop a new class of targeted, electrostatically stabilized iron oxide contrast agents. The development is based on Very Small Iron Oxide Particles (VSOP) developed by Ferropharm GmbH, Berlin, Germany. In contrast to well-known polymer-based iron oxide nano-particles like USPIO or SPIO the size of the newly developed electrostatically stabilized iron oxide nanoparticles has been further decreased to a size less than 4 nm in diameter. This allows for extravasation and renal elimination (~30%). In addition, the bio-availability for targeting various pathologic tissues is highly optimized, while the high magnetic properties for MRI are retained. Pre-clinical proof-of-principle studies demonstrated

1 Size comparison of different particles as markers for molecular imaging.

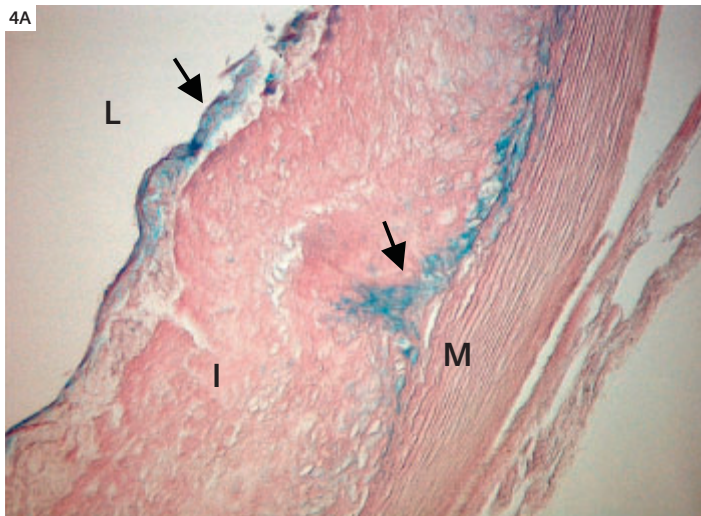




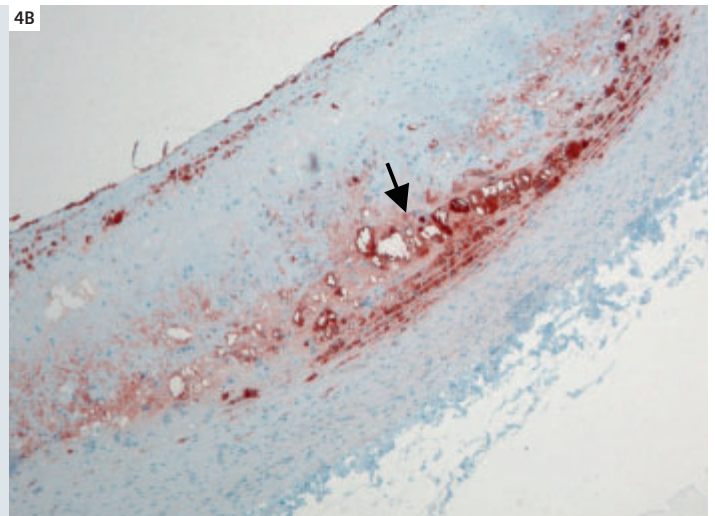
2 VSOP particle with yellow molecules indicating the citrate bound to the iron oxide surface (grey). Functionalization of the particle by specific peptides e.g. Annexin V. (Kindly provided by Eyk Schellenberger, Radiology, Charité, Berlin.)



3 MRI in axial section orientation of the brachio-cephalic trunc and the left common carotid artery (arrows) of a rabbit before **(A)** and after **(B)** administration of VSOP at a dose of 0.06 mMol Fe/kg. Images have been obtained at a Siemens MAGNETOM 1.5 T scanner with a commercially available 4-channel body array coil using a flow-saturated ECG-gated segmented 3D GRE sequence. Luminal signal increase demonstrates free circulation particles which exhibit a strong T1-relaxation time shortening effect. Arterial vessel wall of the left common carotid artery and the right brachiocephalic trunc (arrows in fig. 3B) exhibit a strong signal loss in contrary to the vessel wall of the veins (curve arrows in fig. 3A).



4 (A) Prussian-blue staining of a section from the brachiocephalic trunk 2 hours after administration of VSOP at a dose of 0.06 mmol Fe/kg bw. Areas positive for prussian blue staining are demonstrated in the subendothelial layer and in the area of the intimomedial interface (L = lumen, I = intima, m = media).



(B) Presence of cells positive for RAM-11 antibody with tissue integrity loss in the intimomedial interface could as well be seen in these regions reflecting the complex and advanced pathologic character of this arterial atherosclerotic lesion. According to the data published by Moreno et al. the intimomedial interface damage could be attributed to rupture-prone vulnerable lesions (Moreno et al. 2002 Circulation 105, 21: 2504–2511).

that these VSOP are a valuable tool for the characterisation of atherosclerotic plaque burden and the evaluation of high-risk atherosclerosis by magnetic resonance imaging (MRI).

Nano_AG seeks to optimize VSOPs for vulnerable plaque imaging further by targeting of vulnerable plaque biomarkers. This shall be achieved by linking peptides to VSOPs.

A major aspect of the work of Nano_AG is to obtain mMRI® (molecular MRI) contrast agents which facilitate a fast translation into clinical trials. Development from bench to bedside within a reasonable timeframe is possible only by using biocompatible components which already have been approved. This has been taken into account and the targeted VSOPs are composites of well characterized building blocks: iron oxide, citrate and biologically occurring peptides.

Nano_AG develops further sensitive measurement protocols with high spatial and temporal resolution. This includes off-resonance imaging and navigator sequences, which are mandatory to detect small contrast agent concentrations within the coronaries. Dedicated small animal imaging adaptations for clinical MRI devices have been applied to facilitating preclinical studies in a clinical setting to speed up translational research.

The Nano_AG consortia consists of Siemens Medical Solutions (project manager), the Charité in Berlin, the German Cancer Research Center (DKFZ) in Heidelberg, Freiburg University, MeVis in Bremen, Ferropharm and Bayer Schering Pharma, both in Berlin. Nano_AG is partly funded by the BMBF (German Ministry of Education and Research) grant „Nano for Life“.

Contact

Arne Hengerer, Ph.D.
Siemens Medical Solutions
MED MR PLM D BD
Allee am Röthelheimpark 6
91052 Erlangen, Germany
arne.hengerer@siemens.com

Radiofrequency Coil Innovation in Cardiovascular MRI

Melanie Schmitt, Ph.D.¹; Andreas Potthast, Ph.D.^{1,2}; Lawrence Wald, Ph.D.^{1,3}; David Sosnovik, M.D., FACC^{1,40}

¹Athinoula A. Martinos Center for Biomedical Imaging, Department of Radiology, Massachusetts General Hospital, Harvard Medical School, Boston, MA, USA

²Siemens Medical Solutions, Erlangen, Germany

³Division of Health Sciences and Technology, Massachusetts Institute of Technology, Cambridge, MA, USA

⁴Division of Cardiology, Massachusetts General Hospital, Harvard Medical School, Boston, MA, USA

Introduction

Over the last decade advances in the design of cardiac MRI pulse sequences have allowed the assessment of ventricular function, first-pass perfusion and myocardial viability to be performed with increasing accuracy and speed [1, 2]. Much of this progress has been made possible by significant advances in gradient coil technology, without which the implementation of sequences such as balanced steady state free precession (SSFP, e.g. TrueFISP) would not have been possible. However, despite these important advances, cardiovascular MRI has yet to reach its full potential and additional transformative technological innovations will be needed to improve the spatial resolution, efficiency and speed of cardiac MRI. In this article we describe recent and ongoing innovations in radiofrequency coil design for cardiovascular MRI. After a brief review of existing 32-channel receive coils [3–5], we focus most of the article on a recently developed 128-channel cardiac receive coil and the potential impact of multi-channel transmission coils in cardiovascular MRI [6].

Multi-channel receive coils. Advantages compared to single-channel coils

The sensitivity of multi-element parallel array coils matches the sensitivity of coils with fewer but larger elements in the center of the body, but provides substantial gains in sensitivity closer to the surface of the coil [7–11]. More importantly, multi-element arrays play a crucial role in facilitating parallel imaging with high acceleration factors (R) [3–5]. The signal-to-noise ratio (SNR) during parallel acquisition, SNR_{PA} , is influenced by both the degree of undersampling, described by the ac-

celeration factor (R), and also by the G-factor (G), which is the local geometry factor. SNR_{PA} is thus described by the following equation below.

$$SNR_{PA} = \frac{SNR_{full}}{\sqrt{R \times G}}$$

Simulations and experimental data have shown that G can be reduced, for a given acceleration factor and coil geometry, by increasing the field strength B_0 and/or by increasing the number of coil elements in a phased array coil [12, 13]. The use of multi-channel phased array coils with a high number of individual elements thus not only produces higher SNR values near the coil plane, but also decreases the SNR penalty associated with parallel imaging. Cardiac arrays with 32 coil elements are now commercially available at both 1.5 and 3 Tesla, and have been shown to dramatically impact the ability to accelerate 2D images in one dimension. Highly accelerated 2D cine images have been obtained with these coils, principally using the tSENSE algorithm [14], allowing large volumes of the heart to be imaged in a single breath-hold. The experience with 3D imaging with these coils is less extensive, and is discussed further below. However, it is clear that these 32-element coils constitute a major advance and will have a significant impact on cine, first-pass perfusion and potentially other areas of cardiovascular MRI as well.

New development: 128-channel receive coil for cardiac MRI at 3 Tesla

The appeal of performing parallel acquisition at higher field strengths, such as 3 Tesla, lies not only in the higher unaccelerated SNR obtainable, but

32-element coils will have a significant impact on cine, first-pass perfusion and potentially other areas of cardiovascular MRI.

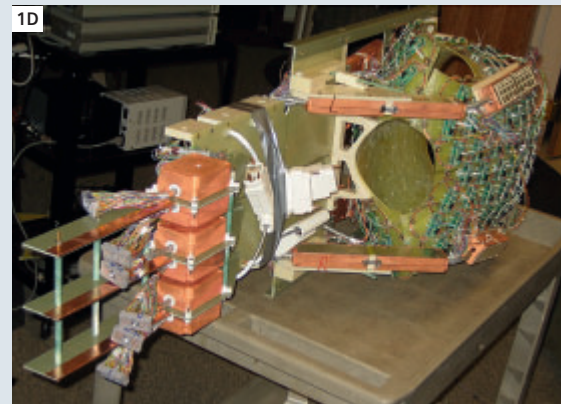
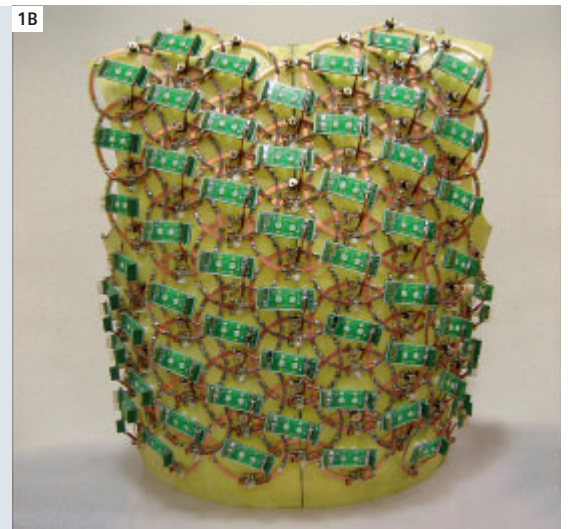
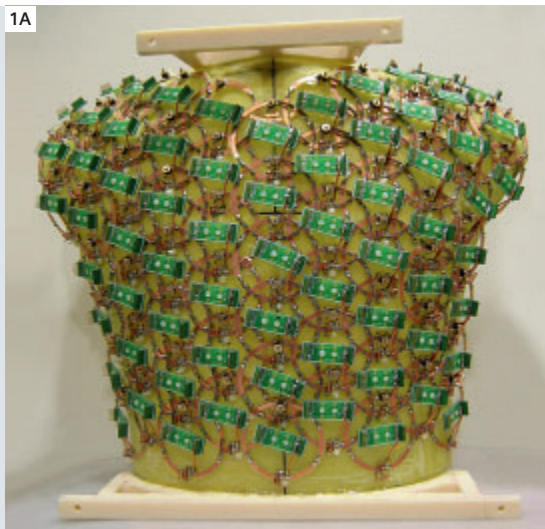
also in the ability to use a larger number of smaller elements without a significant rise in the G-factor. We have thus developed a 128-channel coil for use on a prototype 3T scanner, expanded to 128 independent channels (Figure 1). Our aims in developing this system were to explore the feasibility, challenges and potential benefits of ultra-high element (> 32 elements) receive arrays and determine their potential impact on cardiovascular MRI. The MR system used with this coil is based on a clinical Siemens MAGNETOM Trio, A Tim System 3T scanner with 32 individual RF channels, which was expanded to a system with 128 individual receiving channels [15]. This allows the signal of each individual coil element to be detected with a single receive RF channel. The 128 individual coil elements (mean diameter $d = 75$ mm) are arranged on a fiberglass shell with 68 elements on the posterior portion and 60 coil elements on the anterior part of the coil (Figure 1). SNR and G-factor maps were obtained with the

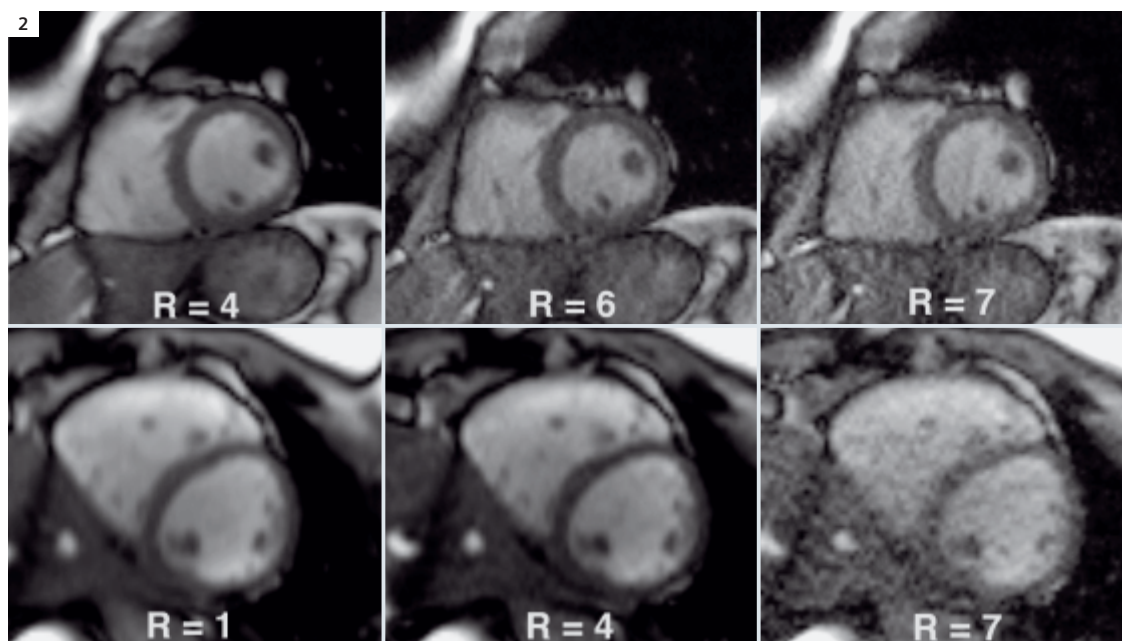
128-channel coil on torso-shaped oil and water phantoms, and compared to those acquired with a commercially available 32-channel coil (InVivo Corporation, Gainesville, FL, USA). At higher acceleration factors ($R = 5, 6, 7$ and 8) maximum G-factors with the 128-channel coil were approximately 50% those with the 32-channel coil. The gains in unaccelerated SNR with the 128-channel coil were more modest, but in human volunteers a gain in unaccelerated SNR at the apex of up to 1.3 could be obtained with the 128-channel versus 32-channel coil. The low G-factors obtained with the 128-channel coil (maximum G-factor of 1.7 at $R = 7$ in left-right direction) facilitated the acquisition of high quality accelerated images in several healthy human volunteers. 2D Cine images of the heart were obtained with a SSFP (TrueFISP) sequence using the following imaging parameters: field of view (FoV) 360 mm, $TE / \alpha / BW = 1.4$ ms / 35° / 965 Hz / Pixel, matrix size: 101 x 192, producing an in-plane spatial resolution of 1.9 mm x 2.9 mm. Slice thickness

1 Prototype 128-channel cardiac coil.

(A, B) The coil consists of a fiberglass mold in a clam-shell geometry, with 60 elements on the anterior portion and 68 elements on the posterior portion of the mold. Each element is 75 mm in diameter and arranged in overlapping hexagonal symmetry to reduce next neighbor coupling. The preamplifier of each element lies 3 cm above the element to improve coil compactness and reduce cable related signal loss.

(C, D) Fully assembled coil with its cover and padding removed. The signal from 32 of the channels is routed to the regular receiving unit of the scanner, while the signal from the other 96 elements is routed to 3 additional receiving units.





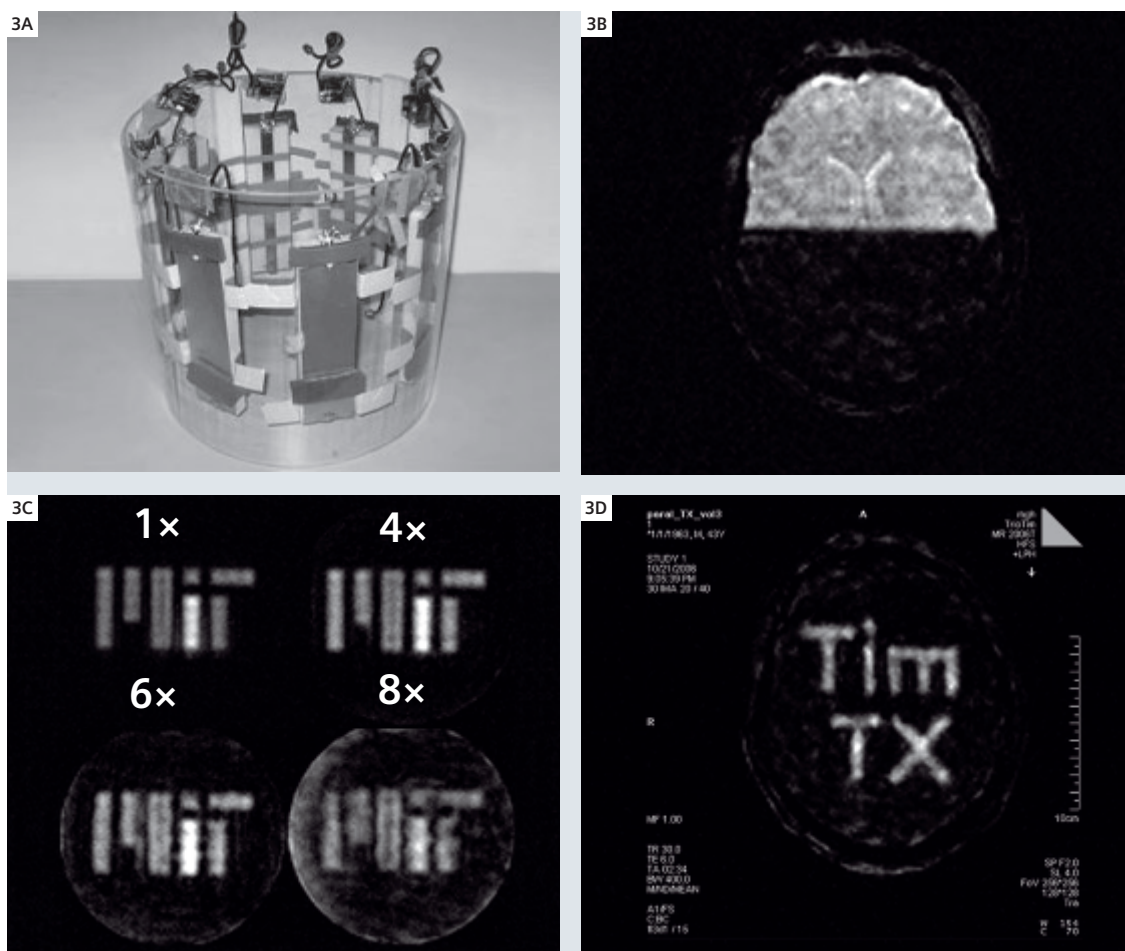
2 Highly accelerated 2D SSFP (TrueFISP) images in a healthy male volunteer (top panel) and a healthy female volunteer (lower panel). The GRAPPA algorithm was used in one direction with an acceleration rate of up to 7. In plane resolution was 1.9×2.9 mm and slice thickness ranged from 6–10 mm. Because of the need to acquire reference lines with GRAPPA, even at acceleration rates of 6 and 7, a maximum of only ten slices could be obtained in a single breath-hold. However, the acquisition of ten 10 mm thick slices, one of which is shown in the male volunteer in the top panel, allowed the whole heart to be easily covered in a single breath-hold. The female volunteer in the lower panel was imaged with a slice thickness of 6 mm and, in addition, the anterior portion of the coil did not lie close to her chest wall, since a rigid design (fitted a male chest) was chosen for this prototype coil to simplify experimental issues. Despite this, the rate 4 images are almost indiscernible from the unaccelerated images, and the rate 7 images remain diagnostic with well-preserved blood-tissue contrast. Future versions of the coil will likely include a flexible anterior portion to lie close the chest of all subjects scanned.

ranged from 6–10 mm and temporal resolution was set to 16 frames per RR interval (Figure 2). Parallel acquisition was performed with the GRAPPA algorithm with acceleration factors up to 7 in one dimension. As shown in Figure 2, image quality was well preserved at acceleration rates as high as $R = 6$ and 7, in both male and female volunteers. The use of spatio-temporal compression algorithms such as tSENSE with these acceleration factors has the potential to allow high quality 2D cines to be acquired sequentially over the entire heart in a single relatively short breath-hold. In addition, 2D acceleration during 3D imaging will likely demonstrate the value of the low G-factors obtained with the 128-channel coil even more dramatically. The current results, obtained with accelerated imaging in one direction, however provide strong proof-of-principle for the use of this 128-channel coil, and suggest that highly accelerated volumetric 3D imaging with this coil will be highly promising.

Multi-channel transmit coils

The concept of multiple independent RF channels is now being applied to RF transmission as well as to RF reception. The potential of parallel RF transmission lies in its ability to allow RF (B_1) shimming as well as spatially tailored excitation to be performed. The challenge of uniform RF (B_1) excitation in the heart becomes significantly more problematic at field strengths of 3 Tesla and higher. Adiabatic excitation pulses can be used to address this challenge, as well shown by Nezafat, Stuber and Pettigrew, but are often long, limited by SAR thresholds and more difficult to implement in a slice selective manner. Vaughan and colleagues have recently shown that RF shimming with multiple RF transmission channels in human brains at 9.4T can be used as an alternative method to address this B_1 inhomogeneity challenge. Perhaps the greatest potential impact of multiple transmission coils, however, lies in their ability

Highly accelerated volumetric 3D imaging with the 128-channel coil will be highly promising.



3 Spatially tailored RF excitation with an 8-channel RF transmission coil. Several different coil configurations have been tested. An example of an 8-channel stripline transmit array is shown in (A). (B) Spatially tailored excitation of the human brain at 3T with an 8-channel transmit array. (C) A spatially selective 2D RF excitation pulse has been used to excite the “MIT” logo in an oil phantom. Without parallel RF transmission, however, the duration of this excitation pulse approaches 10 ms. At rate 4 acceleration the pulse duration can be reduced to approximately 2.5 ms and at rate 6 to less than 1.7 ms. It should be noted that the duration of spatially tailored 3D excitation pulses can reach over 50 ms and the use of parallel RF transmission techniques in this setting may be even more important than in the 2D setting. The reduction of pulse duration with parallel RF transmission also has the benefit of reducing off-resonance effects. At present image quality at rate 7 and 8 acceleration becomes problematic but should improve with the design of better multi-channel RF transmission coils and more efficient algorithms to undersample excitation k-space. Even with present technology, however, complex patterns of spatially tailored excitation can be produced in vivo, as shown in the 3 Tesla image of a normal volunteer (D).

to accelerate spatially tailored excitation pulses, so that the duration of these pulses becomes feasible for clinical implementation. The ability of parallel transmission to facilitate spatially tailored excitation in both two and three dimensions has recently been demonstrated both in phantoms and in the brain in vivo [6]. The experience with spatially tailored excitation in the body is less extensive but could be used, in theory, for the excitation of only a well-defined 2D or 3D region in the body,

such as the heart. The selective excitation of only the heart could then facilitate the reduction of the imaging field of view (FoV), without the penalty of infolding artifacts, and thus facilitate a dramatic increase in either the spatial resolution or speed of a given acquisition.

Prototype 8-channel parallel transmission systems have now been installed on 3, 7 and 9.4 Tesla human scanners. The 3 Tesla prototype system is based on a clinical MAGNETOM Trio, A Tim System scan-

ner using a 8-channel transmission head coil. The 8-channel transmit array is connected to the scanner's original RF channel and operated in a "master-slave" configuration, where the Trio is the master. Cloning the standard Siemens measurement control unit (MPCU) for all 7 slaves makes it possible to run 8 independent sequences with individual RF shapes and characteristics. Using the 8-channel transmission head coil in combination with a 2D spatially tailored excitation RF pulse, the use of acceleration factors as high as $R = 8$ allowed the RF pulse duration to be shortened from 9.47 ms ($R = 1$) to 2.42 ms ($R = 4$), 1.64 ms ($R = 6$) and 1.26 ms ($R = 8$). The image quality in the accelerated images was well preserved even with transmission acceleration factors as high as $R = 6$, as shown in Figure 3. In vivo imaging of the brain could also be performed with this coil and resulted in highly spatially tailored excitation of the human brain (Figure 3).

Conclusion

The breadth, flexibility and soft tissue contrast obtainable with cardiovascular MRI remain unsurpassed. However, further improvements in the speed, efficiency and spatial resolution of cardiac MRI are needed for it to reach its full clinical potential. We have described in this article recent and ongoing technical innovations in radiofrequency design, that have the potential to play a transformative role in cardiovascular MRI. Ultra-high element receive arrays, such as the 128-channel 3T coil described above, could allow high resolution volumetric 3D datasets to be acquired in a single breath-hold. Multi-channel transmission arrays could also dramatically increase both the speed and spatial resolution of cardiac MR acquisitions. While 128-channel receive systems and multi-channel transmission systems remain experimental, both configurations have already been used successfully to scan human volunteers, and 32-channel cardiac receive coils are already commercially available for both 1.5 and 3 Tesla scanners. The translation of ongoing technical innovation in radiofrequency design into routine clinical use thus seems not only highly feasible, but also cause for significant optimism and excitement regarding the future of cardiovascular MRI.

Acknowledgements

The authors wish to acknowledge InVivo Corporation for the use of their 32-channel cardiac coil.

The authors also wish to acknowledge the following collaborators at Siemens Medical Solutions: Franz Hebrank, Franz Schmitt, Ulrich Fontius, Hubertus Fischer, Edgar Mueller, Renate Jerecic, Sven Zuehlsdorff, Ravi Seethamraju and Chung Yiucho.

Contact

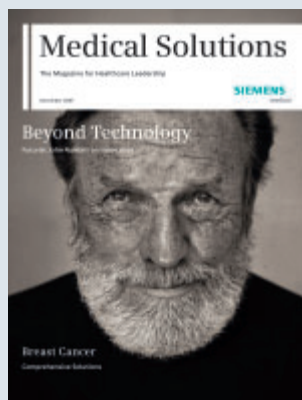
Melanie Schmitt, Ph.D.
Athinoula A. Martinos Center for Biomedical Imaging, Department of Radiology,
Massachusetts General Hospital,
Harvard Medical School, Boston, MA, USA
mschmitt@nmr.mgh.harvard.edu

References

- 1 Barkhausen J, Ruehm SG, Goyen M, et al. MR evaluation of ventricular function: true fast imaging with steady-state precession versus fast low-angle shot cine MR imaging: feasibility study. *Radiology* 2001;219(1):264–9.
- 2 Wilke N, Jerosch-Herold M, Wang Y, et al. Myocardial perfusion reserve: assessment with multisection, quantitative, first-pass MR imaging. *Radiology* 1997;204(2):373–84.
- 3 Pruessmann KP, Weiger M, Scheidegger MB, et al. SENSE: sensitivity encoding for fast MRI. *Magnetic Resonance in Medicine* 1999;42(5):952–62.
- 4 Sodickson DK, Manning WJ. Simultaneous acquisition of spatial harmonics (SMASH): fast imaging with radiofrequency coil arrays. *Magnetic Resonance in Medicine* 1997; 38(4):591–603.
- 5 Griswold MA, Jakob PM, Heidemann RM, et al. Generalized autocalibrating partially parallel acquisitions (GRAPPA). *Magnetic Resonance in Medicine* 2002;47(6):1202–10.
- 6 Setsompop K, Wald LL, Alagappan V, et al. Parallel RF Transmission with Eight Channels at 3 Tesla. *Magn Reson Med* 2006;56(5):1163–71.
- 7 Roemer PB, Edelstein WA, Hayes CE, et al. The NMR phased array. *Magnetic Resonance in Medicine* 1990;16(2):192–225.
- 8 Hayes CE, Hattes N, Roemer PB. Volume imaging with MR phased arrays. *Magnetic Resonance in Medicine* 1991;18(2): 309–19.
- 9 Wang J, Reykowski A, Dickas J. Calculation of the signal-to-noise ratio for simple surface coils and arrays of coils. *IEEE Transactions on Biomedical Engineering* 1995;42(9):908–17.
- 10 Wright SM, Wald LL. Theory and application of array coils in MR spectroscopy. *NMR in Biomedicine* 1997;10(8):394–410.
- 11 Wiesinger F, De Zanche N, Pruessmann KP. Approaching ultimate SNR with finite coil arrays. 2005; Miami Beach Florida, USA. 672.
- 12 Wald LL, Moyher SE, Day MR, et al. Proton spectroscopic imaging of the human brain using phased array detectors. *Magnetic Resonance in Medicine* 1995;34(3):440–5.
- 13 Wiesinger F, Boesiger P, Pruessmann KP. Electrodynamics and ultimate SNR in parallel MR imaging. *Magnetic Resonance in Medicine* 2004;52(2):376–90.
- 15 Wiggins GC, Triantafyllou C, Potthast A, et al. 32-channel 3 Tesla receive-only phased-array head coil with soccer-ball element geometry. *Magnetic Resonance in Medicine* 2006;56(1):216–23.
- 16 Kellman P, Epstein FH, McVeigh ER. Adaptive sensitivity encoding incorporating temporal filtering (TSENSE). *Magnetic Resonance in Medicine* 2001;45(5):846–52.
- 17 Potthast A, Kalnischkies B, Kwapiel G, et al. A MRI system with 128 seamlessly integrated receive channels. 2007; ISMRM, Berlin, Proceedings: page 672.

Siemens Medical Solutions – Customer Magazines

Our customer magazine family offers the latest information and background for every healthcare field. From the hospital director to the radiological assistant – here, one can quickly find information relevant to their needs.



Medical Solutions

Innovation and trends in healthcare. The magazine, published three times a year, is designed especially for members of the hospital management, administration personnel, and heads of medical departments.



AXIOM Innovations

Everything from the worlds of interventional radiology, cardiology, fluoroscopy, and radiography. This semi-annual magazine is primarily designed for physicians, physicists, researchers and medical technical personnel.



MAGNETOM Flash


Everything from the world of magnetic resonance imaging. The magazine presents case reports, technology and product news and "How I do it" sections. It is primarily designed for physicians, physicists, and medical technical personnel.



SOMATOM Sessions

Everything from the world of computed tomography. With its innovations, clinical applications, and visions, this semi-annual magazine is primarily designed for physicians, physicists, researchers, and medical technical personnel.

For details and to order the magazines please visit us at www.siemens.com/medical-magazine



We see a way to evaluate myocardial infarct and vascular disease within one exam without any patient repositioning

Tim

won't let you
miss a beat.

We see a way to determine regional ventricular function in real time allowing free-breathing using 12 matrix coil elements

Proven Outcomes in Cardiology with Tim® (Total imaging matrix technology).

Tim offers unmatched MRI capabilities for all cardiovascular exams without repositioning the patient. Ideal not only in diagnosing subendocardial infarct and congenital heart disease, but also systemic diseases like diabetes and atherosclerosis. With its 76 matrix coil elements and up to 32 RF channels, you enjoy revolutionary acquisition speed with virtually unlimited Parallel Imaging even in double oblique slice orientations. Tim transforms workflow from an exam limited by the dimensions of local RF-coils to one determined by the disease. Tim. Very heart smart.

www.siemens.com/Tim

SIEMENS
medical

MAGNETOM Flash

The Magazine of MR

Issue no. 2/2007
CMR Edition (ESC)
Not for distribution in the US

SIEMENS
medical

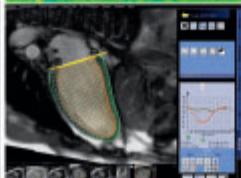
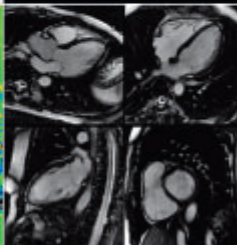
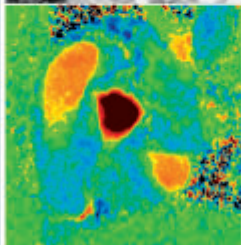
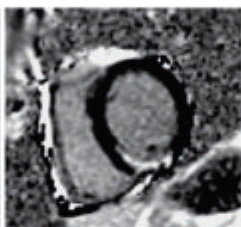
Cardiovascular Magnetic Resonance

Delayed Enhancement
Imaging in Coronary
Artery Disease
Page 14

Differentiation of
Cardiomyopathies
Page 22

Myocardial Stress
Perfusion Imaging
Page 34

Contains a CD with
SCMR Recommended
Protocols
Page 107



MAGNETOM Flash offers product news,
clinical methods, application tips, MR technology
and information on Life.

MAGNETOM Flash

Institution

Title

Name *

Street/P.O. Box *

Zip/Postal Code *

City *

State/Province *

Country *

E-mail

☐ Yes, I consent to the above information being used for future contact regarding product updates and other important news from Siemens MR.

Please print clearly!

Siemens AG
Medical Solutions
Magnetic Resonance
Marketing
P.O. Box 3260

D-91050 Erlangen
Germany



SUBSCRIBE NOW!

– and get your free copy of future
MAGNETOM Flash! Interesting information from
the world of magnetic resonance – gratis to your
desk. Send us this postcard, or subscribe online at
www.siemens.com/MAGNETOM-World

On account of certain regional limitations of sales rights and service availability, we cannot guarantee that all products included in this brochure are available through the Siemens sales organization worldwide. Availability and packaging may vary by country and is subject to change without prior notice. Some/All of the features and products described herein may not be available in the United States.

The information in this document contains general technical descriptions of specifications and options as well as standard and optional features which do not always have to be present in individual cases.

Siemens reserves the right to modify the design, packaging, specifications and options described herein without prior notice.
Please contact your local Siemens sales representative for the most current information.

Note: Any technical data contained in this document may vary within defined tolerances. Original images always lose a certain amount of detail when reproduced.

Not for distribution in the USA.

© 11.2007, Siemens AG
Order No. A91MR-1000-41C-7600
Printed in Germany
CC MR 01000 WS 110720.

Contact Addresses

In the USA:

Siemens Medical Solutions USA, Inc.
51 Valley Stream Parkway
Malvern, PA 19355
Tel.: +1 888-826-9702
Tel.: 610-448-4500
Fax: 610-448-2254

In Japan:

Siemens-Asahi
Medical Technologies Ltd.
Takanawa Park Tower 14 F
20-14, Higashi-Gotanda 3-chome
Shinagawa-ku
Tokyo 141-8644
(+81) 354238489

In Asia:

Siemens Medical Solutions
Asia Pacific Headquarters
The Siemens Center
60 MacPherson Road
Singapore 348615
(+65) 9622-2026

In Germany:

Siemens AG, Medical Solutions
Magnetic Resonance
Henkestr. 127, D-91052 Erlangen
Germany
Telephone: +49 9131 84-0

Headquarters

Siemens AG, Medical Solutions
Henkestr. 127, D-91052 Erlangen
Germany
Telephone: +49 9131 84-0
www.siemens.com/medical